University of Southampton
Faculty of Engineering, Science and Mathematics
School of Ocean and Earth Science

Sand Transport in Northern Venice Lagoon Through the Tidal Inlet of Lido

Author:
Rachel Helsby

Supervisors:
Prof. Carl Amos
Dr. Charlie Thompson

Thesis for the Degree of Doctor of Philosophy
June 2008

The face of the water, in time, became a wonderful book; a book that was a dead language to the uneducated passenger, but which told its mind to me without reserve, delivering its most cherished secrets as clearly as if it uttered them with a voice. And it was not a book to be read once and thrown aside, for it had a new story to tell every day.

- Mark Twain, Life on the Mississippi

'Element opposes element' - Bernardo Trevisan

UNIVERSITY OF SOUTHAMPTON

ABSTRACT

FACULTY OF ENGINEERING, SCIENCE & MATHEMATICS
SCHOOL OF OCEAN & EARTH SCIENCES

Doctor of Philosophy

SAND TRANSPORT IN NORTHERN VENICE LAGOON THROUGH THE TIDAL INLET OF LIDO

by Rachel Helsby

The provenance and transport of sand has been investigated around Lido Inlet, the largest of three tidal inlets in Venice Lagoon, Italy. Morphological analysis has established the presence of an ebb-tidal delta extending from the mouth of Lido Inlet as well as other features typical of tidal inlets. The stability of the inlet, as well as the canals of Treporti and Burano, was determined through the application of the tidal prism/cross-sectional areas relationship theorized by O'Brien (1969). Whilst Lido Inlet and Treporti Canal have both remained in equilibrium in terms of this relationship, Treporti Canal has suffered erosion due to a fluctuating tidal prism. Lido Inlet is slightly flood dominant although grain trend analysis of bottom sediment reveals net export of sand. Treporti Canal is ebb dominant and is the source of this sand, but it is becoming increasingly flood dominant as average current speeds have reduced and ebb currents are weakening at a faster pace than flood currents. This is proposed as a reason to why the northern lagoon is accreting (0.44 cm yr^{-1}), contrary to trends in the southern (-0.37 cm yr^{-1}) and central lagoon (-0.23 cm yr^{-1}). A sediment budget formulated for the whole lagoon has revealed that whilst the overall rate of erosion is reducing, the area subject to erosion is increasing and the rate of accretion is decreasing, resulting in no net change in the net sediment loss rate between 1930-1970 to 1970-2000 (-0.05 cm yr^{-1}). Mineralogical analysis on bottom samples, beach and riverine samples confirmed that longshore transport is from north to south along the northern lagoon; carbonate grains are dominant in the north with proportions gradually replaced by quartz to the south. Lido Inlet proved to have similar mineralogy to the River Piave with a higher calcite/dolomite ratio than inner lagoon samples suggesting a less mature sediment and thus import of sediment. Conversion of ADCP backscatter into bedload transport rate, suspended sand, and suspended fines concentrations has shown that no sand is transported at velocities below $\sim$0.4 m s^{-1}. 55% of sediment transported during an ebb flow was sand in suspension (peak: 527,000 kg hr^{-1}), 37% was fines in suspension (peak: 283,000 kg hr^{-1}), and the remaining 8% of sediment was transported as bedload (peak 68,700 kg hr^{-1}).

Contents

List of Tables

List of Figures

List of Symbols

a	Porosity index
A	Total basin area
A_c	Cross-sectional area
A_i	Intertidal basin area
A_n	Area of body normal to flow
A_w	Advective change in water volume
b	Rouse parameter
b	Bedload (subscript)
B	Bedload sample
C	Calibration sample
C_a	Reference sediment concentration at reference height z_a above the bed
C_D	Drag coefficient
C_f	Fines concentration
C_L	Lift coefficient
S_s	Sand concentration
$C(z)$	Sediment concentration at height z above the bed
d	Median sieve diameter
d	Depth
d_{50}	Median grain size
D	Grain size
D_{cr}	Critical distance between samples
D_*	Dimensionless grain size
E	Spatially integrated evaporation

F_D	Frictional drag
F_G	Gravitational attraction
F_L	Lift
g	Acceleration due to gravity - 9.81 m s^{-1}
G	Groundwater seepage
h	Water depth
H_{sb}	Significant wave breaking height
I_b	Backscatter intensity
I_R	Reflectivity index
k	Number of summed trend vector sites
k	von Karman's constant = 0.4
K_G	Kurtosis
K_l	Empirical coefficient - 0.32-0.39
L	Reliability length
m_s	Mass of dry silt
m_t	Weight of sediment/water mix
M	Near-bed sediment sample
M_{tot}	Total annual littoral drift
OBS	Optical backscatter sensor
p	Pressure along streamline
P	Tidal prism
P	Volume of sediment artificially placed into a system
P_s	Spatially integrated precipitation
P_w	Wetted perimeter
q_b	Volumetric bedload transport rate per unit width
Q	Discharge
Q_r	Channel discharge ratio
Q_t	Tributary discharge
Q_m	Main channel discharge
Q_{max}	Maximum discharge
Q_{pos}	Total flooding discharge
r	Type of inlet
$\vec{r}(x, y)$	Trend vector

R	Tidal range
R	Volume of sediment artificially removed from a system
$\vec{R}_{av}$	Transport vector
R_e	Reynold's number
R_h	Hydraulic radius
$\vec{R}_j$	Summed trend vector from neighbouring site
R_w	Runoff
s	Ratio between ρ_s and ρ
s	Suspended load (subscript)
S	Surface sample
SK_I	Skewness
SSC	Suspended sediment concentration
T	Tidal period
T_s	Transport parameter
u	Horizontal velocity
u_*	Total friction velocity
u_{*c}	Threshold friction velocity
$\overline{U}$	Depth averaged velocity
$\overline{U}_h$	Depth averaged velocity over an hour
U_{100}	Velocity 100 cm above the bed
v	Kinematic viscosity
V_{max}	Maximum velocity
V_t	Volume of sediment/water mix
W_s	Settling velocity
$\overline{y}$	Mean flow depth
y_{cs}	Maximum water depth
z	Height above the bed
z_a	Reference height above the bed
Z_0	Bed roughness
β	Rouse profile constant
Δ_r	Ripple height
ΔV_l	Total volume of the lagoon
ΔV	Net change in volume within coastal cell

Δt	Sum of time
θ_c	Confluence angle
θ	Shield's Parameter
θ_{cr}	Threshold Shield's Parameter
θ_b	Wave breaking angle
γ	Wave breaker index
ρ	Density of water
ρ_s	Density of sediment
τ_0	Bed shear stress (total)
τ_{0s}	Skin friction component of bed shear-stress
$\tau 0f$	Form drag component of bed shear-stress due to bedforms
τ_{cr}	Critical shear-stress
ϕ	Friction angle
u_*	Friction velocity
u_{*c}	Threshold friction velocity
τ_s	Sorting parameter
δ_o	Laminar sub-layer thickness
σ_I	Sorting (phi)
σ_G	Sorting (microns)
σt	Potential density
Φ	Dimensionless bedload transport rate
λ_r	Ripple wavelength

I, Rachel Helsby, declare that the thesis entitled

"Sand transport in northern Venice Lagoon through the tidal inlet of Lido"

and the work presented in the thesis are both my own, and have been generated by me as the result of my own original research. I confirm that:

- this work was done wholly or mainly while in candidature for a research degree at this University;
- where any part of this thesis has previously been submitted for a degree or any other qualification at this University or any other institution, this has been clearly stated;
- where I have consulted the published work of others, this is always clearly attributed;
- where I have quoted from the work of others, the source is always given. With the exception of such quotations, this thesis is entirely my own work;
- I have acknowledged all main sources of help;
- where the thesis is based on work done by myself jointly with others, I have made clear exactly what was done by others and what I have contributed myself;
- parts of this work have been published as:

Helsby, R., Amos, C.L., and Umgiesser, G. (2005). Morphological evolution and sand pathways in northern Venice Lagoon. In P. Campostrini, ed., *Scientific Research and Safeguarding of Venice*, volume 4, pp. 388402. CO.RI.LA, Venice.

Signed:

Date:

To Carl
To Charlie
To Ed

I owe them so much more
than thanks, but here is this thesis
dedicated to you, a small token of
appreciation.

Thanks must be given to the small army of people who have given their time, support and knowledge so that I could undertake this research and write this thesis. Firstly, my supervisors, Carl Amos and Charlie Thompson without whom, I would not be on this path. They have been the strongest team of supervisors a PhD student could ever dream of having, and have provided knowledge and support without fail *with* the hand of friendship thrown in for free. Thanks also to CO.RI.LA, who funded me through the first two years of this project and provided funding and support during the fieldwork undertaken during the course of this PhD.
Thanks are also due to Georg Umgiesser (CNR-ISMAR), the mastermind of the SHYFEM model used throughout this thesis. Not only has he helped immensely with the modeling, but also spent many hours in the boat collecting bathymetry and answering all of my questions about Venice! Thanks also to Christian Ferrarin (CNR-ISMAR), who taught me how to use SHYFEM, and also spent many hours in the boat collecting bathymetry and answering all of my questions about Venice!
Ian West spent many hours in front of a microscope helping me to identify many strange minerals amongst the carbonates and silicas of northern Venice Lagoon and I must thank him strongly for taking a break out of retirement to do so. Bob Jones and John Ford provided the thin sections for this analysis as well as showing me the ins and outs of good diamond jewellery as a sideline to this thesis! I thank you for all of the good conversations and years of good presents to come!
Thanks to my friends who could sympathize with the PhD life, the t@3'rs, a welcome break from 'counting sand', and to my family, who helped when they could. Thanks to the guys at Partrac, who must have wondered how long 'nearly finished' would really take! Special thanks however, must go to my husband Ed, who knew the price of the final six months of a PhD having just completed one, and patiently waited out many lonely evenings whilst I wrote. Thank you.

and thanks to all the fish...

1

Introduction

'Element opposes element'

Thus Bernardo Trevisan described the lagoon of Venice in 1718[i], upon recognition of the conflict between the elements of water, sediment and wind at work within the lagoon. Due to this dynamic nature, Venice Lagoon, as with all lagoons, is just a momentary feature in geological timescales. Once in existence due to eustatic sea level rise (Dyer, 1997), a lagoon can follow only one of two possible fates; complete sedimentation and formation of land, or ingression and eventual envelopment of the sea. Venice Lagoon historically tended towards sedimentation, but due to its success as a maritime power (Norwich, 2003), this trend was incompatible with the ambitions of its citizens, who have sought to control the movement of sediment within Venice Lagoon for much of its history. As such, interest in the sediment transport within Venice Lagoon has been nurtured for several hundred years, with the knowledge first applied in the 14^{th} century when the mouth of the River Brenta was diverted away from the lagoon in an effort to reduce the volumes of sediment imported (Consorzio Venezia Nuova, 1996). The most recent works to the lagoon have been the construction of three jetties at the tidal inlets (Lido, Malamocco, and Chioggia). The largest inlet, Lido, is an amalgamation of three

[i] www.salve.it

channels; Treporti, San Nicolò and Sant'Erasmo canal. Consequently, the current has been constricted, increasing its speed and ability to transport sandy sediments. The hydrodynamics within the inlet have gradually altered as the channel adjusted to find a new equilibrium. Although Tambroni and Seminara (2006a) and Fontolan *et al.* (2007) have studied Lido Inlet in terms of its cross-sectional area, the authors disagree on the status of its stability; Fontolan *et al.* (2007) believes Lido is stable, whereas Tambroni and Seminara (2006a) state that the inlet is prone to deposition; both authors use the relationship of O'Brien (1931). O'Brien studied North American tidal inlets to determine a relationship between the minimum cross-sectional area below mean sea level and the tidal prism (total volume of water entering and leaving during a tidal cycle). As the relationship has been found to be invalid elsewhere in the world (Hicks and Hume, 1996; Shigemura, 1981), it is important to investigate the relationships validity within the Adriatic, as well as that of other relationships to be found within the literature (Le Conte, 1905; Jarrett, 1976; Gao and Collins, 1994). By predicting equilibrium values it may be possible to predict rates of sediment accretion or scour and consequently it is an important management tool. If the same relationship can be proven to be valid along the whole length of the tidal canal (currently the cross-sectional area used is the smallest - the inlet mouth), volumes of sediment accretion and scour can be estimated.

The construction of the jetties has also changed the morphodynamical features of the inlet; prior to their construction, a large spit, formed through longshore transport, extended from Punta Sabbioni (Fontolan *et al.*, 2007) and an extensive flood tidal delta existed adjacent to the (then) barrier island of Sant'Erasmo (see Figure 3.1 for locations). An estimated 300,000 m^3 yr^{-1} of sediment entered the lagoon through the inlets at this time, with post-construction estimations falling between zero (Consorzio Venezia Nuova[ii]) and 50,000 m^3 yr^{-1} (Consorzio Venezia Nuova, 1996). It is important to determine whether or not sand is still being imported into the lagoon as sediment exchange through tidal inlets affects the inner-lagoonal morphology and sediment exchange (Tambroni and Seminara, 2006a). Also, if sand is being dredged from the inlets and canals it is important to ascertain whether it is derived from within the lagoon or outside it; either way, removal of sediment will affect areas further down the transport

[ii] www.salve.it

pathway and may cause further erosion, although sediment-starved areas benefit from dredge-spoil recycling for salt marsh restoration (providing bed stability for pioneer species for eventual entrapment of finer sediment particles).

To determine the provenance of the sediment within Lido Inlet, a high-resolution sediment sampling study has been carried out, with the samples analysed for their grain size and mineralogy. Comparisons between neighbouring samples (Gazzi *et al.*, 1973; Folk and Ward, 1957; Gao and Collins, 1992) will be described and conclusions drawn about the transport pathway and likely sources of the sediment. Although Venice Lagoon has already been widely studied in terms of sediment composition (Albani and Serandrei Barbero, 2001; Bonardi *et al.*, 2002; Umgiesser *et al.*, 2005; Sfriso *et al.*, 2005a), the spatial resolution of these studies is low. One or two samples currently characterise the sediment composition of Lido Inlet, which is hardly indicative of the processes and pathways of sand within the inlet. Therefore, this study is *sui generis* and will aim to represent the sediment composition, sources and sinks, and the transportation pathway within Lido Inlet and the wider sediment cell to which it belongs (longshore transport along the Venice Lagoon shoreline, tributary canals of Treporti and Burano and the nearshore region).

Few estimates of the total sediment budget of Venice Lagoon have been published,; estimates of sediment exchange are limited to a partial story (fluvial input of sediment - Suman *et al.*, 2005, average rates of sedimentation - Sfriso *et al.*, 2005a, modelled export within Treporti Canal - Umgiesser *et al.*, 2006). Sediment loss and accumulation can be determined through comparison of bathymetry and the differences between basins (north, central and south basins) and between canals and intertidal areas. It is difficult to quantify sediment exchange through the inlets via this method due to data limitations. In recent literature however, sediment exchange between the lagoon and sea has been monitored by continually-recording, fixed Acoustic Doppler Current Profilers (ADCP) at each inlet (Zaggia and Maurizio, 2005). Investigations into conversion of backscatter to suspended sediment has resulted in estimations of sediment export of approximately 60,600 m^3 yr^{-1} (Tambroni and Seminara, 2006b) compared to previous estimates of 400,000 m^3 yr^{-1} (Ravera, 2000). As the ADCP is fixed to record data from approximately two metres above the seabed, it is nec-

essary to determine the volume of sediment in transport below this level, including sand transported as bedload. Thus far, the estimates of sediment in suspension have been volumetric, with few attempts to differentiate the mass of sand and fines exported.

This thesis aims to investigate the exchange of sand between the lagoon and the Adriatic Sea through the tidal Inlet of Lido. Within the context of this study, the following questions will be addressed:

- What is the provenance of the sand in Lido Inlet (Albani and Serandrei Barbero, 2001; Bondesan *et al.*, 2004) and what are the characteristics of its transport?
- Is the inlet stable in terms of its cross-sectional area and its relationship with the tidal prism and how does this relationship affect the transport of sediment within the inlet?
- What are the volumes of sand transported through Lido Inlet and has this changed since jetty construction?

1.1 Thesis Overview

This thesis is a study of the dynamics and origins of sand in northern Venice Lagoon, with an emphasis on transport through tidal inlets. It forms part of activities defined within CO.RI.LA's Programma di Ricerca 2003-2006 (Allegato A, linea 3.15), to determine non-cohesive sediment exchange between the lagoon and sea.

- Chapter 4 describes the collection of high-resolution bathymetry and sidescan sonar data of the study area and subsequent analysis of the revealed morphology (U.S. Army Corps of Engineers, 1998, 2002). Stability of the channel cross-sectional area, based on the method first described by O'Brien (1931, 1969), is also investigated within this chapter using tidal prism estimated calculated from discharge data modelled using SHYFEM (Umgiesser, 1997; Umgiesser *et al.*, 2004a, 2006) and bathymetry datasets collected in 1930, 1970, 1990, and 2000.
- 235 bottom sediment samples were collected within the study area, and at possible sources of sand (along the beaches bordering Venice Lagoon and the major

regional rivers to the north and south). Statistical analysis of these samples is described within Chapter 5, and grain-trend analysis has been applied to qualitatively illustrate the sand transport pathways within the inlet (Gao and Collins, 1992).

- A quantitative assessment of sediment in transport within the inlet is investigated in Chapter 6, evaluating the conversion of Acoustic Doppler Current Profiler (ADCP) backscatter data into estimates of suspended sediment concentrations (both sand and fine-grained particles). The chapter will also use ADCP velocity measurements to estimate bedload transport using equations outlined in Soulsby (1997).

- Chapter 7 will analyse the lagoon-wide bathymetry datasets of 1930, 1970, and 2000 to determine areas of net erosion, net deposition and areas of stability. The volume of sediment change will be calculated and an overall sediment budget discussed.

- The final chapter will summarize and conclude the findings of the preceding chapters, with a discussion in terms of the aims and objectives outlined within this current chapter.

2

Background and Theory

2.1 Coastal Lagoons and Tidal Inlets

Coastal lagoons account for 13% of the coastal zone worldwide (Cohen *et al.*, 1997), and are found predominantly along low-lying plains that have been subject to submergence within their recent geological history (Kirk and Lauder, 2000). Lagoons are important as a unique habitat for plants, animals, birds and fish, some of which are commercially exploited, e.g. fish farms. Lagoons provide relatively warm, sheltered and nutrient-rich water for 'nurseries' for commercially important fish such as salmon, trout and shellfish. Lagoons are also economically important for shipping and recreational boat use (tourism) as they act as natural harbours providing shelter. It has been estimated that tidal estuaries, tidal marshes and wetlands have an average economic value of \$1.58 per m^2 $year^{-1}$ (\$2.28, \$0.99 and \$1.48 per m^2 $year^{-1}$ relatively) compared with an average value of less than \$0.02 of arable/pasture land (Costanza *et al.*, 1997). It is therefore of great economic and environmental importance to retain the lagoonal ecosystem through an understanding of the unsteady equilibrium the lagoon maintains during its existence. The system is self-regulating with negative feedback loops maintaining the equilibrium during natural changes such as sea level rise and subsidence. The mobility and dynamics of this system are incompatible with the

permanent boundaries maintained by man and so control of the lagoonal environment becomes increasingly difficult as equilibriums are sought.

2.2 The Lagoon System

2.2.1 Definitions and Categories

A lagoon is defined by Kjerfve (1994) as:

'a shallow coastal water body separated from the ocean by a barrier, connected at least intermittently to the ocean by one or more restricted inlets, and usually orientated shore-parallel.'

Kjerfve further subdivided this definition depending on the limits of water exchange between the lagoon and sea, reflecting the forcing (wave or current dominance) and the time-scale of hydrologic variability (see Figure 2.1):

Choked lagoons have a single, narrow inlet along wave dominated coastlines with significant long-shore transport. The single channel serves as a 'dynamic filter' and restricts tidal oscillations and currents within the lagoon.

Restricted lagoons are large and generally shore-parallel with two or more tidal inlets. They have a well defined tidal circulation and are well-mixed due to wind effects and short residence times, although salinity ranges from brackish to oceanic.

Leaky lagoons are elongated, tidally dominated shore-parallel water bodies with numerous wide inlets, characterised by unimpaired water exchange between the lagoon and sea.

2.2.2 Evolution of Lagoons

Lagoons are predominantly formed during eustatic sea level rise (less so during sea level fall - Dyer, 1997) in low-lying coastal plains. The most recent period of eustacy, the Flandrian Transgression, began 18,000 years BP as glacial ice sheets melted, raising global sea levels an estimated 100 metres over a period of 15,000 years (Graham *et al.*,

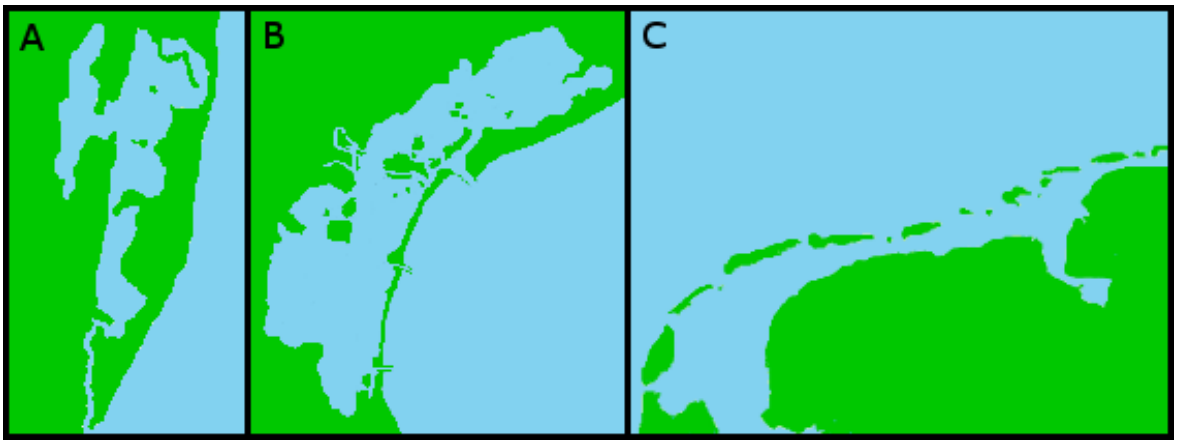

Fig. 2.1: Lagoon types: **A.** Choked lagoon (St. Lucia Lake, S. Africa). **B.** Restricted lagoon (Venice Lagoon, Italy). **C.** Leaky lagoon (Wadden Sea, Netherlands).

2003). Most modern lagoons were formed as the eustacy rate slowed to levels less than 1 m per century (Woodroffe, 2002) when sea level reached current levels between 6,000 to 3,000 years ago. A plentiful supply of sand is required to form barrier islands, eventually separating the lagoon from the open sea and forming intertidal marshes. The wave climate must also be sufficient to transport this sand and shape the barrier islands (Kirk and Lauder, 2000). It is not known for certain how barrier islands form; one long-held theory hypothesized by Gilbert (1885) is that longshore transport of sediment forms long spits where the coast 'indents' (Figure 2.2A). The spits become breached during storms to form tidal inlets and barrier islands (Figure 2.2B).

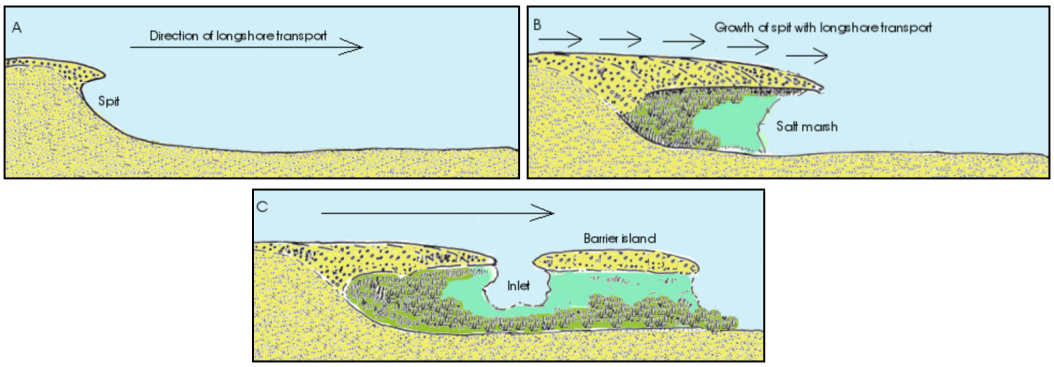

Fig. 2.2: Formation of barrier islands due to spit breach after Gilbert (1885).

This type of barrier island formation has been recently witnessed in locations such as Cape Cod (U.S. Army Corps of Engineers, 1998); however, work by Hoyt (1967) suggested that this can only be the case in small coastal sections with a plentiful sediment supply, and cannot be responsible for the growth of large barrier islands. He also noted that the sand on some barrier islands did not match the corresponding landward beach sand and therefore must have been derived from an offshore source rather than longshore transport. Hoyt refined the theory originally formed by McGee (1890), that encroachment of the sea onto a 'beach-and-dune complex' (U.S. Army Corps of Engineers, 1998) floods the low-lying beach and marsh either side of the dune systems, with only the dunes remaining exposed. Waves and currents are then responsible for shaping and maintaining the new barrier island. However, if the tidal range of the area is above 4 m (macrotidal), then it is unlikely that the island will remain (Hayes, 1965, cited by Martin and Dominguez, 1994) because of reduced localisation of breaking waves as a sand deposition mechanism.

The tidal range affects the shape and size of the barrier islands; a mesotidal coast will be more conducive to leaky lagoons, with shorter barrier islands and numerous inlets; a microtidal coast will have more restricted lagoons with long, slender barrier islands with few tidal inlets and less well developed tidal deltas (Kjerfve, 1994; Hayes, 1979). Choked lagoons are similar, but the barrier island accumulation of sand is more intense, resulting in fewer tidal inlets remaining. It is possible for the lagoons to lose all tidal inlets and become completely isolated from the sea, as occurred with the choked-lagoon, Lake Sibaya (the neighbour of the choked lagoon example in Figure 2.1) in South Africa, 5,000 BP (Wright *et al.*, 2000). These choked lagoons are also present in areas of coastal retreat, such as along South Island, New Zealand, but tend to regress inland with the erosion, rather than become marine (Kirk and Lauder, 2000). Tidal inlets tend to form as a breach in a barrier island during storm events. Most breaches silt up due to the continuation of longshore transport, but some are maintained (if flow speeds continue to exceed sediment suspension thresholds) and become permanent tidal inlets (Woodroffe, 2002; Hayes, 1979).

There are two types of barrier island; transgressive, which gradually move landwards due to limited sand supply and are susceptible to sea-level rise, and regressive

barrier islands, which are progradational with a plentiful sediment supply (Woodroffe, 2002).

Lagoons are by nature a geologically temporary feature on a dynamic coast with tendencies towards marine or land amalgamation (Consorzio Venezia Nuova, 1997; Ravera, 2000). A lagoon will only maintain an uneasy stability if sedimentation and erosion are equal. However, if fluvial and marine sedimentation exceeds subsidence and erosion, then the lagoon will silt up and become *terra firma*. This has occurred to the ancient Ravenna Lagoon (on the Adriatic coast just south of Venice). Like Venice, Ravenna was built on a lagoon, but due to siltation, the city is now 10 km from the coast (Keahey, 2002). If the volume of sedimentation is not sufficient to overcome erosion then the lagoonal barriers will be eroded away and the area will become fully marine.

Infilling of a lagoon will not be constant due to negative feedback cycles changing the dominance of tidal currents. The longevity of the flood tide is related to the strength of ebb currents, thus a long flood phase is due to strong ebb currents; a short flood phase is due to weak ebb currents. The difference is due to the balance of the tidal range (R) to inlet water depth (h) ratio identified by Speer and Aubrey (1985) and the area of intertidal basin (A_i) to total basin area (A). A large R/h ratio usually signifies flood dominance; a large A_i/A signifies ebb dominance (Crossland *et al.*, 2005). Flood dominance, and thus sediment import, is more probable for recent basins, but as the intertidal area increases, and scour deepens the inlet, the lagoon will become ebb dominant as it evolves, and less sediment is imported (negative feedback)(Crossland *et al.*, 2005).

2.2.3 Lagoon Morphology

Lagoons are dependent on their geomorphology for balances of salinity, heat and water. This morphology is based on five categories: inlet configuration, lagoon size, orientation to prevailing winds, bathymetry and mean depth (Smith, 1994). Water exchange is controlled primarily by the dimensions and number of inlets and can be represented by the hydrologic equation (2.1). This describes the change in water volume, both fresh

and saline (Smith, 1994):

$$\frac{\Delta V_l}{\Delta t} = P_s - E + R_w + G \pm A_w \tag{2.1}$$

where ΔV_l is the total volume of the lagoon, Δt is time, P_s and E are spatially integrated precipitation and evaporation, R_w is runoff, G is groundwater seepage and A_w is the advective change in water volume. Water input into a lagoon is mainly tidally forced, but atmospheric pressure differences can push water into the lagoon. This can be wind driven, especially if the inlet is orientated with the prevailing wind, or through low pressure storm surges, increasing the sea level.

The principal morphological features of lagoons are found in association with tidal inlets as large volumes of sand are transported with the flood/ebb tide and deposited when current speed falls below critical threshold for suspension. Estimates of sand export can thus be determined through analysis of ebb-tidal delta volume and how this alters over time (Hicks and Hume, 1996).

2.2.4 Tidal Inlets

Tidal inlets may be a natural or artificial (such as Ancão Inlet in Portugal - Vila-Concejo *et al.*, 2003) conduits between a back-barrier basin and the sea (Fenster and Dolan, 1996). They provide a natural flushing mechanism to maintain water quality and nutrient availability within the back-basin, producing a unique habitat (Seabergh, 2003). They are hydrodynamically complex and will migrate to attain equilibrium depending on the wave climate, currents and surrounding geomorphology. This complexity makes current modelling techniques of sedimentation and erosion imprecise (U.S. Army Corps of Engineers, 2002). Inlets can be classified into three types: wave dominated, tide dominated and mixed energy (Hayes, 1979). Wave-dominated coasts tend to produce long, thin and highly mobile inlets (examples include Fire Island Inlet, NY, which migrated 6.4 km in 100 years, and Nauset Inlet, NY, which migrates 1.2 to 1.7 m yr^{-1} - Woods Hole Group, 2006), whereas tidal-dominated coasts form shorter, wider and more stable inlets. Tidal inlet stability has been shown to be linked with the tidal prism (the volume of water that enters and exits during a tidal cycle) and inlet cross-sectional area (O'Brien, 1931; Escoffier, 1940; Bruun, 1978; Hume and Her-

dendorf, 1988; Walton, 2004; Fontolan *et al.*, 2007); this is discussed further in relation to the study area in Chapter 4.

Circulation within inlets is primarily governed by tidal forcing although bay geometry, inlet geometry (Bertin *et al.*, 2004), the presence of jetties, bottom topography, and wind and river inflow all have a significant role. The tidal forcing is commonly asymmetrical in inlets; a factor that strongly affects the net sediment transport direction as the '*bias in peak velocity creates a difference in the amount of material being transported on flood and ebb tides*' (Fitzgerald, 1988). An ebb dominant inlet will flush sand to maintain an efficient inlet, whereas a flood dominant inlet will import sand.

2.2.5 Tidal Inlet Morphology

The morphology of a tidal inlet reflects the local sediment characteristics and hydrodynamics, and consequently can be used to determine the movement of sand (Seabergh, 2003); therefore information on the morphology and how it alters (morphodynamics) is useful in the management of an inlet. Figure 2.3 shows the morphology generally associated with tidal inlets as described by Hayes (1975). Tidal currents converge in the 'gorge' (throat) of the inlet, and travel along ebb or flood dominant channels before diverging once no longer restricted by the inlet. A bias in the peak flow can result in a difference between the volume of sediment transported in the flood and ebb tide effecting the morphology associated with either phase.

2.2.5.1 Ebb-Tidal Morphology

Ebb-tidal currents converging in the inlet are restricted, and therefore increase in velocity to form an 'ebb jet' (Joshi, 1982). Jettied inlets accelerate flow velocities due to deflection and constriction of currents flowing adjacent to the walls; thus causing scour along the jetty wall (Hughes, 1997). As the current is deflected into the centre of the channel, it decelerates and deposits some of its load. This continual erosion near the wall and deposition in the centre of the channel eventual moves the deep channel closer to the jetty wall . The proximity of the channel to the wall forms steep velocity gradients, causing turbulent eddies that initiate scour. This is particularly prevalent at the tips of the jetty walls, where turbulence increases as a result of flow convergence

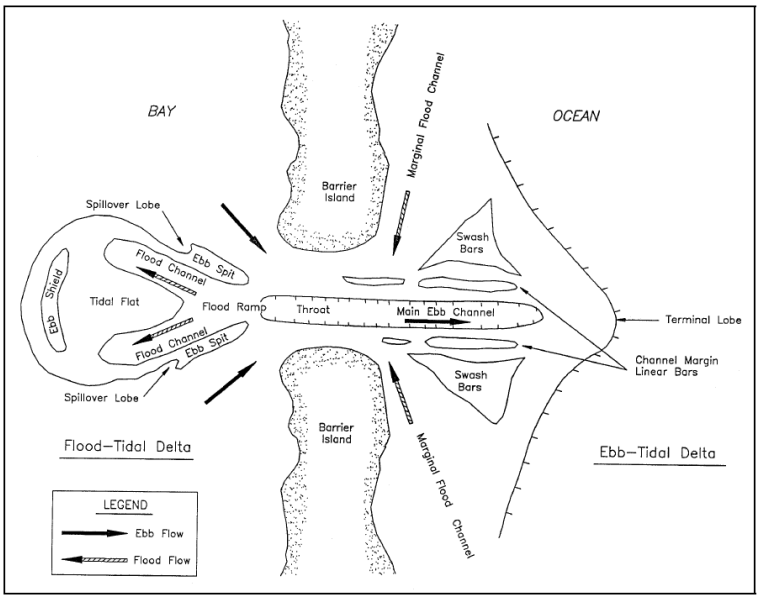

Fig. 2.3: Morphology associated with tidal inlets. From Hayes (1975); U.S. Army Corps of Engineers (2002)

between the ebb jet and wave-generated, shore-parallel currents (Mitello and Hughes, 2000). The channel is shouldered by parallel, channel margin linear bars shaped by wave and current interaction. Once the ebb jet is no longer restricted by the inlet it expands and decelerates, and coarser grains held in suspension deposit to form an ebb-tidal delta or shoal (Joshi, 1982). Most sediment is deposited before the terminal lobe (usually indicated by a straightening of contour-lines - Stauble, 1998). These sediments can then be reworked by wave activity to form swash bars. Towards the edge of the delta, these bars are dominated by wave-generated currents and migrate in the wave direction towards the shoreline, eventually helping to build up sandy barrier islands. Interaction between longshore currents and the ebb jet can cause asymmetry of the ebb tidal delta. Deposition of sediment on the downstream side of the inlet mouth orientates the tidal channels (outside of the inlet) upstream (van Leeuwen *et al.*, 2003). If longshore currents exceed the effects of the tidal current, then the ebb delta will be restricted in length seawards, however it will be skewed in the direction of longshore transport. Stronger tidal currents will elongate the delta shore normal (Oertel, 1988). Ebb tidal deltas are significant sources and sinks of sand and can effect sediment supply

to nearby beaches particularly if there are any changes in delta volume due to alterations in the tidal prism (Hicks and Hume, 1997; Oertel, 1988) such as those caused by jetty construction. Studies by Walton and Adams (1976) show that the size of an ebb tidal delta is directly related to the tidal prism of its inlet with variability caused by differences in wave climate (Fitzgerald, 1988).

2.2.5.2 Flood-Tidal Morphology

Inlets also restrict flood-tidal currents, keeping peak velocities at the centre of the inlet. Entrainment of sediment by this flood jet within the inlet decreases current velocity, causing it to spread and therefore weaken (when out of the influence of jetties). As the current weakens, it begins to deposit larger and/or heavier sediment grains to form a 'flood ramp' (all definitions after Hayes, 1975); this ramp further weakens the current, leading to the formation of a flood tidal delta (shoal) and an ebb shield. Daboll (1969) (in Davis, 1978) states that the ebb shield is generally composed of a larger grain size than the flood ramp; this is probably a function of wave activity (if the ebb shield is inter-tidal) removing all but the coarsest of grains (grain sorting). When the tide turns, the ebb current gradually strengthens and traction of the flood tidal delta sediments can occur, forming subaqueous ebb spits in the deeper water adjacent to the delta. Flood tidal deltas occur within micro- and meso-tidal environments ($<$ 1 to 4 m tidal range). Sand accumulating along the flood ramp is often maintained as sand waves, which slowly migrate to the top of the delta and may eventually form part of the ebb shield. This is the highest and oldest part on the flood tidal delta, and may be bio-stabilized. The ebb shield diverts ebb currents away from the flood delta reducing erosion. However, this diversion of the ebb current can form ebb spits on either side of the delta, which are also shaped by flood currents and storm activity. Breaches in the ebb spits or shield due to ebb currents are known as spill over lobes (U.S. Army Corps of Engineers, 2002).

2.2.5.3 Tidal Inlet Dynamics

Tidal currents are the predominant force acting on sediments at the inlet throat (the minimum cross-sectional area of an inlet), with wave effects increasing seaward towards the ebb-tidal delta, and alongshore, providing a potential sediment source to the inlet.

The mobility and large sediment supply to inlets make them unpredictable in terms of navigability and as a result, many be artificially restricted by jetty construction. By decreasing the cross-sectional area, the inlet becomes unstable and is forced to accommodate the tidal prism by scouring the seabed and increasing in depth. Tidal inlets are susceptible to scour when hydrodynamic bottom shear-stresses exceed the critical shear stress for sediment mobility (Hughes, 2003). This may be due to focussing of wave energy by structures, localised increases in wave orbital velocities, acceleration or separation of flow, or changes in bed type from resistive to erodible. Scour at jetty tips is caused by flow separation from turbulent eddies formed during a flood tide. The scour is maintained by the ebb jet, which restricted by the jetty walls, forms a fast, non-rotational, steady flow.

Wave climate affects the size of tidal deltas, with wave-dominated coasts tending to support larger ebb deltas, but smaller flood deltas. Lagoons with no tidal flats or high tidal marshes are more likely to have flood dominant tidal inlets; however, as the surface slope increases with sedimentation (thus development of tidal flats), ebb dominance will prevail (Mota Oliveira, 1970).

2.2.6 Inner Lagoonal Processes and Morphology

The inner-lagoonal canal system is a network of tidal creeks cut within intertidal marshes. They are major sinks of sediment in low-energy areas and thus are important in the lagoon sediment cycle. Salt marshes originate as mudflats, which, under an increase in sediment supply (U.S. Army Corps of Engineers, 2002, Allen, 2000, see Marani *et al.*, 2006), stabilize with an initial colonization of microphytobenthos and pioneer halophytic plants such as *Spartina maritima, Juncus* spp. (Marani *et al.*, 2006). These plants help to attenuate wave energy and impede tidal-currents, trapping sediment in the process. This sediment is generally finer (fine sand to clayey silt - Packham and Willis, 1996) and better sorted than other intertidal areas (U.S. Army Corps of Engineers, 2002), but accumulates slowly. If subsidence exceeds sediment supply and accretion, then environmental stress on the halophytes increases (too much salt, water inundation), which kills them, resulting in sediment loss and flattening of the marsh surface (Meijer, 2005) with the sediment infilling the inner-lagoon canals

(Ravera, 2000).

Scour can occur when the current flow of two canals combine. The resulting confluence scour holes are usually associated with separation zone bars that form adjacently due to flow separation. This low velocity region is a sink for tributary channel sediment (Best, 1988; Bristow *et al.*, 1993), whilst little erosion or deposition occurs in the maintained scour hole. Scour holes are formed from erosion of the bed due to '*high turbulence along the combined flow shear layer and greatly increased velocities along the confluence*' and are maintained due to the lack of sediment that travels through the scour hole (Best, 1988). The scour hole orientation is a product of the channel discharge ratio (between the main and tributary flow - $Q_r = Q_t/Q_m$), aligning increasingly with the tributary flow, and becoming deeper with an increase in confluence angle (Bristow *et al.*, 1993) - see Figure 2.4. The scour depth is a function of total discharge

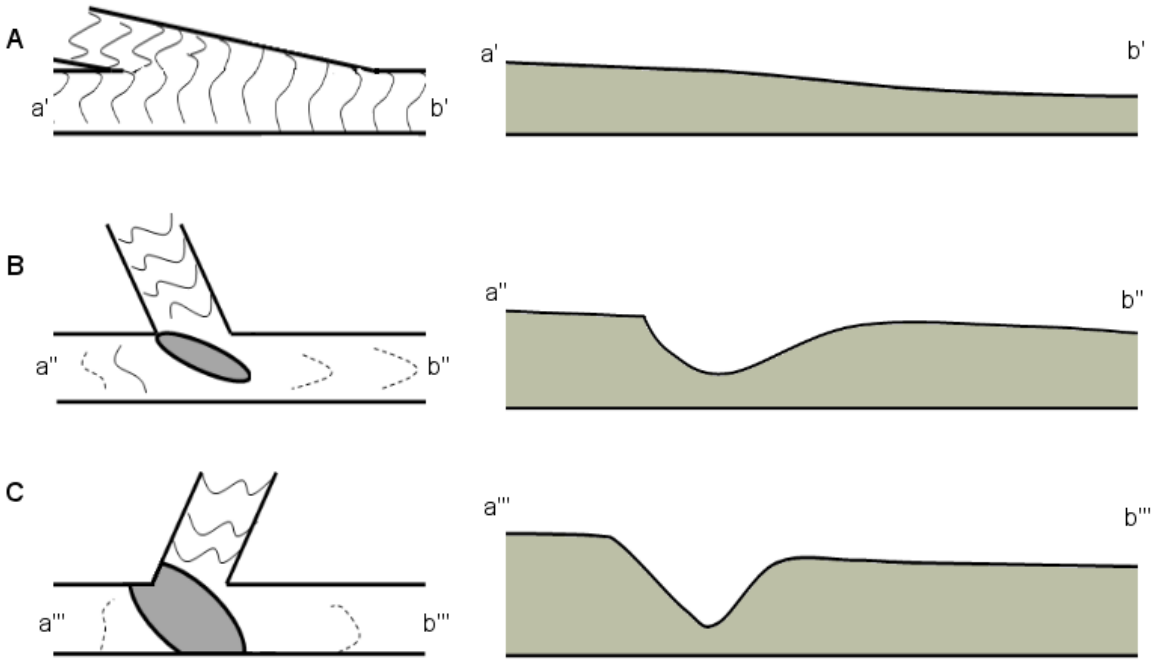

Fig. 2.4: Scour hole orientation and depth after Best (1988), with total discharge equal to unity. A: shallow angle (15°) confluence with no confluence scour produced. B: 70° confluence angle. C: 105° confluence angle. Cross sections are taken from a to b.

and confluence angle as described by the equation for fine sand (Klassen and Vermeer,

1988 cited in Melville and Coleman, 2000):

$$\frac{y_{cs}}{\overline{y}} = 1.29 + 0.037\theta_c \tag{2.2}$$

where y_{cs} is the maximum water depth, $\overline{y}$ is mean flow depth, and θ_c is confluence angle[i]. Thus the scour depth increases with the confluence angle. The depth is further exaggerated with an increase in mean grain size (sands and gravels; $y_{cs}/\overline{y} = 2.24 + 0.031\theta$, cohesive muds; $y_{cs}/\overline{y} = 1.01 + 0.030\theta$ - Melville and Coleman, 2000).

2.2.7 Outer Lagoonal Processes

Longshore transport (also called littoral drift) describes the sediment transported parallel to shore. Waves and their associated sediment load, approach the shore at an oblique angle, and retreat at a 90° angle, causing sand particles to move gradually along the beach. Net drift of sediment may conceal volumes moving in the opposite direction, with changes in total transport affected by annual meteorological conditions such as storm events, which may move a large volume of sediment in a different direction to the general trend in calm conditions (Stauble and Morang, 1992). The morphology of the coast can indicate longshore transport direction. However, it can also affect transport due to changes in the way waves are refracted along the shore (from the presence of headlands, river mouths and inlets for example). Changes in longshore transport direction define boundaries of a coastal cell; 'areas of coast where no inflow or outflow of sediment occurs' (Smith and Sayao, 1989). Estimates of longshore transport rates in volume per unit time (Q_l) can be found by the CERC equation (U.S. Army Corps of Engineers, 2002; Bayram *et al.*, 2007):

$$Q_l = \frac{\rho\kappa\sqrt{g/\gamma_b}}{16\left(\rho_s - \rho\right)\left(1 - a\right)} H_{sb}^{2.5} \sin\left(2\theta_b\right) \tag{2.3}$$

where γ is the breaker index (0.78), ρ and ρ_s are the densities of water and sediment, a is the porosity index ($\cong 0.4$), g is acceleration due to gravity, H_{sb} is the significant wave breaking height, θ_b is the wave breaking angle and K_l is an empirical co-efficient taken to be approximately 0.32-0.39 (Wang *et al.*, 2002). This equation is thought to

[i]This equation was originally formulated for braided rivers

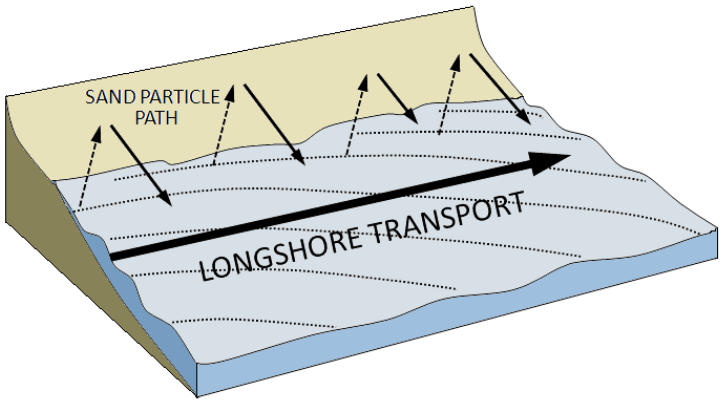

Fig. 2.5: Longshore transport. Waves travelling obliquely to shore, transports sediment onto the beach. It is then transported perpendicularly back down the beach face with backwash, gradually moving along the coast.

be 30-50% accurate, although subsequent equations are generally unable to replicate field results (Wang *et al.*, 2002) despite inclusion of a wider range of factors such as breaker type, beach slope and grain size. An increase in the median grain size has been shown to result in a decrease in longshore transport rates (King, 2005), although it is not represented in the original CERC formula (Equation 2.3). Similarly, Vanoni (1975) has shown viscosity to affect sediment transport in rivers, leading Rosati (1985) to conclude that longshore transport must also be susceptible to changes in water temperature (affecting viscosity).

2.2.8 Sediment transport in tidal inlets

Littoral sand is transported into tidal inlet systems through wave action and by tidal currents, although some sediment is transported offshore by rip currents. Tidal current flow through tidal inlets interrupts longshore transport driven by waves, affecting the sediment supply to downdrift beaches (Fitzgerald, 1982; Balouin and Howa, 2002). Wave action updrift of the inlet will either transport sand into the inlet, or it will bypass the inlet and continue longshore transport. There are three methods of inlet bypassing as described by Bruun and Gerritsen (1959) and Davis and Fitzgerald (2004) and shown in Figure 2.6. These include:

stable inlet processes, where the inlet does not migrate. Sand import to the inlet occurs due to longshore transport, tide and wave currents passing thorough flood channels and through wave breaking over ebb-delta bars. The sand is then removed from the inlet by ebb currents, subsequently forming part of the ebb delta. Wave activity over the delta lobe forms swash bars, which migrate slowly towards the shore to be transported by longshore drift (Figure 2.6A).

ebb-tidal delta breaching occurs within stable inlets with migrating ebb channels (Figure 2.6B). Sand is imported into the inlet but instead of forming bar complexes, it accumulates on the updrift portion of the delta, forcing the ebb channel to migrate towards the downdrift shore. This reduces the tidal flow, and eventually a new, more efficient channel is breached, leaving the accumulated sand now downdrift of the channel. The sand is then able to form bar complexes and migrate towards the shore and continue on the longshore transport pathway. An example of this process is found in Willapa Bay Inlet (Davis and Fitzgerald, 2004), which undergoes a 16 year cycle of delta breaching and channel migration. It is thought that El Niño is a driver for this cycle, increasing the tidal prism and current speed enabling a new channel to be cut.

inlet migration caused by spit formation due to dominant longshore transport processes (Figure 2.6C). The spits are liable to breaching due to water level differences either side of the spit, forming new inlets. The sand of the previous inlet system moves onshore due to wave action. In jettied inlets, sand may also bypass by passing through porous jetty walls (U.S. Army Corps of Engineers, 2002).

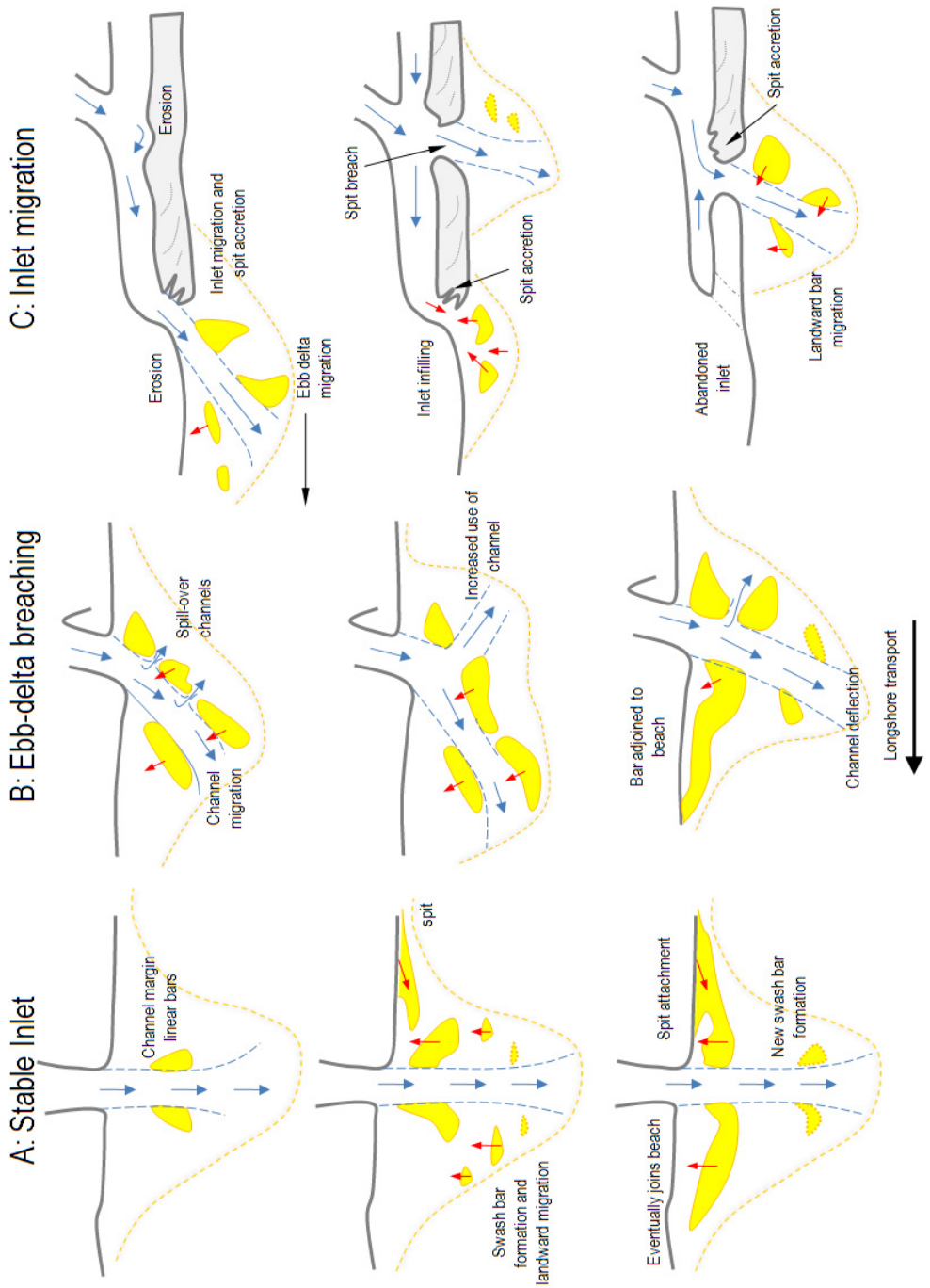

Fig. 2.6: Sediment pathways near tidal inlets showing: (A) stable inlet bypassing, (B) ebb-delta breaching, and (C) inlet migration. After Fitzgerald *et al.* (2000)

Sand will accumulate around the tidal inlet in either the ebb or flood tidal-delta (and to a lesser extent, ebb spits and sand bars), which affect the local wave climate. The morphology of these deltas is related to the balance between longshore currents and tidal currents (Oertel, 1988; Komar, 1996; van Leeuwen *et al.*, 2003). An increase in the tidal prism results in an increase in the volume of the ebb delta (Walton and Adams, 1976) and a corresponding decrease in the inlet width:depth ratio, which reduces wave energy, allowing the ebb delta to move further seawards (Hicks and Hume, 1996). Ebb deltas are important in the exchange of water and sediment between the sea and back-barrier basin (Fenster and Dolan, 1996; van Leeuwen *et al.*, 2003). Bedforms and sediment characteristics of ebb-tidal deltas have been described by Krüger and Healy (2006) during a study of a New Zealand inlet. They found coarse sand limited to wave-influenced, outer swash bars, with medium sand deposited in a central fan shape and modelled into small dunes, controlled by the ebb-jet. Fine sand was found in all the other areas of the delta, exhibiting both wave and current generated bedforms.

Variation in hydrodynamics due to storms and other low pressure wind events such as the Mediterranean bora winds, which can cause surges of over a metre (Keijzer and Bobovic, 1999). This has a great impact on sediment transport in the tidal inlet vicinity, causing sediment to accumulate in some areas (an annual accumulation of 15,000 m^3 occurs at the end of the northern jetty of Lido Inlet, Venice, mainly due to Sirocco wind events- Consorzio Venezia Nuova, 1997), or erode (Currumbin Creek, Australia - Castelle *et al.*, 2006). To determine the effect of the inlet on longshore transport, the following has been formulated (Bruun and Gerritsen, 1959 cited in Castelle *et al.*, 2006),:

$$r = \frac{P}{M_{tot}} \tag{2.4}$$

where P is the tidal prism (m^3) and M_{tot} is total annual littoral drift (m^3). The r values define types of inlet, with $r > 150$ describing a tidal-dominated inlet, with stable, deep channels. These inlets tend to be poor ebb-delta bypassers, whereas inlets with smaller r values tend to be increasingly wave-dominated and unstable, but bypass sand well through the ebb-delta (Carr and Kraus, 2001; Castelle *et al.*, 2006).

2.3 Fluid and Sediment Dynamic Theory

Quantifying and describing sediment transport is important in coastal system management for navigational dredging, coastal protection (beach nourishment, coastal erosion) and habitat protection (maintenance of salt marshes, dune systems, pollutant tracing).

Sediment transport is controlled by fluid flow, produced by tidal forcing or waves (wind-produced or boat wake). A fluid moving past a solid body (seabed) is retarded by frictional drag caused by a pressure differential, reducing its momentum and producing shear stress. This frictional drag (F_D) is defined as:

$$F_D = C_D A_n \frac{\rho u^2}{2} \tag{2.5}$$

where C_D is a drag coefficient, A_n is the area of the body normal to the flow, ρ is the fluid density, and u is horizontal velocity. In simple terms, the drag force of a body is approximately proportional to the square of the velocity as long as turbulent flow is created. As C_D is dependent on, amongst others, bed roughness (Z_0) it is usually evaluated by experimentation (Dyer, 1986; Soulsby, 1997; Thompson, 2003). Moving away from the bed, frictional drag and shear stresses reduce and momentum increases to free-stream velocities. The fluid layer affected by shear stress friction between the flow and a solid body is known as the boundary layer. The fluid next to the solid is constrained by a 'no-slip' condition, which dictates that the fluid velocity goes to zero at the boundary (Schlichting and Gersten, 1999). Moving away from this solid body, eddy viscosity falls and velocity increases parabolically until it reaches 99% of the freestream velocity at the edge of the boundary layer (Heathershaw, 1988). The thickness of the boundary layer reflects the amount of momentum delivered to the bed, which has implications on sediment transport as the ability of a flow to transport sediment is a function of bed shear-stress (Nielsen, 1992). Thin boundary layers, such as those created in wave-dominated environments, create greater shear stresses as the velocity gradient in the boundary layer (defining bed shear-stress) remains large, causing sediment resuspension as velocities are high closer to the seabed (see Figure 2.7). Due to the oscillatory nature of waves, wave-entrained sediment is transported away by currents. Thicker boundary layers associated with tidal currents have smaller velocity

gradients and thus apply smaller shear stresses to the bed resulting in less resuspension. Boundary layer flow can either be laminar or turbulent (see Figure 2.8). Laminar

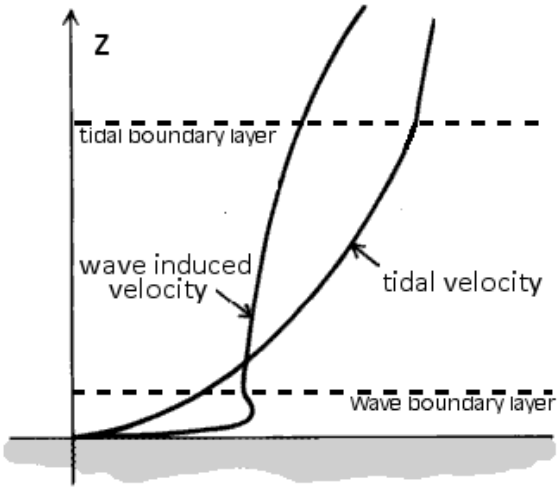

Fig. 2.7: Velocity profile under tidal currents and waves.

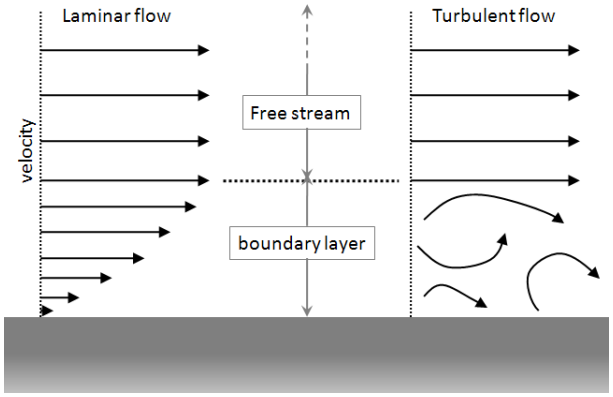

Fig. 2.8: Boundary layer in laminar and turbulent flow conditions.

flow generally occurs at lower velocities (depending on Reynolds number) with any induced disturbance controlled by fluid viscosity. It is not as conducive to sediment transport as turbulent flow, which occurs when velocities increase, and inertial forces exceed viscous forces to cause turbulent mixing (Thompson, 2003). Most natural flows

are turbulent with boundary layer forces controlling sediment transport above critical shear-stress. Bed-shear stress is the frictional force exerted by the flow per unit area of the bed ($\tau_0 = \tau_{0s} + \tau_{0f}$) and is contributed to by τ_{0s}, the skin friction component (which will be the total contribution to bed shear stress in a flat bed case), and τ_{0f}, the form drag produced by pressure differences over rough beds. This threshold of motion is defined by Soulsby (1997):

$$\overline{U}_{cr} = 7\frac{h}{d_{50}}^{1/7}[g(s-1)d_{50}f(D_*)]^{1/2} \tag{2.6a}$$

where:

$$f(D_*) = \frac{0.30}{1+1.2D_*} + 0.055[1-\exp(-0.020D_*)] \tag{2.6b}$$

$$D_* = \left[\frac{g(s-1)}{v^2}\right]^{1/3} d_{50} \tag{2.6c}$$

where D_* is the dimensionless grain size, s is the ratio of sediment and water densities (ρ_s/ρ), v is the kinematic viscosity, and h is water depth. Once this critical threshold is exceeded, transport occurs as bedload or as suspension depending on grain size, shape and flow speed. The sediment transport rate is generally proportional to the third or fourth power of either current velocity or wave height (HR Wallingford, 2002).

A grain will fall through a column of water at terminal velocity (gravitational force - F_G). This velocity is the result of a balance between the weight of the immersed grain and drag forces imposed on it by the water (see Figure 2.9). This immersed weight is determined by the difference in the lift forces of drag from the surrounding fluid and buoyancy, and gravity (Komar and Reimers, 1978). This is defined by:

$$F_G = \frac{1}{6}\pi D^3(\rho_s - \rho)g \tag{2.7}$$

This equation can then be balanced with the fluid drag (F_D) applied to a grain (Equation 2.8) to determine the settling velocity (w_s) when the buoyant and frictional drag forces equal gravitational forces:

$$F_D = C_D A\frac{\rho w_s^2}{2} \tag{2.8}$$

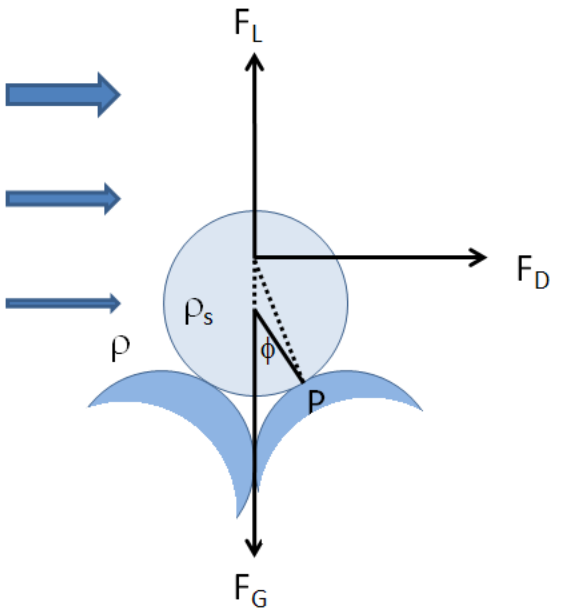

Fig. 2.9: The forces affecting a static grain at the threshold of movement. If the friction angle (ϕ) is overcome then the grain will roll out of its current position. ρ is water density, ρ_s, is particle density, F_L, F_D, and F_G are the respective forces of lift, fluid drag and gravitational attraction.

$$w_s = \left[\frac{4}{3}\frac{1}{C_D}\frac{(\rho_s - \rho)}{\rho}gD\right]^{\frac{1}{2}} \tag{2.9}$$

where C_D is the drag coefficient, a dimensionless quantity to describe the level of drag applied to an object:

$$C_D = \frac{4}{3}\frac{(\rho_s - \rho)}{\rho w_s^2}gD \tag{2.10}$$

The drag coefficient is related to the Reynolds number (R_e), which is the ratio between inertial forces and viscous forces (Reynolds, 1883 as cited in Bridge, 2003). Laminar flow occurs when viscous forces exceed inertial forces ($R_e < 1$), known as the 'Stokes range', where Stokes law of viscous drag can be applied (normally to grains smaller than 63 μm; $C_D = \frac{24}{R_e}$). Laminar flow separation occurs in the boundary layer when 1 $> R_e <$ 1000, leaving a turbulent wake (domination of fluid drag over viscous drag). $R_e >$ 1000 describes a state of total form drag with the generation of a turbulent boundary layer and wake region. At Reynolds numbers over 1, the settling velocity or

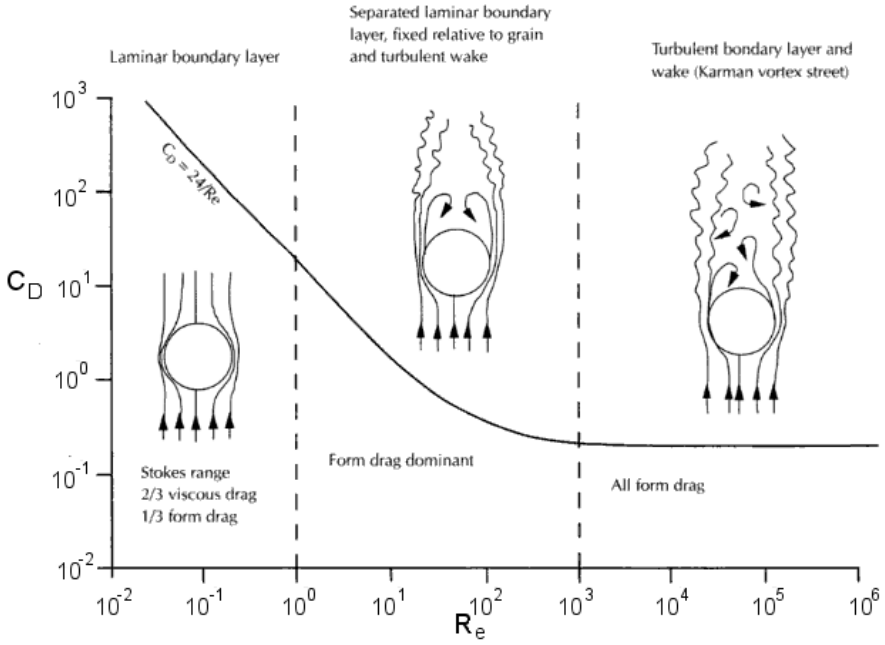

Fig. 2.10: Drag coefficient against Reynolds number for a single spherical grain in still water conditions (modified after Bridge, 2003.)

w_s of a grain can be determined by its size, shape and density, as well as the viscosity of the settling medium (Soulsby, 1997). w_s of sand can be calculated by Soulsby's settling formula (Soulsby, 1997, Chp 8), which is based on the dimensionless grain size D_*:

$$D_* = \left[\frac{g\,(s-1)}{v^2}\right]^{\frac{1}{3}} d \tag{2.11}$$

where v is the kinematic viscosity of water, d is the median sieve diameter of the grains and s is ρ_s/ρ_w. Soulsby's formula is:

$$W_s = \frac{v}{d}\left[\left(10.36^2 + 1.049D_*^3\right)^{\frac{1}{2}} - 10.36\right] \tag{2.12}$$

According to this formula, very coarse quartz sand will settle at a rate of 20 cm s^{-1} whilst very fine quartz sand will settle at 0.4 cm s^{-1} (freshwater at 20°C - see Figure 2.11). 90% of the results of this formula are within 20% of the actual settling rate (Soulsby, 1997).

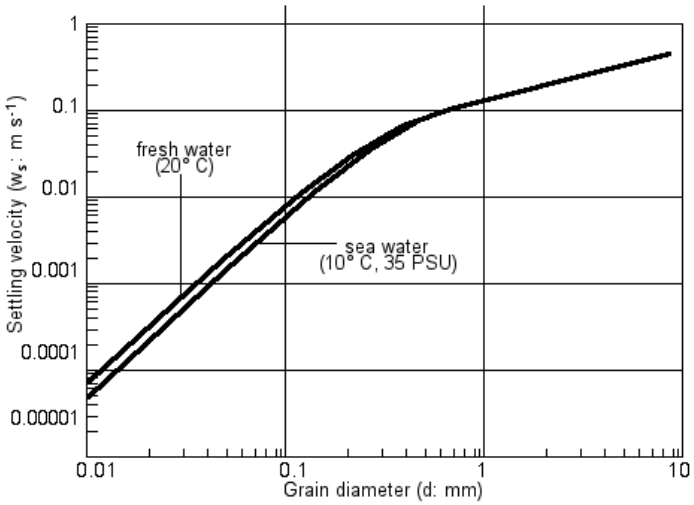

Fig. 2.11: Settling velocities calculated by Equation 2.12 for a quartz grain (ρ_s = 2650 kg m^{-3}.)

Sand grains increase bed roughness, and thus alter the flow of a current due to deflection. This distortion causes flow acceleration and a corresponding decrease in pressure vertically across the grain defined by Bernouilli's equation:

$$\rho g h + p + \rho \frac{U^2}{2} = constant \tag{2.13}$$

where g is acceleration due to gravity, h is the height of the fluid, and p is the pressure along the streamline. A decrease in this pressure difference across the grain causes lift as velocity increases. This force can be defined as:

$$F_L = \frac{1}{2} \rho C_L A_n U^2 \tag{2.14}$$

where C_L is the lift coefficient. This force is increased by backspin (spinning opposite to velocity gradient), which reduces the pressure difference due to faster (relatively) fluid velocities. The force is however, reduced to zero within one grain diameter of the bed (Bagnold, 1974; Dyer, 1986). For grain transport to occur, the forces of F_L and F_D must be sufficient enough to overcome F_G (see Figure 2.9). The moment of lift is

known as the *threshold of motion* and occurs at a *critical velocity*. The depth-averaged critical velocity ($\overline{U}_{cr}$) for a non-cohesive sediment of $D_* > 0.1$ can be calculated as;

$$\overline{U}_{cr} = 7\left(\frac{h}{d_{50}}\right)^{\frac{1}{7}}\left[g\left(s-1\right)d_{50}f(D_*)\right]^{\frac{1}{2}} \tag{2.15}$$

where

$$f(D_*) = \frac{0.3}{1+1.2D_*} + 0.055[1-exp(-0.02D_*)], \tag{2.16}$$

and s is the ratio ρ_s/ρ_w and v is the kinematic viscosity of water (Soulsby, 1997). This results in a $\overline{U}_{cr}$ of 0.28 m s^{-1} for a mean grain size of 1 mm in 10 m of water. The threshold of motion can also be defined in terms of bed shear stress (τ_0). It is also described by the Shield's Parameter (θ) which is a dimensionless form of the bed shear stress directly related to the sediment grain size (Soulsby, 1997). It is defined as:

$$\theta = \frac{\tau_0}{g(\rho_s-\rho)d} \tag{2.17}$$

To find the threshold Shields parameter (θ_{cr}), τ_0 can be replaced with the critical bed shear stress (τ_{cr}) to calculate the threshold of movement According to these formulas, a quartz grain with a 1 mm diameter could be expected to move when bed shear stresses exceed 0.45 Nm^{-2}.

Once the threshold of motion has been reached, a sediment grain will be transported in suspension or as bedload by rolling or saltation, all of which influences the degree of sediment sorting.

Bedload transport begins above the threshold of motion with some grains beginning to roll upon exceeding the critical friction angle ϕ (see Figure 2.9). Stronger currents cause saltation, where lift and drag exceed gravity momentarily and cause the grain to lift into the flow at an angle of 50° before returning to the bed within two to four grain diameters above the seabed (Francis, 1973 in Dyer, 1986). Saltation sorts sediment according to shape with angular grains moving slower than more rounded grains (Dyer, 1986).

When the threshold of movement is exceeded, sediment starts to be transported as bedload (rolling or saltation) or suspension. The transport of sediment in suspension is controlled by the transfer of momentum from the water column to the particle, so the concentration of sediment in suspension is controlled primarily by the amount of energy present in the water, which is usually provided by tidal/river currents or through waves. The ability of a flow to transport a sediment is influenced by the shear stresses it induces at the bed, thus waves will suspend greater volumes of sediment than tidal currents. Even if tidal velocities are greater than wave-induced velocities (Figure 2.7), wave-generated shear stress will still be the controlling factor in sediment motion (Nielsen, 1992). Suspension occurs once the settling velocity of a grain is less or equal to the vertical component of turbulent velocity (Dyer, 1986) and so is more likely to occur with finer-grained material. Greater volumes are transported as suspension than as bedload (Soulsby, 1997).

The proportions of sediment transported as suspension or bedload are controlled by the ratio between the ambient friction velocity (u_*) and threshold friction velocity (u_{*c}) (see Figure 2.12). Transport begins near the threshold of movement, with exposed

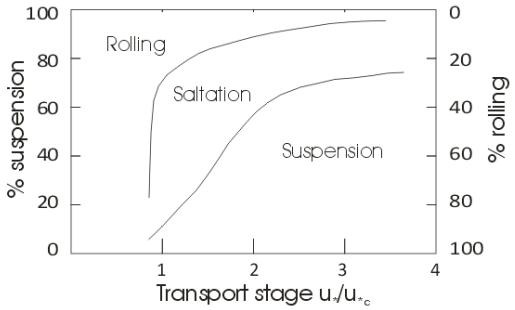

Fig. 2.12: The proportion of sediment transported as rolling, saltation, and suspension as a function of velocity. From Dyer (1986)

grains rolling until they reach a stable position. A further increase in velocity at transport stage 1 (Figure 2.12) causes momentary lift of grains, moving them at an angle of 50° (Dyer, 1986) before they return to the bed at a concave projection. When $u_* \approx W_s$, the trajectory of the grains becomes higher and longer, with a wavy path of suspension, although if the grain comes within two or three diameters of the seabed,

settling is likely before commencement of another saltation or suspension event. The transport stage is affected by the grain size, although authors disagree on exactly how to relate grain size to suspended transport; Ackers and White (1973) argued that the d_{35} for the bed grain size of a river gave the most accurate predictions of sediment transport, whereas Whitehouse (1995) proposed that the d_{50} of sediment in suspension is correlated with the d_{10} of bed sediment grain size. Work by van Rijn (1984a,b,c) shows a relationship between the d_{50} of both suspended load (s) and bedload (b) sediment, using a sorting (σ_s: Equation 2.18) and transport (T_s: Equation 2.19) parameter:

$$\sigma_s = 0.5 \left(\frac{d_{84}}{d_{50}} + \frac{d_{50}}{d_{16}} \right) \tag{2.18}$$

$$T_s = \frac{(\tau_{0s} - \tau_{cr})}{\tau_{cr}} \tag{2.19}$$

via:

$$\begin{aligned} \frac{d_{50}}{d_{50,b}} &= 1 + 0.011\,(\sigma_s - 1)\,(T_s - 25) \quad \text{for } 0 < T_s < 25 \\ &= 1 \quad \text{for } T_s \geq 25 \end{aligned}$$

These equations may give a general estimate of the sediment transport if velocity and the grain size distribution of the bed is known.

3

Study Area

3.1 Study Site - Venice Lagoon

3.1.1 Introduction

Venice Lagoon is a restricted, shallow, coastal embayment (Kjerfve, 1994) located on the north east coast of Italy at 45° N 12° E. It is separated from the northern Adriatic Sea by a series of slender, sandy barrier islands typical of a microtidal coast (Hayes, 1979). The islands are divided by three tidal inlets - Lido , Malamocco and Chioggia, through which water and sediment exchange occurs (see Figure 3.1). The maximum discharge through the three tidal inlets is 20,000 m^3 s^{-1}, equivalent to between 175 million m^3 during neap tides and 350 million m^3 of discharge during spring tides (Mazzacurati, 1995). The tide is semidiurnal with an average range of 55 cm increasing to 110 cm during spring tides (see Appendix A.1). An average depth of 1 m, ensures that the lagoon is well-mixed (Pritchard, 1952; cited in Woodroffe, 2002) with a residence time of between 24 hours close to the inlets (Carbognin and Cecconi, 1997; Ravera, 2000) and 30 days in the inner lagoon (Cucco and Umgiesser, 2005; Molinaroli *et al.*, 2007). The drainage basin of Venice Lagoon is 1877 km^2 (Consorzio Venezia Nuova, 1997), providing 35.5 m^3 s^{-1} of freshwater input, most of which comes from the north-

Fig. 3.1: Venice Lagoon and its location in Italy (inset)

ern tributaries of the Silone (35% of total discharge) and Dese (21.1%) (Molinaroli *et al.*, 2007). As most fluvial input is into the northern basin of the lagoon (see Figure 3.2), not only is the salinity lower but there are more nutrients available as it receives 50% of the total annual sediment load (Zuliani *et al.*, 2005).

The lagoon is exposed to two major wind events; the sirocco, an autumnal/spring south-easterly wind from the Sahara, and the bora, a north-easterly wind that peaks in the winter. The bora induces a drop in the water level in the north and and rise in the south, which increase velocities in Chioggia Inlet and reinforces flood currents at Lido Inlet, reducing residence times to three days (Fletcher and Spencer, 2005). These

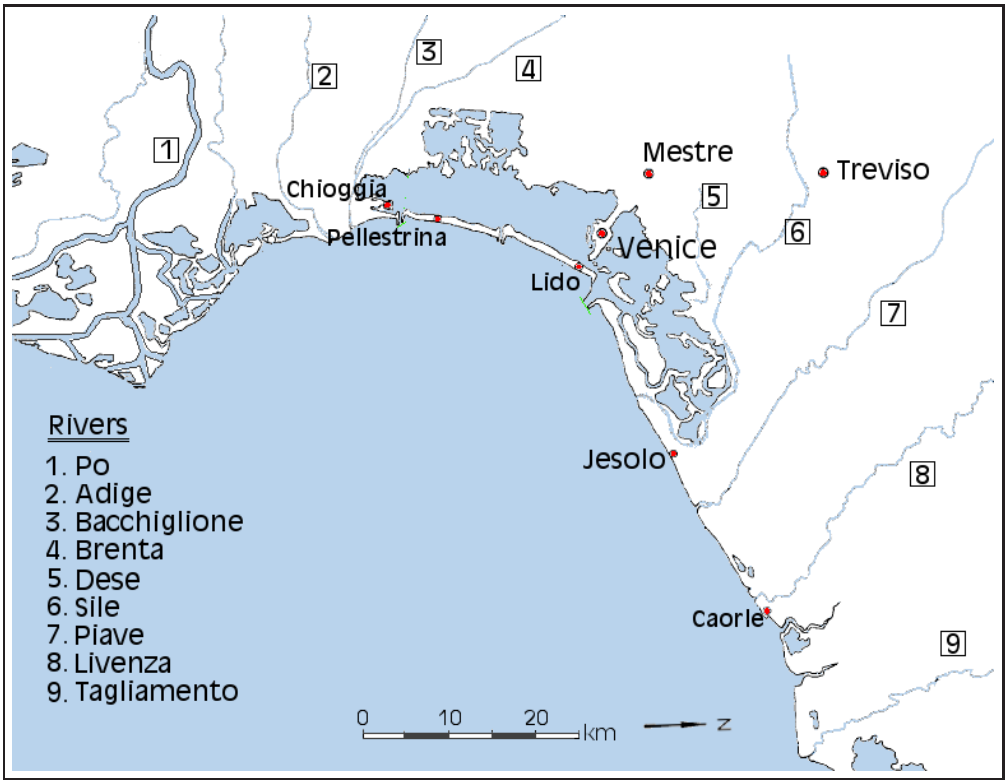

Fig. 3.2: The rivers of Venice Lagoon

winds cause major resuspension of sediment particularly in the south (bora) and west (sirocco) of the lagoon (Nielsen, 1992 and G. Umgiesser, Pers Comm). In Lido Inlet, high concentrations of sediment occur along the inside (bora) and at the tip (sirocco) of the northern jetty. Both winds cause build up of sediment (approximately 150,000 m^3) near to the mouth of Lido Inlet (Consorzio Venezia Nuova, 1996), in the position of the ebb-tidal delta (Helsby *et al.*, 2005).

3.1.2 Evolution of Venice Lagoon

Venice Lagoon is the principal survivor of a series of post-glacial lagoons, which formed about 6,000 years BP along the eastern Italian coast as a result of the Flandrian marine transgression (Gatto and Carbognin, 1981). The climate at the time was hot and humid, a controlling factor in the increased sediment load (accelerating weathering of the surrounding bed rock - Birkeland, 1999) carried by the rivers, causing the ancient

Piave and Adige river deltas (Gatto and Carbognin, 1981) to prograde towards the Adriatic Sea. The sediment was then distributed along the coast by wave and current action to form a well-defined littoral line characterised by a series of sandy barrier islands and lagoons.

The lagoon was originally much smaller than the present day one (see Figure 3.3A), expanding into the mainland to retain the original position of the littoral line (Gatto and Carbognin, 1981). Venice Lagoon was originally subject to fresh water and sediment input from five major rivers; the Piave, Brenta, Tagliamento, Adige and Sile, and had eight portals (in 1000 AD - Gatto and Carbognin, 1981) to the sea for water and sediment exchange (Carbognin and Cecconi, 1997), which meant that Venice Lagoon had a natural tendency for siltation. This tendency is evident in the disappearance of similar, neighbouring lagoons as documented by Mazzacurati (1995). The siltation of the lagoon was so great that 14th Century Venetians feared that ships would not be able to reach Venice, and trade would be lost. Works were subsequently undertaken to divert the mouth of the River Brenta away from the city (Albani and Serandrei Barbero, 2001) reducing fluvial import of sediment from 700,000 m^3 yr^{-1} to 30,000 m^3 yr^{-1} (Suman *et al.*, 2005). Further schemes to protect the lagoon have continued to the present day, through further river diversions (including moving the Po River in 1604 - Mazzacurati, 1995), coastal protection engineering (sea walls along the barrier islands in 1700s - CVN website[i]) and jetty building starting with Malamocco (1808 to 1840), Lido (1890 to 1910), and finally Chioggia (1911 to 1933). Prior to the construction of the jetties, sediment influx from the longshore transport pathway has been estimated at approximately 300,000 m^3 yr^{-1} (Consorzio Venezia Nuova, 1996). This transport is evident as spits/deltas extending from the eastern edges of the inlets (Fontolan *et al.*, 2007). If these engineering works had not been carried out, it has been estimated that Chioggia Inlet and perhaps Malamocco Inlet would have silted up. Instead beach nourishment schemes have been required to protect the southern shoreline from *lack* of sedimentation (Mazzacurati, 1995).

The current sediment influx is insufficient to compensate the natural average subsidence of 0.4 cm yr^{-1} (Carbognin and Cecconi, 1997), resulting in erosion of salt

[i]http://salve.it/uk/eco/default.htm - 29/11/07

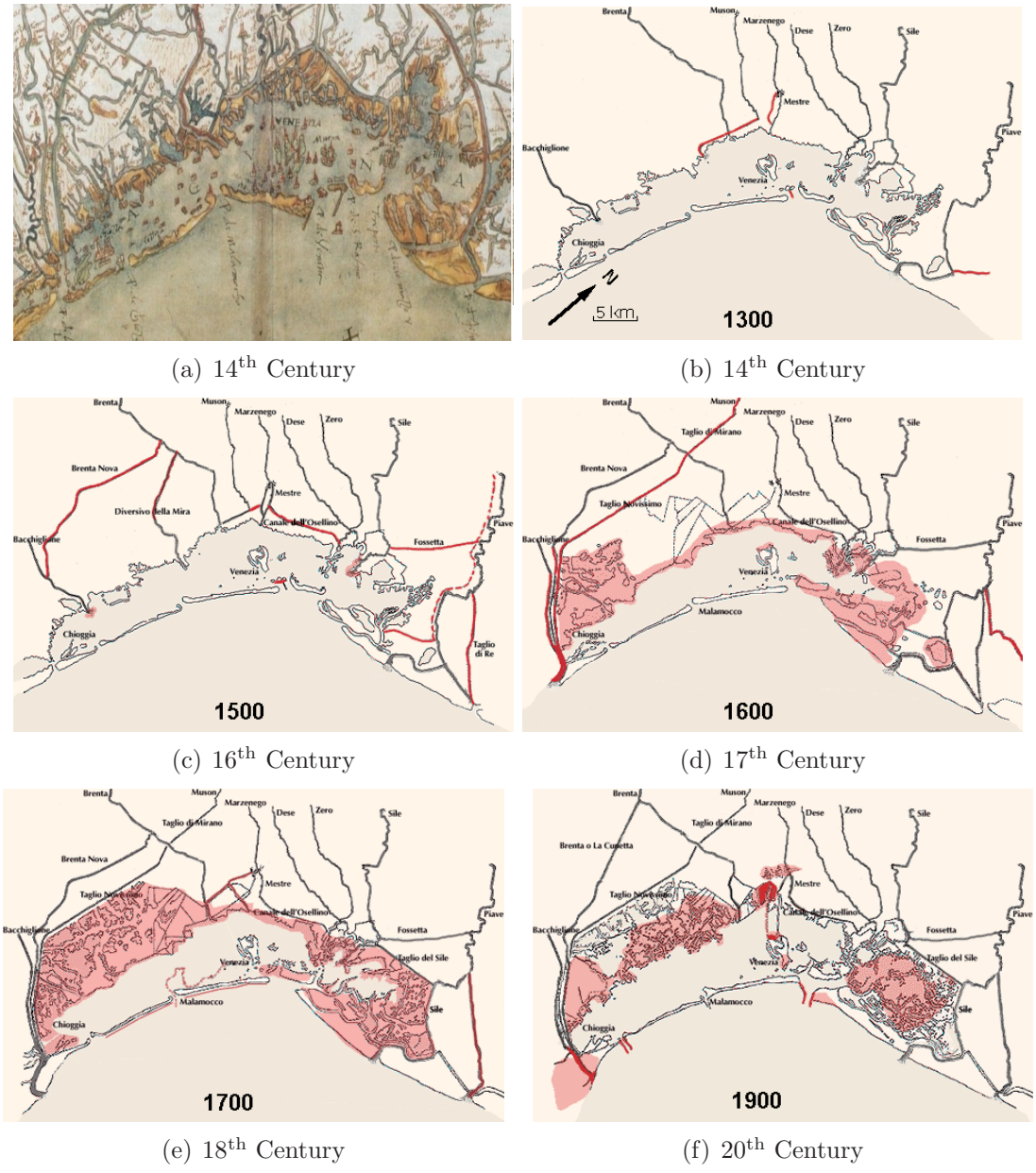

(a) 14th Century

(b) 14th Century

(c) 16th Century

(d) 17th Century

(e) 18th Century

(f) 20th Century

Fig. 3.3: The anthropogenic evolution of Venice Lagoon. Figure (a) is an old map showing the lagoon before any engineering works - from www.corila.it. Figures (b-f) show the diversion of all of the main rivers away from the lagoon, the seawalls (murazzi), and jetties (changes are shown as pink). Scale is approximate across all figures. From Consorzio Venezia Nuova website (www.salve.it)

marshes, infilling of channels and greater wave energy (Ravera, 2000). The subsidence has been exacerbated by eustatic sea level rise of 0.127 cm yr^{-1} and industrial groundwater pumping during the 1950s, 60s and 70s, which caused anthropogenic subsidence of up to 1.4 cm yr^{-1}[ii] (Consorzio Venezia Nuova, 1996). These factors have lead to Venice 'sinking' by 12 cm over the last century relative to sea level (Tosi *et al.*, 2002; Consorzio Venezia Nuova, 1997), meaning that parts of Venice now flood with a normal spring tide of one metre (Fletcher and Da Mosto, 2004). However, if the spring tide coincides with a low pressure event such as the sirocco, storm surges can inundate the city; flood-waters reached 194 cm AMSL[iii] in 1966, leaving St Mark's Square under 1.2 m of water. Extreme flood events (over 110 cm AMSL), that flood 12% of the city, have increased in frequency, occurring (if at all) once or twice a year before 1960, but in the last decade have occurred at least four times a year (Fletcher and Da Mosto, 2004). Critical flood events (over 140 cm) have flooded 90% of the city five times since 1966[iv]. These floods affect the whole lagoon, causing currents and waves to reach areas that otherwise would have remained protected from water-generated erosion.

Sea-level change in the Adriatic is greatest along the western and north-western edge due to tectonic pressure from the subduction of the Adriatic plate under the Appenine plate (- 0.3 mm yr^{-1} in Venice), which is overcompensated for by isostatic readjustment along the Italian coast (0.7 mm yr^{-1} in Venice). This shows that sea-level change in Venice is localised (di Donato *et al.*, 1999). The relative increase in water level has increased wave energy in the lagoon resulting in increased erosion and flattening of the bottom (Ravera, 2000).

The reduction in sediment supply has affected the salt marshes in the south and central lagoon, with 70,000 m^3 of sediment eroded annually (Mazzacurati, 1995). Lateral erosion of the marsh front is occurring due to increased wave energy from relative sea-level rise and an increase in boat traffic has resulted in areas that were protected from natural waves now experiencing constant impacts from artificially-generated ones. The area covered by salt marsh (including reclaimed land) totals 33.5 km^2 at last esti-

[ii] in 1968

[iii] Above Mean Sea Level

[iv] 03/11/68 (144 cm), 22/12/79 (166 cm), 01/02/86 (158 cm), 08/12/92 (142 cm), and 06/11/00 (144 cm): www2.comune.venezia.it/maree/allstoriche.asp - 03/12/07

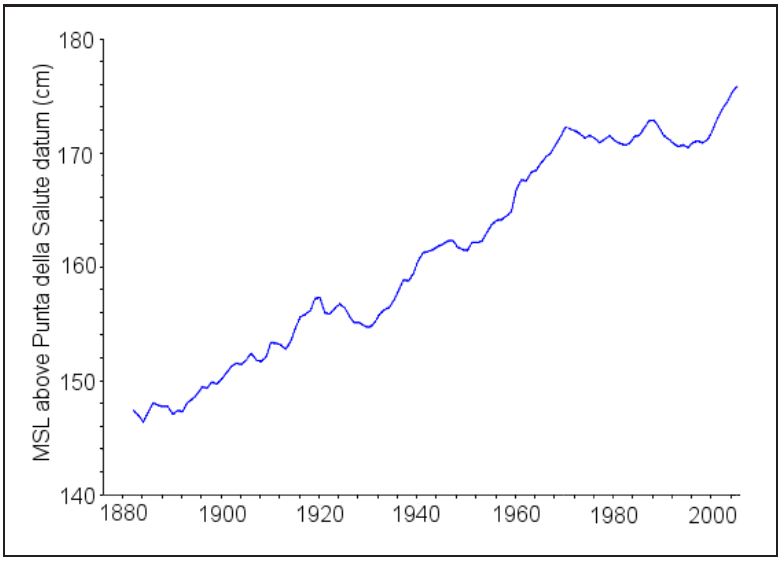

Fig. 3.4: Mean sea-level change between 1880 and 2005. Data from APAT (2006).

mate (1999) from 115 km^2 in 1810 (Fletcher and Spencer, 2005). At the current rate of destruction (average loss of 4 cm yr^{-1} at the marsh front according to Day *et al.*, 1998), salt marshes in Venice will have disappeared by 2045 (see Figure 3.5). Contrary to this

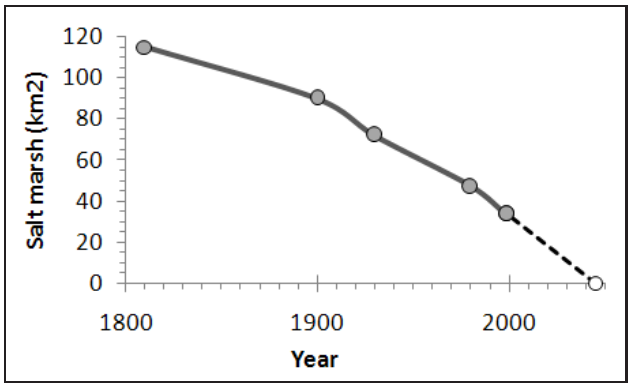

Fig. 3.5: The rate of salt marsh depletion between 1800 and 2050. Data from Consorzio Venezia Nuova (1996); Fletcher and Spencer (2005).

trend, salt marshes in the northern basin have been found to be accreting 1.52 cm yr^{-1}, due to bio-stabilisation inducing a increase in shear strength, and increased sediment input because of the location within the relatively well supplied northern basin

(Cappucci *et al.*, 2004). Signs of rapid accumulation in the salt marshes has also been noted by Day *et al.* (1999), who found plastic sheeting buried 30-50 cm in the Punta Cane marsh (southern basin). This sediment accretion is highest during storm activity, although the vegetation edge of this marsh is being eroded by 1.2 to 2.2 m yr^{-1} due to wave impacts. This has been especially noticeable around the Petroli Canal, built in the '60s to allow passage of oil tankers to the industrial port of Mestre/Marghera. An estimated 50-100 cm has been eroded from the shallows and salt marshes in this area since 1900 (Fletcher and Spencer, 2005), with sediment settling in the channels requiring maintenance dredging. Thus Venice Lagoon has evolved from a small, water body, decreasing in size due to net sediment influx, to a larger, highly engineered, brackish environment suffering the effects of net sediment loss.

3.1.3 Sediment Exchange

Gazzi *et al.* (1973) states that the sedimentary environment in the Gulf of Venice is controlled by longshore transport (also found by Bonardi *et al.*, 1997), which has been interrupted by the construction of groynes and jetties, resulting in turbulent eddies. Sediment supply in the vicinity of Lido Inlet is plentiful, demonstrated by the rapid accretion of Cavallino Beach that occurred after the jetties were built (15.8 m yr^{-1} between 1908 and 1933, slowing to 8.5 m yr^{-1} between 1980 to 1987 - Consorzio Venezia Nuova, 1989; cited in Fontolan *et al.*, 2007; Mazzacurati, 1995; Consorzio Venezia Nuova, 2000). The accretion of Cavallino Beach and the evolution of Lido Inlet is shown in Figure 3.6.

Whilst the longshore transport rate is estimated to be 150,000 m^3 yr^{-1} (Consorzio Venezia Nuova, 1989 cited in Fontolan *et al.*, 2007), the supply is limited at the southern end of the lagoon, suggesting that much sediment is transported offshore or trapped by the Lido jetties. Fontolan *et al.* (2007) has investigated the ebb-tidal delta off Lido Inlet, and found it to be immature, containing 5.81 x 10^6 m^3 of sand, which is just 10% of its estimated equilibrium volume of between 6.05 x 10^7 m^3 and 7.18 x 10^7 m^3 as calculated by the Residual Method of Walton and Adams (1976) (in Hicks and Hume, 1996). The Residual Method determines idealized 'no inlet' contours from the bathymetric contours. The difference between this and the real bathymetry provides an estimate to the total sediment present in an ebb-tidal delta (Fontolan *et al.*, 2007).

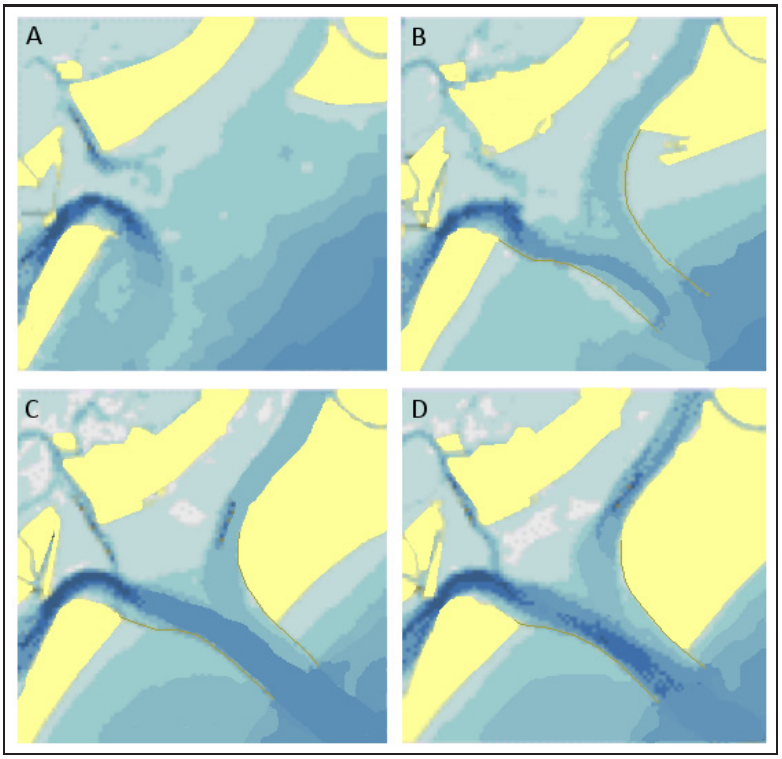

Fig. 3.6: The evolution of Lido Inlet: 1809 (A), 1897 (B), 1934 (C), 2003 (D). After Balletti (2006)

The delta immaturity affects the sand supply to down-drift beaches, as sand is not easily bypassed (Bruun and Gerritsen, 1959). The -5 m contour off Lido Beach has receded 600 m closer to shore between 1886 and 1997, due to loss of sediment supply although some sand has recirculated by ebb-jet related eddies to accrete by the beach adjacent to the southern jetty (some of this sand may be a relic of the ebb-spit present prior to jetty construction). Beach nourishment has occurred on south Lido Beach and Pellestrina Beach, supplied by 2 million m^3 of sand from a 5,000 year old palaeo-beach 20 km offshore (see Figure 3.7) from Malamocco Inlet (Danish Hydraulics, 1996; Cecconi and Ardone, 2000; Consorzio Venezia Nuova, 2000). Frequent dredging to maintain the shipping channel into Lido Inlet, as well as a wave energy of just 15.61 m^2 s^2 (a mean significant wave height of 0.5 m and 5 m for Bora and Sirocco events) has slowed down the equilibrium process for the ebb delta in terms of the tidal prism (Fontolan *et al.*, 2007).

The near-shore region along the lagoon is dominated by very-fine sand, which is di-

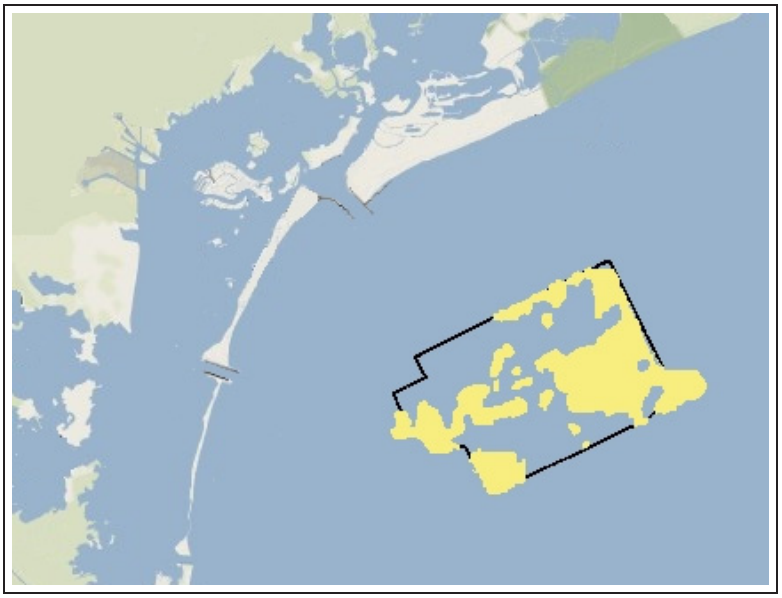

Fig. 3.7: The source of sand for beach nourishment for Cavallino and Pellestrina, and Lido beaches. Modified from Cecconi and Ardone (2000).

verted offshore with the ebb current at Lido Inlet, leaving medium to fine sand south of the inlet along Lido Beach due to selective removal of fine-grained sediment. A 5 km wide 'mud belt' is present 2-3 km offshore, stretching along the length of the lagoon (Albani *et al.*, 1998); the silts and clays are thought to have been supplied by the northern Adriatic rivers such as the Piave (Brambati *et al.*, 1973 cited in Wang and Pinardi, 2002). Sand is present further offshore (Albani *et al.*, 1998), in the form of the palaeo-beaches described previously.

Increased agitation of bed sediment has occurred in recent years, due to a combination of the use of mechanical dredges instead of manual dredges in the harvesting of the clam *Tapes philippinarum* and a reduction in the presence of bed-stabilizing macroalgae. Sfriso *et al.* (2005a) state that concentrations of suspended particulate matter have increased by a factor of ∼70 in the decade since 1988. This has been estimated to be the equivalent losing 1.6 cm yr^{-1} of sediment on average, or 2.4 million m^3 yr^{-1} (11 cm) during 1994-2001, which was the peak clam harvesting period. During the dredging process, fine sediments are resuspended above the boundary layer, where

velocities exceed settling velocity, and are transported away.

Amos *et al.* (2002) studied the water and sediment exchange in the inner-lagoon canal system of Burano-Treporti-Lido and found evidence of submerged beaches in the Burano region, providing an area of shelly-sand to the otherwise silty inner-lagoon. These beaches are biostabilized by seagrasses which strongly attenuate wave energy through sand entrainment, protecting salt marshes as observed by Cappucci *et al.* (2004). Umgiesser *et al.* (2006) used the hydrodynamic model SHYFEM (Umgiesser, 2000; Umgiesser *et al.*, 2004a) with the sediment transport model SEDTRANS05 (Li and Amos, 2001; Ferrarin, 2005) to model sediment transport in the Burano-Treporti-Lido system and found that sediment transport is inversely proportional to grain size and also distance from Lido Inlet. During conditions of tidal forcing, sediment is exported from the lagoon except during Bora wind conditions, when sediment is imported along Treporti Canal. Umgiesser *et al.* (2006) states that sand found in Treporti Canal is reworked from an ancient sand barrier, resulting in no distinguishable trends. The high velocities in Treporti Canal inhibit sedimentation meaning that the northern basin is losing sand rather than importing it.

The geology of the Veneto Region (shown in Figure 3.8) is predominantly alluvium from the River Brenta, with alluvium from the River Piave (Figure 3.1) present from the southern limits of Treviso (25 km north of the lagoon) to the north-east of the lagoon. The barrier islands of Venice however, are predominantly medium/fine sand mainly from the Piave, but with some characteristics of Brenta alluvium. Only the very northern marshes are recent Piave alluvium. Alluvial sediments from the River Adige are predominant just south of the lagoon, occupying a relatively thin strip between the regions of Po and Brenta river alluvium (APAT, 1960a,b,c). Mineralogy of the lagoonal sediments has been carried out in detail by Bonardi *et al.* (2005). They determined that the average percentage of sand (as opposed to clay or silt) was highest in the southern basin and lowest in the northern basin, despite evidence that Lido Inlet is sandy (see Chapter 5), and submerged beaches have been found in the Burano area (Amos *et al.*, 2002). Bonardi *et al.* (2005) found that the northern basin had greater proportions of silt and clays than the other two basins (south and central). The authors also found that carbonate minerals were dominant in the northern basin, and

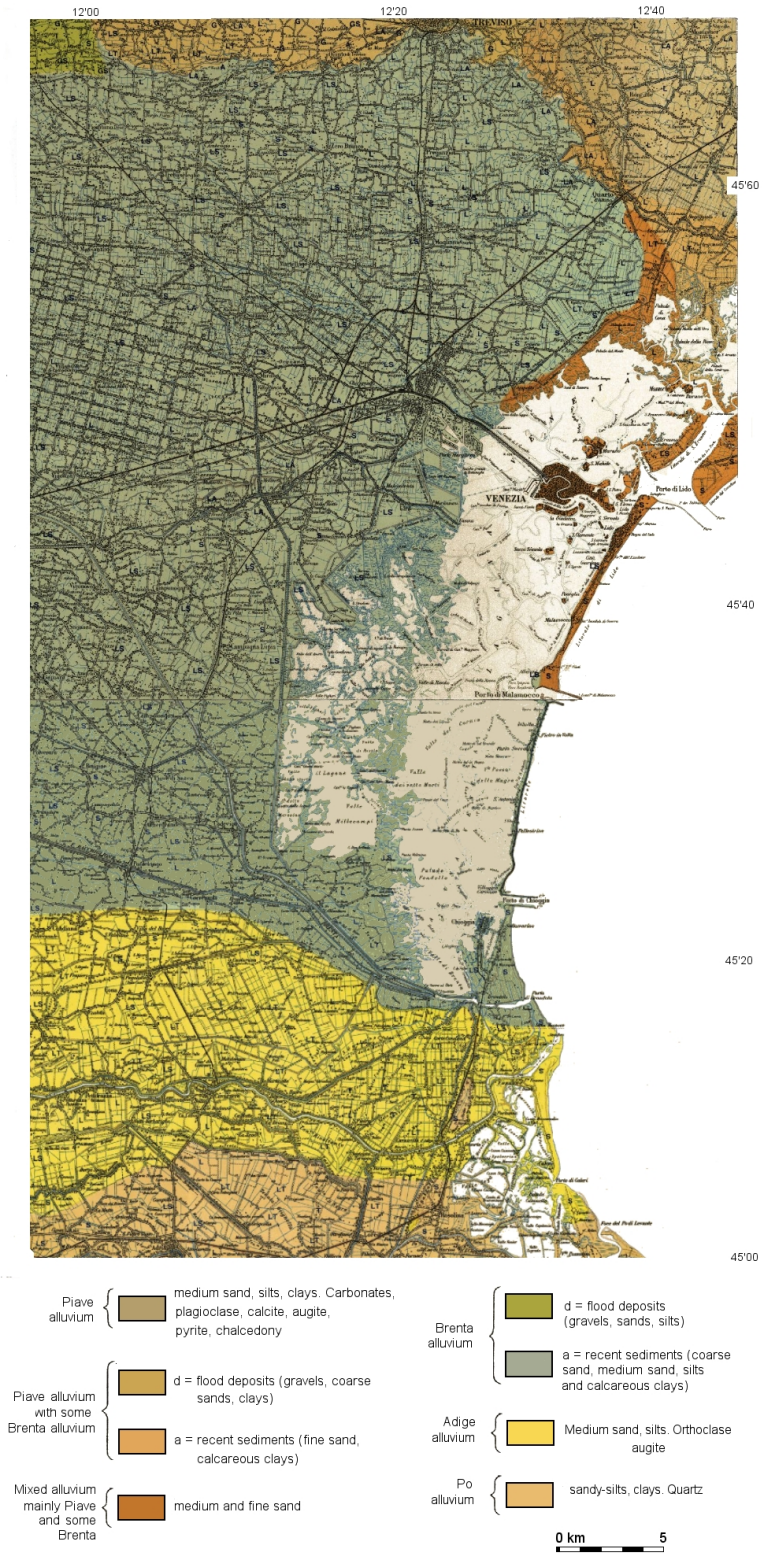

Fig. 3.8: The geology of the Venice Lagoon region. From APAT (1960a,c).

silicates in the south. These findings are in agreement with mineralogical analysis of Gazzi *et al.* (1973) and modelled results of Weltje (1995), who hypothesised that carbonates were transported down the rivers Tagliamento and Piave (see Table 3.1) from the Dolomite Mountains to the north to the beaches. The rivers are also an ancient source of northern lagoonal sediment. Model results from Weltje (1995) agreed with sedimentological findings of Gazzi *et al.* (1973), who showed that longshore transport was from north to south from the Tagliamento to Pellestrina but travelled from south to north from the Po delta to Pellestrina. Thus, silicate minerals carried by the rivers Po, Adige and Brenta are transported north towards the southern basin.

River	Quartz (%)	Dolomite (%)
Tagliamento	15	20
Piave	10	20
Brenta	15	15
Adige	35	15
Po	20	0

Tab. 3.1: The percentage of quartz and dolomite in the main rivers around Venice Lagoon as described by Ravaioli *et al.* (2003)

4

Character and Morphology of the Seabed

4.1 Introduction

The character and morphology of the seabed around a tidal inlet is the result of a combination of hydrodynamics, sediment properties and aquatic biology. Through investigation of the morphological features and how they change over time, it is possible to gain an understanding of the pathways of sand transport, and how this transport reflects the stability of the tidal inlet.

This chapter will describe the methods used to collect bathymetric and reflectivity data from Venice Lagoon, and will discuss the transport of sand in the context of bathymetric change and seabed texture. From these results the tidal prism/cross-sectional area relationship will be evaluated. The following questions will be discussed:

- What are the main transport pathways, sources and sinks of sand in northern Venice Lagoon and how has the sand shaped the morphology of the region?
- To what extent is the morphology of the region controlled by the tidal prism?
- Has the tidal prism of Lido Inlet changed between 1930 and 2000 and is it possible

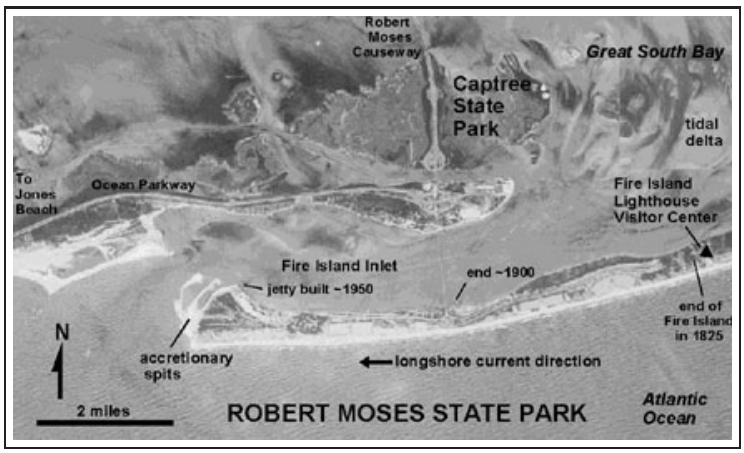

Fig. 4.1: Ariel photo of Fire Island inlet showing the migration trends from 1875 to present. From USGS website - http://3dparks.wr.usgs.gov/nyc/parks/loc74.htm

to apply the tidal prism relationship of O'Brien (1931) along the canal system of Lido Inlet, Treporti Canal, and Burano Canal?

- Can areas of peak sand transport be determined using changes in morphology and through seabed classification?

4.1.1 Tidal Inlet Stability

A tidal inlet is a short channel maintained by tidal currents, which connects an enclosed water body to the sea (Hayes, 1975; Fitzgerald, 1988). They are important to a lagoon as they flush lagoonal/bay waters which may otherwise become nutrient depleted or polluted. They are also economically important as a passageway for ships into sheltered harbours. A tidal inlet is the most dynamically active component of a lagoon, as revealed by frequent alterations in its morphology and position. The migration of the Fire Island Inlet in New York state is an example of this mobility (shown in Figure 4.1) as it has migrated west approximately four miles in 100 years. This is an example of sediment bypassing by inlet migration (see page 19). Inlet mobility is a sign of instability between the current flow and the geomorphology of the site that can cause navigational problems as maps quickly become obsolete. Therefore it is economically beneficial to determine how stable a tidal inlet is and if it requires artificial stabilization by jetty construction. Work by O'Brien (1931) has demonstrated that inlet stability

can be determined by comparing the tidal prism (the total volume of water passing through an inlet at its smallest cross section) during a tidal cycle and the cross-sectional area at mid spring-tide. This relationship between the cross-sectional area (A_c) of an inlet and its tidal prism (P) has been investigated by numerous authors (Le Conte, 1905; O'Brien, 1931, 1969; Escoffier, 1940; Jarrett, 1976; Hume and Herdendorf, 1988, 1990). All have concluded that the relationship can be expressed by a variation of the general formula:

$$A_c = xP^n \tag{4.1}$$

where x and n are constants. If an inlet follows this relationship, then it can be regarded as stable in terms of its equilibrium with the tidal prism. An inlet with a smaller cross-sectional area or larger tidal prism than the relationship predicts, may be unstable and should erode to increase the cross-sectional area in order to accommodate the tidal prism, and vice versa. However, as the inlet cross-sectional area changes, the tidal discharge and velocity must also be affected and by analogy the tidal prism. It is therefore important to consider this relationship in terms of inlet management as the depth (for navigation) can be controlled if the inlet width is restricted by jetties.

Le Conte (1905); O'Brien (1931, 1969) and Nayak (1971) used data collected from inlets along the Pacific coast of North America to define a standard relationship of inlet stability. In addition, O'Brien (1969) distinguished a difference between natural inlets (Equation 4.2) and jettied inlets (Equation 4.3), which results from a slightly larger cross-sectional area found in the jettied inlets:

Natural inlets

$$A_c = 7.607 \times 10^{-3} P \tag{4.2}$$

Jettied inlets

$$A_c = 7.489 \times 10^{-4} P^{0.86} \tag{4.3}$$

Jarrett (1976) published a summary of cross-sectional area/tidal prism relationships using data on inlets along the Pacific, Atlantic, and Gulf coasts of N. America. He concluded that inlets on the Atlantic coast followed a different relationship to those on the Pacific coast, that they have a larger cross-sectional area to a given tidal prism:

Atlantic coast

$$A_c = 3.039 \times 10^{-5} P^{1.05} \tag{4.4}$$

Pacific coast

$$A_c = 2.833 \times 10^{-4} P^{0.91} \tag{4.5}$$

Pacific and Atlantic coasts are subject to different tidal conditions as the former has a large diurnal inequality (one high tide is significantly larger than the second high tide of the day); the latter is semidiurnal. Jarrett (1976) however, concluded that the wave climate and ratio of the inlet width to the hydraulic radius (R_h - the ratio between the cross-sectional area and the wetted perimeter) were more significant in creating differences in these relationships. The mean wave height in the Pacific is greater than in the Atlantic by over a metre; this influences the magnitude of the littoral drift of sand and hence the hydraulic radius of the channel. The greater the magnitude of littoral drift, the smaller the hydraulic radius becomes (Jarrett, 1976). Inlets restricted by bedrock will shift geographically with littoral drift action (Bertin *et al.*, 2004), and reduce the tidal prism through the formation of ebb-tidal deltas (Walton and Adams, 1976), so that the relationship remains valid. The O'Brien relationship is not always suitable and new relationships have formulated, for example, in Japan (Shigemura, 1981) and in New Zealand (Hume and Herdendorf, 1990).

The inlets of Venice Lagoon have only recently been studied in terms of their stability. Tambroni *et al.* (2005) determined that all three inlets corresponded to the general tidal prism/cross-sectional area relationship (Equation 4.1), although they tested the stability of the inlets through a relationship between maximum velocity and depth. Their results show that both Lido and Chioggia inlets are unstable and liable to deposition due to relatively slow velocities when compared with depth, whilst the artificially deepened Malamocco Inlet is near a 'critical condition' with velocities faster than predicted for its depth. Fontolan *et al.* (2007) researched the relationship between Adriatic inlets and their ebb-delta volumes (V) using variations of the general formula $V = xP^n$ (note the similarity with Equation 4.1). Their results describe an immature ebb-tidal delta associated with Lido Inlet, with just 10% of the volume predicted using the formula $V = 8.157 \times 10^{-15} P^{1.4636}$ of Hicks and Hume (1996). Their investigations

also show Lido Inlet to be stable in accordance with the relationship of O'Brien (1969), contrary to the findings of Tambroni *et al.* (2005). However, whilst Tambroni *et al.* (2005) used recent modelling techniques to determine their results, Fontolan *et al.* (2007) used discharge data that is almost two decades old (Consorzio Venezia Nuova, 1989). The stability of Lido Inlet is still clearly debatable and requires further study; therefore, this chapter will investigate the validity of the O'Brien (1969) relationship within Lido Inlet and whether the relationship can be extended to any cross section within a tidal canal to quantify the stability of channels within the lagoon.

4.1.2 Bathymetry and Texture

The mapping of morphology is important for sediment transport investigations. Hence deeper channels are representative of high-energy environments with sediment transport as suspended load and bedload. Similarly, shallow areas can depict a low-energy environment and thus are a likely sink of sediment. Changes in the seabed bathymetry over time can also provide an indication of the type of environment through erosion (high-energy) and accretion (low-energy). Large scale bedforms can also provide information on sand transport, for example, sand waves are produced by mean velocities greater than 0.4 m s^{-1}, with sediments coarser than 200 μm (Tucker, 1991). Sediment characteristics, such as grain size and shape, provide an indication of the hydrodynamics; for example, coarse material in a predominantly fine-grained area could be the result of scour (armouring), caused by turbulence in the water column (Hoffmans and Verheij, 1997). Changes in the sediment type of the seabed can be detected through differences in the way they reflect acoustic waves, thus sidescan sonars (Nitsche *et al.*, 2007; Collier and Brown, 2005) and echosounders (Burczynski, 2001; Lied *et al.*, 2004; Tęgowski, 2005) have been used to characterise the seabed by its reflectivity. The authors generally concede that grain size is positively correlated with an increase in backscatter (Collier and Brown, 2005); fine-grained sediment absorbs sound energy, thus is distinguished by low reflectivity, whereas sand is generally more reflective due to its hard, flat surface. Reflectivity must still be calibrated with sediment samples as it is affected by other variables such as the turbidity, presence of bubbles, and water chemistry of the water column, which can absorb acoustic energy. The reflectivity of the seabed can subsequently be compared with these sediment samples to produce a

high-resolution map of seabed texture. An example of seabed classification by Nitsche *et al.* (2007) depicting the River Hudson is shown in Figure 4.2.

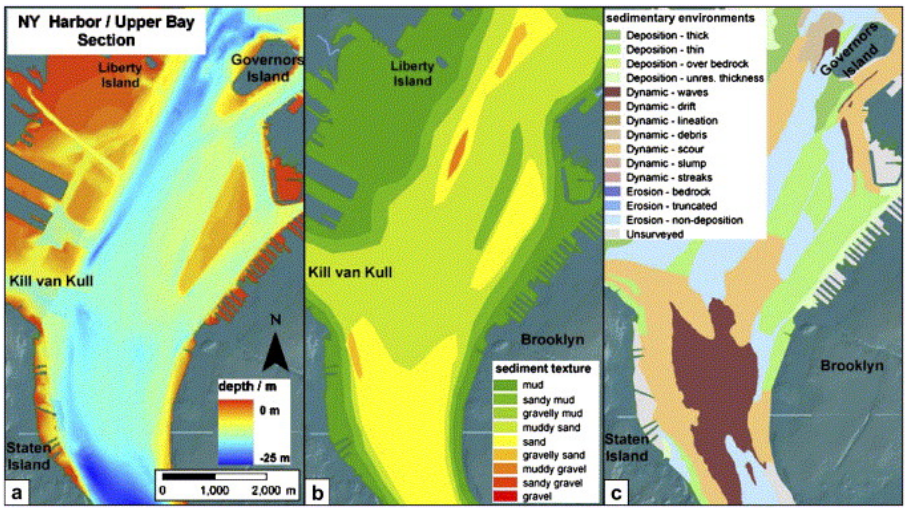

Fig. 4.2: Example of the seabed classification maps of the Hudson River produced by Nitsche *et al.* (2007).

The use of reflectivity and bathymetric data will be used to determine the morphology of the study area resulting in hypotheses of hydrodynamics (areas of peak/minimum velocity, eddy formation and scour, areas of wave and tidal current domination) and sediment dynamics (sand wave production, scour, deposition and erosion). From this it may be possible to determine potential sources (scour) and sinks (deposition, fine-grained beds) of sediment as well as the average direction of sediment transport (skewing of morphological features).

4.2 Methods

4.2.1 Bathymetry Survey

540 line kilometres of bathymetry and sector-scanning sonar data (in sidescan mode) were recorded during February 2003, February 2004 and May 2004 within the Lido Inlet, Treporti and Burano canals, and in the Adriatic Sea around the mouth of Lido Inlet. The track lines are shown in Figure 4.3. Further bathymetry data from 1930,

1970, 1990, and 2000 (provided by CNR-ISMAR) were also used, as well as historical charts of Venice Lagoon up to 500 years old (Baso *et al.*, 2003).

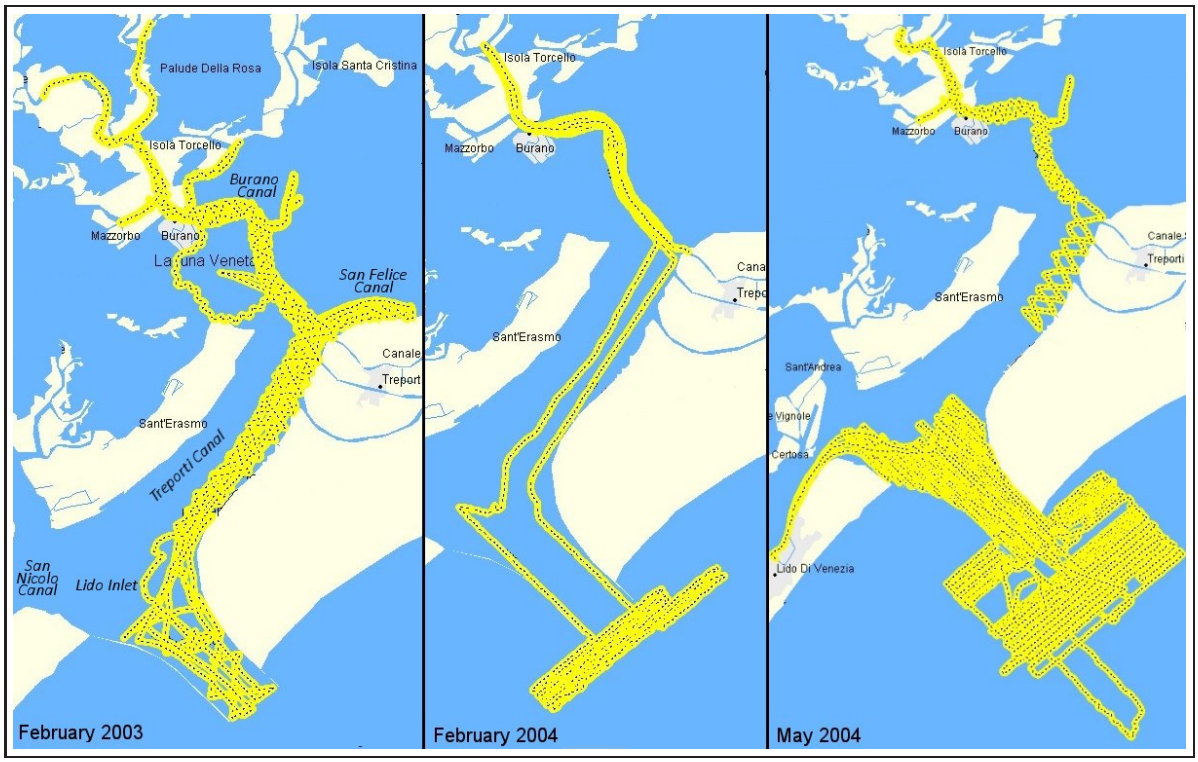

Fig. 4.3: Survey lines for bathymetry and reflectivity (sonar) data for 2003 and 2004.

Bathymetric data strings were recorded at 1 Hz from a single-channel echosounder at a vertical resolution of 3 cm. The data were geo-referenced with a Garmin® GPS (recording at 1 Hz into a separate file) through correlation of time stamps saved within each line of data in both data files. Tidal corrections (available at 5 minute intervals) using measurements from a tidal gauge in Lido Inlet were interpolated and applied to the data as were corrections for draft and depth (Figure 4.4); the echosounder was calibrated during each survey for changes in the speed of sound in seawater. All of the datasets were corrected relative to the Punta Salute Datum in the Grand Canal, Venice, with any obvious outlying data-points removed.

Longitude and latitude (in decimal degrees) and depth (in metres) were transferred into a text file readable by Generic Mapping Tools (GMT) for imaging (Wes-

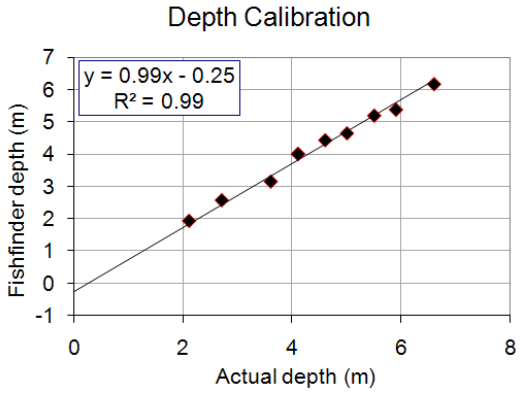

Fig. 4.4: The depth calibration for the Fishfinder echosounder. Standard error of the difference is 0.16 m.

sel and Smith, 1991). The data were plotted initially as trackpoints, and cross-over points (where the boat tracks intersected) were compared to ensure the data had been corrected sufficiently. The average discrepancy between crossover points (excluding

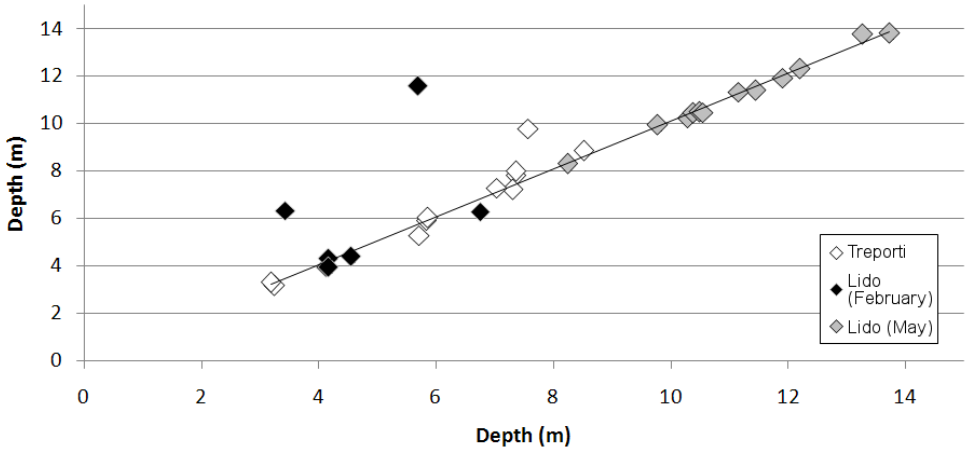

Fig. 4.5: Comparison of depths where boat tracks intersected (cross-over points).

three outliers seen in Figure 4.5) was 0.05 m with a standard error of 0.23. The data were subsequently gridded at 0.001° intervals using GMT algorithms (Wessel and Smith, 1991) to calculate the hypothetical value of desired fixed-grid datapoints using nearest-neighbour real world values, and imaged as layers in a postscript graphic. Further image layers were added to show the locations of islands, which were digitized

from a recent map of Venice Lagoon (Bondesan *et al.*, 2004). Contour plots of the whole lagoon as well as sections focussing on Lido Inlet, Treporti and Burano Canals and outer Lido were created to show bathymetry in the years of 1930, 1970, 1990, 2000, and 2004. To show changes in morphology and areas of erosion and deposition the difference map method (DMM) was employed (Stauble, 1998); the bathymetric gridfiles were compared using a further GMT algorithm (algorithms used are shown in Appendix B). The disparity between two datapoints occupying the same gridpoint but for separate years were calculated and the result written into a new file also providing the grid coordinate. The resulting gridfile was then used to determine temporal changes in bathymetry and to quantify erosion and deposition rates. By analysing these maps, changes in morphological characteristics could be determined and sediment transport pathways hypothesized.

4.2.2 Tidal Inlet Stability

The hydrodynamic model SHYFEM (Umgiesser *et al.*, 2004a,b) was used to determine the channel stability as theorized by O'Brien (1969), and to investigate the applicability of the relationship to inner-lagoonal channels. A model was used instead of taking actual data measurements so that discharge and thus tidal prism could be calculated for the years with available bathyemtry. 11 profiles, selected to correspond to nodes within the SHYFEM model, were drawn across sections of Lido Inlet, Treporti Canal and Burano Canal (for positions see Figure 4.7) and the cross-sectional area calculated from the gridded, lagoon-wide, bathymetry datasets for the years of 1930, 1970, 1990 and 2000. The bathymetry was gridded using GMT algorithms and data extracted at equal intervals along each profile (x in Equation 4.6). The depth (d) was then assumed to be uniform for each of these intervals (dividing the cross-section into rectangles of equal width. See Figure 4.6) so that a trapezoidal calculation could be performed:

$$A_c = \sum_{i=1}^{n} d_i \Delta x \tag{4.6}$$

where n is the total number of individual trapezoids.

SHYFEM was used to calculate the tidal prism through simulation of a typ-

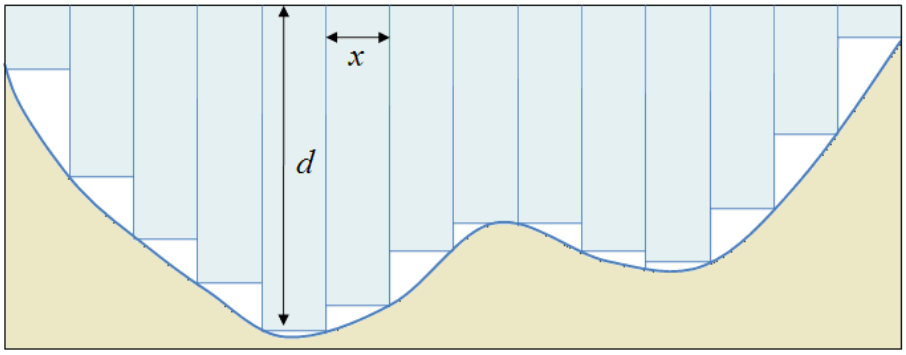

Fig. 4.6: Calculation of cross-sectional area. The white-shaded areas are not included in the calculation but only appear significant in this image due to the relative exaggeration of the axes and length x.

ical spring tide in Venice Lagoon. The model was run using all four lagoon-wide bathymetry datasets to predict discharge, tidal elevation and current velocity across each profile every 300 seconds of the tidal cycle. The tidal prism was then calculated using three different methods, which were compared to determine the most accurate method. The first method (Equation 4.7) was that of O'Brien (1931, 1969), where A_c is cross-sectional area, V_{max} is the maximum velocity and T represents the tidal period:

$$P = \frac{A_c V_{max} T}{\pi} \tag{4.7}$$

The second method, uses maximum discharge during the flooding tide (Q_{max}), after the U.S Army Corps. of Engineers (Seabergh, 2002):

$$P = \frac{T Q_{max}}{\pi} \tag{4.8}$$

The final method directly sums the discharge passing the profile during the flooding tide (Q_{pos}) with the result multiplied by 300 (Δt):

$$P = \sum_{0}^{T} \Delta t Q_{pos} \tag{4.9}$$

The tidal prism and cross-sectional area were plotted against the O'Brien relationship

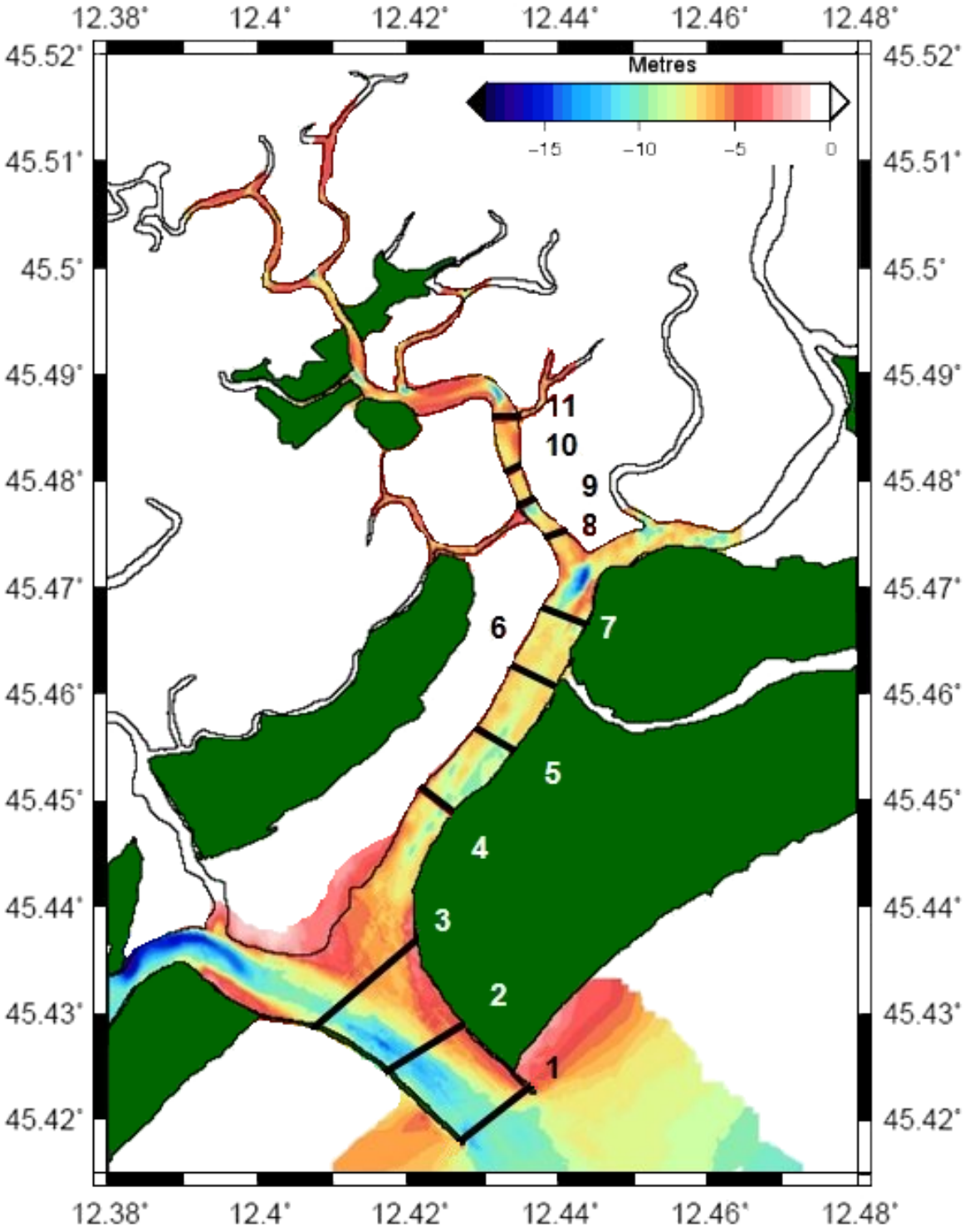

Fig. 4.7: The location of cross sections used to determine the stability of Lido Inlet.

as well as other cross-sectional area/tidal prism relationships (Jarrett, 1976; Le Conte, 1905). The cross sections were compared to quantify erosion and deposition in the years 1930, 1970, 1990, 2000, and 2004, and to determine if channel shape has altered.

4.2.3 Reflectivity

A Marine Electronics image profiling sonar operating at 500 kHz, collected reflectivity data concurrently with the bathymetry data (see Figure 4.3). The sonar was hull-mounted on a downrigger, which restricted the survey speed to 7-8 km/hr to reduce reverberation and turbulence. Degradation of the signal occurred due to turbulence and bubbles left in the wake of ships (Lido Inlet is the thoroughfare to Venice for ferries and cruise ships) crossing the survey path.

Each acoustic ping was displayed in real time on the onboard PC and saved automatically approximately every three minutes (Figure 4.8). These data, saved as an image file were then converted into text file with each bin having a value from 0 to 255, 0 being lowest reflectivity (blue pixels in Figure 4.8) and 255 being maximum reflectivity (fully saturated and represented by red pixels in Figure 4.8).

GPS coordinates were not integrated with the sonar system, therefore the save time from each sonar file was correlated with the save time from the bathymetric dataset in order to determine the co-ordinates of the data. Water depth was also correlated with the sonar data so the seabed return could be identified by subtracting the water depth from the first return (taking into account draft). The seabed return was averaged to reduce error and then plotted using GMT. This method produced only adequate results, showing a large variation of backscatter, probably due to boat roll and variation in the width of the seabed return (see Figure 4.8), which could not be taken into account. To improve the quality of the results the image files were processed using a more laborious, manual method, which involved the definition of colour scales between 1 and 30 (arbitrary units, subsequently referred to as reflectivity index or I_R shown in Figure 4.9) with dark blue (no backscatter) having a value of zero, and the red (fully-saturated backscatter) having a value of 30 I_R, and the colours between split into 5, 10, 15, 20, and 25 I_R. Six images which corresponded well to each of these

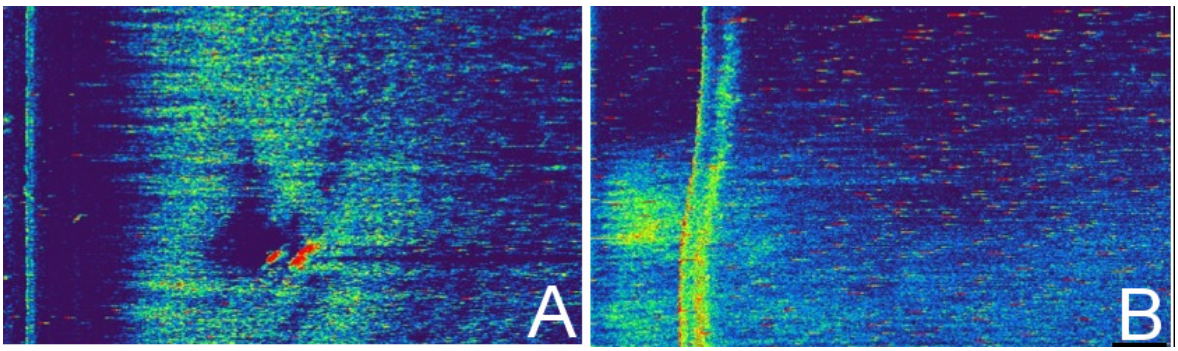

Fig. 4.8: An example sidescan image showing shadowing around navigation poles and a thin seabed return (A) and a change in seabed texture and a thicker seabed return (B).

benchmarks were used to compare with all the remaining images, with intermediate values (such as 8 or 27 I_R) used when the backscatter was not a precise match to the reference images.

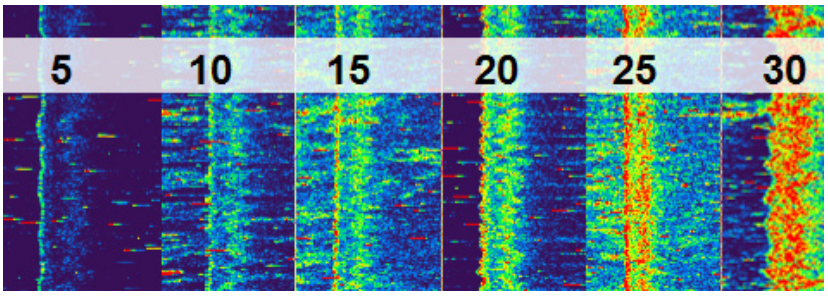

Fig. 4.9: Reflectivity spectrum of the data showing the reference I_R increasing from 5 to 30.

The save time of each image was used to determine the position which was then combined with the I_R data, depth and sonar gain into a text file readable by GMT.

Corrections to the data were required to standardize the different gains used through the survey, and also to correct for depth induced errors. The I_R of several pairs of images which were consecutive but had different gains, was compared to find the average change in I_R (1.5 I_R per increment in gain). This difference was used to normalize all images to a gain of 7. These values were subsequently mapped and compared with the initial uncorrected map to evaluate the success of the calibration. Neighbouring datapoints now showed similar I_R, unless the seabed characteristics changed. The

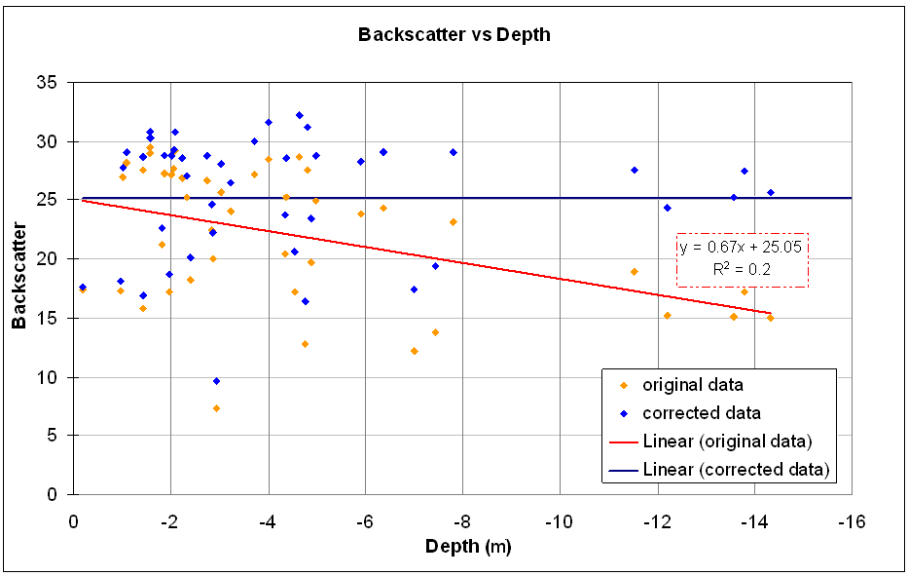

Fig. 4.10: Backscatter reflectivity versus depth. The original data is shown in orange, the corrected data, in blue.

height of the water column also affects reflectivity as sound is attenuated with distance travelled. Therefore the return signal can be over-saturated in shallow water but very weak in deeper water. A graph (Figure 4.10) of I_R versus depth (h) was plotted and a regression line fitted ($I_R = 0.6753h + 25.046$) to show the mean I_R at each depth. To correct the data for depth, the regression line was de-trended as shown by Figure 4.10. The result of this calibration was to retain the mean I_R at 25 (the mean I_R at zero depth). As the maximum I_R was now greater (33.9) than the defined maximum of 30, the results were multiplied by 0.885 to restore the scaling.

4.2.4 Seabed Classification

The reflectivity data were used in conjunction with sediment classification (determined through grab sampling and discussed in Chapter 5) and bathymetry data to categorize the seabed. Three morphodynamic zones were identified and mapped: high energy (e.g. areas of maximum current strength, or wave foci), medium energy (e.g. dynamic conditions - waves, tidal currents) and low energy (sheltered due to short fetch or water depth). Areas of significant deposition (over 2 m between 1990 and 2004), deposition

(0 to 2 m), erosion (0 to -2 m) and scour (over -2 m erosion) were also added to the same diagram.

4.3 Results

4.3.1 Morphological Changes in Venice Lagoon

Venice Lagoon has suffered widespread erosion between 1930 and 2000 (Figure 4.11); comparison between the datasets of these two years reveals loss of sediment principally around the Petroli Canal (passage for oil tankers leading from Malamocco Inlet to the industrial port of Marghera - see Figure 3.1), Venice and Chioggia Inlet. This is in agreement with the conclusions of Magistrato alle Aqua (1993) and Ravera (2000). The average rate of erosion is approximately 1.5 cm yr^{-1}, although this doubles to 3 cm yr^{-1} around Chioggia Inlet and increases to over 10 cm yr^{-1} around the Petroli Canal[i]. An erosion 'aura', where bed elevation has decreased at a rate of 5 cm yr^{-1}, extends about 2 km around the canal's 90° bend[i]. Deposition at an average rate of 2 cm yr^{-1} occurs in the northern intertidal area and along the shoreline of the mainland. Further results regarding volumetric changes in the morphology of the lagoon are discussed in Chapter 7.

4.3.2 Morphological Features of the Study Area

4.3.2.1 General Morphology

Lido Inlet contains many of the typical features normally associated with tidal inlets (as shown in Figure 4.12) as defined by Hayes (1975). In 1930 it was slightly ebb dominant, although from approximately 1980 the tidal dominance shifted and it is currently slightly flood dominant (ebb/flood ratio is 7:8 during June 2007[ii]; see Figure 4.13) and from observation it appears that the strongest current flows along the deepest part of the channel running adjacent to the southern jetty. An ebb-tidal delta is present at the mouth of the inlet that extends about 4 km into the Adriatic Sea (Amos, 2005; Donde *et al.*, 2008). The delta is skewed to the south-west, in the direction of longshore

[i]This rate is calculated from a 1970-2000 comparison map as the canal was not completed until 1969.

[ii]Data (in hours) from Comune di Venezia.

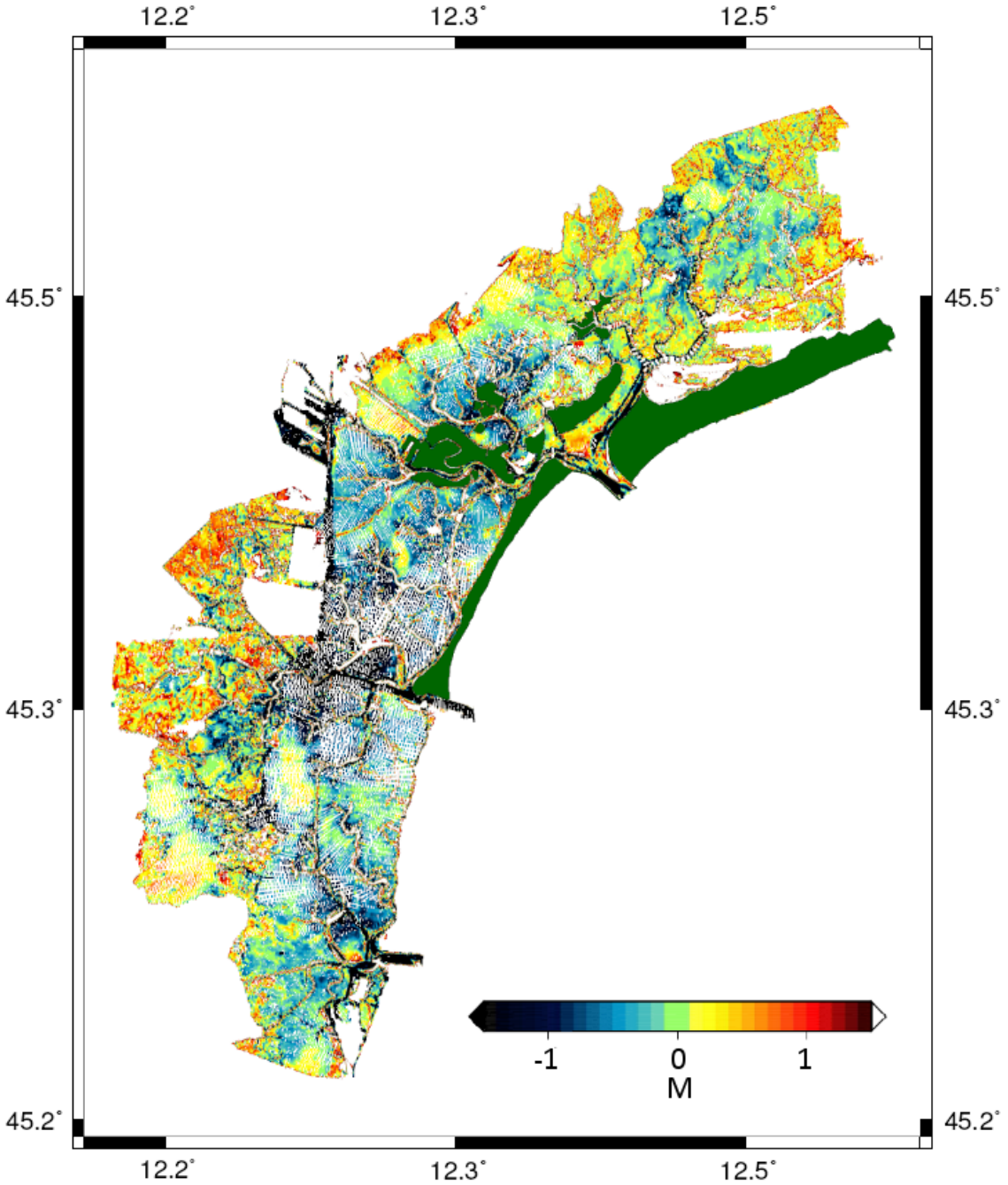

Fig. 4.11: Areas of erosion and deposition in Venice Lagoon between 1930 and 2000. Note deposition in the northern intertidal areas, and erosion around the Petroli Canal extending from Malamocco Inlet.

transport (Gazzi *et al.*, 1973). There does not appear to be any marginal flood channels or channel-margin linear bars. The deepest part of Lido Inlet is adjacent to the southern jetty and is well defined; the maximum depth is around 18 m (MSL) compared to an average depth of approximately 5 m elsewhere in the inlet. There are no channel-margin linear bars within the inlet, although a sub-aqueous ebb tidal spit is attached to Punta Sabbioni extending parallel to the tidal channel for about 1 km. A flood-tidal delta separates Treporti Canal and San Nicolò Canal; whereas the San Nicolò Canal is a continuation of the deep tidal channel and reaches depths of over 20 m, the channel leading into Treporti Canal is shallow at 4 m.

Flood-ramp sand waves are visible on satellite images (see Figure 4.14), which are orientated perpendicularly to the tidal currents and lead up to a shallow area of deposition inaccessible to the boat survey. A bio-stabilised ebb shield is attached to the eastern edge of the delta. Treporti Canal is strongly ebb dominant exhibiting greater discharge (by 14%) and faster average current-speeds than during flood (modelled by SHYFEM as 0.50 m s^{-1} compared to 0.48 m s^{-1} during flood). However, the modelled results (used to calculate the tidal prism) reveal that the flow of Treporti Canal is becoming increasingly flood dominant as ebb currents have decreased at a greater rate than the flood currents (see Figure 4.13 and Table 4.1).

Channel	Date	Ebb	Max Ebb Speed	Flood	Max Flood Speed
Lido	1930	-37.03	-0.78	36.71	0.70
	1970	-37.55	-0.79	37.46	0.73
	2000	-34.97	-0.72	35.23	0.69
Treporti	1930	-32.18	-0.57	27.15	0.59
	1970	-32.95	-0.60	27.93	0.60
	2000	-26.47	-0.50	23.13	0.48
Burano	1930	-22.71	-0.50	25.10	0.42
	1970	-20.33	-0.44	23.92	0.42
	2000	-17.05	-0.37	18.86	0.36

Tab. 4.1: Flow characteristics of Lido Inlet, Treporti and Burano canals (cm s^{-1}). Ebb and flood are calculated from summation of all modelled velocity data over the period of a typical spring tide.

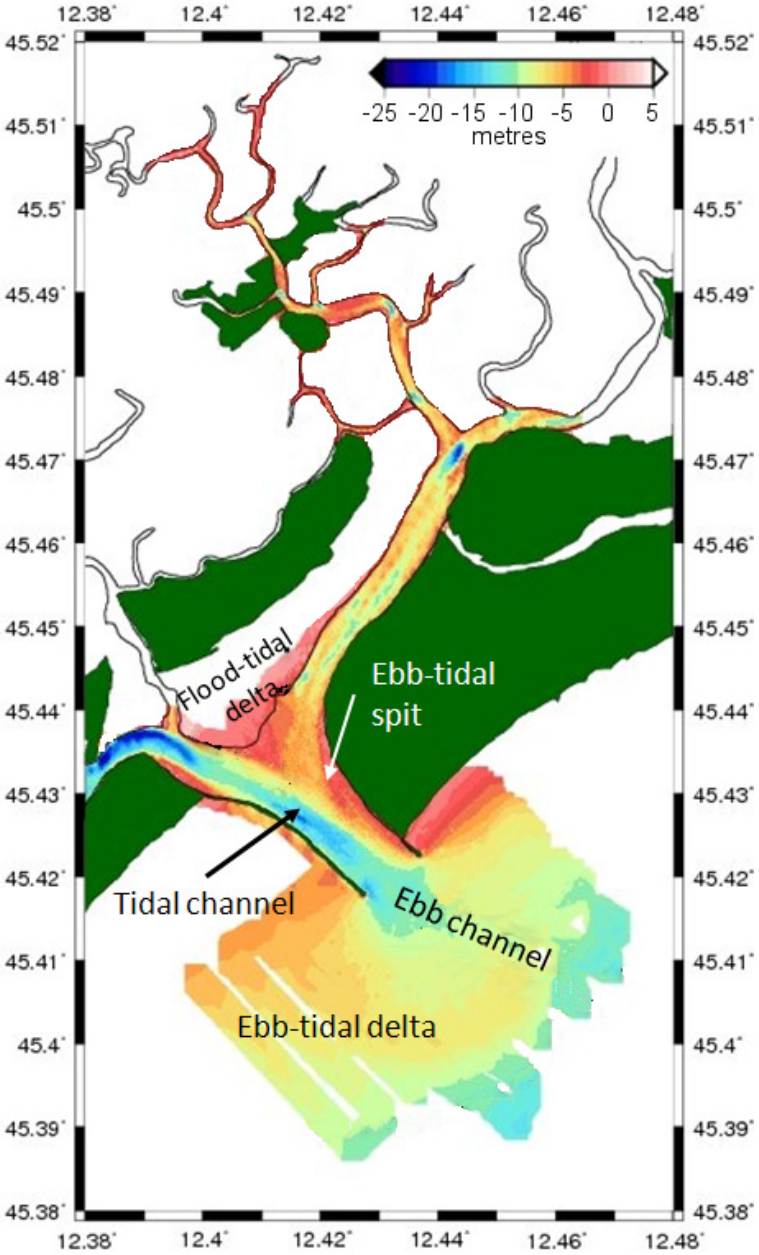

Fig. 4.12: Morphology of the study area showing the tidal deltas.

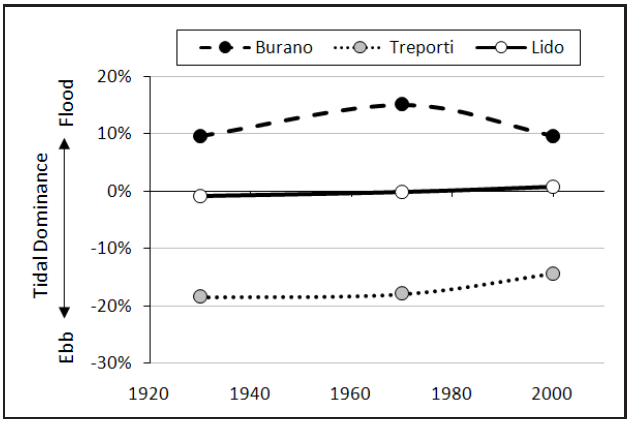

Fig. 4.13: Changes in tidal dominance (ebb discharge to flood discharge ratio) in Lido Inlet, Treporti and Burano canals. The percentage difference in the total discharge in a typical spring tide as modelled by SHYFEM.

Fig. 4.14: Satellite image (from Google Earth) showing the flood delta with sand waves on the flood ramp and a bio-stabilised ebb shield.

The canal has a 10 m deep tidal channel which is bordered by a channel margin linear bar reducing the depth to around 4 m. The deepest part of the canal is at the

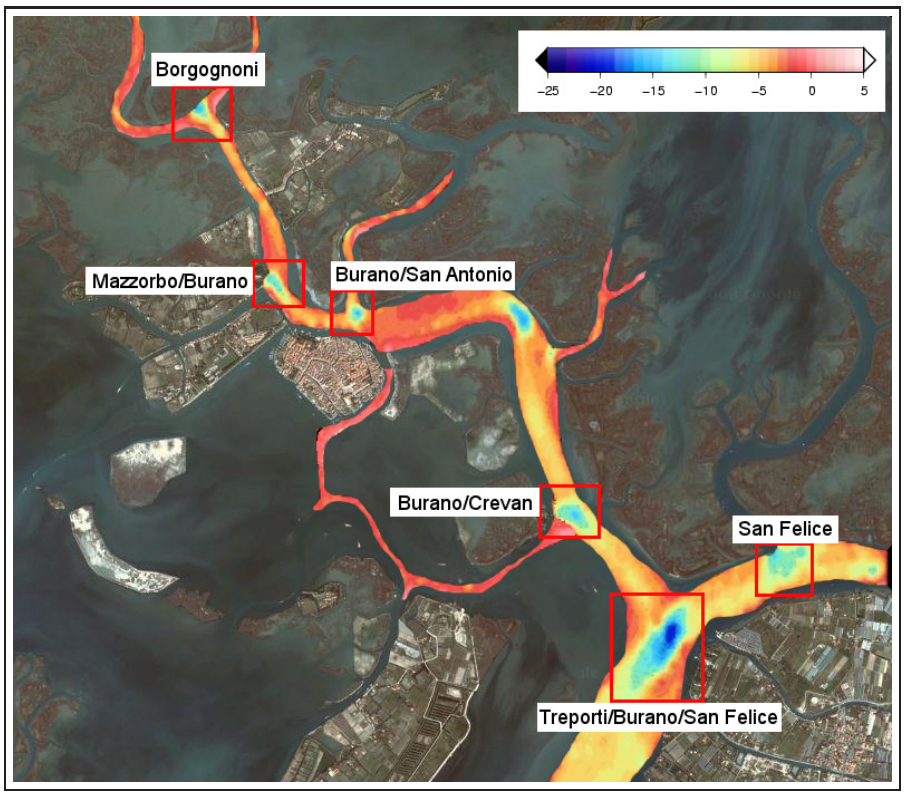

Fig. 4.15: Confluence scour holes along Burano Canal. Bathymetry from 2000 (in metres) with satellite image from Google maps.

junction with Burano Canal and San Felice Canal where a 20 m deep confluence scour hole exists. These confluence scour holes are a significant feature of Burano Canal, appearing at most tributary confluences (see Figure 4.15). They have been referred to as 'triple-junction scour holes' in a study of the region by Amos (2005). The depth of Burano Canal ranges from an average of 6 m at its mouth to 3 m at source, and is up to 15 m deep at the scour holes. Scour is also present half way along the canal where the course changes direction by 90°. Burano Canal is flood dominant, and like Treporti Canal, this dominance is reducing gradually as current speeds have fallen by around 15 to 20% between 1930 and 2000.

4.3.2.2 Morphological Changes: Erosion and Depositional Trends

The tidal channel in the narrowest section of Lido Inlet has deepened by 3 m between 1930 and 2004 (4 cm yr^{-1}). This ebb scour, B in Figure 4.16, extends past the limits of the jetties, with maximum scour (approximately 14 cm yr^{-1}) occurring 500 m off the southern jetty, skewing slightly towards the south west. A second area of erosion

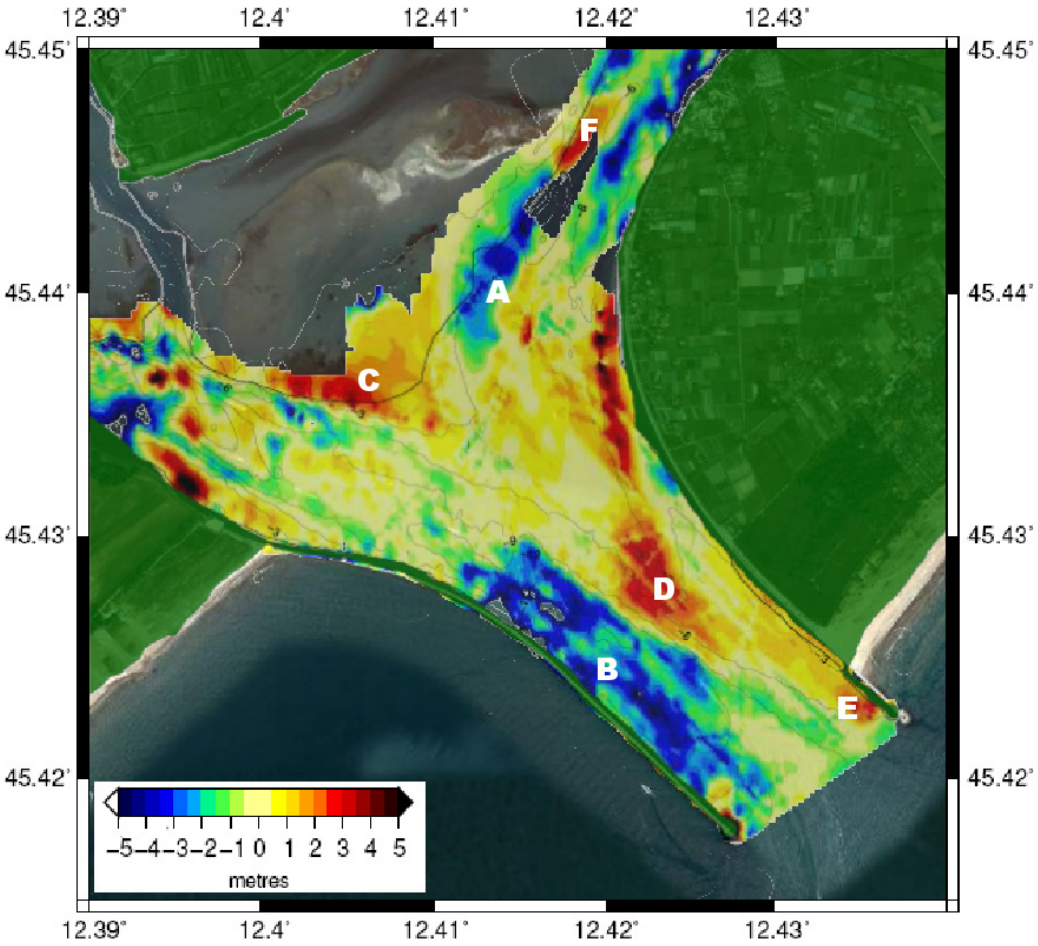

Fig. 4.16: Bathymetric changes in Lido Inlet between 1930 and 2004. Areas of erosion have formed where current flow from Treporti Canal (A) has been altered by deposition on the ebb shield (F), and in the tidal channel (B). Deposition has occurred on the western edge of the flood delta (C), the ebb spit (D) and at the northern jetty where sand enters the inlet (E).

with a relative increase in depth of up to 1 m between 1990 and 2004, exists 2 km to the south east of the jetties, positioned in line with the tidal channel. The ebb-tidal delta lobe begins about 1.5-2 km from the southern jetty, beyond the ebb scour. The delta has experienced deposition of around 10 cm yr^{-1}; sediment has been deposited in a 'half-moon' shape, south-west from the inlet mouth.

Rapid deposition has occurred on the beach side of the northern jetty as water depth has decreased by over 4 m between 1990 and 2004 (Figure 4.17). This deposition is related to the rapid progradation of Cavallino Beach (8.5 m yr^{-1} - Consorzio Venezia Nuova, 1989). If the beach has prograded to the end of the jetty, it is likely that some of its sediment will enter the inlet during a flood tide; a small area of deposition just inside the inlet adjacent to the northern jetty, has appeared since the 1970 dataset was collected, suggesting this has occurred. Deposition has occurred on the large ebb tidal spit within Lido Inlet (Figure 4.16D) at an average rate of 8 cm yr^{-1} between 1930 and 1970. This corresponds to around 387 m^2 of sediment deposited in cross-section

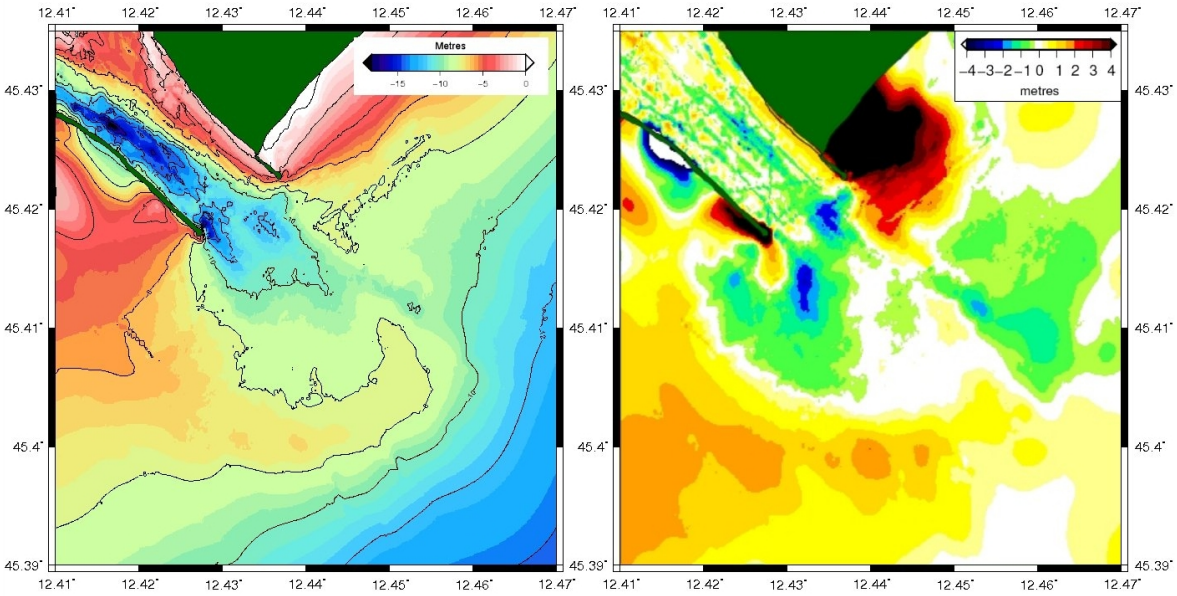

Fig. 4.17: A. The bathymetry of the ebb-tidal delta in 2004 and B. The patterns of erosion and deposition between 1990 and 2004.

2 (see Figure 4.7 for location). Deposition post 1970 has been negligible, with erosion of around 2.5 cm yr^{-1} occurring where the ebb spit extends away from the northern

jetty. Sediment is also being deposited at a rate of 7-8 cm yr^{-1} near to the mouth of Lido Inlet adjacent to the northern jetty (Figure 4.16E). However, this is relatively recent as no significant deposition occurred here prior to 1970. The rest of the inlet has remained stable between 1930 and 2004. The flood-tidal delta has experienced slight deposition on the flood ramp (Figure 4.16C) and the western section of the ebb shield (1 cm yr^{-1}) with a maximum rate of deposition (2.5 cm yr^{-1}) occurring on the western edge of the flood delta. The eastern edge of the flood delta has been severely affected by sediment removal, with water depths increasing around 3 m between 1930 and 2004; a rate of 4 cm yr^{-1}.

Cross sections of Lido Inlet reveal that the tidal channel has deepened by a similar volume (387 m^2; see also Chapter 7) as the ebb spit has gained since 1930 (see Figure 4.18). In 1930, the inlet had a 'u' shaped profile, but since 1970 the depth of the

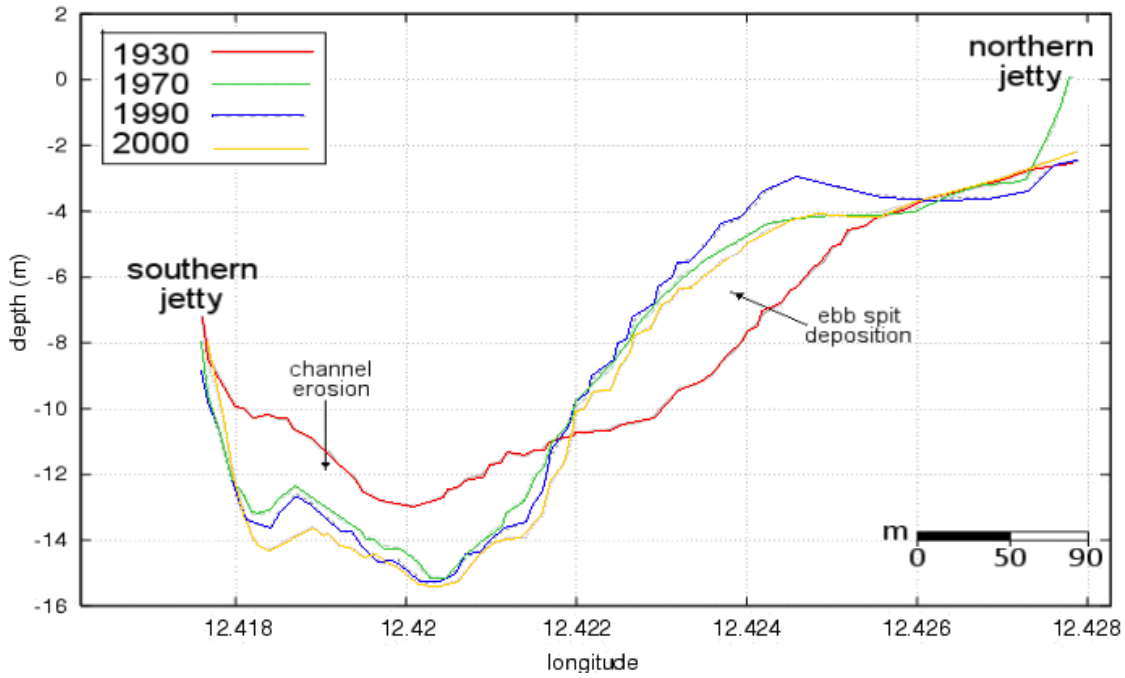

Fig. 4.18: The cross-sectional profile midway up Lido Inlet for the years of 1930, 1970, 1990, and 2000 (MSL).

tidal channel has increased by around 2 m, whereas the area of the ebb spit has become

shallower by an equal volume creating an asymmetric profile. The cross sections also show that the tidal channel is 'v' shaped in contrast to the 'u' of the channel leading into Treporti Canal. The tidal channel has deepened by around a metre between 1930 and 2000, whereas the shallower, northern part of Lido Inlet has a depositional tendency (see Appendix B for all cross sections).

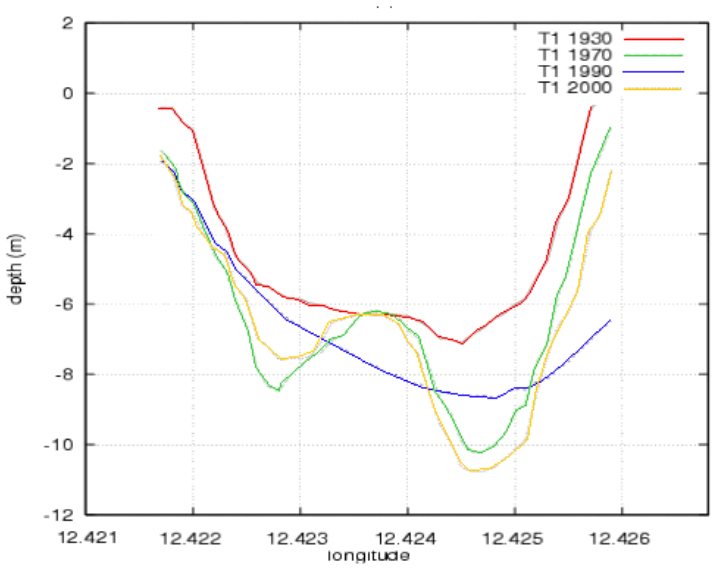

Fig. 4.19: The change in cross-sectional area in the first profile of Treporti Canal (profile 4 in Figure 4.7).

Treporti Canal has become increasingly intrenched between 1930 and 2004 as the channel margin linear bars have remained relatively stable, whilst the water depth in the tidal channel has increased by about 3 m. The cross sections of Treporti Canal show that the channel changed shaped from 'u' shaped in 1930 to 'w' shaped from 1970 due erosion of part of the channel (Figure 4.19).

Burano Canal experienced an average deposition of 4 cm yr^{-1} between 1930 and 1970, although the mouth adjoining Treporti Canal was eroded slightly. After 1970 however, the canal has remained relatively stable, with changes around the scour holes, located at channel junctions. Infilling affected these holes when the canal was depositional; the Mazzorbo-Burano scour hole was reduced to a third of its 1930 size

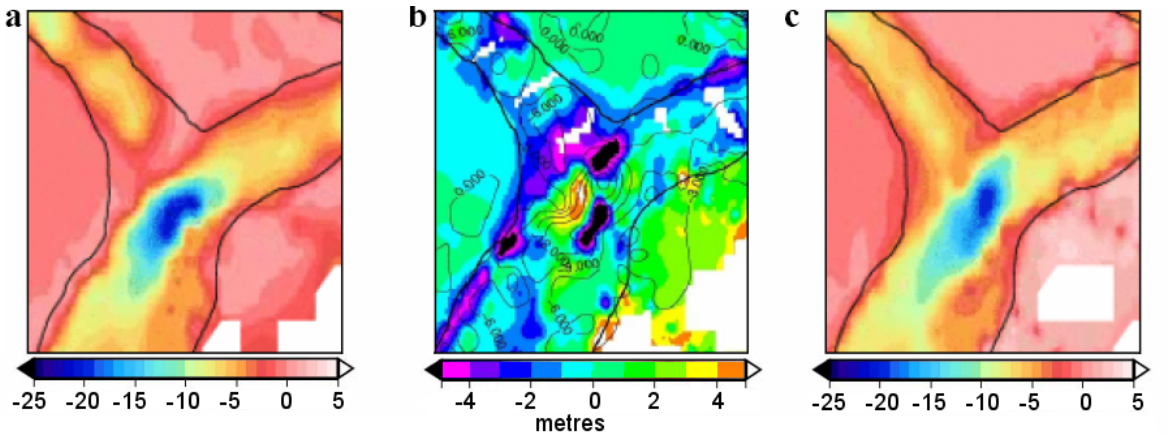

Fig. 4.20: Bathymetry of the confluence scour hole at Burano and Treporti canals: in 1930 (A), a comparison between 1930 and 2000 (B), and in 2000 (C).

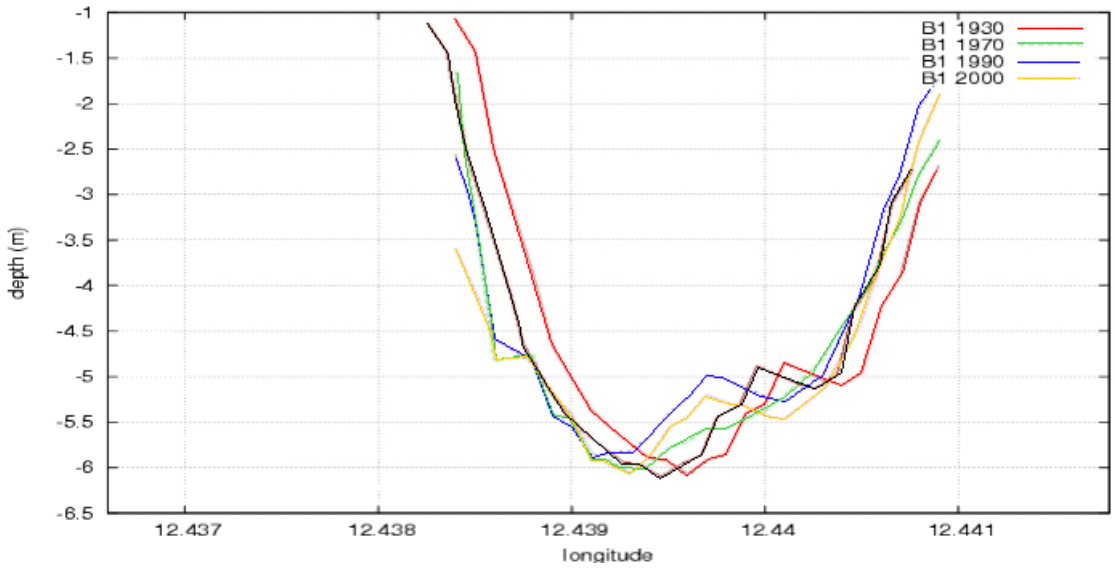

Fig. 4.21: The cross sectional profile at the mouth of Burano Canal showing the channel in 1930, 1970, 1990, 2000, and the position of the 1930 profile (black) assuming error in the positioning of the 1930 dataset.

by 1970. The confluence scour hole between Treporti and Burano canals experienced a decrease in water depth (deposition) of 4 m on its western edge between 1930 and 2004 and an increase of over 5 m depth (erosion) on its northern and eastern edges in the same time frame (see Figure 4.20). Direct comparison of the bathymetry from both

these years show the scour hole has become streamlined with the dominant flow (see Figure 4.20). The cross sections of Burano Canal show that the 1930 profile is offset in comparison to subsequent profiles (see Figure 4.21), which have remained relatively stable in terms of depth and profile shape. This suggests that the canal may have shifted its position.

4.3.3 Tidal Prism

Different methods of calculating the tidal prism were compared (results shown in Figure 4.22). The direct discharge equation (Equation 4.9) compared favourably (within 2.6%; $\sigma = 4.5\%$) with the trapezoidal calculation favoured by Seabergh (2002) of the U.S. Army Corps of Engineers (Equation 4.8). The velocity method of O'Brien (1969) (Equation 4.9) differs by over 10% when compared to the direct discharge calculation in Lido Inlet despite being similar to the results for the Treporti and Burano canal profiles ($\sigma = 15.6\%$). For this reason, the U.S Army Corps discharge method (Equation 4.8) was used to calculate the tidal prism as it appears to provide a better fit than the velocity method and is simpler than the direct discharge calculation.

The ratio of the tidal prism and cross-sectional area (CSA) in 1990 shown in Figure 4.23A, reveal that the cross-sections were on average, 29% larger than predicted by the O'Brien relationship. However, the profiles in Treporti increased by an average of 7% between 1970 and 2000 though some deposition occurred between 1990 and 2000. Also, Lido Inlet remained relatively stable between 1990 and 2000 despite needing to reduce its cross-sectional area by a minimum of 20% to be stable according to the O'Brien relationship. Larger cross section/tidal prism ratios are indicative of the Pacific coast inlet relationship described by Jarrett (1976) and so were compared with the cross-sectional profiles from the current study. These results are shown in Figure 4.23B. The data from Venice Lagoon (green diamonds) fit the relationship for Atlantic coast inlets (blue line) better than the relationship of O'Brien (red dashed line). Burano Canal has a relatively large cross-sectional area for the tidal prism, even when compared to the Atlantic relationship. However, it does fit a relationship for inner harbour entrances (dotted blue line in Figure 4.23B) formulated by Le Conte (1905).

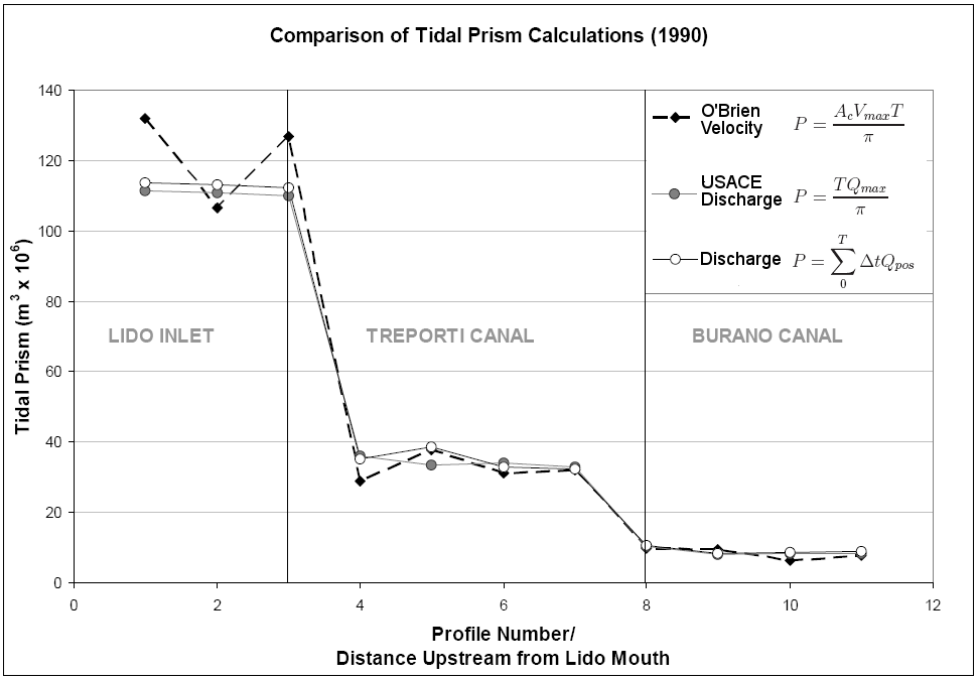

Fig. 4.22: A comparison between methods of tidal prism calculation

The stability over time of the northern Venice Lagoon canals was determined by repeating the analysis with bathymetry data from 1930, 1970, and 2000 to provide answers to two important questions; has the tidal prism changed within the last 70 years, and are the tidal channels stable? The model results show the tidal prism to be relatively stable, albeit with an increase in 1970. As the results are similar in 1930, 1990, and 2000, it may be that the 1970 data is an outlier (see Figure 4.24). Profiles 2 and 3 (well within Lido Inlet - see Figure 4.7) have remained stable between 1930 and 1970 in terms of cross-sectional area, but experienced change by 2000; profile 2 increased its cross-sectional area by 3%, whilst profile 3 experienced a decrease of 3%. Profile 1 agreed with the results of Tambroni *et al.* (2005), and experienced a 7% increase in its cross-sectional area between 1930 and 1970 before gradually infilling and returning to its 1930 dimensions. This prompts the question; why was the cross-section significantly larger in 1970 if subsequently the cross-sectional area returned to previous dimensions and thus, is returning to an equilibrium level? The results from the tidal

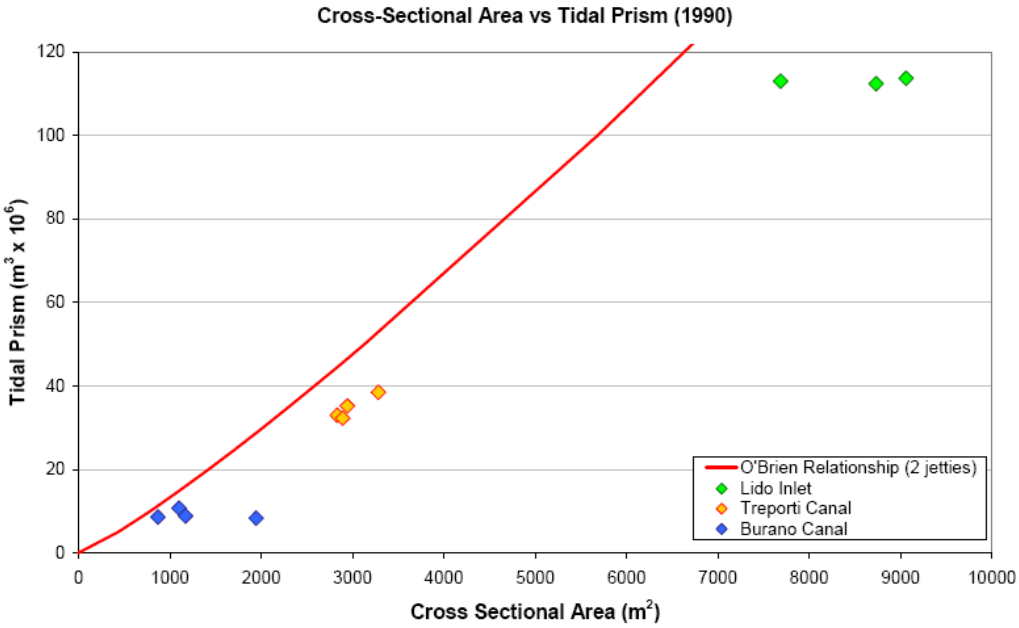

(a) Cross-sectional area against tidal prism of 11 profiles in the Lido Inlet-Treporti-Burano canal system of northern Venice Lagoon; a comparison with the O'Brien (1931, 1969) relationship.

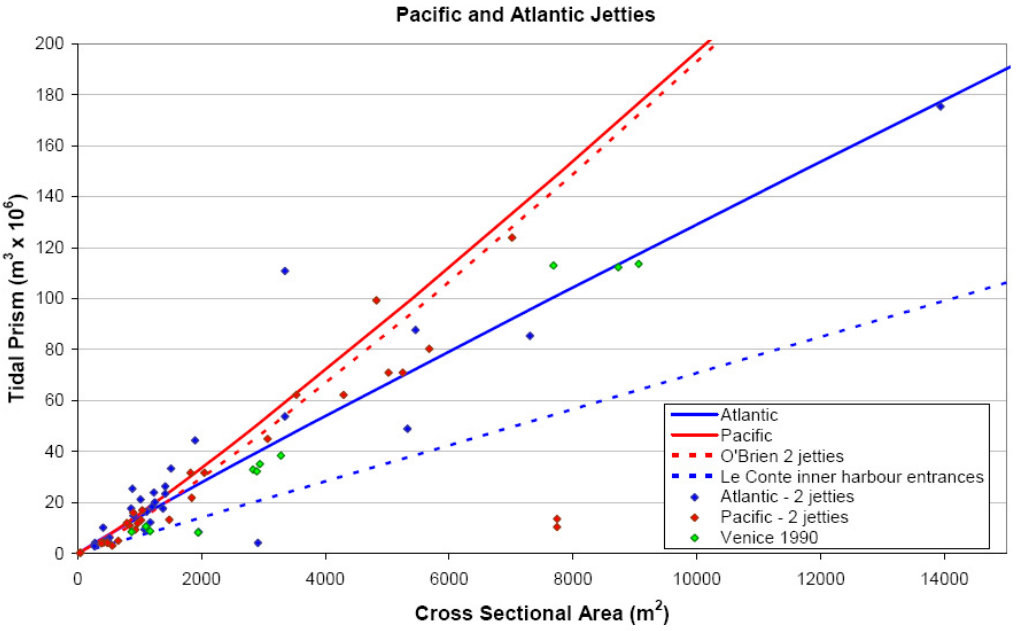

(b) The tidal prism and cross-sectional area data from Venice in comparison to data from jettied tidal inlets on the Pacific and Atlantic coasts. The relationships of Le Conte, 1905, Jarrett, 1976 and O'Brien, 1969 are also plotted.

Fig. 4.23:

prism calculations also show an increase of 2% (an extra 8,633,000 m^3) in the total volume of tidal water entering and leaving profile 1 between 1930 and 1970, although by 2000, this had returned to the same tidal prism as seen in 1930 (see Figure 4.24).

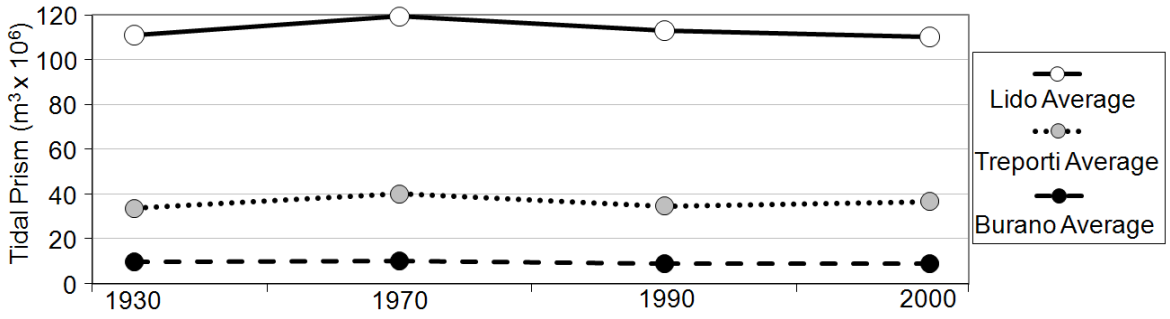

Fig. 4.24: Tidal prism calculations for 1930, 1970, 1990, and 2000. Note the outlying increase for 1970.

Location		CSA (m^2)				Tidal Prism ($\times 10^6$ m^3)			
Channel	Profile	1930	1970	1990	2000	1930	1970	1990	2000
Lido	1	8709.33	9317.28	9058.65	8684.25	111.38	120.00	113.66	111.00
	2	7770.25	7659.26	7682.75	8019.49	111.08	119..44	113.02	110..33
	3	9007.46	9048.95	8728.82	8743	110.03	118.86	112.36	109.65
Treporti	4	2036.58	2792.57	2940.01	2929.28	33.73	40.51	35.19	37.31
	5	2506.21	2871.00	3280.73	3154.92	36.99	43.82	38.45	39.93
	6	2555.67	2724.50	2829.45	2965.00	32.39	38.48	32.96	35.61
	7	2619.69	2445.56	2890.80	2662.55	31.59	37.85	32.26	34.23
Burano	8	1096.62	1141.95	1099.53	1152.99	11.08	11.47	10.68	9.53
	9	1634.93	2004.99	1942.45	1885.55	9.42	9.50	8.28	8.50
	10	972.60	895.56	866.81	993.62	8.68	9.47	8.56	8.92
	11	1082.21	972.71	1168.91	1221.29	9.59	10.12	8.83	9.27

Tab. 4.2: Cross-sectional area and tidal prism for each profile.

The tidal prism/cross-sectional area relationship was also calculated for the other two inlets of Venice Lagoon (Malamocco and Chioggia) as they are thought to drain hydraulically separate basins (the northern, central and southern basin - Serandrei Barbero *et al.*, 1999; Solidoro *et al.*, 2004) but have similar tidal and geological characteristics so should be directly comparable to Lido Inlet (Figures 4.26A & 4.26B). Both the cross-sectional area and tidal prism calculations for Malamocco Inlet reflect the artificial deepening of the channel for the Petroli Canal, however it appears that equilibrium values may now have been reached 30 to 40 years after construction. However, this equilibrium is not in agreement with the O'Brien relationship as the cross-sectional area is much smaller than expected (Figure 4.26B). The tidal prism in Chioggia Inlet is gradually increasing (by almost 1 million m^3 between 1930 and 2000), as is its cross-sectional area (by 1000 m^2 in the same time frame). This is the only inlet that has reached equilibrium according to the relationship of O'Brien, although its continually changing state suggests that it is not stable.

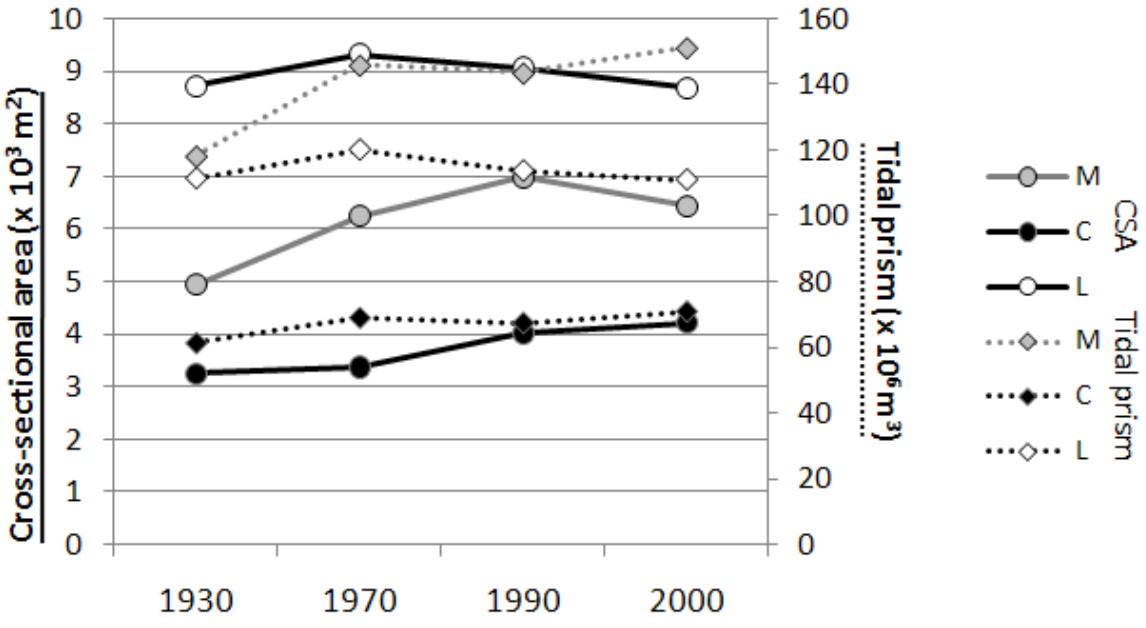

Fig. 4.25: Tidal prism (dotted lines) and cross-sectional area (solid lines) for Malamocco (M; grey), Chioggia (C; black) and Lido (L; white) inlets.

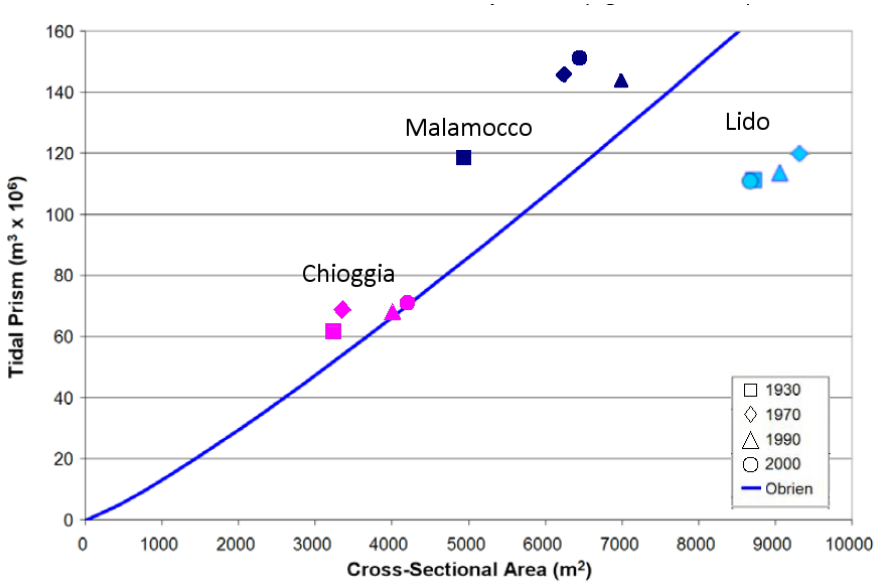

(a) The tidal prism/cross-sectional area relationship of the three inlets of Venice Lagoon Lido, Malamocco, and Chioggia.

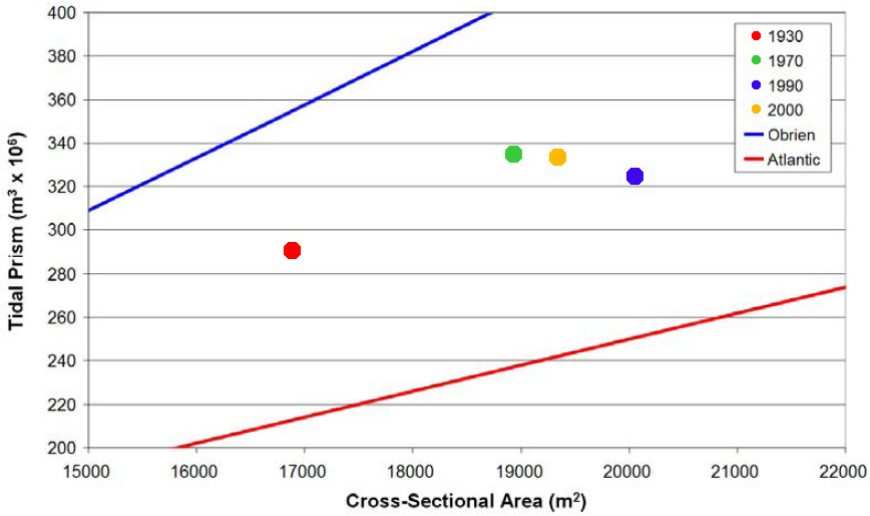

(b) The summed tidal prism and cross-sectional area of the three Venice Lagoon inlets in 1930, 1970, 1990, and 2000. Shown with the O'Brien relationship and the Atlantic relationship (after Jarrett, 1976).

Fig. 4.26: Cross-sectional area/prism relationships.

4.3.4 Seabed Texture and Classification

The mapped results of corrected reflectivity are shown in Figure 4.27A. Areas of high reflectivity are located around the southern jetty, along Cavallino Beach and extend

into Lido Inlet around the northern jetty, as well as the confluence between Treporti Canal and Lido Inlet. The lowest reflectivity is found off Cavallino Beach, extending around the area of high reflectivity off the southern jetty.

Collier and Brown (2005) state that backscatter is generally positively correlated with mean grain size although in the present study, the coefficient of error (R^2) of the regression is very low (0.05) so the likelihood of using backscatter to accurately determine grain size in this case is limited. However, direct comparison between the reflectivity and grain size maps (see Chapter 5 for more information and diagrams), show that there are some similarities. The area of low reflectivity (Figure 4.27A) is located in the region of the mudbelt described by Albani *et al.* (1998) but also where very fine sand has been sampled during this study (see Figure 5.10B and 4.27B). The area of high reflectivity (4.27A) corresponds to areas with gravel or high sand content. This is not the case in area D on the flood-tidal delta, which has high reflectivity but is composed of muddy sand. The area is however, much shallower and intertidal.

A summary diagram of the 'seabed classification' is shown in Figure 4.27C. The sediment type and reflectivity are analogous, showing a low energy environment (fine sand and low reflectivity) to the south east of the inlet mouth and a high energy environment (high reflectivity and coarse sediment) near the flood-tidal delta. There is some agreement to where scour (high energy) occurs at the southern jetty, but it is not well defined compared to the other areas of low and high energy environments (defined on Page 58).

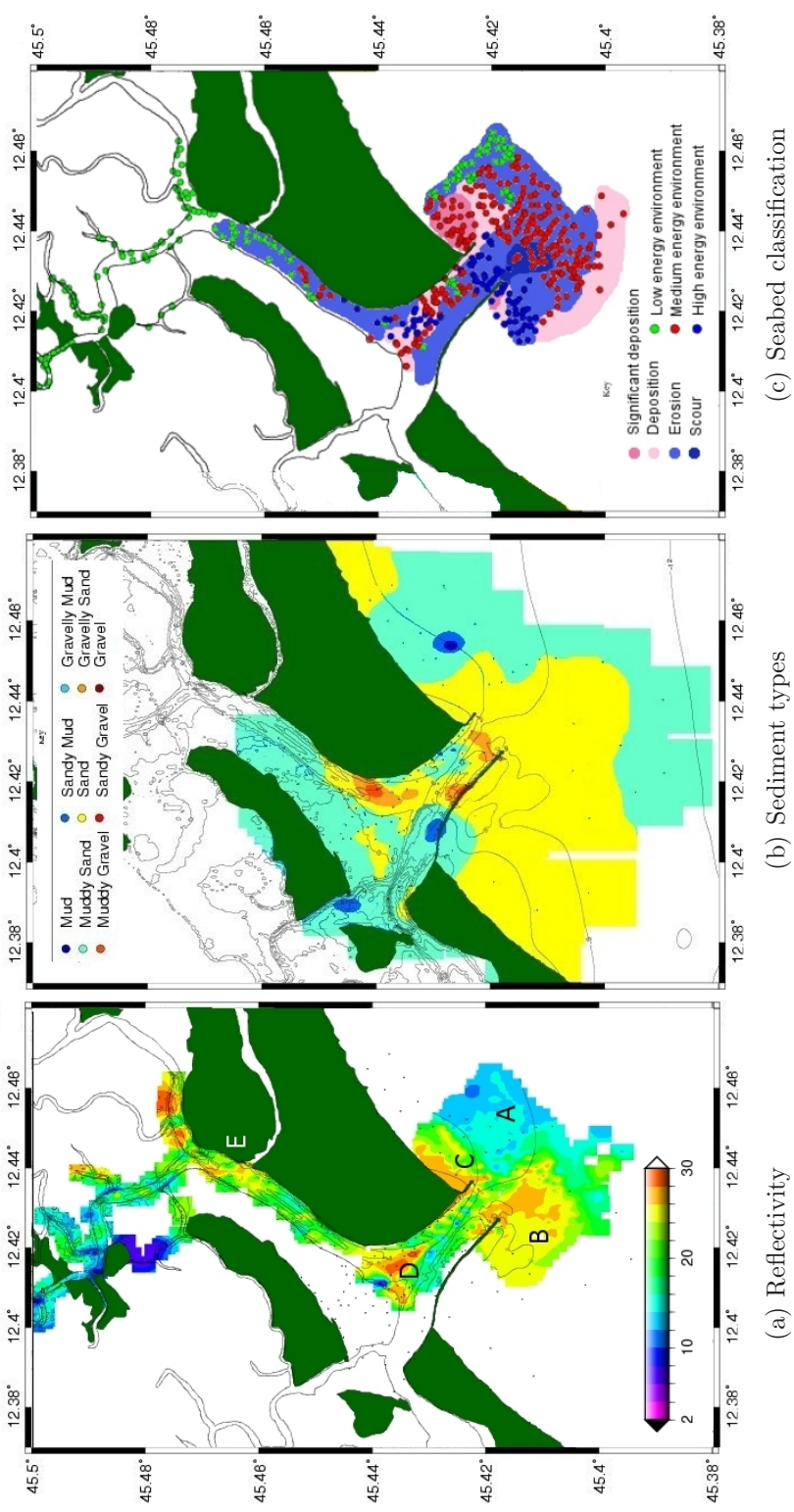

(a) Reflectivity (b) Sediment types (c) Seabed classification

Fig. 4.27: (a) Depth corrected reflectivity from sidescan sonar in I_R arbitrary units; blue is low reflectivity, red is high reflectivity. Significant features include (A) the mudbelt, (B) ebb delta and scour, (C) import of beach sediment, (D) Treporti scour and (E) a possible sediment jet from Podeglio Canal. (b) Sediment type around Lido Inlet. (c) Seabed classification showing ambient energy and bathymetric change.

4.4 Discussion

4.4.1 Lagoonal Morphology

Venice Lagoon is separated from the Adriatic Sea by sandy barrier islands, which are divided by three tidal inlets through which sediment and water exchange occur. Few rivers drain into the lagoon and so the morphology is primarily driven by marine processes. Wind-driven current and waves are also an important factor due to the size of the lagoon (Umgiesser, 1997), although longshore drift (Gazzi *et al.*, 1973) has an effect on morphology outside.

Venice Lagoon has suffered severe erosion at least since 1930. This is significant as the average depth of the lagoon is only 1 m (Consorzio Venezia Nuova, 1996). The greatest degree of erosion has occurred around the Petroli Canal, which was constructed between 1952 and 1969 to allow passage of oil tankers from the Adriatic Sea to the mainland industrial port of Marghera (see Figure 4.11). This dredging, combined with significant subsidence (Gatto and Carbognin, 1981), has altered the current hydrodynamics and increased the Malamocco Inlet tidal prism by 28% between 1930 and 2000 (from 1.18×10^8 to 1.51×10^8). This increase in the volume of water entering into this canal has caused erosion (Gatto and Carbognin, 1981; Ravera, 2000). Waves generated by the tankers and other boat traffic have exacerbated this erosion by scouring the fine sediment of the mudflats and salt marshes surrounding the Petroli Canal (Ciavola *et al.*, 2002). In total, these effects have caused bed elevation to decrease at a rate of 10 cm yr^{-1}.

The edges of the lagoon as well as most of the northern basin have experienced accretion between 1930 and 2000. Some of this deposition was artificial; the result of attempts to protect the salt marshes (Scarton *et al.*, 2000; Fletcher and Spencer, 2005). However, work by Cappucci *et al.* (2004) and Day *et al.* (1999) reveal that rapid deposition is occurring naturally in the northern basin.

4.4.1.1 Morphological Features of the Study Area

The predominant feature in the nearshore off Lido Inlet (outer Lido) is an asymmetrical ebb-tidal delta that is skewed to the south-west in the direction of longshore transport as defined by Gazzi *et al.* (1973). The skew suggests that longshore currents exceed the effects of tidal currents, which enhance the seaward growth of the delta (van Leeuwen *et al.*, 2003). Comparison between the bathymetries of 1990 and 2004 reveal that the outer part of the ebb-tidal delta has accreted by a maximum of 2 m between 1990 and 2004, whilst the inner part, directly adjacent to the mouth of Lido Inlet, has eroded by about 1 m. Figure 4.28 shows that this is because the delta has expanded seawards (Stauble, 1998). Growth is also indicated by an increase in width of the 8 m contour (the thickest part of the delta), suggesting that an increased volume of sand is being stored within the delta. Marino and Mehta (1987) and Hicks and Hume (1996) note that ebb-tidal delta growth is linked to an increase in the tidal prism, a decreasing inlet width/depth ratio and decreasing wave energy, and that a seaward extension of the delta is linked with only with decreasing wave energy. The ebb delta of Lido Inlet has appeared since the construction of the jetties in the early 20th Century (Amos, 2005; Fontolan *et al.*, 2007); the width/depth ratio has reduced from 320:1 just after construction, to 80:1 in recent years (data from MAV-CVN, 1992; Tambroni and Seminara, 2006a - see Figure 3.6), altering the cross-sectional area/tidal prism relationship to cause scour. The change in wave energy is unknown, although the both the intensity and frequency of bora wind events has reduced due to warmer temperatures in the polar regions (Pirazzoli and Tomasin, 1999), resulting in a decrease in bora-generated waves. This could decrease wave energy in the north Adriatic and thus enhance the expansion of the ebb-delta seawards (Marino and Mehta, 1987).

Scour has occurred at the mouth of Lido Inlet extending from the tidal channel (Figure 4.16B), to a kilometre offshore. The seabed has deepened by 2 m here between 1990 and 2004; this has been caused by the ebb-jet, a high velocity flow formed due to constriction of ebb currents by the jetties, able to erode sediment (Joshi, 1982). As the flow starts to weaken when the ebb jet is no longer constricted beyond the jetties, the suspended sediment becomes influenced increasingly by the longshore current and sand begins to be deposited to the south-west onto the ebb-tidal delta as velocity drops

below the suspension threshold (Joshi, 1982). Fine sediments are transported further into the offshore mudbelt (Albani *et al.*, 1998). The composition of the ebb delta is therefore likely to be a mix of lagoonal sands and beach/river sands from the north (longshore transport); this will be discussed further in Chapter 5.

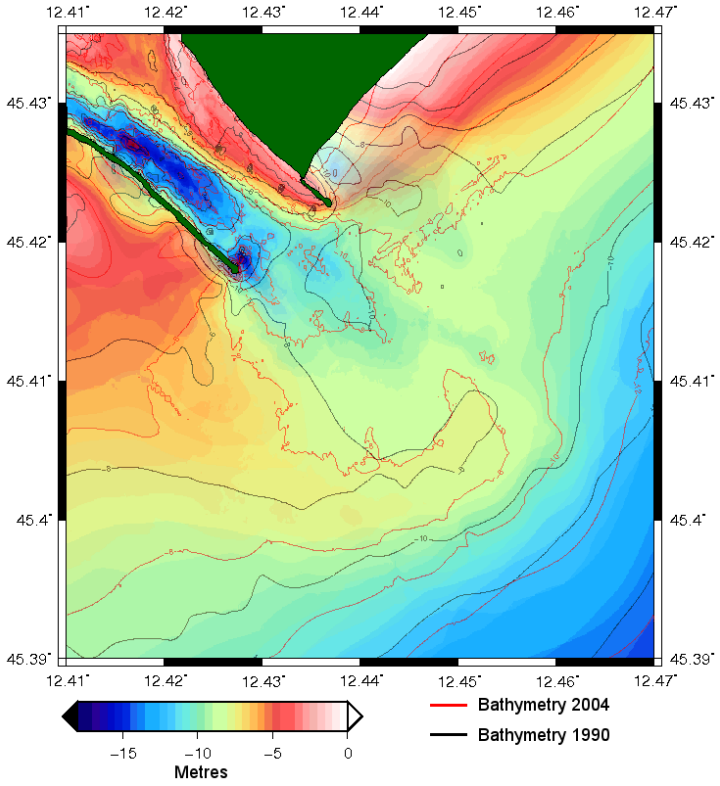

Fig. 4.28: The bathymetry of the ebb-tidal delta area in 1990 (black contours) and 2004 (red contours), showing the seawards migration of the delta.

Lido Inlet is slightly flood dominant. The strongest currents flow along the deepest part of the channel, which leads into the San Nicolò Canal towards Venice. The channel has experienced scour averaging 4 cm yr^{-1} between 1930 and 2000 in the region of fastest velocities (see Chapter 6 for velocity profiles), thus it is this region that has the greatest potential for sand transport. The ebb spit extending from Punta Sabbioni on the northern side of the inlet has accreted by 4 m between 1930 and 1970 in proportion to the scour in the flood channel. Thus Lido Inlet is stable in terms of

its cross-sectional area (which has changed by 1%) despite these large changes in shape (Figure 4.18). The inlet morphology post-1970 has remained relatively unchanged so these two features are probably interlinked. It may be that the channel was deepened by dredging to accommodate the large cruise ships travelling to Venice. The ebb spit has built up naturally as a response, according to the tidal prism relationship proposed by O'Brien (1931). Between 1970 and 2004, the water depth decreased by around 2 m in the area adjacent to the northern jetty (Figure 4.16E). This suggests that sediment is entering the inlet at this point by longshore transport, as Cavallino Beach has prograded at an average rate of 20 m yr^{-1} (see Figure 3.6) since the jetties were built and has now reached the tip of the northern jetty. The beach sand first started to enter the inlet between 1970 and 1990 as between 1930 and 1970 there was no sand accumulation adjacent to the northern jetty.

A flood-tidal delta is attached to the southern shoreline of Sant'Erasmo island at the landward end of Lido Inlet. An ebb shield is present across the back of the flood delta (although not attached to the shore of Sant'Erasmo), the eastern edge of which is bio-stabilized (as shown by Figure 4.14) suggesting that this area has experienced the weakest tidal flow. There are at least two washover lobes; one in the middle of the shield, which looks as if may have been breached during storm activity as the shield is about 200 m wide at this point. The second is at the western extreme. Small spits also occur to the eastern edge of the shield, pointing to the west away from Treporti Canal. This suggests that the channel dividing the island of Sant'Erasmo and the delta is ebb dominant, but that Treporti Canal is flood dominant (which is the case - see Figure 5.18 and Umgiesser *et al.*, 2006). Between 1930 and 2004, the flood delta accreted approximately 2 cm yr^{-1} , although on the western edge (Figure 4.16C) the average depositional rate was in general double that. It also appears that the eastern bio-stabilized ebb shield is extending into Treporti Canal causing a redirection of current to scour the inlet edge of the delta (Figure 4.16F). This accounts for a maximum increase of 4 m in water depth in this location.

4.4.1.2 Treporti and Burano Canal Morphology

Treporti Canal is erosional; between 1930 and 2004 the erosion rate was up to 1 cm yr^{-1} on the channel margin linear bars and 5 cm yr^{-1} within the main channel. The flow of Treporti Canal has been diverted by the ebb shield to erode the south eastern edge of the flood delta. The peak flow from Treporti continues along the tidal channel of Lido Inlet (Chapter 5) and is directed away from the ebb spit. This flow direction was probably instrumental in the formation of the ebb spit due to reduction in current speed as the channel widened upon entry to Lido Inlet.

Burano Canal has been infilling at an average rate of 2 cm yr^{-1} between 1930 and 2000. Most of this deposition occurred between 1930 and 1970, with the canal stabilising post 1970. The cross sections show that the southern part of the canal (see Appendix Figure B.4(a)) has migrated around 30 m to the west. Erosion of the banks has increased the cross-sectional area, especially between 1970 to 2000, and is probably indicative of increased wave height due to boat traffic (Day *et al.*, 1998; Ravera, 2000; Fletcher and Spencer, 2005). Eroded sediment has decreased the water depth of Burano Canal and partially infilled the confluence scour holes. These scour holes suffered erosion along the upstream side between 1930 and 1970 (as seen on the bathymetric maps), therefore Burano Canal may have been flood dominant at this time. The removal of this sediment post 1970, and the erosion of the triple junction scour holes in the downstream direction, suggest that Burano Canal has become ebb dominant, and thus more efficient at exporting sediment (Walton, 2002). This is supported by the fact that the largest scour hole within Burano Canal (Burano-Crevan, near to the Treporti Canal confluence; Figure 4.15) was a eroding when Burano Canal was infilling and accreting when Burano Canal eroded.

Vertical accretion of 4 m of sediment on the western edge of the confluence scour hole of Treporti, Burano and San Felice canals has been balanced by erosion of around 5 m of sediment along the northern and eastern edges. This is mainly a transformation of shape, as the scour hole became more streamlined with the flow from Treporti Canal. Figure 4.20A shows the original 'dogleg' appearance of the scour hole in 1930, while Figure 4.20C shows a straighter shape in 2000 as the scour increasingly

responds to discharge coming from Burano, causing the orientation to shift to bisect the confluence angle (Bridge, 2003). This is despite overall discharge (as modelled by SHYFEM) falling between 1930 and 2000 in Burano, San Felice and Treporti canals.

4.4.2 Tidal Inlet Stability

The canals of northern Venice Lagoon do not fit the O'Brien relationship; only 5 data-points fall within 10% of the predicted cross-sectional area and half of the data-points have a cross-sectional area at least 25% larger than predicted. If the O'Brien relationship is assumed to be valid then the canals, especially Lido Inlet, should be depositional. Table 4.3 shows the change in area of each cross-section between 1930 and 2000 and shows that, by contrast, all the cross-sections have increased in size (i.e. erosion has occurred) by an average of 9% between 1930 and 2000.

Lido Inlet was accretional between 1970 and 2000, which reduced the average cross-sectional area by 2%. However, the average cross-sectional area should have decreased by an average of 25% to become stable according to O'Brien's relationship. As the cross-sectional areas of Lido Inlet haven't altered by more than 7% between 1930 and 2000, it would appear that the inlet is already relatively stable, so why does O'Brien's relationship not fit with this data? Jarrett (1976) proved that the inlets on the Atlantic coast did not fit with O'Brien's relationship, although they still conformed to the theory that tidal prism and cross-sectional area are linked. A new relationship, defining a larger cross-sectional area for a given tidal prism was formulated. This difference in cross-sectional areas may be a result of the local wave climate; the Pacific Ocean has a much larger mean wave height than the Atlantic Ocean, and therefore greater wave energy and, as Jarrett (1976) explains, littoral sand transport. Consequently, more sediment is transported into the Pacific inlets. This creates a smaller cross-section than would be expected for an equivalent inlet on the Atlantic coast. Another explanation could be the inlet width to hydraulic radius ratio ($R_h = A_c/P_w$). This is generally smaller for the Pacific inlets, indicating a narrow, deep, and thus more hydraulically efficient channel than the wide, shallow inlets on the Atlantic coast. Jarrett reasons that this allows the Pacific inlets to accommodate more water (i.e. a larger

Profile	Date			
	1930-2000	1930-1970	1970-1990	1990-2000
1	0%	7%	-3%	-4%
2	3%	-1%	0%	4%
3	-3%	0%	-4%	0%
Lido Average	0%	2%	-2%	0%
4	30%	27%	5%	0%
5	21%	13%	12%	-4%
6	14%	6%	4%	5%
7	2%	-7%	15%	-9%
Treporti Average	17%	10%	9%	-2%
8	5%	4%	-4%	5%
9	13%	18%	-3%	-3%
10	2%	-9%	-3%	13%
11	11%	-11%	17%	4%
Burano Average	8%	1%	2%	5%
Total Average	9%	4%	3%	1%

Tab. 4.3: The change in the area of each cross section (%). Blue (-ve) values indicate deposition, and red (+ve) values indicate erosion.

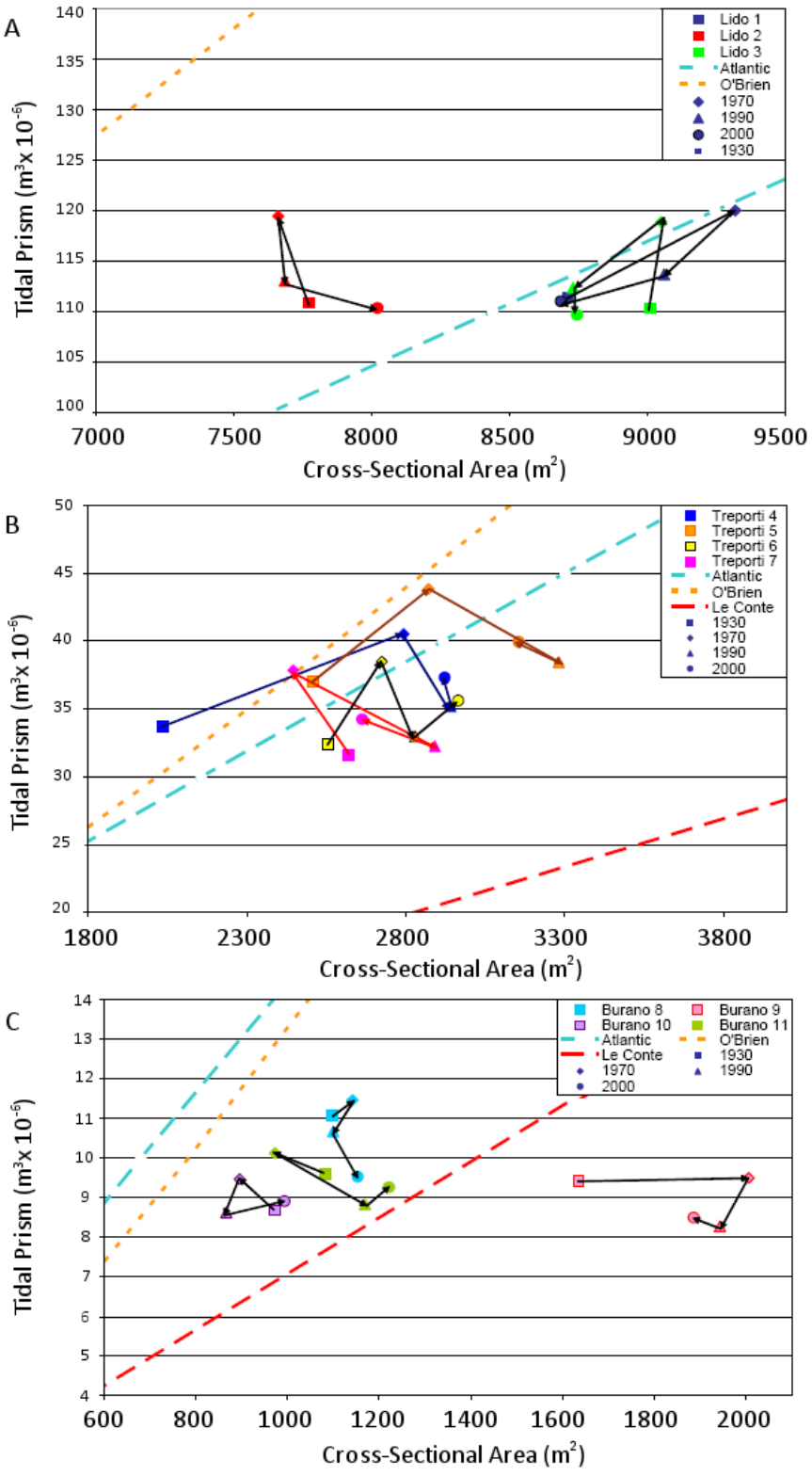

Fig. 4.29: Change in the tidal prism/cross-sectional area for Lido Inlet (A), Treporti Canal (B), Burano Canal (C) and comparison with the O'Brien's, 2 jetty relationship, and Jarrett's Atlantic relationship (for locations see Figure 4.7).

tidal prism) than their Atlantic counterparts. The lack of change in the bathymetry over the last 40 years indicates that Lido Inlet is probably stable (see Table 4.3); this is confirmed by the correspondence to the Atlantic relationship (see Figures 4.23B & 4.29A). Treporti Canal was net erosional between 1930 and 2000, although this incorporates a period of slight accretion between 1990 and 2000 (see Table 4.3). Treporti Canal fits the Atlantic relationship fairly well also, and is in equilibrium in relation to this (as the tidal prism changes, a corresponding change in cross-sectional area occurs). However, it cannot be defined as stable as the canal has lost 2-3 cm yr^{-1} over the last 70 years; it is clearly unstable in terms of bed level.

Burano Canal does not fit either O'Brien's relationship or Jarrett's Atlantic relationship. This not unexpected as Burano Canal is sheltered from the waves that effect inlets such as Lido. Le Conte (1905) created a formula for inner harbour entrances, which takes into account the circumstances of a tidal channel further from the open sea. The data from Burano (discounting the data form Profile 9, which extends across a confluence scour hole) appears to fit this relationship. Between 1930 and 1970, when Burano Canal was eroding slightly (but becoming increasingly flatter through deposition in the channel) and flood dominant (Helsby *et al.*, 2005, Table 4.3), it appeared to move towards the Atlantic relationship line by depositing sediment whilst the tidal prism increased. However, post 1970, Burano Canal experienced a greater degree of erosion, which increased the cross-sectional area. With a concurrent reduction in the tidal prism (Table 4.2), the relationship increasingly followed the line of Le Conte (1905). Profile 11 became stable according to Le Conte's relationship (Le Conte, 1905) in 1990, and responded to the change in tidal prism by the removal of a proportionate amount of sediment to remain that way. Therefore, it seems likely that, for the last 30 years, that Burano Canal has responded to the Le Conte inner harbour relationship and is eroding in order to reach stability.

4.4.3 Error in the Method

Error in the calculation of cross-sectional area or tidal prism is likely to be fairly high due to poor resolution of bathymetry data (especially in 1930 and 1970) and the

positioning of the profiles (using SHYFEM nodes increased the accuracy of the tidal prism calculations but may not have been positioned in the same position or orientation as profiles used for previous work - Fontolan *et al.*, 2007; Tambroni *et al.*, 2005). Modelling the tidal prism may produce error, even though SHYFEM has been well calibrated (Umgiesser, 1997). To estimate the error the results of Fontolan *et al.* (2007) and Tambroni *et al.* (2005) are compared with the results from this study. The cross-sectional area of Chioggia (deemed to be stable according to O'Brien's relationship by this study and that of Fontolan *et al.*) is within 3% of estimates by Tambroni *et al.* (2005), although Fontolan *et al.* (2007) proposes a cross-sectional area (and tidal prism) 15% larger than this. Estimates of the cross-section of Lido are larger by 8% in the current study over those of Fontolan *et al.*; however, the calculated tidal prism is also larger (by 23%). These differences are partially explained by the use of discharge data from 1984 by Fontolan *et al.*; especially when the current study shows the tidal prism to have reduced since 1970. The tidal prism did appear to increase between 1930 and 1970 before reducing back to 1930 levels by 2000; work by Tomasin (1974) revealed an increase of 10% in the tidal amplitude between 1909 and 1972, which would affect the tidal prism by the amount calculated in this current study (8% greater discharge in 1970 compared to 1930 through profile 1). This change corresponded to a period of relative sea-level rise of 4 mm yr^{-1} (exacerbated by subsidence - Carbognin and Cecconi, 1997); between 1970 and 2000, the average sea-level rise was negligable (see Figure 3.4).

4.4.4 Seabed Classification

A classification system to convert reflectivity data into seabed classes, such as that designed by Nitsche *et al.* (2007) could not be utilised for this study due to the lack of sub-bottom profiling. However, the change in bathymetry, reflectivity data and sediment type all give clues to the type of environment present. Low-energy environments occurred in Burano Canal and off-shore to the east, represented by low reflectivity and muddy sediments. Burano Canal is relatively sheltered, current speeds are roughly 40% slower than in Lido Inlet (Table 4.1) and the residence time of water is longer than the Venice average (Cucco and Umgiesser, 2005), allowing the accumulation of finer sediments. Nearshore Cavallino Beach is low energy due to a combination of water

depth (around 12 m) and distance away from the breaker zone and the ebb jet of Lido Inlet. It includes the mud-belt that runs parallel to the shore (Albani *et al.*, 1998), interrupted only by river or inlet deposits. Most of the study area has been classed as medium energy (able to transport sand-sized sediments) and includes the beginning of the ebb-tidal delta and nearshore Cavallino Beach adjacent to the northern jetty. The remaining areas are high energy, where armouring of the seabed occurs (lag deposits by Punta Sabbioni), the shelly area south of the southern inlet, and where scour occurs at the mouth of Lido Inlet.

4.5 Conclusions

Venice Lagoon is evolving into a marine habitat due to a combination of sea level rise and subsidence, both natural and anthropogenic. This caused an increase in the total volume of water passing through the lagoon between 1930 and 1970 (the tidal prism), which has caused inner-lagoonal channels such as Burano Canal to widen. The resulting sediment has deposited in the channel bed, resulting in a flatter, wider channel, although the relatively fast current speeds resulted in confluence scour holes to increase in size. The tidal prism reduced after 1970, with a corresponding fall in average current speeds; Burano Canal also became decreasingly flood dominant. This has resulted in infilling of the confluence scour holes within the canal and a streamlining of the large confluence scour at the Treporti/Burano/San Felice junction. The canal is nonetheless stable following the tidal prism/cross-sectional area relationship of Le Conte (1905). Due to this stability, it is unlikely that it is a present source of sand, although this does not discount it from transporting sand from further within the lagoon.

The ebb-dominant Treporti Canal was highly erosional between 1930 and 1970 although the rate of erosion decreased between 1970 and 2000. However, the cross-sectional area has remained in equilibrium with the tidal prism. Treporti Canal is able to transport sand. This is indicated by the composition of the sea bed (bottom classification by Bondesan *et al.*, 2004 and in Chapter 5) and evidence that it is erosional; it may therefore be a source of sand to Lido Inlet. Treporti Canal is ebb dominant, but becomes less so as average current speeds fell with the reduction of the tidal prism

post-1970. The flow has eroded part of the eastern edge of the flood-tidal delta (a sediment sink located at the end of Lido Inlet), removing finer sediments and leaving behind lag deposits (seen by the sonar as high reflectivity). The rest of the delta is stable with maximum rates of deposition on its western side and an ebb shield spanning its width.

The morphology of Lido Inlet suggest that sand is principally exported. This is shown by the direction of growth of the ebb spit and the seaward growth of the ebb-tidal delta. Scour occurs only where the ebb jet exits adjacent to the southern jetty. Lido Inlet has been stable in terms of its cross section and tidal prism (following the Atlantic relationship of Jarrett, 1976) since 1970. Sediment has been removed from the deepest part of the channel but has been balanced by the evolution of the ebb spit on the northern edge. This sediment may be a combination of sand transported from within the lagoon, and also of sand imported from Cavallino Beach. An ebb-tidal delta is present about 2 km from the mouth of Lido Inlet and is extending seawards due to low wave energy (Fontolan *et al.*, 2007), storing sediment exported from Lido Inlet.

From the orientation and dimensions of seabed morphology and through reflectivity data it is possible to determine that the likely sand transport pathway is from the inner canals of the lagoon (such as Treporti, which is erosional and ebb dominant; both of which encourage export), through Lido Inlet (shown by the seaward orientation of the ebb spit and seaward growth of the ebb delta) and into the Adriatic Sea. Peak sand transport is likely within Treporti Canal and in the deep flood-channel of Lido Inlet, as both areas have experienced erosion/scour.

This study confirms that a tidal prism/cross-sectional area relationship is valid for other channels within the lagoon; it is not necessary to use the minimum cross-sectional area as define by O'Brien (1969), although this simplifies comparison in the future. The type of relationship may alter with distance from the open sea; Burano Canal follows a relationship of sheltered inner harbour entrances (Le Conte, 1905), whereas Treporti Canal and the three Venice Lagoon inlets follow the Atlantic coastline relationship of Jarrett (1976).

5

Source, Transport and Sinks of Sand

5.1 Introduction

The morphology of the seabed, as investigated in the previous chapter, represents the large-scale result of sediment transport as a product of the local hydrodynamic conditions. Thus general observations on the movement of sand can be generated. However, as the rate of transport of sand is controlled by the physical characteristics of its individual particles (grain size, shape, density, mineralogy), it is only by analysis of the sediment that conclusions can be drawn on the characteristics of its transport. Key questions are: what is the direction of sand transportation? Is the sediment part of a sink or is it a source to other areas?

This chapter will describe the methods used to collect bottom sediment samples in Venice Lagoon and the analysis involved to determine the properties of the sediment to find the direction of transport and possible sources. The aims of the chapter are as follows:

- Do the trends in grain properties of the sediment agree with transport hypotheses derived in the previous chapter?

- Is the sediment of the ebb tidal delta sourced from inside the lagoon or is it transported to the study site by littoral drift?
- Lido Inlet is known to be comprised of sand (Gazzi *et al.*, 1973; Albani *et al.*, 1998; Albani and Serandrei Barbero, 2001) but how variable are the characteristics of this sand and can transport within the inlet be determined from these characteristics?

5.1.1 Grain Characteristics

There are three significant characteristics of sand important in the understanding of the processes of sediment transport. These are size, density, and shape. The grain size of a sediment sample is primarily a function of the source material and the local environmental conditions (Folk, 1974). Exposed to erosion and weathering, the grain size will decrease (although the rate of abrasion will vary depending on how the environmental characteristics interact with those of the sediment), which has some significance in terms of the determination of provenance and the transport direction. Grain size affects the mobility of a sediment; generally, finer grains will be transported before coarser grains due to the increase in lift required to overcome the increase in mass. This is described by the Hjulström curve, which describes the transport stage (erosion, transport, deposition) as a function of current velocity against grain size, as shown in Figure 5.1. The threshold of motion of a grain is described by the Shields Diagram (Figure 5.2), which describes the dimensionless shear-stress required to transport grains of various dimensions (threshold Shields parameter - θ_{cr}; Equation 2.17). Using this assumption, the presence of large grain sizes may then indicate the maximum current velocity at the time of deposition (Folk, 1974) as the current must have reached a certain velocity in order to transport this size of grain.

Grain size is usually described by the Wentworth-Udden scale (Figure 5.3), which defines size classes from clay (< 3.9 μm) to boulders (> 256 mm) and includes five sand size classes (very fine sand, fine sand, medium grained, coarse and very coarse sand). The sizes are expressed as sieve diameters, so does not account for grain shape; however, the sieve diameter can be converted into a sphere of an equivalent volume by multiplying by 1.32 (Komar and Cui, 1984; le Roux, 2005). The Wentworth-Udden

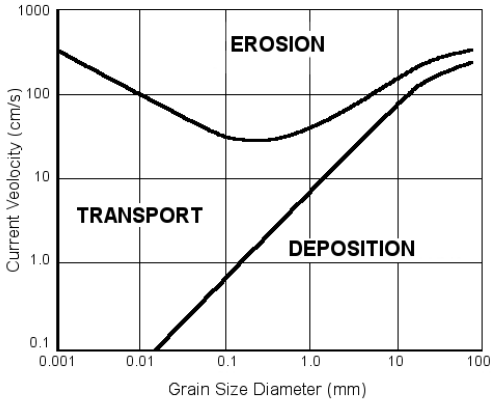

Fig. 5.1: The Hjulström Curve, showing the critical velocity boundaries for erosion, deposition and transport of different grain sizes.

scale was modified by Krumbein (1936) to include a logarithmic scale in phi (ϕ). This was principally to equalise the size intervals and to ensure that each class was limited by an integer, simplifying subsequent statistical analysis (as described in Section 5.1.2). Sand-sized particles are usually separated into these classes by sieving or settling (where grain size is calculated from its settling velocity). Both methods have advantages and disadvantages but generally, sieving can be more accurate (De Lange *et al.*, 1997), whereas settling is far quicker. Both methods were used in this study and are described further in Section 5.2.1.

The shape of a grain is usually assumed to be spherical as a generalisation when calculating sediment transport. This is not particularly accurate, as grains are very rarely this shape. However, the more a grain deviates from a spherical shape, the greater the drag force is (and thus the internal friction angle - Komar and Reimers, 1978), which decreases the settling velocity and consequently the grain mobility in turbulent conditions. Shape can be described by a grains sphericity or roundness; sphericity is defined as the 'cube root of the volume of the particle divided by the volume of the circumscribing sphere' (Dyer, 1986). This parameter is controlled by the original 3D shape of the crystal structure and is unlikely to alter greatly over transport, unlike roundness, which Dyer defines as 'the average radius of corners and edges

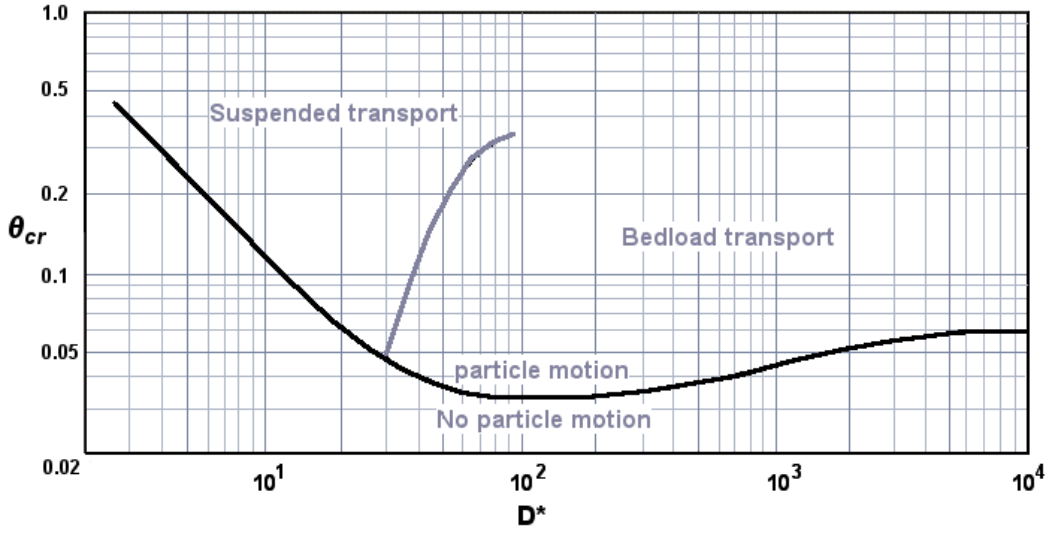

Fig. 5.2: A modified Shields diagram describing the threshold Shields parameter (dimensionless shear-stress; θ_{cr}) required to effect motion in a grain size (D) related in terms of the thickness of the laminar sub-layer (δ_o). After Hoffmans and Verheij (1997).

divided by the radius of the circumscribing circle'. Roundness is particularly affected by abrasion as any outliers on the grain will be smoothed more than any depressions. This variation in exposure eventually rounds the grain. This difference between angular and rounded grains affects sediment transport as rounder grains are preferentially moved first as the friction angle is smaller (Folk, 1974).

Rollability is another method of determining the grain shape as there is a high correlation between rollability and shape (Winkelmolen, 1969). Grain shape will affect the erodibility of the bed, due to sorting and packing of the sediment. The more 'rollable' a grain is, the quicker it will be sorted out from the main sediment and be transported away. This has been proven by Winkelmolen (1969) who passed grains of the same size class through a slightly tilted (2° 30' above horizontal) rotating drum. The most rollable (i.e. spherical or allantoid grains) quickly separated from the remaining sediment and accumulated in the collector (as described by Dyer, 1986). The shape of a grain also affects the efficiency of packing; important in terms of erodibility as a well-packed sediment is less porous (the ratio of water volume to sediment volume),

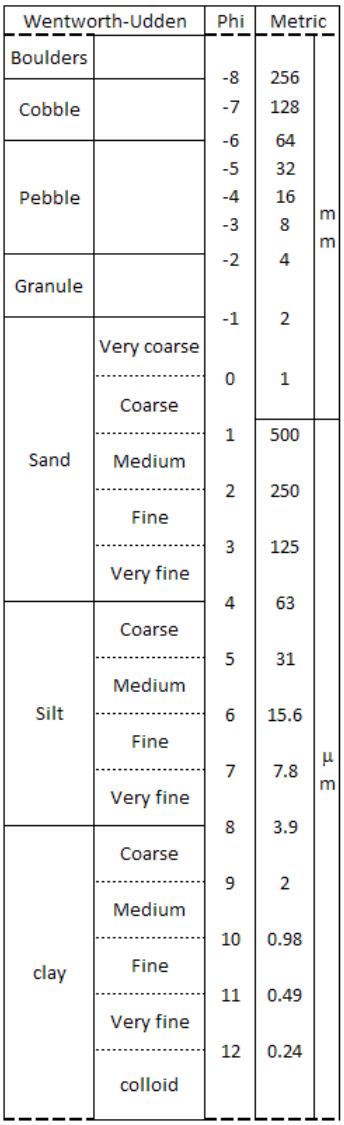

Fig. 5.3: Grain size scale with the Wentworth-Udden classes, with metric and the logarithmic phi scale (Krumbein, 1936).

.

Grain size	Porosity (%)
Coarse Sand	39-41
Medium Sand	41-48
Fine Sand	44-49
Fine Sandy Silty Clay	50-54

Tab. 5.1: Typical porosity values for different grain sizes (Soulsby, 1997).

thus requiring greater energy to move it than a loosely-packed grain. Generally, the smaller the mean grain size is, the higher the porosity (see Table 5.1).

Grain density is controlled by the component mineral. It can be measured by specific gravity (SG), which is the grain density divided by water density at 4°C. Quartz has an SG of 2.65 and is less dense than dolomite, which has an SG of 2.86. Although specific gravity is dimensionless, pure water has a known density of 1000 kg m^3, so the density of quartz can be calculated as 2650 kg m^3 (Fredlund and Rahardjo, 1993). Denser grains have a faster settling velocity so this has implications in sediment transport as more energy (i.e. flow velocity/turbulence) is required for the vertical components of turbulence to exceed the resistive forces. Grains of a greater density tend also to be more resistant to erosion (Briggs, 1986) and concentrate in areas of high energy where less dense and erosion-prone grains are abraded or transported away (selective entrainment/kinetic sieving). These denser grains include minerals such as zircon (SG = 4.6), gold (SG = 19.3) and haematite (SG $\approx$ 5.0).

5.1.2 Sediment Characteristics

A sediment sample can be characterised by the distribution of its individual grain sizes. These statistical measures are sorting, kurtosis and skewness.

5.1.2.1 Sorting

Sorting, in statistical terms, is the standard deviation of a grain size distribution. The smaller the standard deviation is, the greater the degree of sorting. Each sediment grain in transport has characteristics which affect the ease in which it is carried. Therefore

over time, the sediment will be sorted by a combination of its grain size, density and shape. A 125 μm sand grain will usually be transported in preference to a grain twice the size; a less dense quartz grain should move before a denser dolomite grain; a 'rollable' grain should move preferentially over a more angular grain. However, this is not always the case and determining transport becomes more complicated. For example, shear sorting affects grains of different densities in 'liquefied' sediment such as found in the swash zone of a beach. Gravity causes the smaller grains to drop down into the space between larger grains, with the larger and denser grains moving to the surface; the area of least shear strain (Inman, 2002). Also, an allantoid (sausage-shaped) grain may be highly rollable in one axis, but if this face is perpendicular to the current, then it becomes more streamlined and less drag force is produced, which inhibits transport. More energy is therefore required to transport the grain. The degree of sorting is dependent principally on the source material; Folk (1974) gives the example of waves eroding a glacial till cliff and a river running through a sandstone bedrock outcrop. The glacial till cliff will provide a wide range of grain sizes from boulders to clay, making the beach poorly sorted, but the river will carry very well-sorted sediment though both samples are adjacent to the source. A graph of grain size versus sorting can help to evaluate the degree of sorting in this case. Current intensity will also affect the degree of sorting. An intermediate current of constant strength will be more efficient at sorting than a weak or strong current, or a current which is constantly fluctuating (Folk, 1974).

Sorting (in ϕ) is defined by Folk and Ward (1957) as:

$$\sigma_I = \frac{\phi_{84} - \phi_{16}}{4} + \frac{\phi_{95} - \phi_5}{6.6} \tag{5.1}$$

or in geometric (μm) terms as:

$$\sigma_G = \exp\left(\frac{\ln P_{16} - \ln P_{84}}{4} + \frac{\ln P_5 - \ln P_{55}}{6.6}\right); \tag{5.2}$$

the result (σ_I and σ_G) refers to descriptive classes as shown in Table 5.2.

Sorting	Geometric (μm)	Logarithmic (ϕ)
Very well sorted	< 1.27	< 0.35
Well sorted	1.27 - 1.41	0.35 - 0.50
Moderately well sorted	1.41 - 1.62	0.50 - 0.70
Moderately sorted	1.62 - 2.00	0.70 - 1.00
Poorly sorted	2.00 - 4.00	1.00 - 2.00
Very poorly sorted	4.00 - 16.00	2.00 - 4.00
Extremely poorly sorted	> 16.00	> 4.00

Tab. 5.2: The degree of grain size sorting using μm (geometric) and ϕ (logarithmic) using Folk and Ward (1957).

5.1.2.2 Kurtosis

Kurtosis describes the 'peakedness' of a grain size distribution curve, thus illustrating how far the sample deviates from the median grain size. A platykurtic size distribution describes a sample which has an even spread of size classes and a large standard deviation, whereas a leptokurtic curve describes a sample with a small deviation from the median grain size (see Figure 5.4 and Table 5.3). It is defined as:

$$K_G = \frac{\phi_{95} - \phi_5}{2.44(\phi_{75} - \phi_{25})} \tag{5.3}$$

Kurtosis	ϕ & μm
Very platykurtic	< 0.67
Platykurtic	0.67 - 0.90
Mesokurtic	0.90 - 1.11
Leptokurtic	1.11 - 1.50
Very leptokurtic	1.50 - 3.00
Extremely leptokurtic	> 3.00

Tab. 5.3: The classes of kurtosis for both geometric and logarithmic size scales, using Folk and Ward (1957).

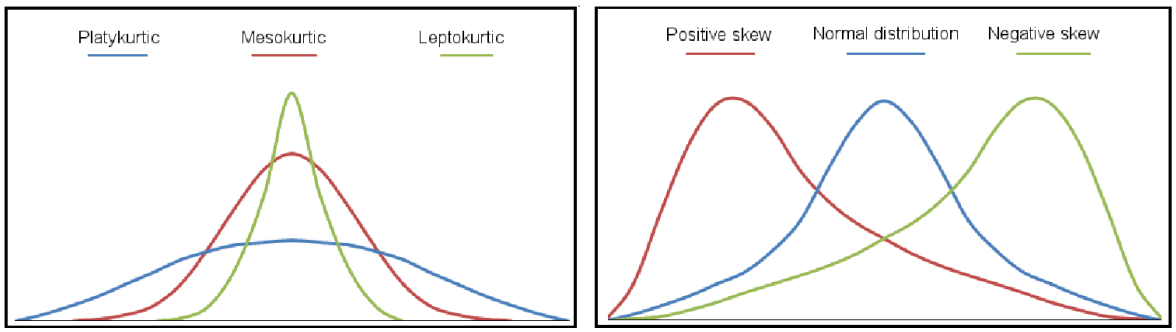

Fig. 5.4: Description of kurtosis (left) and skewness (right) in graphical form

.

5.1.2.3 Skewness

The skewness of a sediment sample describes the distribution around the median grain size and which grain sizes are predominant. If the distribution is normal then the mean, median and mode will all be the same. However, if the sediment is mainly composed of coarse sediment then the mode and median will be positive in relation to the mean and the skewness will be positive or *coarsely skewed*. If the median and mode are negative relative to mean, then the sediment is dominated by fine-grained material and is negative or *fine skewed* (see Fig 5.4).

$$SK_I = \frac{\phi_{16} + \phi_{84} - 2\phi_{50}}{2(\phi_{84} - \phi_{16})} + \frac{\phi_5 + \phi_{95} - 2\phi_{50}}{2(\phi_{95} - \phi_5)} \tag{5.4}$$

Skewness	ϕ & μm
Very fine skewed	-0.3 to -1.0
Fine skewed	-0.1 to -0.3
Symmetrical	-0.1 to +0.1
Coarse skewed	+0.1 to +0.3
Very coarse skewed	+0.3 to +1.0

Tab. 5.4: The classes of skewness for both geometric and logarithmic size scales, using Folk and Ward (1957).

5.1.2.4 Considerations in Grain-size Analysis

Shells in sediment are usually broken up but can cause positive skewness, making the sediment seem coarser than it actually is. Despite being generally larger than sand grains, shells are hydrodynamically equivalent to quartz grains due to their flat shape (Dyer, 1986). Consequently, shells can also be used as a tracer as they are softer than quartz and will be eroded the longer they remain in transport. Heavy minerals within a sample can also cause positive skewness (compared to the results if the same sample was sieved) if the grain-size distribution is calculated from settling velocities as they settle faster than equivalently-sized quartz or carbonate grains. However, this may be an advantage within a study focussed on the transport of sand grains, as heavy minerals are generally hydrodynamically equivalent to larger sand grains (White and Williams, 1967).

5.1.3 Grain Trend Analysis

Grain size trends over a transport pathway have long been studied as a method to assess not only sediment movement in modern coastal areas, but also ancient environments (Emery, 1955; Folk and Ward, 1957; McLaren, 1981; Gao and Collins, 1992; Gao *et al.*, 1994; Hill and McLaren, 2001; Lucio *et al.*, 2004). The assumption that grain size should decrease along a pathway is superficially sensible (erosion and abrasion reduces grain size), however this is not always the case. If fine-grained material is readily eroded and leaves behind a coarser-grained component, then it may appear that sediment becomes coarser over the transport pathway, although the sediment will become better sorted and increasingly skewed; the key identifiers in the grain-trend model of Gao and Collins (1992), which is described herein. A grain size distribution is the result of primarily the source material and the variables controlling the way each individual grain is transported. These variables according to Krumbein (1938) are:

- the gradual erosion, loss, or addition of sediment en route;
- the nature of fluid flow (laminar or turbulent), and
- authigenic changes after deposition.

McLaren and Bowles (1985) used the characteristics of seabed sediment to infer the direction of transport (McLaren, 1981). The authors write that a grain size distribution is independent of the transportation process and depositional environment, but instead relies on "clearly identifiable trends from source to deposit" resulting from erosion/abrasion, partial deposition and total deposition, which are disclosed in the statistical parameters. McLaren and Bowles therefore use changes in mean grain size, sorting and skewness to provide three possible cases of sediment transport between two neighbouring samples.

Case I/lag deposit: if sample 2 (d_2) has a larger mean grain size, is better sorted and has more positive skew than sample 1 (d_1), then sample d_2 is a 'lag deposit' of d_1 from the same source. No transport direction can be gauged.

Case II/fining sediments: if d_2 has a smaller mean grain size, but is better sorted and more negatively skewed than d_1, then the transport direction is from d_1 to d_2. Coarser grains are not transported as far as the finer particles of the source sediment.

Case III/coarsening sediment: d_2 has a larger mean grain size and is also better sorted and more positively skewed than d_1. The direction of transport is also from d_1 to d_2 but explained by the trapping of the finer sediment (shielded by coarser surface grains).

This method was criticized by Gao (1991) and Gao and Collins (1992) as a 'one-dimensional' model. The authors argue that sediment transport can occur even if McLaren's Case II or III is false (see Table 5.5), and so proposed a new two-dimensional version of the model, using 'transport vectors'. This model has been utilised to gauge transport of sediment within the study area. Consequently it is discussed in greater detail in the methods section (5.2).

5.1.4 Mineralogy

The mineralogy of a sediment is useful in the determination of sediment transport pathways (Folk, 1974; Cox, 2002) due to a presence of a natural tracer (e.g. garnet) or through a change in the mineralogical composition as softer minerals (e.g. mica) erode

Observed Changes			Environment	Author(s)
μ	σ	S_k		
+	u	u	Alluvial fan	Blissenbach, 1954
+	-	u	Beach	Pettijohn & Ridge, 1932
-	n	n	Beach	Schalk, 1938
+	-	n	Beach	Schalk, 1946
-	-	+	Beach	Carr, 1969
+	-	+	Beach	Self, 1977
-	u	u	Beach	McCave, 1978
-	-	u	Beach	Bryant, 1982
+	n	-	River	Plumley, 1948
+	u	u	River	Basumallick, 1966
-	-	+	River	McLaren & Bowles, 1985
-	-	+	Spit	McLaren & Bowles, 1985
-	-	u	Spit	Nordstrom, 1981
+	n	u	Spit	Nordstrom, 1989
+	-	-	Delta\lake	McLaren & Bowles, 1985
+	u	u	Submarine Canyon	Hand & Emery, 1964
-	-	u	Flume	Bagnold, 1968

Tab. 5.5: Observed changes in grains size parameters in the direction net transport (u is unknown, n is no change). From Gao (1993).

at a greater rate than more resistive minerals.

The mineralogical composition of sediment within a sediment cell should be comparable to its source (assuming a singular source); therefore, a sudden change in composition can signal a boundary with another cell and thus a change in the transport direction. Changes within each sediment cell will occur as the result of erosion along the transport pathway. An indicator of this erosion specific to Venice Lagoon is the change in dolomite relative to calcite (dolomite/calcite ratio) due to the greater resistance to weathering of the former. Not only is calcite softer (3 on the Mohs scale, compared to 4 to 4.5 for dolomite), but it is more liable to dissolution in seawater than dolomite (Kramer, 1959). Therefore, the lower the calcite/dolomite ratio becomes, the longer the sediment will have been transported and exposed to erosive forces. Problems in interpretation occur with the introduction of sediment from a secondary source, as

occurs when a river divides a beach.

Quartz also is a robust indicator of sediment maturity due to its hardness (7 on the Mohs scale) as it will remain after minerals such as dolomite have been removed. Shape is also an indicator; angular quartz will be relatively young and close to source, whereas a well-rounded quartz will either have been in transport for an extended time or have been exposed within a high-energy environment such as a swash bar. Other minerals such as mica, also indicate lack of maturity by virtue of their presence. Mica is easily eroded due to a combination of its hardness (around 2.5 Mohs) and structure (a sheet structure separated by weak bonds).

5.2 Methods

5.2.1 Grain Size Analysis

204 sediment samples were collected in February 2004 in the Lido Inlet vicinity, along the seaward-side beaches of Cavallino/Jesolo, Lido, Pellestrina and Chioggia (see Figure 5.5). Samples from the Rivers Brenta, Piave and Tagliamento were also collected as possible sources of the sediment into the study area. The offshore samples were collected using a Van Veen sediment grab whilst the beach and intertidal samples were collected by hand (surface sample imitating volume collected by the grab). Only samples containing sand were retained. Other sand samples from Treporti Canal collected in a 2003 study were also available for this analysis (Umgiesser *et al.*, 2006). Broken shells were not removed as the method used to remove them would also destroy the carbonate minerals known to be present (Gazzi *et al.*, 1973).

The samples were processed to determine the proportion of fines ($< 63\ \mu$m), sand (63 μm to 2 mm) and gravel (> 2 mm). The samples were wet sieved, with material less than 63 μm retained in measuring cylinders and allowed to settle before before both fractions were weighed (as dry-weight). Due to the large volume of fine-grained material, alternative methods were investigated to quicken the process. The Amos and Sutherland (1994) method to quickly gauge the dry mass of sand in a saturated sample was adjusted to see whether the technique was valid for fine sediment. The

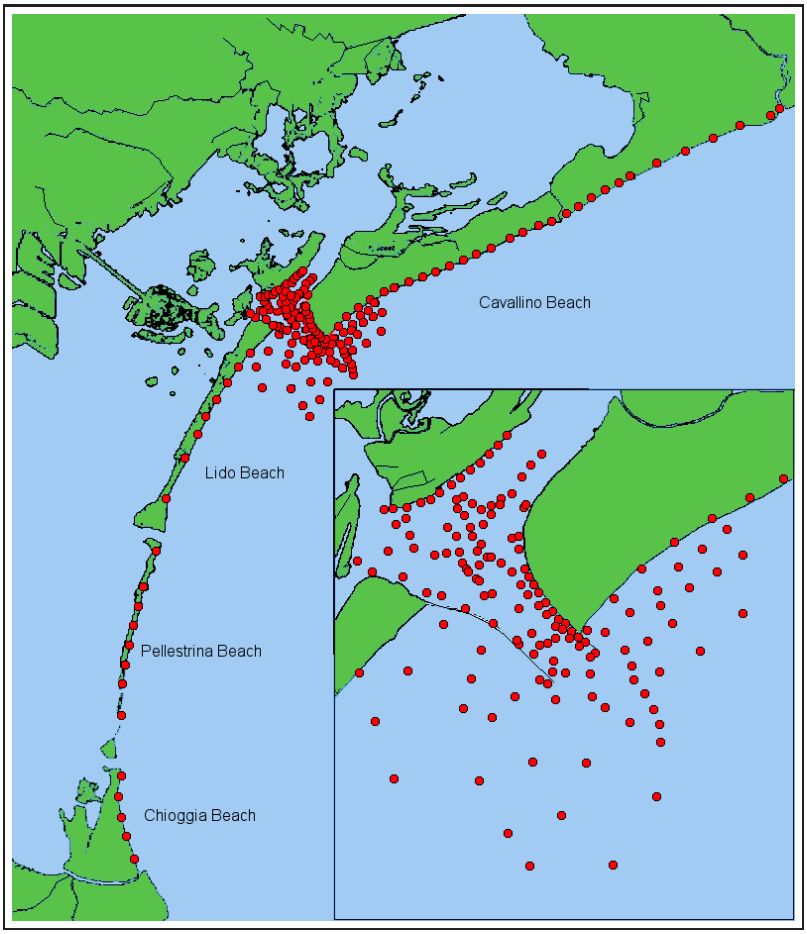

Fig. 5.5: The location of the sediment sampling sites. Samples were also collected in the rivers Tagliamento, Adige and Brenta.

sediment/water mix which had passed through the 63 μm sieve during wet sieving was weighed to 1 cg and the volume measured to the nearest 5 ml; the following formula was applied:

$$m_s = \rho_s(m_t - \rho_w V_t) \tag{5.5}$$

where m_s is the mass of dry silt, ρ_s is the sediment density (2800 kg m^{-1}), ρ_w is the density of tap water (998 kg m^{-1}), m_t is the weight of the water/sediment mix, and V_t is the volume of the water/sediment mix. The results were compared to samples where the weight of fine sediment was known and was found to be comparable to within 0.4 g, however, these samples were particularly abundant in fine-grained material. Other

samples measured this way exhibited larger errors. Thus, it is likely that the method is only valid when the concentration of fine sediment is significant (over 20% fines). It is not therefore, suitable for the majority of these predominantly sand samples.

The quickest and most accurate method was to dry each sample at a low temperature, as not to bake the fine fraction and to measure the total dry weight. The samples were then wet sieved at 63 μm to remove the fine-grained component and oven dried prior to separating the sands and gravels with a 2 mm sieve. The mass of fines was then calculated from the dry weight of the sands and gravels. Error is introduced if sand grains are caught in the sieve mesh, as they contribute to the fines content (any gravel stuck in the 2 mm sieve was clearly visible and removed from the sieve).

The sand fraction was analysed further using the National Oceanography Centre's settling column ; a long glass tube filled with water of a known density used to determine the settling velocity of particles. Each sand sample was divided in a splitter to provide a subsection of approximately 5 g. This was then poured onto the rough plate of the settling column, dampened with distilled water and spread equally over the plate. Any excess water was then absorbed by a tissue lightly pressed against the side of the plate. This was found to be the most effective way to ensure the whole sample adhered to the plate, rather than the usual method of pressing the damp plate into a dish of the dry sample, which tended to leave smaller particles behind due to sheltering by larger grains. The thoroughly damp sand ensured that minimal air was trapped between particles, which can prevent the grains from entering the water due to air bubble formation (see Figure 5.6). Releasing a lever at the top of the tube drops the roughened plate into the water releasing the sediment, which falls through the water column at different speeds according to the size and shape of the different grains (Equation 2.12, page 26). At the same time, the lever triggers a connected computer to start recording the cumulative weight of sediment landing on the connecting dish at the base of the tube (connected to a balance correct to 1 mg). Error was reduced by ensuring that no sand from previous experiments was in suspension at the start of each test. Other precautions included minimizing air movement around the balance, which reduced the error by around 3%. Unavoidable error in this technique results from turbulence caused by water displacement as the grains enter the water, which

Fig. 5.6: Air bubbles forming on the settling column rough plate after deployment

lifts some grains in the resultant eddies, thus affecting the time it take for them to settle. Boundary layer conditions exist along the wall of the settling column, which reduces the settling velocity of grains in the vicinity. The error produced by this effect is negated by a centimetre gap left between the collecting plate and the wall ensuring that affected grains pass by uncollected. Error may be produced if particles stick to the rough plate and drop during the coarse of the experiment, although this is thought to be less than 1% (Syvitski, 2008)

The results (a text file of cumulative weight recorded in 0.16 second time steps) were processed using a Matlab script (Neumeier, 2005). The script uses the settling velocity formula (Equation 2.12) of Soulsby (1997) to determine the grain size classes ($\frac{1}{8}$ phi) defined by Folk and Ward (1957) - see section 5.1.4. Error is reduced by calculating the settling velocity once turbulence (from the release of grains into the water) has subsided after ≈ 7 seconds. GRADISTAT, a Microsoft Excel add-on package written by Blott and Pye (2001) was used on the resultant data for statistical analyses to determine:

mode - the most inhabited class size,

percentiles (median/d_{50}) - the class size at the d_n of the distribution ,

mean - the average class size,

sorting - the standard deviation of the sample (Equation 5.1 and 5.2).

kurtosis - the degree of peakedness of the distribution (Equation 5.3).

skewness - measure of asymmetry of class sizes (Equation 5.4).

A resultant data sheet is produced as in Figure 5.7, showing these characteristic statistics as well as percentiles and descriptions of class type present. A particle size distribution graph is also produced to show the general trend.

5.2.2 Data Visualisation

The processed data were combined with coordinates and plotted as maps created by Generic Mapping Tools (GMT - Wessel and Smith, 1991) to view the distribution of different grain attributes over the sampling area:

- very fine sand
- fine sand
- medium sand
- coarse sand
- very coarse sand
- mean grain size (Folk and Ward, 1957 in mm or ϕ)
- skewness
- kurtosis
- sorting

5.2.3 Grain Trend Analysis

The statistical parameters described in the previous section can be used to determine the likely direction of sand transport (Gao and Collins, 1992; McLaren, 1981). The mean grain-size ϕ, sorting, and skewness were used to calculate transport vectors, which were plotted onto a map of the study area (see results section). The initial step of the Gao and Collins (1992) grain trend model is to illustrate *trend vectors* through the comparison of neighbouring samples. In this case, a neighbour was defined as any sample (S_2) located within a 500 m critical distance (D_{cr}) of the initial sample site (S_1). This distance was chosen as it was large enough to allow most lagoonal samples to have

SAMPLE STATISTICS

SAMPLE IDENTITY: **L60** ANALYST & DATE: Rachel Helsby,

SAMPLE TYPE: Unimodal, Very Well Sorted TEXTURAL GROUP: Slightly Gravelly Sand

SEDIMENT NAME: Slightly Fine Gravelly Fine Sand

	μm	ϕ
MODE 1:	155.4	2.688
MODE 2:		
MODE 3:		
D_{10}:	116.8	2.509
MEDIAN or D_{50}:	151.4	2.724
D_{90}:	175.6	3.098
(D_{90} / D_{10}):	1.504	1.235
(D_{90} - D_{10}):	58.87	0.589
(D_{75} / D_{25}):	1.216	1.109
(D_{75} - D_{25}):	29.32	0.282

GRAIN SIZE DISTRIBUTION

GRAVEL:	0.5%	COARSE SAND:	0.0%
SAND:	99.5%	MEDIUM SAND:	0.5%
MUD:	0.0%	FINE SAND:	84.2%
		V FINE SAND:	14.7%
V COARSE GRAVEL:	0.0%	V COARSE SILT:	0.0%
COARSE GRAVEL:	0.0%	COARSE SILT:	0.0%
MEDIUM GRAVEL:	0.0%	MEDIUM SILT:	0.0%
FINE GRAVEL:	0.5%	FINE SILT:	0.0%
V FINE GRAVEL:	0.0%	V FINE SILT:	0.0%
V COARSE SAND:	0.0%	CLAY:	0.0%

	METHOD OF MOMENTS			FOLK & WARD METHOD		
	Arithmetic	Geometric	Logarithmic	Geometric	Logarithmic	Description
	μm	μm	ϕ	μm	ϕ	
MEAN ($\bar{x}$):	171.7	150.0	2.737	148.5	2.751	Fine Sand
SORTING (σ):	301.2	1.358	0.442	1.182	0.241	Very Well Sorted
SKEWNESS (Sk):	13.63	6.692	-6.692	-0.211	0.211	Fine Skewed
KURTOSIS (K):	189.3	76.14	76.14	1.252	1.252	Leptokurtic

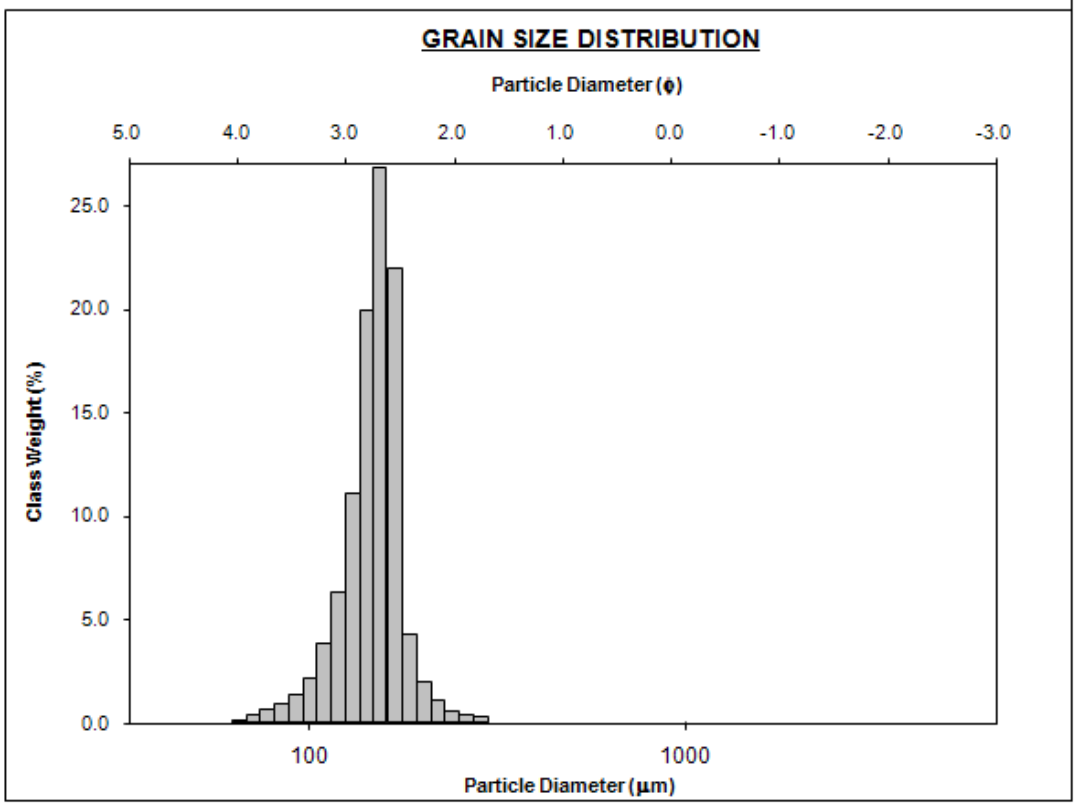

Fig. 5.7: Example data sheet produced by the GRADISTAT Excel macro (Blott and Pye, 2001) showing grain size distribution and statistical characteristics. This particular sample is from the shallow-side of the inlet.

at least one neighbouring sample, but small enough not to encompass the majority of the inlet width which could affect results due to the averaging of vectors in the latter stages of the model. The samples outside Lido Inlet had a D_{cr} of 1 km, due to the wider spacing between samples. Each neighbouring sample had its sediment characteristics compared and if either Case 1 or Case 2 proved true, then a *dimensionless trend vector* was applied (the length is unity) in the direction of the neighbouring sample.

$$\text{Case 1: } \sigma_2 \leq \sigma_1 \text{ and } \mu_2 > \mu_1, \text{ and } S_{k2} \leq S_{k1}$$

$$\text{Case 2: } \sigma_2 \leq \sigma_1 \text{ and } \mu_2 < \mu_1, \text{ and } S_{k2} \geq S_{k1}$$

The majority of samples had more than one neighbour, therefore it was necessary to sum the resultant vectors to produce a singular trend vector for each site. This was achieved by applying:

$$\vec{R}(x,y) = \sum_{1}^{n} \vec{r}(x,y)_i \tag{5.6}$$

where n is the number of trend vectors for the site, $\vec{r}(x,y)_i$ is a trend vector and $\vec{R}(x,y)$ is the sum of the trend vectors. Noise still exists where more than one neighbouring site adheres to either case. To remove the noise the vectors must be averaged with vectors of neighbouring sites. Using the same D_{cr} defining distance, the following is applied to each site:

$$\vec{R}_{av}(x,y) = \frac{1}{k+1}\left[\vec{R}(x,y) + \sum_{1}^{k} \vec{R}_j\right] \tag{5.7}$$

where $\vec{R}_j$ is a summed trend vector from a neighbouring site resulting from Equation 5.6 and k is the total number of such sites. The resulting vectors are defined as *transport vectors* now that noise has been significantly reduced. If neighbouring vectors follow similar directions then transport pathways can begin to be established. However, it is still necessary to test the reliability of that each vector is displaying the real direction of transport. Assuming that noise alone is responsible for a grid of neighbouring trend vectors, it is likely that the averaging protocol previously described will cause vectors to cancel each other out, producing short transport vectors. To determine if the vector length is reliable, Gao and Collins (1992) ran the following significance test, where

length (L) increases with increased reliability:

$$L = \sum_{1}^{N} \left| \vec{R}_{av} \left(x, y \right)_i \right| \tag{5.8}$$

where N is the number of sites. Due to the uneven grid pattern in the current study (distance between sites varies between 100 m to 1 km), the longer vectors cover up the small vectors on the map making them difficult to distinguish. Therefore, using Equation 5.8, L was assigned a colour instead of a length; red is an unreliable indicator of transport, and purple is very reliable.

5.2.4 Mineralogy

A subsection of samples within the study area was chosen to represent potential sand transport pathways (as determined by the literature and the results of the grain trend analysis). Samples were also chosen to represent the major morphological features including Chioggia, Lido and Cavallino beaches, the ebb and flood tidal deltas, and the ebb and flood channels.

Each sample was embalmed in resin and fashioned into a thin section[i], which were stained using alizarin red and potassium ferricyanide to differentiate between calcite and dolomite (both ferrigenous and non-ferrigenous). Each thin section was viewed under a Zeiss Photomicroscope III with a rotating stage and adjustable specimen holder. Each mineral was classified into one of the following classes, chosen as they are relatively common in these samples (Gazzi *et al.*, 1973; Weltje, 1995) and easy to identify:

Dolomite: A sedimentary carbonate, either fine grained or orthorhombic cleavage. Colour is either pale (translucent) or stained deep blue if ferroan; salmony rainbow extinction colours. Identified by a change in relief upon rotation.

Calcite: A sedimentary or metamorphic carbonate, also has a change in relief upon rotation. Stained pink or purple (if ferroan).

[i]By Bob Jones and John Ford of the National Oceanography Centre

Monocrystalline quartz: relatively slow crystal growth in hydrothermal conditions. Grey extinction although slightly yellow in comparison to feldspars, relatively free of inclusions, but not aligned if present and usually rounded.

Polycrystalline quartz: rapid crystallization in hydrothermal conditions. Multiple crystals of quartz. Also includes microgranular chert.

Potassium feldspar: igneous mineral always the same composition but different crystal structures depending on temperature during formation. Orthoclase (clear grey extinction, stable above 500° C) and microcline (tartan extinction, often has dirty appearance from inclusions which are often aligned, stable below $400°C$).

Plagioclase feldspar: twinning giving stripy grey appearance.

Mica: slowly formed igneous muscovite (clear, low relief, high interference colours) or metamorphic biotite (brown, highly pleochroic).

Shell: identified to differentiate biogenic sediment from terrigenous.

Rock fragment: all other fragments including heavy minerals.

The degree of error in counting between the beginning and end of the analysis was found by replicate analysis. 99% of the grains were identified as the same mineral during both counts. The data were then mapped using GMT to visualise the change in composition around the Lido Inlet and along the shore face of Venice Lagoon and ternary diagrams created to correlate patterns and determine possible transport pathways.

5.3 Results

Morphology and seabed characterization has been used in the previous chapter to hypothesize sand transport routes as well as possible sources and sinks. The proposed transport pathway begins in the ebb-dominant Treporti Canal, where sand is scoured from the channel bed; some sand passes through Treporti from Pordelio Canal (flowing through the sandy barrier island of Cavallino) and possibly from Burano and San Felice canals. Some of this sand is deposited on the ebb spit, whilst the majority is exported into the longshore transport pathway with some deposition on the ebb-tidal delta. Finer sediments are deposited on the flood-tidal delta, although the source for this sediment is unclear. These pathways will be further investigated within this chapter using grain-size analysis, grain trend analysis, and mineralogical analysis.

5.3.1 Grain Size Analysis

5.3.1.1 Distribution of Sediment Size Classes

The initial analysis of the Venice Lagoon sediments (divided into fines, sands, and gravels) show an area dominated by sand (Figure 5.8). The 'baseline' sand content of the lagoonal channels appears to be around 60-70%, but this increases to 85-100% around the lobe of the flood tidal delta, and the Punta Sabbioni ebb spit. The sand content is over 80% outside Lido Inlet, with 'lobes' of 90% sand content extending from Cavallino Beach and around the ebb tidal delta. Sediment with a substantial volume of fine grains is found well into Treporti Canal, where proportions reach 50%. Fine-grained sediment is also found between the ebb spit and jetty, and in the main channel of Lido around the confluence of Treporti and San Nicolò. Gravel-sized sediment is mainly composed of shells and is predominant off Punta Sabbioni, and from here, seawards along the remainder of Treporti Canal into the deep channel of Lido Inlet. The mean grain size (Figure 5.9) of the study area is approximately 170 μm but increases towards the southern edge of Lido entrance where gravel is present. The grain size on the ebb tidal delta is around 180 μm, much coarser than the rest of the seabed outside of the lagoon, where it falls to less than 100 μm just off Cavallino Beach and south of the ebb delta.

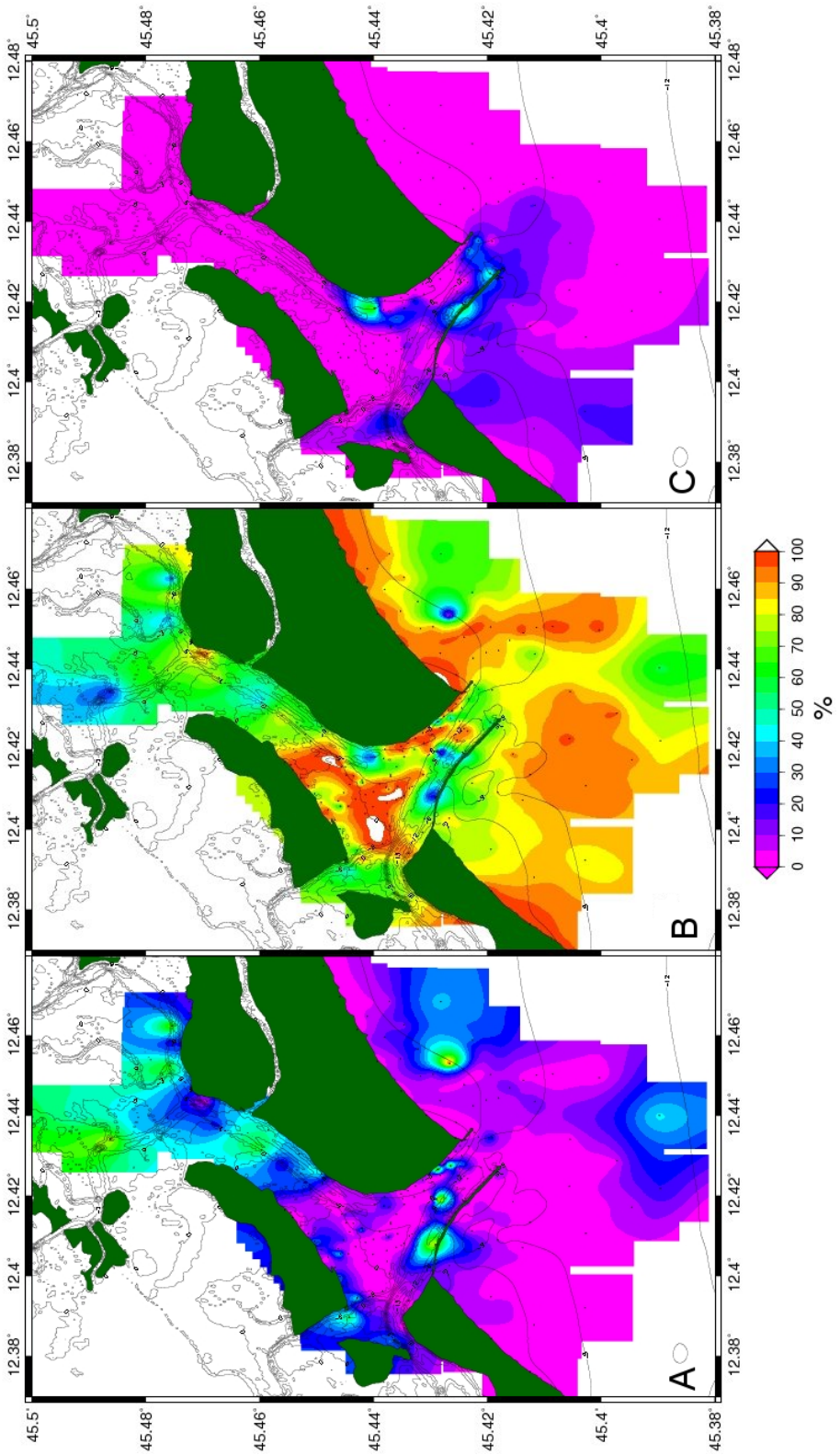

Fig. 5.8: Percentage composition of **A**, fines (< 63 μm), **B**, sand (63 μm to 2 mm) and **C**, gravels (> 2 mm) in the Lido Inlet vicinity. Note the predominance of sand on the tidal deltas, spit and along Cavallino Beach.

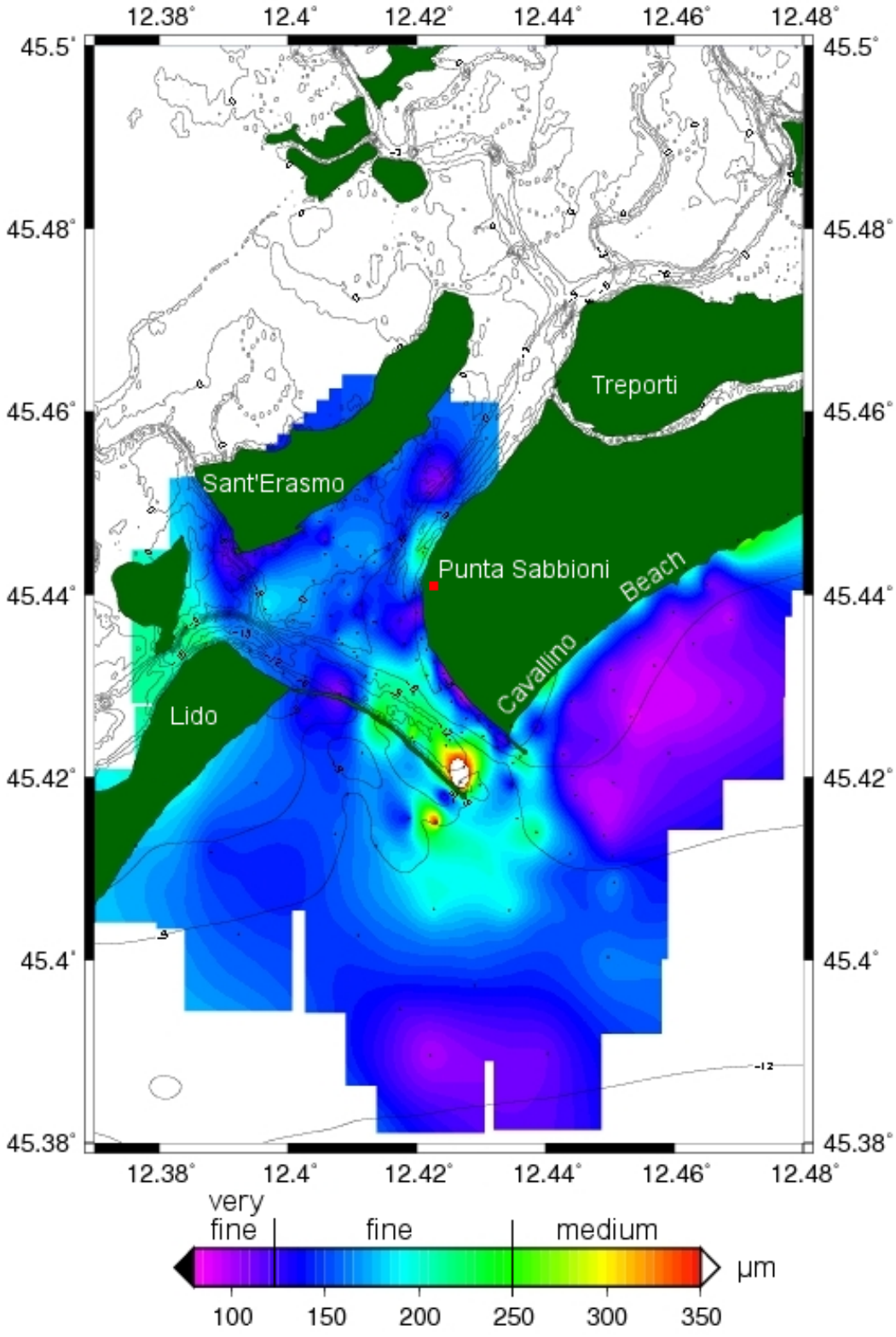

Fig. 5.9: Mean grain size in microns of the study area using the method of Folk (1974).

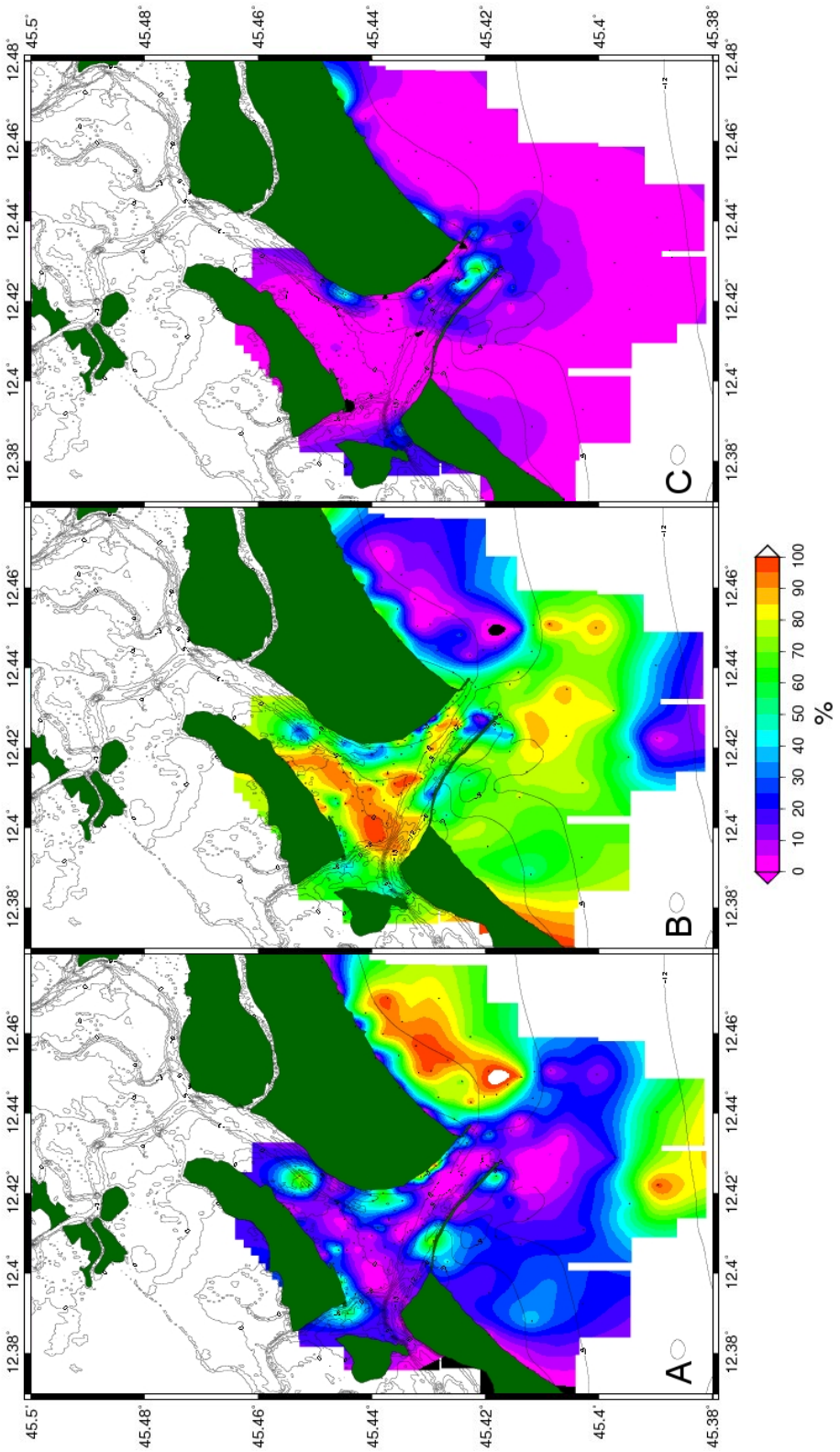

Fig. 5.10: Percentage composition of **A**, very-fine sand (63 - 125 μm), **B**,fine sand (125 - 250 μm) and **C**, medium sand (250 - 500 μm) in the Lido Inlet vicinity. Coarse sand is found at the mouth next to the southern jetty in quantities of no more than 10%.

The maps showing the different classes of sand (Figure 5.10) indicate that these areas have a seabed composed of between 70% to 100% of very fine sand (63 μm to 125 μm), whereas the rest of the study area is composed of only 20% on average of this sized sand. The map of fine sand (Figure 5.10A) shows that the seabed of the study area is approximately 70% sand between 125 μm and 250 μm in size. The flood-delta lobe is almost completely constructed of this fine-grained sand, with fine-grained 'patches' continuing down the centre of the Lido Inlet channel and onto the ebb-tidal delta. Sand sizes larger than 250 μm are not predominant anywhere in the study area, though concentrations of up to 20% are present along Treporti Canal, Lido Inlet, the ebb delta, and also along Cavallino Beach. Coarse sediment (between 500 μm and 1 mm) is only present in small quantities (below 10%) off Punta Sabbioni and along both sides of the southern jetty. There appears to be no significant amounts of sediment between 1 mm and 2 mm in diameter.

5.3.1.2 Statistical Parameters

Maps were created to show the statistical parameters of the sediment in the study area (Figure 5.11). The sorting of the sediment can show where transport pathways combine if sorting worsens. Most of the study area is very well sorted with the exception of the deepest parts of the tidal channels and the shore to the west of Lido Inlet where sorting deteriorates. The grain distribution curve or skewness, is basically symmetrical, with a tendency towards a finer skew (predominance of fine sediments) in Treporti Canal, the tidal deltas and adjacent to the beach. Within the tidal channel of Lido, and west of the inlet, there is a tendency towards a coarser skew. The maps of kurtosis show a gradual east to west change from mesokurtic (mainly nearshore) to leptokurtic.

Maps showing the d_5 and d_{95} percentiles of grain size were also generated (Figure 5.12) as Folk (1974) states that maximum seabed grain-sizes can indicate areas of peak sediment transport. Minimum seabed grain-sizes can also be used in a similar way as relatively large, minimum grain-sizes indicate that smaller grains are transported as suspension and the area must be of high velocity and/or high turbulence.

Figure 5.12A displays the d_5 percentile (the smallest $\frac{1}{20}$ of the sample). The

minimum grain-size increases from an average of approximately 100 μm over the whole study area to over 140 μm in the tidal channel of Lido, but only where the inlet width is at its narrowest. The d_5 of the seabed adjacent to the northern jetty is finer than 70 μm and this band of d_5 fines extends to Punta Sabbioni at the mouth of Treporti Canal. Both the ebb- and flood-tidal deltas have slightly higher than average d_5 values (110 μm), although the d_5 grain size of the ebb delta gradually decreases with distance from the inlet mouth (extending in a south-west direction). The beaches also have higher-than-average d_5 values (between 120 and 180 μm) although the minimum grain-size falls to below 70 μm in the nearshore area by Cavallino Beach.

The d_{95} values (largest $\frac{1}{20}$ of the sample, shown in Figure 5.12) reach a maximum at the inlet mouth (covering most of the inlet width including the tip of the northern jetty), although values rapidly fall from over 2 mm to about 500 μm further into the inlet (falling below 70 μm on the northern edge of the channel). The tip of Punta Sabbioni also has relatively large grains in the 95^{th} percentile (above 1500 μm); these areas of high d_{95} values are abridged by a region of moderately high d_{95} values (500 μm), whilst the rest of the seabed in the inlet (including the flood delta, San Nicolò and Treporti canals) has maximum grain sizes no higher than 300 μm. The d_{95} grain size of the ebb-tidal delta gradually decreases with distance away from the inlet mouth in a pattern similar to that seen with Figure 5.12.

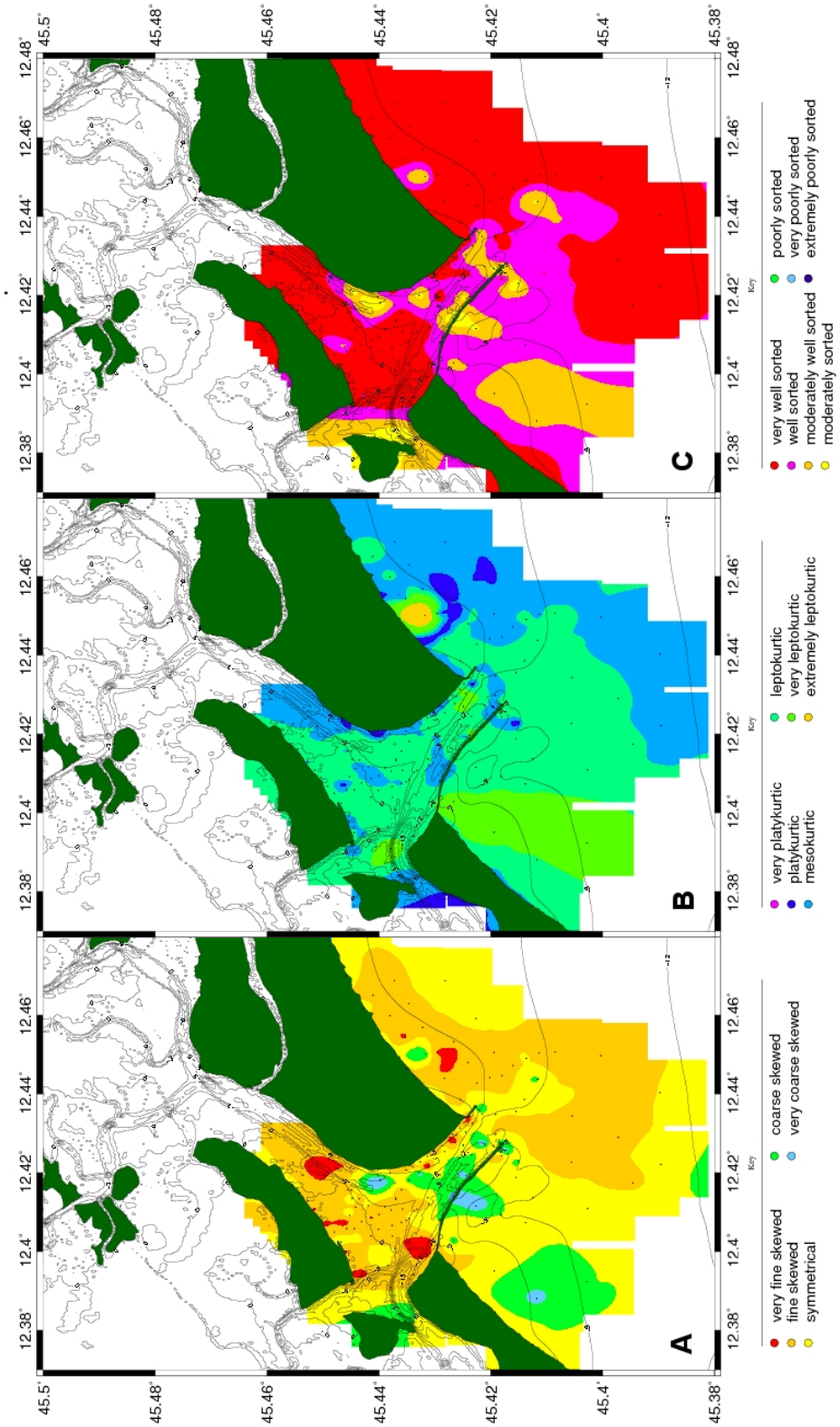

Fig. 5.11: Maps of skewness (A), kurtosis (B), sorting (C).

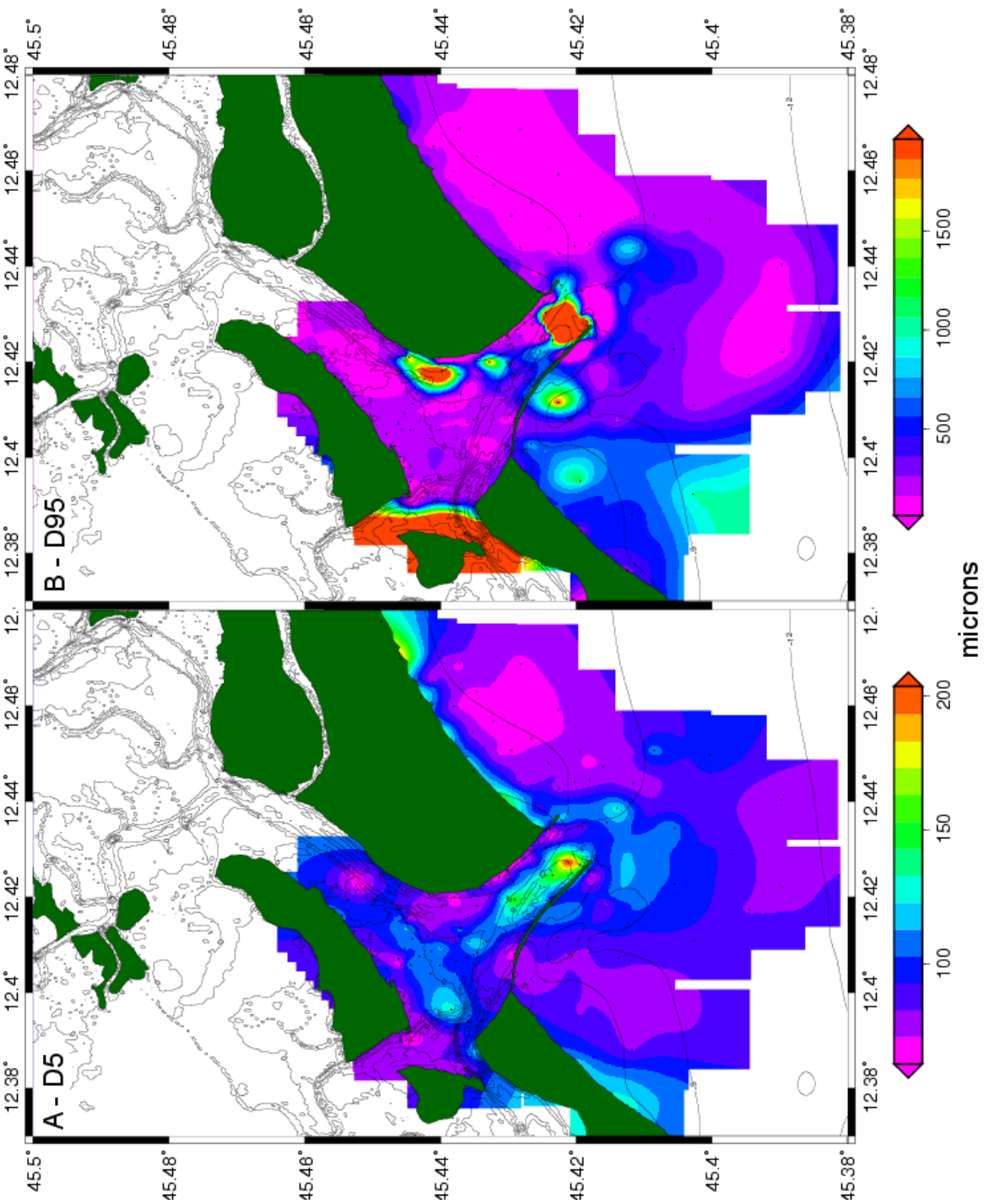

Fig. 5.12: d_5 (A) and d_{95} (B) percentile grain sizes showing peak and minima transport. (Folk, 1974).

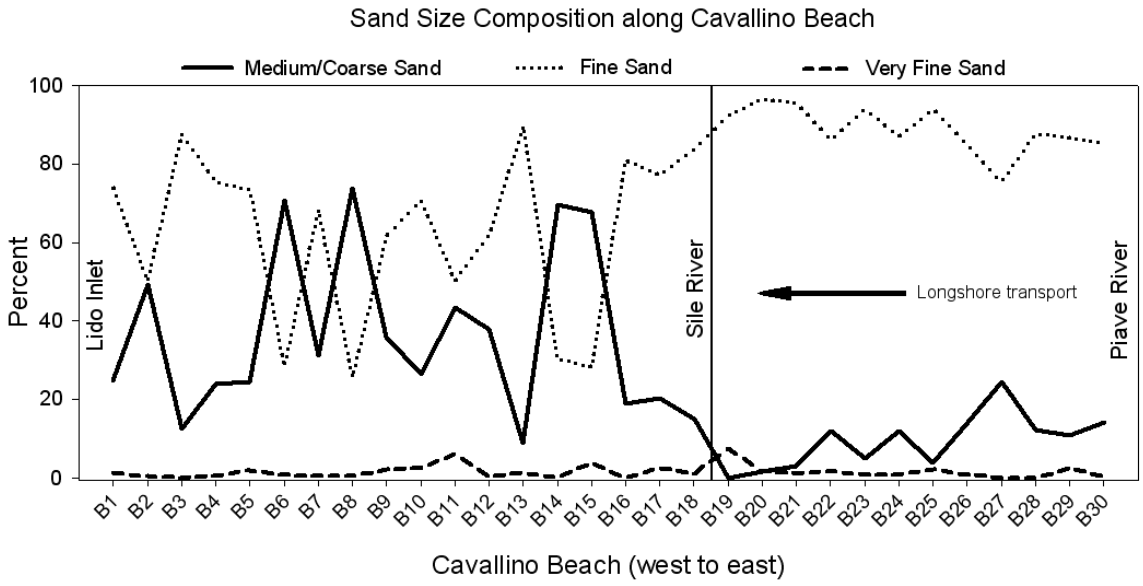

Fig. 5.13: The changes within sand grain sizes along Cavallino Beach. Sample B1 was taken adjacent to Lido Inlet, B30 is adjacent to the Piave River and the vertical line shows the position of the Sile River mouth.

Figure 5.13 shows the change in proportions of three different sand size classes (very fine, fine, and medium/coarse sand) along the transport route from the Piave River-mouth (site B30), along Cavallino Beach to the mouth of Lido Inlet (site B1). The grain size fluctuates little until the mouth of the Sile River is reached. The sediment is mainly fine sand suggesting that the sediment is from one source. There is a slight trend of decreasing proportions of medium/coarse sand and a corresponding increase in proportions of fine sand moving south from the Piave mouth. This is the result of grain abrasion, decreasing the average grain diameter along the transport pathway (Folk, 1974). The Sile River mouth dissects Cavallino Beach 12.3 km south-west from the Piave River, between sites B18/B19 (shown by the vertical line in Figure 5.13). An immediate change in the grain-size composition occurs as an increase in the concentration of medium/coarse grains from negligible proportions up to 20%. The levels of this size class peaks at approximately 70% at site B15. The proportions of very fine sand do not fluctuate, remaining at 1 or 2% along Cavallino Beach, but the proportions of both fine and medium/coarse sand alter greatly with the medium/coarse sand proportions varying between 15% and 75%.

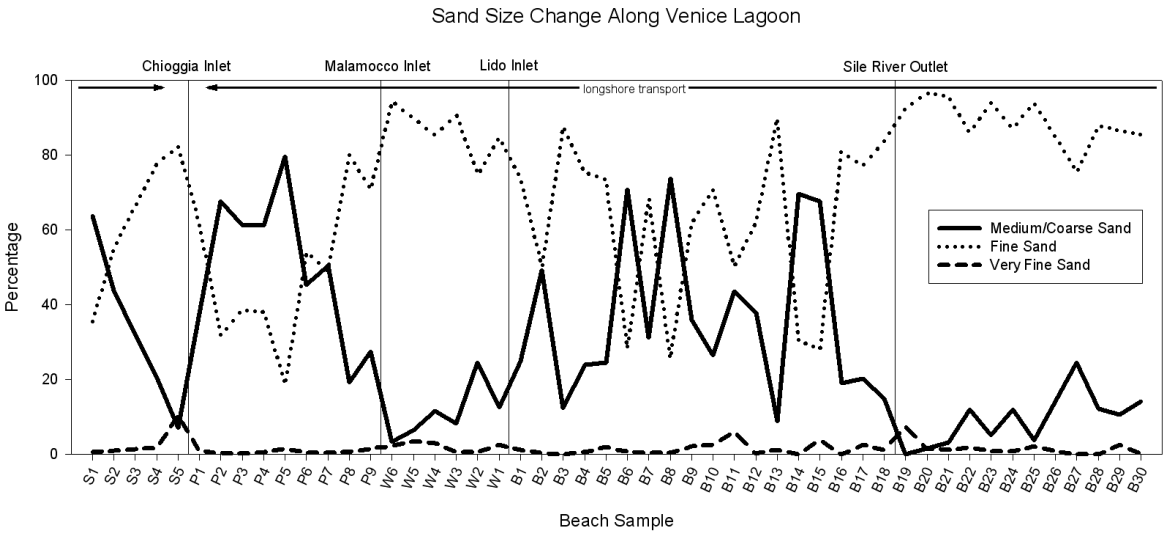

[h]

Fig. 5.14: The changes within sand grain sizes along the beaches of Venice Lagoon including Chioggia Beach (S1 to S5), Pellestrina Beach (P1 to P9), Lido Beach (W1 to W6) and Cavallino Beach (B1 to B30).

5.3.2 Transport

5.3.3 Grain Trend Analysis

The results of the Gao and Collins (1992) grain trend model are presented in Figure 5.15. The general transport pathway (as shown by the vectors) is from Treporti Canal into the deep tidal channel of Lido Inlet (adjacent to the southern jetty) and then out of the lagoon. These vectors are cold colours and are therefore a highly reliable indicator of the transport direction of sand. The vectors change direction from south to south west at the mouth of the inlet to point the same way as the vectors adjacent to Cavallino Beach. The vectors on the south shore of Sant'Erasmo island initially point in a northerly direction and gradually turn to a southerly direction progressing from the east to the west end of the island. These vectors are of low reliability however as they are adjacent to the shoreline and thus do not have enough neighbouring samples with which to compare characteristics. Outside of the lagoon, the vectors appear to point in all directions. The vectors pointing in a southerly direction are generally more reliable (appearing as colder colours) than the northerly vectors, suggesting that this is the more likely direction of transport. However, as this area is subject to changing

current directions, no conclusions should be made from the results of the grain trend analysis.

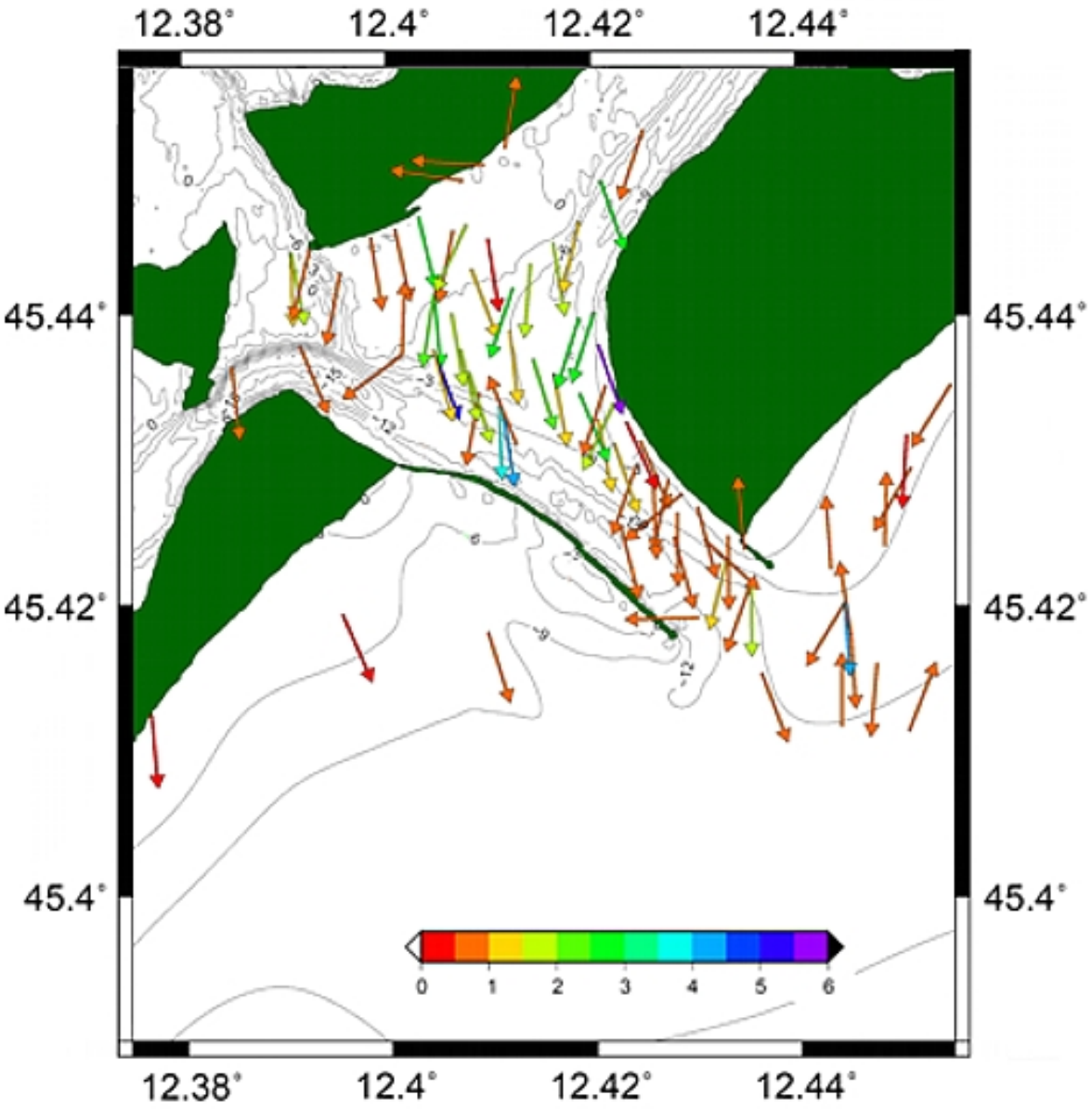

Fig. 5.15: Grain trend analysis using the method of Gao and Collins (1992). Colour denotes reliability of transport direction; purple is very reliable and red is of low reliability.

5.3.4 Mineralogy

Maps of the percentage composition were created to form a visual representation of the sea bed composition. The data were also presented in a variety of ternary diagrams.

Quartz is found predominantly south of Chioggia Inlet and makes up around 30% of the sediment. The levels reduce further to the north to under 20% at Lido Inlet, and less than 10% past Cavallino Beach. There are a couple of outliers on Cavallino Beach, where the composition is 20% quartz. This quartz is predominantly polycrystalline (60%) with monocrystalline quartz accounting for the remaining 40%.

The sites north of the lagoon are composed of over 80% carbonate (Figure 5.16A), though this drops to between 50 and 75% around Lido Inlet and Lido Beach. At Chioggia Inlet, the percentage of carbonate is significantly lower (under 20%). Two outliers exist along Cavallino Beach; the northern outlier contains only 20% carbonate and the adjoining site increases to 40%. The general pattern is of a reduction in carbonate from north to south. This carbonate is mainly dolomite, with calcite representing no more than 20% of the whole sample. Outliers of calcite appear along Pellestrina Beach, where percentages reach 40% just north of Chioggia Inlet. South of this inlet, levels drop once again to less than 5%.

The calcite/dolomite ratios are much higher south of Chioggia Inlet (0.9) and at sites of beach replenishment (> 0.8) than around Lido Inlet. The lowest ratios (0 to 0.3) occur in the ebb and flood tidal deltas of Lido Inlet and on the ebb spit. The ratio increases to 0.5 within the flood channel, Treporti Canal and also along Lido and Cavallino beaches.

The pattern of percentage of rock fragments follows that of quartz. High levels (40%) occur south of Chioggia Inlet, but small amounts are found north of the lagoon ($< 5\%$). Levels are between 10 and 30% around Lido Inlet, but increase at the same outlier sites described above for quartz (Figures 5.16B and C).

Feldspar, mainly potassium feldspar, comprises of up to 30% of the sediment

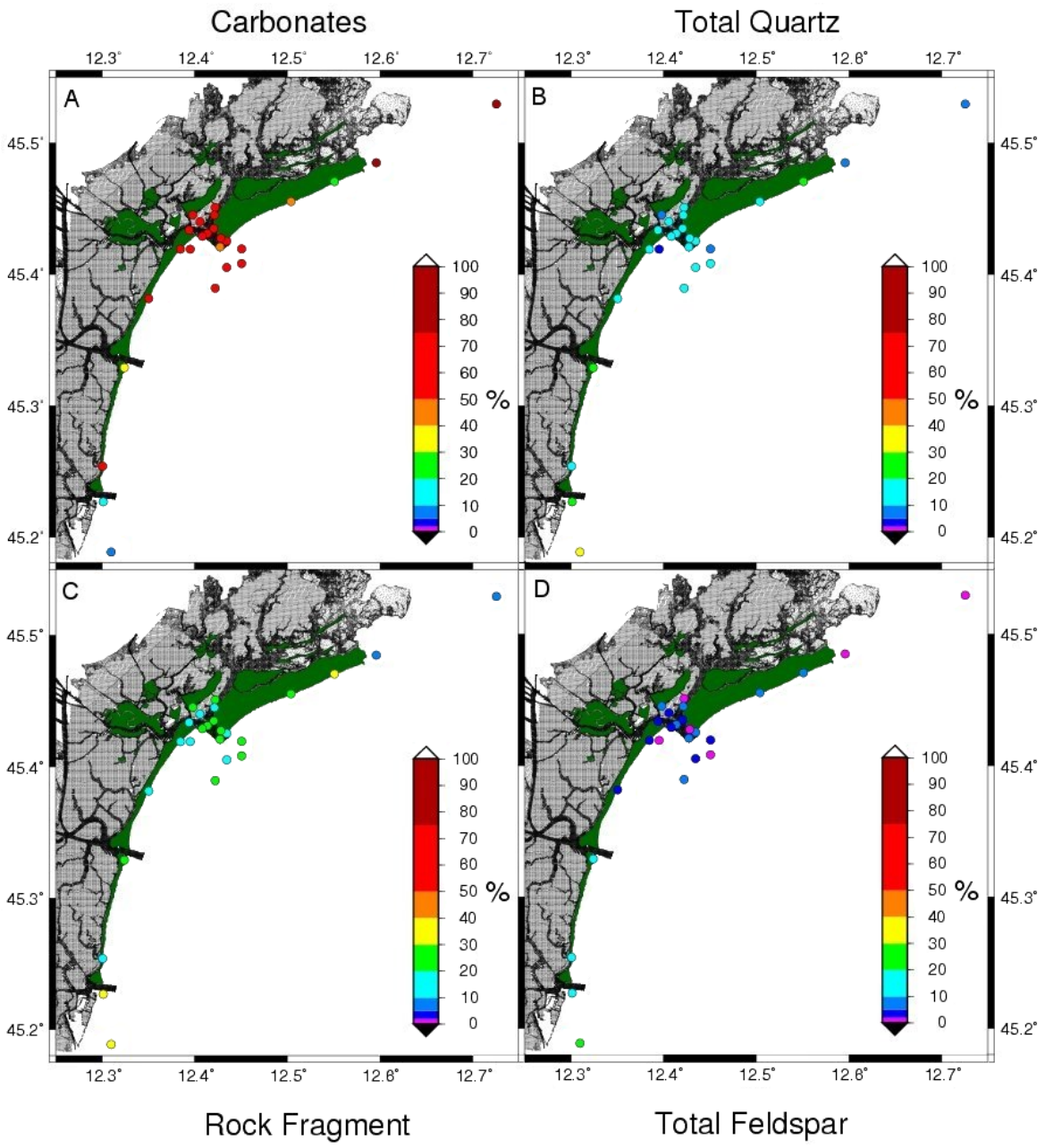

Fig. 5.16: The percentage composition of carbonates (A), quartz (B), rock fragments (C), and feldspar (D).

south of Chioggia Inlet, although levels fall towards the north (Figure 5.16D). Lido Inlet has less than 10% feldspatic content within its sediment, and this drops to trace levels north of the lagoon.

Shell fragments are only found at one or two sites within the lagoon, and along Lido Beach, though levels are never more than 10% of the whole sample. Mica is also uncommon in the area; found only south of Chioggia Inlet at levels less than 10%, where there are high levels of quartz and rock fragments.

Figure 5.17A is a ternary diagram discriminated by source, with axes of gravels, sands, and fines. It shows the dominance of sand over the study area, increases in the proportion of silt towards the inner lagoon (up to 85% fines in Treporti Canal), and an increase of gravels in the flood and ebb channel (30-55%) as well as parts of Treporti Canal. The sandiest section of the study area is the flood delta lobe, the beaches and nearshore beach areas. Figure 5.17B describes the distribution of sand sizes in finer detail (very fine, fine and medium/coarse sand) for the beaches and nearshore beach areas. It shows the beaches to be predominantly fine sand ($> 50\%$), decreasing in size in the Cavallino nearshore area (50 to 100% very fine sand) and Lido Beach, although the nearshore Lido Beach samples are poorly sorted with a mix of all three grain sizes.

The mineralogical data were also subdivided; Figure 5.17C compares lagoonal samples with riverine and beach samples to see if the likely source could be determined. All of the lagoonal samples cluster around the Cavallino Beach, Piave and Tagliamento river sources, showing high levels of rock fragments and carbonates (over 70%). Only the beach samples show any similarity with the sample from the Brenta River, with 20 and 30% of quartz (the Brenta sediment is around 38% quartz), although they also have a greater feldspar content than any of the rivers.

Figure 5.17D also shows mineralogical compositions, but separates the carbonates. The data shown are representative samples along the length of Cavallino Beach, as well as Lido, Pellestrina, and Chioggia beaches and the riverine samples. North and south Cavallino Beach samples are similar in composition to the Tagliamento River sample with carbonate levels of around 70%. Mid Cavallino Beach samples however,

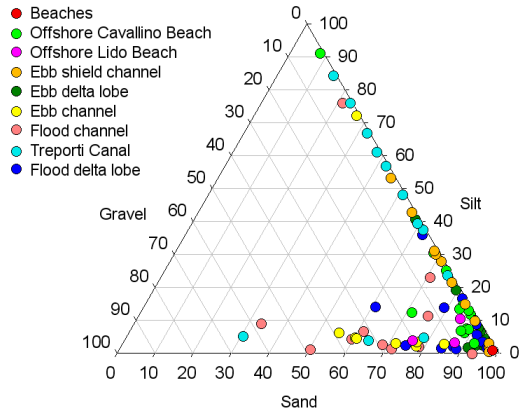

(a) Grain size distribution of beach, nearshore, channel, and delta samples

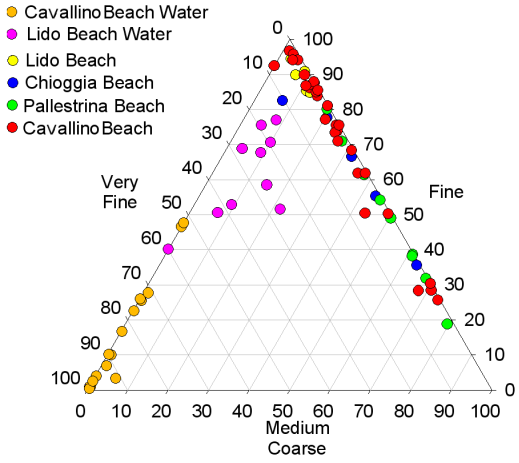

(b) Sand size distribution of beach and nearshore samples

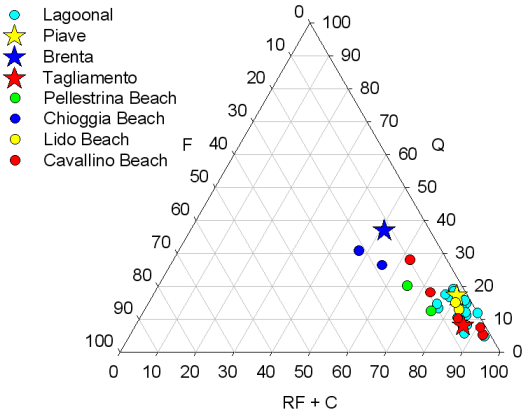

(c) Mineralogical composition of river and lagoonal samples

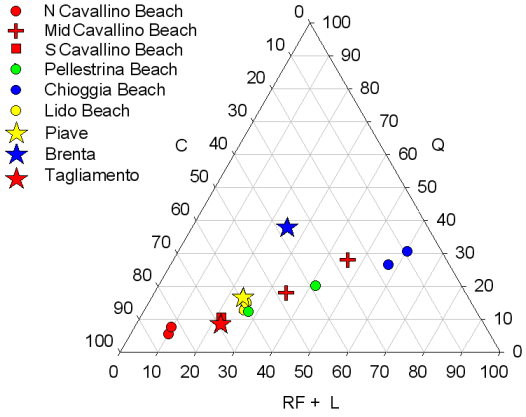

(d) Mineralogical composition of river and beach samples

Fig. 5.17: The composition of sediment samples from the study area. Mineralogical definitions are: quartz (Q), carbonates (C), feldspar (F), rock fragments (RF) and lithics (L).

have much higher quartz and rock fragment levels but less carbonate. Lido Beach samples have almost the same mineralogical composition as the Piave River, as does the southern-most sample from Pellestrina Beach. Chioggia Beach samples have the highest quartz proportion, but is composed of more rock fragments than the River Brenta (which has similar levels of quartz).

5.4 Discussion

The transport pathway of sand was investigated in the previous chapter in terms of the morphology of the study area. The morphology (and changes in it over time) can reveal regions where the hydrodynamics alter to conditions suitable for suspension (transportation) or deposition (accretion/sink). An estimated transport pathway of sand was hypothesised; sediment is scoured from Treporti Canal and transported through Lido Inlet out of the lagoon and onto the ebb-tidal delta. The aims of the current chapter attempt to verify the sand transport pathways through seabed sampling and application of grain trend analysis.

5.4.1 General Sediment Patterns

Sand is the predominant size class found around Lido Inlet as grain-size distributions reveal that seabed sediment is comprised of 60-70% sand. As the lagoon was created due to the formation of sandy barrier islands (Gilbert, 1885; Bonardi *et al.*, 1997), the dominance of sand is expected. Also, the lagoon was originally fed, and is still surrounded by, rivers carrying sandy sediment from the Dolomite mountain range to the north. These rivers are thought to be the general source of sediment to the lagoon (discussed in section 5.4.2).

The major morphological features of the inlet (ebb- and flood-tidal deltas, and the ebb spit) have higher proportions of sand (80-100%) suggesting that selective entrainment has removed the finer material present further within the lagoon. The velocity in these areas must be high enough to remove finer material without resettling, but not fast enough to transport the sand away as occurs in the main tidal channel (in regions where gravel is present). The 5^{th} percentile map shows that transport potential increases in the tidal channel of Lido as soon as the flow becomes restricted by

the jetties, indicating the presence of an ebb jet (Joshi, 1982); the 95th percentile map shows more specifically that peak sediment transport occurs at the mouth of Lido but is reduced once the flow becomes unrestricted. The gravel within the tidal channel is further evidence of scour and the position of peak turbulent velocities, which must be frequently above the suspension threshold of fine sand ($\sim$0.44 m s^{-1} following Equation 2.6a) to remove most sediment below 250 μm.

The flood-tidal delta has been formed by a drop in velocity due to the increase in the size of the cross-sectional area relative to the inlet mouth; as soon as the channel widens, the proportion of sand increases from around 60 to 80%. The delta is shaped by ebb currents from Treporti Canal to the north-east as well as flood tidal currents from Lido. This is indicated by the direction of sand transport as shown by the results of the grain-trend modelling. Flow entrainment by the flood-lobe induces sand in suspension to be deposited and transported as bedload, forming sand waves (seen in Figure 4.14). The grain size increases from the lobe to the delta (shown in Figure 5.9) due to selective removal of finer grains as the sediment is reworked by waves and tidal action (Daboll, 1969). The transport potential of the mid section of the delta (running parallel to Sant'Erasmo) is still high as shown by the comparatively large d_5 grain size.

The ebb-tidal delta is formed by deceleration of the ebb jet as it ceases to be restricted beyond the jetties. Sand in suspension (discussed fully in Chapter 5.5) settles out as flow speeds fall below the suspension threshold to form the ebb delta. The mean grain-size is relatively large at around 190 μm as the medium-grained sands fall out of suspension first (particle-size analysis shows little evidence of coarse- and very coarse-grained sands) before the fine sands and silts, which are transported further offshore. This grading of sediments is illustrated in Figure 5.12 of the 5th and 95th percentile of the grain-size distribution. The ebb delta extends 4 km from the mouth of the inlet, suggesting that the velocity remains above the suspension threshold for sand to this point, although it is likely that sand from longshore drift is mixed with the lagoonal deposits here. The sand south of the inlet is relatively poorly sorted, more so nearshore, suggesting that sand from two sources has intermixed (Folk, 1974) as predicted in the previous chapter. The position of this mixed sediment south of the inlet implies that longshore transport moves sediment from north to south, as previously

observed by Gazzi *et al.* (1973) and Brambati *et al.* (1978).

The greatest concentration of gravel in the study area is located at the tip of Punta Sabbioni suggesting this to be a source of larger grain sizes. The sediment in this area has grain sizes above 1500 μm in the 95th percentile of the grain-size distribution, which is well above average for the study area. This suggests that the transport potential of sand is very high; however, the below-average grain sizes in the 5th percentile of the distribution also imply that this is an area of deposition for fine-grained sediment. The shape that the contouring produces in each percentile map may provide an answer to this contradiction; the map of d_5 grain-size shows a contour tapered into Lido Inlet, whereas the contour tapers into Treporti Canal in the d_{95} grain-size map. It may be possible that the transport potential for coarse-grained particles reaches a peak during the flooding tide when the flow is compressed into the smaller channel of Treporti, but reduces significantly to the extent of deposition of fine-grained material when the tide turns and the flow from Treporti Canal expands into Lido Inlet.

The map of fines ($< 63\mu$m) shows that this size class makes up to 40% of the seaward end of Treporti Canal. This location is sheltered from waves propagating through Lido Inlet and waves generated from sirocco winds (from the south-east) by the barrier island to the south. The canal is orientated to the north-east, parallel to the bora winds, but due to the short fetch, is still relatively sheltered to the north-east. The weak wind-generated waves and relatively slower tidal velocities (Umgiesser, 2000) prevent the same degree of selective sorting as seen in Lido Inlet allowing finer-grained sediment to remain. The channel present between the ebb shield and Sant'Erasmo island also has a relatively high percentage of fine sediment ($\sim$20%), suggesting that this area is also sheltered. Residual currents predicted by Umgiesser (2000) show lower average currents (Figure 5.18). Note that the mean current shows slight flood dominance in Lido Inlet as found in Chapter 4 (page 58). There are also fines present in the northern edge of main tidal channel ($\sim$20%) and between the ebb spit and the northern jetty wall ($\sim$60%). This latter area is relatively sheltered by the ebb spit, and is away from the strongest flows (in the main tidal channel), allowing the settling of fine-grained material due to low velocities. The fines within the tidal channel occur where the jetties widen near the Lido island, and so are present where the flow is less

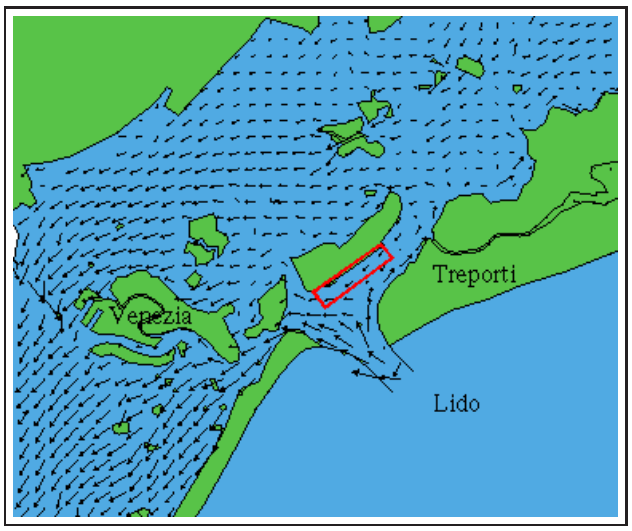

Fig. 5.18: The residual modelled current for 1987, showing low current velocity in the sheltered area above the ebb shield (within red rectangle). (Umgiesser, 2000).

restricted and the velocities are lower. Alternatively, their presence may be the result of sediment trapping, where the peak flow from the flood current continues in a straight line instead of following the jetty wall, so that velocity by the wall is below transport threshold. However, this would need to be confirmed through modelling or in situ current measurements. It also appears that some sediment may pass through the jetty wall as fine-grained sediment is present on both sides, despite coarser sediment being present elsewhere on the seaward side.

5.4.2 Source

The mineralogy of the lagoonal sediments is most similar to the Piave and Tagliamento rivers (see Figure 5.17). It is therefore likely that these rivers are the source of the sediments in the study area. Work by Bellucci *et al.* (2005) found calcite/dolomite ratios to be low (approximately 0.3) in the central lagoon, corresponding to values (from this study) around the deltas and ebb spit. Low ratios characterise re-worked mature sediments, so it is likely that the sediment was sourced from the rivers when they were still discharging into the lagoon, rather than being imported now they have been diverted. Therefore, it could be concluded that the ebb and flood deltas are comprised of lagoonal sediment rather than beach (fluvial) sediment as the ratios here are also

below 0.3. The sediment in the rest of the inlet has slightly higher calcite/dolomite ratios so may be intermixed with grains sourced from the beaches (and thus the rivers), which have ratios of 0.3-0.5.

The work of Gazzi *et al.* (1973) shows that the longshore transport around Venice Lagoon is part of a sediment cell moving sand from the north along the coast to Chioggia Inlet, which is also the boundary to another sediment cell transporting sediment from the south. Figure 5.13 shows a trend in decreasing grain size from north (by the Piave River) to south (the Sile River), as grains are abraded during transport. The introduction of a secondary source may be responsible for varying grain sizes south of the Sile River; however, the predominant signal is more likely to be from beach replenishment schemes in the '90s (Cecconi and Ardone, 1998). Sediment was dredged from a region about 14 km to the south-east of Lido Inlet (Cecconi and Ardone, 2000) and pumped onto the beaches. This source most likely would had varying grain sizes, accounting for the trend seen along Cavallino Beach. Although grain sizes do not infer transport direction here, it is apparent that sand continues to move towards the south due to the significant accretion of Cavallino Beach immediately to the north of Lido Inlet (see previous chapter).

Figure 5.14 shows the change in sand grain size along the Venice Lagoon beaches. Chioggia Beach follows a similar trend to the northern part of Cavallino Beach (north of the Sile River), in that the proportions of medium/coarse sand grains decreases relative to fine sand as abrasion reduces the grain size over time (the longer a grain has been in the transport pathway the longer it is exposed to erosive forces - Folk, 1974). The trend on Chioggia Beach (unlike Cavallino and Lido Beach) is south to north, agreeing with trends highlighted by Gazzi *et al.* (1973). The trend is also seen in the mineralogy, as these beach samples are high in quartz and mica - minerals which are less prevalent further north, but are found in the rivers to the south. The calcite/dolomite ratios do not follow this trend however, with the most southern Chioggia Beach sample having a high ratio (1), suggesting relatively unworked sediment, but at the northern end of the beach, the sediment has a very low ratio (0.14) suggesting well-worked, mature sediment. However, as this latter sample contains mica (a maturity indicator), it is more likely to be a recent sediment, indicating that the sediment here has recently

been added to the transport pathway. Along Pellestrina Beach, transport pathways have been obscured due to recent beach replenishment.

Sand from Cavallino Beach enters Lido Inlet; this can be seen in the map of sand (Figure 5.8) by a small tail of high percentage sand entering Lido around the northern jetty. It is also indicated by a change in the sorting from very-well sorted both inside the lagoon and offshore, to moderately to well sorted within the confines of the jetties suggesting that two sources of sediment are mixing within this area - one from Cavallino Beach, and the other from within the lagoon. Unfortunately, the mineralogy does not provide conclusive results. However, the results of the Gao and Collins grain trend modelling showed that sand is mainly exported from Treporti Canal and out of the lagoon through Lido Inlet. This suggests that the source of the inlet sediment is from within the lagoon, supporting the conclusions made in the previous chapter.

5.4.2.1 Error

The sediment samples were collected over a period of days in February 2003 during both the ebb and flood tidal phases, which may have affected the direction of sediment transport. However, the sample depth (∼4 cm) of the Van Veen grab is sufficient to capture sediment transported over numerous tidal cycles to provide a composite sample and thus provide an modal transport direction. It may however be conducive to repeat this study during different seasons (as (Tambroni and Seminara, 2006b) state seasonal changes in the direction of net transport within the inlet).

5.5 Conclusion

Sand from the Piave and Tagliamento rivers is transported south by longshore drift. This is shown by a decrease in the mean grain-size and a decrease in medium/coarse sand (corresponding with an increase in very-fine sand). The mineralogy of the Piave and Tagliamento river samples corresponds well with the northern Cavallino Beach samples; all are carbonate rich with little quartz, unlike the Brenta River (a likely source for Chioggia Beach). The mid-beach Cavallino samples are an exception caused

by annual beach replenishment which began in the '90s (Cecconi and Ardone, 1998). This sand is more quartz rich with larger quantities of rock fragments, but become more carbonate rich towards the south due to mixing with the natural sediment travelling in the same sediment cell. The area adjacent to Lido Inlet is the only section of Cavallino Beach naturally accreting due to trapping by the northern Lido jetty. This sediment is mineralogically a mix between the natural fluvial sediment and the sand from the beach replenishment further updrift. Once the sediment reaches the tip of this jetty, the majority is transported 3-4 km offshore with the ebb jet, however, a small quantity enters the lagoon adjacent to the northern jetty. This is best seen in Figure 5.8B, where the plume of sand extends away from the lagoon and the 'tail' of sand enters near the jetty. The tail is also visible in the reflectivity data described in Chapter 4. Further, the mineralogy of sample D13, which is located inside Lido Inlet adjacent to the northern jetty, is similar to sample B1 on the accreting section of Cavallino Beach. How far this sand travels into the lagoon is unclear, as the source rivers originally fed directly into the lagoon and sediment deposited prior to the diversion of the rivers may still be a source of sand within the lagoon. The mineralogy of most of the lagoonal samples is similar to one another to within 10%, with variations in the levels of lithics occurring in areas of scour. Therefore it is difficult to determine the extent of sand import using mineralogical methods. The grain trend modelling hints at a short penetration, with one vector of low reliability pointing north where the jetty extends seawards, but again, this is not sufficient to categorically determine the transport of sand into the lagoon.

The sand is exported from Treporti Canal and out of the lagoon through Lido Inlet. The principle evidence for this is the grain trend modelling (Gao and Collins, 1992), as most transport vectors follow the ebb currents along Treporti Canal and either closely follow the Punta Sabbioni shoreline and the northern jetty, or passing into the deep tidal channel. The vectors also suggest that sediment in the flood tidal delta channel between Sant'Erasmo and the ebb shield move in the ebb direction before draining into the San Nicolò Canal and out of the lagoon through the inlet. The calcite/dolomite ratios indicate that the sediment is reworked from sources within the lagoon as they are lower than the ratios of the beach samples. The sediment is then transported about 3-4 km out of the lagoon with the ebb jet and settles to form the

ebb-tidal delta, over which longshore transport occurs. The confluence of sediments from different sources is evident in the map of sorting (Figure 5.11C); each source (from inside and outside the lagoon) is very-well sorted. At Lido Inlet, the sediment becomes less-well sorted, indicative of mixing.

The longshore transport of sand continues north to south past Lido Inlet. Figure 5.8B shows that the plume of sand from Cavallino Beach passes the inlet and moves closer towards Lido Beach. This outlines the area of the ebb tidal delta described in Chapter 4. The area adjacent to the southern jetty is subject to eddies recirculating the sediment back towards the north (Brambati *et al.*, 1978). This is visible in satellite images (Figure C) although Figure 5.8C suggests the area is affective at trapping gravel sized sediment from the Lido Inlet. The grain size of Lido Beach is similar to the northern section of Cavallino Beach, where a gradual decrease in medium/coarse grained sand with a corresponding increase in fine-grained sand is evident (see Figure 5.14). This supports the hypothesis of north to south longshore transport. However, the mineralogy shows that there is an increase in quartz levels on Cavallino Beach, indicative of the recent beach replenishment (Cecconi and Ardone, 1998). The north to south longshore transport appears to continue past Pellestrina, although replenishment of the whole beach has occurred (Cecconi and Ardone, 1998). There is a lack of mica (present in Chioggia Beach), so if south to north transport was occurring along Pellestrina, some mica should be present in the samples. Chioggia Beach is mineralogically different from the other beaches, with more than twice the average volume of quartz and less than half the quantity of carbonates. It follows the same pattern of decreasing medium/coarse grained sand and increasing fine grained sand with the direction of transport, although that direction is from south to north. The Brenta River is thought to contribute to the south-north sediment transport pathway, as the samples are mineralogical similar, although there are significantly more rock fragments and lithics in the Chioggia samples. These may be from the Adige or Po rivers, located further to the south. The hypothesized sediment transport route is summarized in Figure 5.19. Sand is transported north to south along Cavallino Beach. At Lido Inlet, some sand enters the lagoon, but the main direction of sand transport is out of Treporti Canal, through Lido Inlet and onto the ebb delta (shown as very fine sand by Albani *et al.*, 1998). A band of medium to fine relic sand is present offshore (Cecconi

and Ardone, 1998) and it is unlikely to be rejuvenated on a large scale by sand from the present-day sediment cell. Thus, sand exported from the lagoon continues south within the longshore transport pathway to the cell boundary at Chioggia Inlet. Some sand must be lost along the pathway; the thickness of the barrier islands reduces from approximately 2 km in the north to a strip less than 50 m wide in the south. Where does this sand go? Is the carbonate fraction abraded and/or dissolved? Is it transported offshore past the mudbelt? These are questions that need to be answered by further data collection (sediment sampling) and modelling.

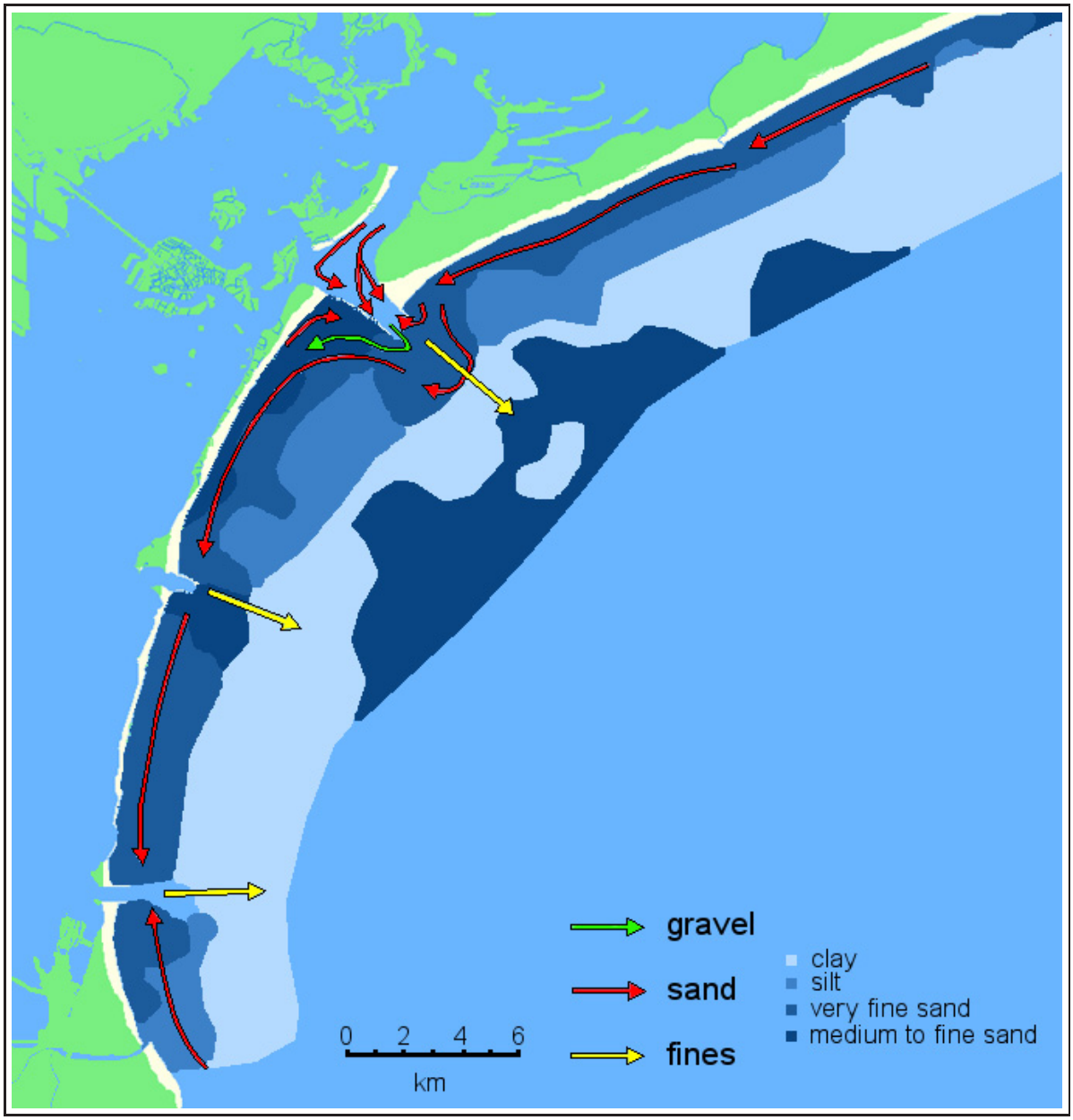

Fig. 5.19: The transport of sand, gravels and fines in Lido Inlet and along the coast of Venice Lagoon. The contours show the sediment of the seabed after Albani *et al.* (1998).

6

Channel Dynamics and Sand Transport

6.1 Introduction

The volume of sediment transported as suspension is the most important control of the sediment budget in a coastal system. Because sediment in suspension is transported within the current flow, the volume transported is much greater than the volume of sediment travelling as bedload (Raudkivi, 1998; Edwards and Glysson, 1999). When flow velocity falls, sediments are deposited from suspension, and this influences the morphological evolution of the system by infilling channels for example (Simon and Senturk, 1992). Suspended sediments are also responsible for the distribution of pollutants and toxins which readily adhere to fine-sediment particles (Yuan *et al.*, 2006), and affect the level of light attenuation important for photosynthesis and the biological food chain (Gartner, 2004).

In order to estimate the export of total Suspended Sediment Concentration (SSC) in Venice Lagoon, upward-looking RDI Acoustic Doppler Current Profilers (ADCPs) were fixed to the seabed in each of the three tidal inlets. The ADCPs have been continuously recording velocity and backscatter data since 2003 to provide estimates of long-term sediment transport in the inlets (Zaggia and Maurizio, 2005). To determine

the velocity and backscatter across the whole channel profile, an additional survey was undertaken with traversing RDI ADCPs. Water column and epi-benthic sediment sampling was also performed to calibrate the backscatter into SSC as backscatter recorded by the ADCP is directly related to suspended matter in the water column (Gartner, 2002). The bottom metre of the water column affects the acoustic reflection (side-lobe echoes Rotaru *et al.*, 2006) of the traversing ADCP, and the fixed ADCP is upward looking and thus does not record any data from the bottom metre either. There is therefore a need to be able to model the concentration of suspended sediment in the lower metre of the water column; possible through application of the Rouse Profile (described in Soulsby, 1997). Furthermore, using data collected from the traversing ADCP it should also be possible to model the bedload transport rate (Soulsby, 1997) so a total mass of sediment in transport can be determined. This can then be used to estimate a sediment budget and be used in the calibration of SHYFEM/SEDTRANS (Ferrarin, 2005), currently under development.

The aim of this chapter is to:

- determine total suspended sediment transport within Lido Inlet by correlating backscatter from the traversing ADCP with various sediment sampling methods and using this to calibrate the fixed ADCP.
- further refine the calibration to differentiate the total suspended fines and total suspended sands.
- calculate the total suspended sediment transport in the bottom metre below the fixed and traversing ADCPs using the Rouse parameter.
- calculate bedload transport using velocity data from the ADCPs.

6.1.1 Methods to Determine Suspended Sediment Concentrations

Traditional methods of sampling Suspended Sediment Concentration (SSC) involve direct sampling of the water column with sediment traps (e.g. Helley-Smith bedload traps shown in Figure 6.4A), Niskin Bottles, and pump sampling. However, there are inherent problems with these techniques; water sampling is limited by small sampling

volumes (increasing potential error) and some samplers (Niskin bottles) are susceptible to accidental triggering resulting in a sample of unknown depth/wrongly assumed depth. Settling within the bottle below the output tap will also remove larger particles from the analysis. The technique is also highly labour intensive and requires time commitment although the efficiency is very high due to the instantaneous collection of water and any suspended particulate matter. Sediment traps can sample much larger volumes but provide average concentrations over the deployment time, which can encompass several resuspension events (Bloesch, 1994). Adaptations of bedload samplers such as the Helley-Smith have also been used but the efficiency falls rapidly with decreasing mesh size from ∼100% between mesh sizes of 0.5 mm to 16 mm (Batalla and Martin-Vide, 2001) to 4% with a 63 μm mesh (Amos *et al.*, 2008). A further disadvantage to the Helley-Smith trap is that it collects only the larger particles in suspension; thus further investigation is required if a complete particle size distribution is required. Optical and acoustical instruments such as Optical Backscatter Sensors (OBS) and laser diffraction particle size analysers (LISST) measure relative turbidity. Turbidity can subsequently be converted into estimates of SSC by calibration (Yuan *et al.*, 2006), with LISST also providing data on the particle size distribution, and are able to sample a greater size range of particles in suspension[i]. OBS instruments work by measuring backscatter, LISST particle size analysers work by measuring laser diffraction. Algorithms are applied to the signals to determine sediment size distribution (LISST) and sediment concentration (LISST and OBS). There are disadvantages in the use of these instruments; OBS calibration is arduous as the sensor is sensitive to fine grain-sizes. Therefore sand will produce lower turbidity readings (NTU) than the same concentration of fine-grained material (Hitchcock *et al.*, 1999; Gartner, 2002). Thus the calibration sample must be representative of the grain-sizes measured in suspension. Sediment colour also effects the reflectivity (Sutherland *et al.*, 2000) although this shouldn't be an issue if un-oxidised sediment from the study site is used to calibrate the sensor. Success of long-term deployment may be affected by biological fouling obscuring the optical sensor (Gartner, 2002), although recent designs have a self-wipe mechanism that limits this problem[ii]. Both instruments (more so the LISST) affect the current flow of the water that they sample (Yuan *et al.*, 2006) and record as single

[i] From manufacturers website: www.sequoiasci.com/products/LISST_Inst.aspx
[ii] www.ysi.com/products - May 2008

point sources. Use of acoustic backscatter methods (Acoustic Doppler Current Profiler - ADCP), which can sample a transect of the water column without affecting the flow in the sampling area, in the determination of suspended particulate concentrations has been investigated since the early 1990s (Thevenot *et al.*, 1992).

6.1.2 ADCP

An Acoustic Doppler Current Profiler (ADCP) is principally used to determine the current velocity throughout the water column. It works by transmitting a high frequency sound pulse (ping) that reflects off particles in the water back to the instrument. Due to the Doppler effect, particles moving away from the instrument return acoustic reflections that are low frequency, particles moving towards the instrument return higher frequency waves. Using the frequency shift, it is possible to calculate the direction and velocity of the water current. The time taken for the pings to return is also recorded so current velocities throughout the water column can be calculated[iii]. As the ADCP uses particles in the water column to determine velocity, in theory it should be possible to estimate SSC, as an increase in sediment concentration will affect the return signal intensity or backscatter to the ADCP (Yuan *et al.*, 2006).

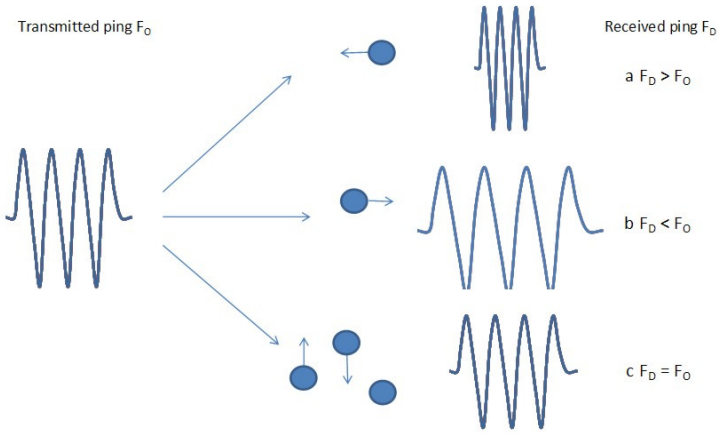

Fig. 6.1: Principles of the operation of an ADCP.

[iii]From Sontek website: http://www.sontek.com/princop/adp/adppo.htm - accessed 23/09/2007

Since the first studies in the determination of SSC using ADCP was published by Thevenot *et al.* (1992), much work has been carried out in an attempt to overcome the inherent difficulties and produce an accurate method to estimate SSC from backscatter (Gartner, 2002; Merckelbach, 2006). Continuous sampling can provide a complete picture of sediment transport over time with no interruption to the flow. Although calibration is still required, the data can be used to provide a long-term estimate of volumes of sediment being imported and exported.

ADCP data are affected by beam attenuation, which is affected by water viscosity and transducer attributes, although this has been solved by authors such as Yuan *et al.* (2006) and is now taken into account by software packages such as WinRiver (Teledyne RDI) and Sediview (Dredging Research Ltd). A further consideration arises as the acoustic ping can be reflected off any floating particle including suspended sediment, organic matter, turbulence/bubbles or even fish; hence separating the proportion of the signal reflected from suspended sediment is difficult. The degree of backscatter is also dependent on particle characteristics such as particle size (the ADCP is more sensitive to larger grains, Yuan *et al.*, 2006), shape and density (Hoitink and Hoekstra, 2005). Sand grains in suspension are thought to be homogeneous in terms of backscatter (Sheng and Hay, 1988; Hoitink and Hoekstra, 2005), but the signal from other suspended matter (organics, fine-grained material) must also be accounted for. These problems are because the instrument operates at a single frequency, thus a change in grain size may be difficult to distinguish from a change in concentration (Gartner, 2002). Merckelbach (2006) states that gauging SSC from ADCP has been carried out successfully using random-phase, acoustic-backscatter modeling as applied in the Sediview software[iv] used by Gartner (2004) and others. Whilst Merckelbach managed to find a good correlation between the model results derived from the echo intensity of the ADCP and actual SSC, the model significantly overestimated the SSC when current speeds exceeded 0.7 m s^{-1} (the echo intensity increased without the expected increase in SSC). Water samples confirmed that there was no increase in the particle sizes in suspension which may have explained the trend. Merckelbach concluded that the difference could be explained by the spatial distribution of particles; randomly spaced particles reflected backscatter with incoherent wave phases, whereas spatially coherent

[iv]DRL Software LTD for RDI ADCPs.

particles could reflect backscatter waves that are in phase and thus produce a stronger echo intensity. The presence of turbulence-induced density fluctuations provides some coherence to the suspended particles over some critical velocity threshold and reflect in-phase acoustic waves. Therefore velocity must be taken into account when using backscatter to derive suspended sediment concentrations.

Wall *et al.* (2006) state that using an ADCP for calculation of SSC should be used as a tangent rather than a replacement to conventional methods because of the level of post-processing and additional measurements or assumptions required to resolve the reasons why echo intensity varies. Also error in SSC estimations increases as the ratio between particle size and acoustic wavelength nears unity (Gartner, 2004). However the benefits of using ADCP may outweigh any disadvantages as they can be operated by ships of opportunity (ferries, container ships[v]) or left unattended on the seabed, and can therefore provide a much larger dataset at a fraction of the cost than can be collected by conventional methods.

Problems with using an ADCP mount from the lack of usable data adjacent to bed; fixed ADCPs are located above the bed and so do not 'see' the water column below the sensor. Traversing ADCPs return bad data from this same area due to the production of side-lobe echoes, which can affect the calculation of velocity and produce artificially high backscatter values (Rotaru *et al.*, 2006). The Rouse profile (Rouse, 1939; Soulsby, 1997) can produce estimates of suspended sediment in this bottom metre (or at any height above the bed) assuming a parabolic reduction in concentration throughout the water column. A reference concentration from near the bed is required along with the Rouse parameter (b):

$$b = \frac{W_s}{\beta \kappa u_*} \tag{6.1}$$

This formula uses the settling velocity (W_s) of the median sediment grain size d_{50}, with von Karman's constant ($\kappa = 0.4$), and the total friction velocity (u_*). The value of β is generally assumed to be unity although this is controversial as values have been obtained both above and below unity (Dyer, 1986; Soulsby, 1997). Lees (1981) evaluated

[v]Ferrybox website: http://www.ferrybox.org/ - November 19, 2007

β using velocity and concentration measurements in the sea and determined that it varied with grain size, changing from ∼1 for very fine sand, and increasing to ∼10 for medium sand (Dyer, 1986). Further to this, an inverse relationship exists between β and SSC 1 m above the seabed reaching unity at around 180 mg l^{-1} (Lees, 1981). For Rouse parameters less than unity, sediment is suspended throughout the water column; greater than unity means that settling dominates vertical mixing and maximum concentrations are found close to the bed (Ralston and Stacey, 2007). Solving the Rouse parameter enables an estimate of suspended sediment concentration at any depth to be calculated:

$$C(z) = C_a \left[\frac{z}{z_a} \cdot \frac{h - z_a}{h - z} \right]^{-b} \tag{6.2}$$

where $C(z)$ is the sediment concentration at height z above the bed, C_a is the reference sediment concentration at reference height z_a above the bed and h is total water depth. The Rouse profile assumes that eddy diffusivity varies parabolically with height and is therefore more suited to riverine environments; a linear diffusion for open-sea conditions requires the *power-law profile* (Soulsby, 1997).

The b parameter is related to grain size relative to flow; a large W_s/u_* (> 2.0) indicates a large grain size in a weak flow, meaning that most transport is as bedload, a small W_s/u_* (< 0.8) indicates smaller grain sizes in a faster flow travelling as suspension (Dyer, 1986; Ogston, 2006).

6.1.3 Bedload Estimations

Most sediment in coastal areas is transported in suspension but a significant volume of sediment will still be transported as bedload; this is important to quantify as it controls the morphology of the channel in the long term. Not only is it the primary method of transportation below transport stage 1 (when $u_*/u_{*c} = 1$ - see Figure 2.12), but it will also occur when most sediment is in suspension and for grains coarser than 2 mm (Soulsby, 1997). The threshold for transport as bedload is related to bottom shear stress and can be determined by the form:

$$\Phi = func(\theta, \theta_{cr}) \tag{6.3}$$

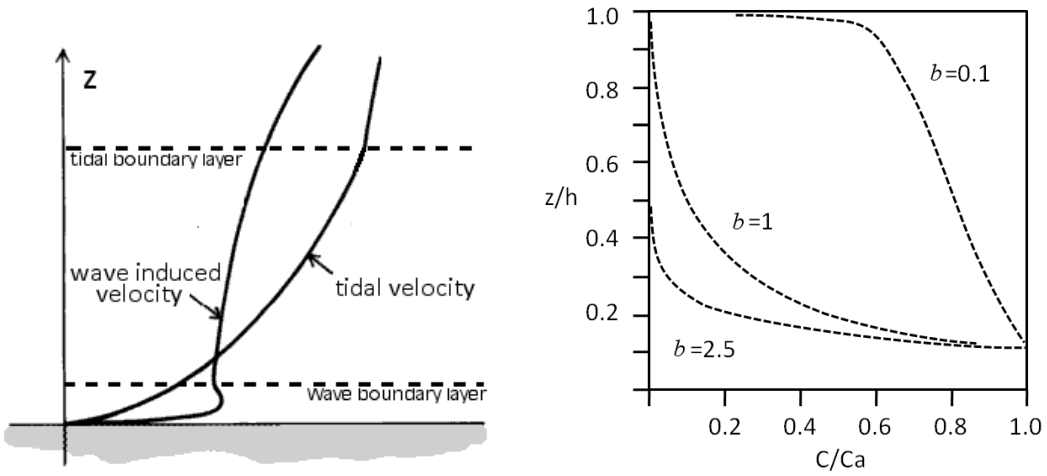

(a) Velocity (b) Suspended sediment concentration

Fig. 6.2: (a) Velocity profiles for wave and tidal velocities showing the smaller boundary layer from wave induced velocities. From Nielsen (1992). (b) Relative concentration profiles for varying Rouse parameters.

where Φ is the dimensionless bedload transport rate: $\Phi = q_b[g(s-1)d^3]^{1/2}$, θ is the Shield's Parameter: $\theta = \tau_0 g\rho(s-1)d$, τ_{cr} is the critical threshold of movement, and q_b is the volumetric bedload transport rate per unit width. Soulsby (1997) summarizes the most common variations of this formula (6.3), but has determined that the equation derived by Nielsen (1992) is well suited to sand transport as bedload under currents as it has been verified by real data, theory and experimentation (Soulsby, 1997). Nielsen's formula follows:

$$\Phi = 12\theta^{1/2}(\theta - \theta_{cr}) \tag{6.4}$$

To convert this dimensionless transport rate into actual bedload rate, the following equation is applied:

$$q_b = \Phi[g(s-1)d^3]^{1/2} \tag{6.5}$$

where q_b has units of $\mathrm{m^2 s^{-1}}$.

6.1.4 Fixed ADCP project - Venice Inlets

Fixed ADCPs (600 kHz RDI Sentinals) have been recording current flow in the three inlets of Venice Lagoon since 2001 as part of ongoing programme to monitor the exchange

of water, sediments and dissolved substances for habitat management and preservation (Zaggia and Maurizio, 2005). Sediview software has been used to calibrate the ADCP using water samples collected by Niskin bottles. The results suggest a narrow range of sediment sizes although there is an acoustical underestimation when the particle size distribution is finely skewed. The average concentration in Lido Inlet was found to be 10 mg l^{-1}, and was found to be strongly modulated by the tide.

The fixed ADCP is located 1 m above the seabed (see Figure 6.3) and therefore does not collect any data in the bottom metre of the water column where much sediment is transported in suspension and as bedload. However, if the sediment concentration (C_z) is known at a reference height (z_a) above the bed, then the Rouse profile can be used to determine sediment concentration in this bottom metre. The fixed ADCP records backscatter and velocity data in the water column directly above it, so in order to estimate the total SSC across the whole channel profile, traversing ADCP profiles have been collected and to SSC derived from the backscatter data. In situ suspended samples collected in collaboration with these profiles provide points of calibration. This chapter will describe the methods used to determine SSC from ADCP backscatter data in order to estimate the total volume of sand and fine-grained sediment in transport.

6.2 Methods

6.2.1 Field Survey

A survey was undertaken on the 19th, 20th, and 21st September 2006 to determine suspended and bedload sediment transport in Lido Inlet and to calibrate the fixed ADCP. Bedload and suspended sediment samples were collected as calibration points in order to process optical backscatter from the traversing and fixed ADCPs into suspended sediment concentration. The survey consisted of two simultaneous operations; the *Litus* was stationed adjacently to the northern jetty opposite the fixed ADCP to collect sand in suspension, with the *Henetus* undertaking ADCP transects between the *Litus* (see Figure 6.3 for positions and Appendix D for sampling times) and the fixed ADCP (N45.42250 E12.42650). Two Helley-Smith bedload samplers fitted with 63 μm mesh were deployed from the *Litus*. The first trap sat directly on the bed to sample

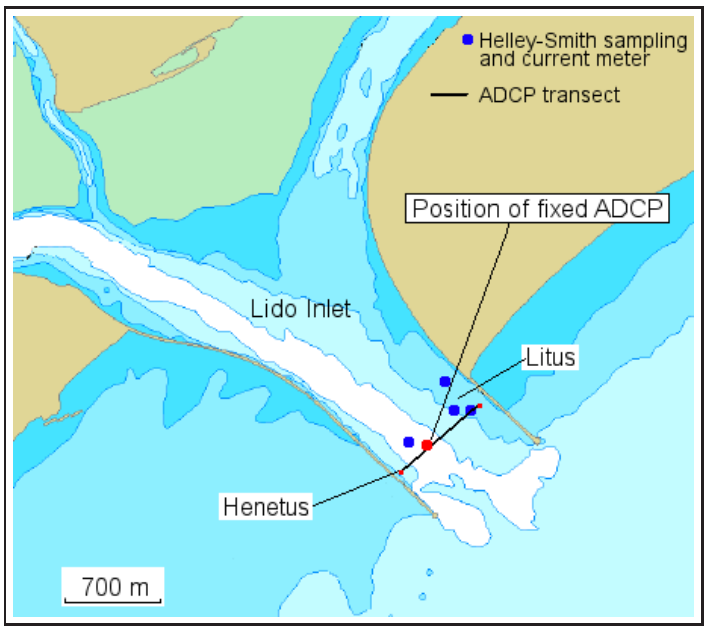

Fig. 6.3: Location of the fixed ADCP in Lido Inlet.

bedload transport (including grains saltating up to 15 cm above the bed); the second trap had skis attached to lift the mouth 13 cm above the bed and sampled sand in suspension (travelling 13-28 cm above the bed). Any sand in suspension in the surface layers were sampled using a streamer bag, also fitted with a 63 μm mesh (see Figure 6.4 for dimensions of the traps and streamer bag). Calibration samples were collected at the surface using a 14 litre bucket. The bucket was filled 40 times during each sampling interval and the water filtered through a 63 μm sieve. Sand retrieved from the traps was also filtered through a 63 μm sieve to remove finer particles. Deployment of all traps for 20 minutes occurred each hour on the commencement of each ADCP transect. A frame with a Valeport current meter (recording at 4 Hz for 6 minutes every 30 minutes), a LISST particle sizer (4 Hz every minute), and an Optical Backscatter Sensor (OBS) were deployed in the same area. An ADV was deployed concurrently with the traps recording at 25 Hz in 5 minute intervals. Finally, a CTD rosette was deployed at the end of each ADCP transect by the *Henetus* with triggers set at 2 m, 10 m (in line with the fixed ADCP), and 12 m to collect Total Suspended Solids (TSS). Profiles of density, temperature, oxygen, salinity and pH were also recorded by the CDT. Velocity data recorded by the fixed ADCP for the water column was also

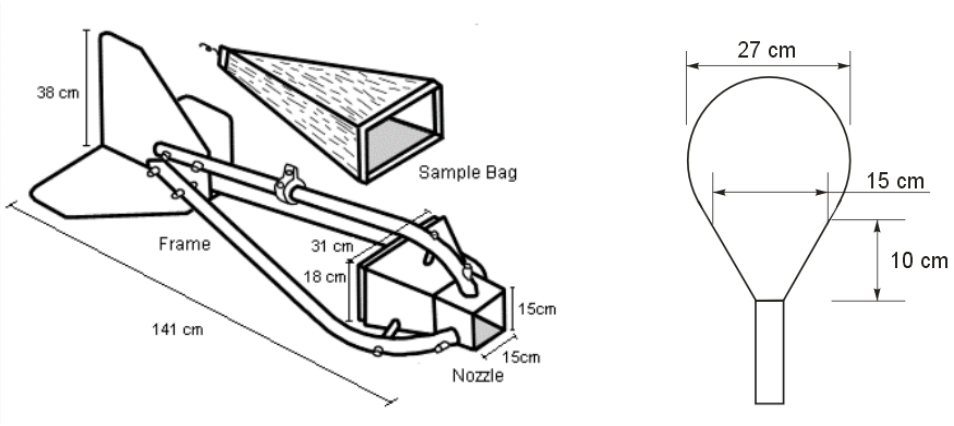

(a) The Helley-Smith sand trap fitted with a 63 μm mesh (Emmett, 1980). A ski attached to the frame near the nozzle lifts the mouth a further 13 cm.

(b) The surface sampler (also fitted with 63 μm mesh).

Fig. 6.4: Sand traps used in Lido Inlet on the 19th, 20th and 21st September, 2006.

available in ten minute bursts for the month of September 2006.

6.2.2 Survey Error

The small size of the mesh on the sand traps results in a reduction in water velocity and potential blockage from clays and larger particles; this means that most water and any associated suspended matter is diverted away at the mouth and is not collected. This is evident in the low efficiencies determined by calibration. Calibration of the Helley-Smith sampler would normally be carried out using pumps but this option was limited due to the volume of water sampled during this survey. Therefore surface water samples were collected using a bucket; approximately 560 litres was passed through a 63 μm sieve to determine mass of sand in suspension. An error of approximately 7% occurs in this method if the bucket was underfilled by just 1 cm (approximately 1 L) as the volume was estimated rather than measured accurately due to time constraints and ease of method. Only the surface sampler bag could be calibrated in this way and was found to have an efficiency of approximately 3±3.5%. The Helley-Smith traps were assumed to have a similar efficiency in the absence of other calibration data.

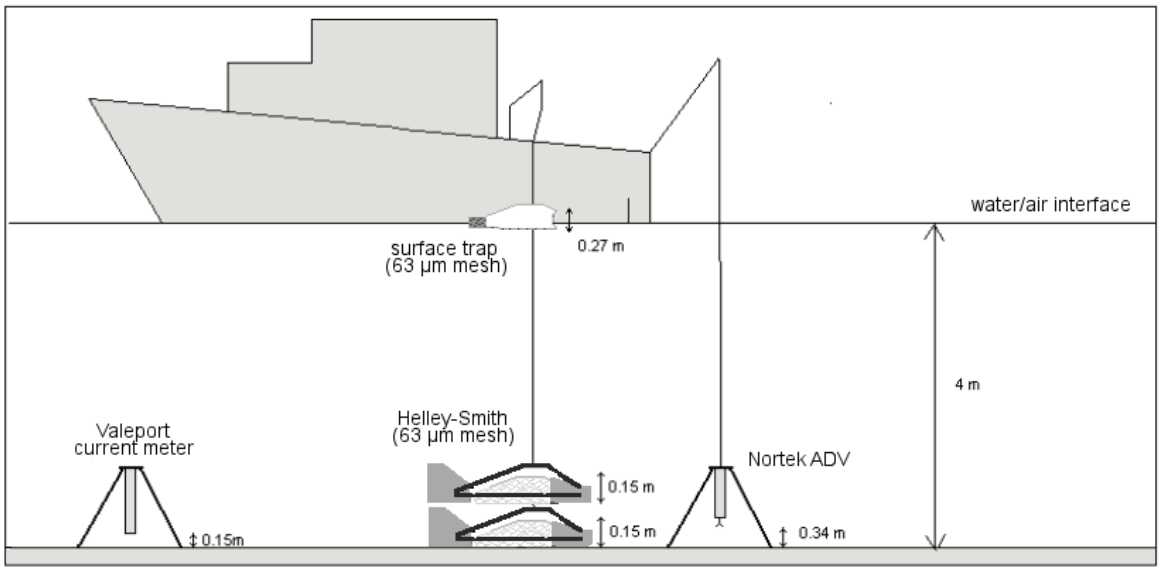

Fig. 6.5: Cross-section diagram showing the positions of deployed instruments from the *Litus* in the September 2006 survey (modified after Venturini, 2007)

6.2.3 Processing and Analysis

The surface (S) and calibration (C) samples from the *Litus* and the niskin bottle samples from the CTD drop (also washed through a 63 μm sieve) were filtered through pre-weighed glass-fibre filters and rinsed with distilled water to remove salt residue. The filters were oven dried and the weight of the residue calculated before being incinerated at 380 °C for 4 hours to determine the percentage of organic and inorganic matter present (loss on ignition). The Helley-Smith samples of near-bottom suspended load (M) and bedload (B) were dried and sub-samples incinerated for total organic carbon. Grain-size distribution of the sand trap samples was determined using the National Oceanography Centre settling column (see page 104).

Velocity of the current taken from the traversing ADCP was used to estimate the total volume of water passing uninhibited through the sand traps so the total concentration of suspended sands (mg l^{-1}) could be determined. The trap efficiency, calculated through comparison with SSC of the calibration samples, was used to produce a final concentration of sand in suspension. Error is introduced if the bedload sampler agitates sediment upon landing on the seabed; this may have produced an

overestimation of the volume of sediment travelling as bedload. Underestimation of sediment may occur if the mesh was blocked by organic matter or sediment.

6.2.4 Suspended Sediment Concentration: Traversing ADCP

6.2.4.1 Method Development

The ADCP data were viewed and processed by WinRiver software[vi] to show acoustical backscatter (dB), which could then be correlated with the calculated SSC. The top metre is not recorded as the sensor head sits below the surface and the bottom metre is disregarded due to side-lobe echoes reflecting from the seabed, which can affect the calculation of velocity and produce artificially high backscatter values (Rotaru *et al.*, 2006).

The main components of suspended matter are inorganic sands and silts, organic particulate matter and macrophytes; the composition of organic and inorganic matter was determined from the sand trap samples and Niskin bottle samples by loss on ignition (see 6.2.3). Sand concentration was determined from the sand trap samples and Niskin bottle samples provided the concentration of fine-grained sediment. Several different combinations of size classes can potentially produce the same backscatter signal (i.e. a low-density sand plume with some silt may produce a similar backscatter signal to that of a high-density silt plume with some sand). To determine the SSC, some characteristics of sediment transport have to be assumed:

- Sand in suspension is less likely above the benthic boundary layer (up to 4 m in this case - Amos *et al.*, 2008), so a linear probability relationship above 4 m is applied.
- Sand in suspension is unlikely to occur in current velocities below the suspension threshold for sand.
- The concentration of fines in suspension is likely to be constant over the water column.

[vi] Teledyne RD Instruments

- A Rouse profile can be define sediment concentration in the bottom metre of the water column.

The raw ADCP data were processed within WinRiver to extract the ensemble number (count), depth of bin, velocity magnitude and direction, backscatter intensity (dB) and water depth. Sediment concentrations were calculated using regressions between backscatter and sample concentrations. Sand concentrations were determined through a regression of backscatter and sand trap samples corrected for efficiency: $C_s = 1.697I_b - 116.15$, where I_b is backscatter intensity. Fines concentration was found using a straight-line function, where m and c were derived from a regression of backscatter and fines concentration at depths of 2, 10, and 12 m (see Table 6.1 and Figure 6.6). The gradient and intercept from the three equations were plotted to gain

Depth (m)	Fines Concentration Equation	R^2
2	$y = 0.59x - 33.31$	0.44
10	$y = 0.77x - 44.36$	0.59
12	$y = 0.73x - 43.45$	0.37

Tab. 6.1: The equations derived from Niskin fines concentration and backscatter at different depths.

two further equations (Equations 6.6 and 6.7) to derive the gradient and intercept for any depth(x), allowing fines concentration to be calculated (y).

$$m = 0.247 \ln(x) + 0.156 \tag{6.6}$$

$$c = -18.6 \ln(x) + 0.886 \tag{6.7}$$

This presumes that backscatter is a direct function of fines concentration, so the following assumptions were also applied:

1. if $U_{100} < 0.2$ m s^{-1} (below the suspension threshold of sand); then only the calibration for fines is applied throughout the water column.
2. if $U_{100} > 0.2$ m s^{-1}; then:

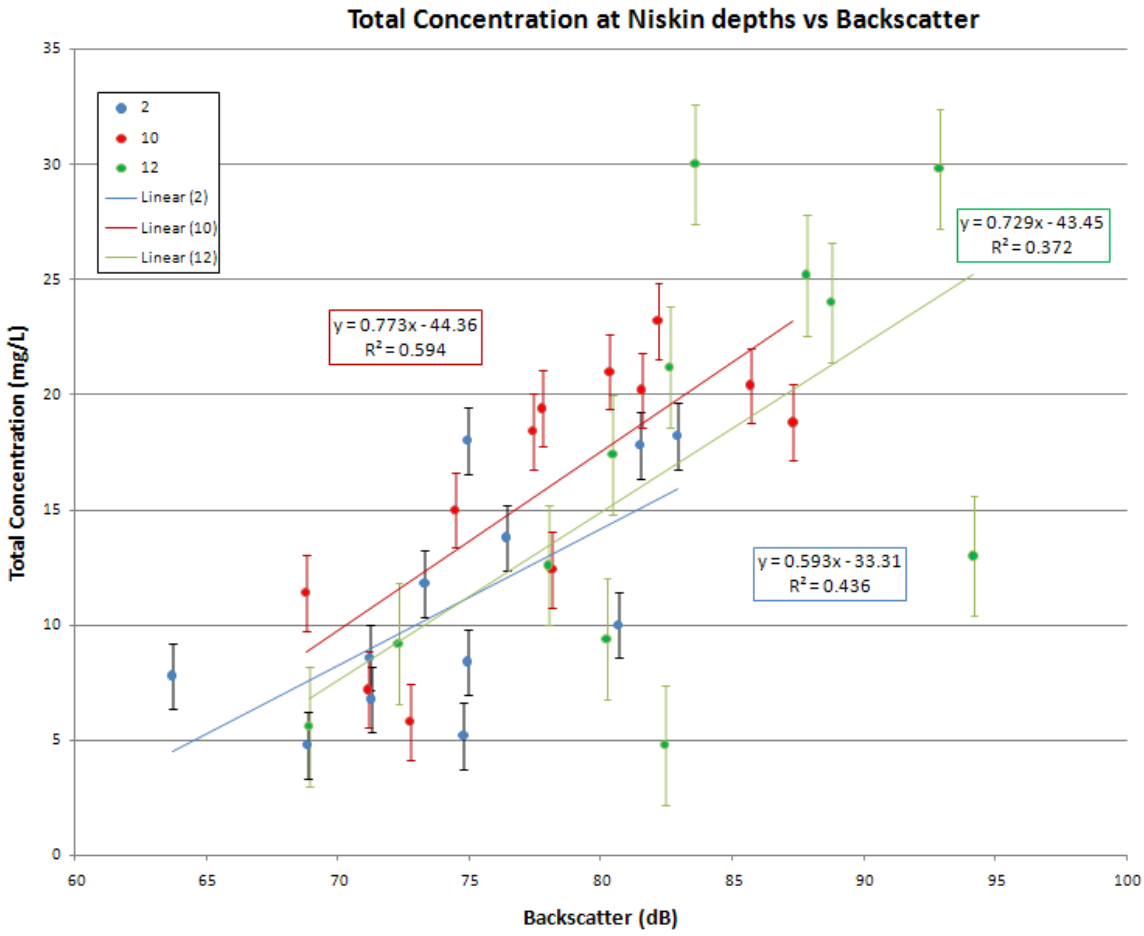

Fig. 6.6: Correlation between backscatter and fine sediment concentration for the three survey days. Standard error is applied to show similarity of regression.

(a) the backscatter is calibrated for sand in bottom 4 m;

(b) a linear probability function is applied to the sand calibration between 4 and 8 m (the estimated concentration of sand is more likely to be correct closer to the bottom);

(c) the backscatter is calibrated for fines at a constant concentration above 8 m.

(d) the backscatter is calibrated for fines above 8 m (as sand will not be present above 8 so backscatter is a function of fines).

The Rouse profile was calculated to determine suspended sediment concentration in the bottom metre of the water column. The deepest bin of the ADCP data from which the sediment concentration had been calculated, was used as the reference concentration (C_a) and reference depth (z_a) of Equation 6.2. Settling velocities of sand (D_{50} = 125 μm) and fine-grained sediment (D_{50} = 30 μm) were determined (0.0225 and 0.0073 m s^{-1} respectively) and WinRiver-style profiles created to show concentration of sand, fines and total inorganic suspended matter (see Figure 6.7). These diagrams showed representative pictures of sand and fine-grained sediment in suspension at lower velocities; however at higher velocities, the profile appeared very striated, and contours of SSC appeared affected by the shape of the profile rather than the intensity of backscatter (Figure 6.7B). The sand and fines concentrations are derived separately for this method, which is the predominant reason to why this method is dubious. As the backscatter signal is a function of all suspended particles it is difficult to undertake separate regression analysis for each class (e.g. sand, fines, organics). Therefore the resultant relationship within the method described above for either fines or sands cannot be reliably attributed to either sediment size, based solely on the backscatter signal; i.e. the regressions falsely assume that backscatter is a product solely of sand or fine sediment, whereas it is a product of both sizes (and also other floating particulate matter). Thus the ideal sampling dataset would include the percentage of fines and sand to show exactly what the backscatter is being reflected off. Difficulties in obtaining this type of data derive from sampling methods; the sediment traps collect only sediment larger than 63 μm, and although able to collect an entire particle size distribution, water sampling can misrepresent the concentration of sands due to the small sampling volume. However, as the sampling depth and volume is known at three positions within the water column (2, 10, and 12 m), Niskin-derived fines concentrations can be used as the first step in developing the method.

6.2.4.2 Further Development of the Method

Standard error was applied to the regression of Niskin fines concentration and backscatter (in Figure 6.6) to verify whether that there was no backscatter variation due to

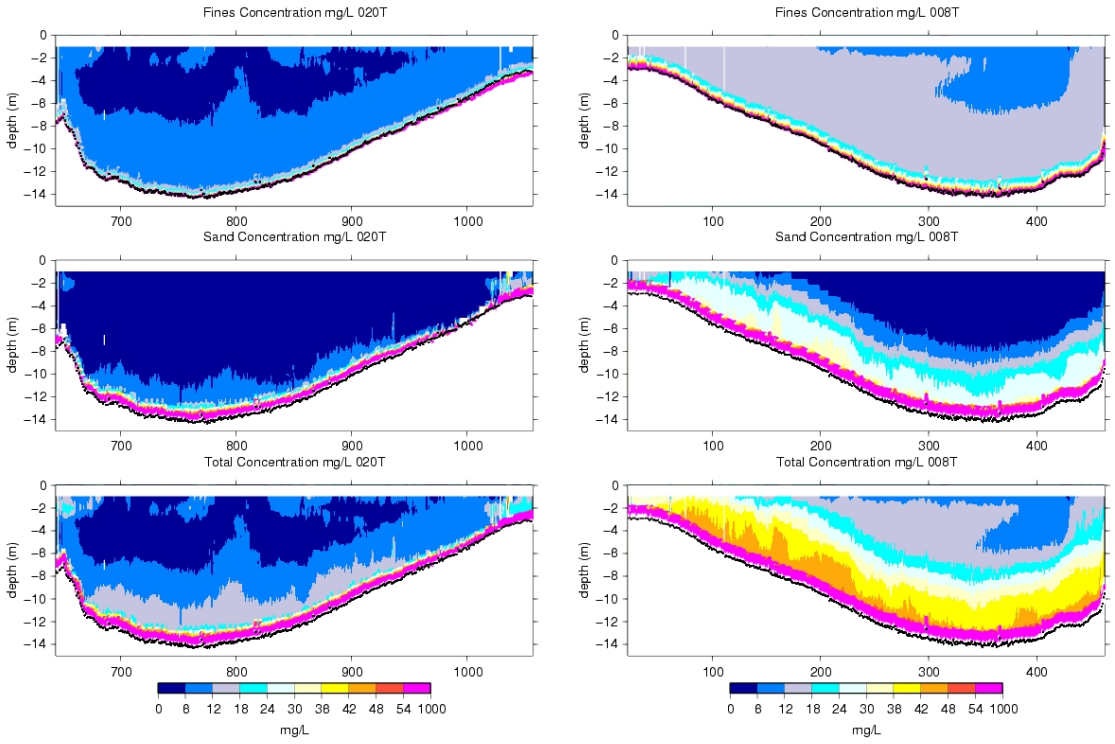

(a) 20th September - low velocity

(b) 19th September - high velocity

Fig. 6.7: Results from the initial method showing fines (top), sand (middle) and total concentration (bottom). Note that high velocities show the weakness of the method - linearisation.

depth (depth effects should have been removed during correction of echo intensity). There was significant overlap between the depths proving that the samples were similar and the backscatter produced is not dependent on depth. The regression was therefore replotted without accounting for depth, producing the correlation;

$$C_f = 0.889 I_b - 54.34 \tag{6.8}$$

where C_f is fine sediment concentration and I_b is backscatter (dB). The regression was applied to the backscatter from the traversing ADCP files and profiles imaged to show fine-grained sediment concentration. Accuracy of the results were compared to those determined by SediView, a popular, commercially available piece of post-processing

software (USACE, 2007; Zaggia and Maurizio, 2005)

The regression is derived from only fines concentration and using separately derived sand concentrations from the sand traps has already been shown not to work. The use of a LISST instrument was therefore employed to give further information on the grain size distribution of the water column. The LISST (Laser In-Situ Sizing/Scattering and Transmissometry) instrument was deployed on the same frame as the Valeport and OBS sensors, recording data every minute for the duration of the survey each day to give the particle concentrations (ug l^{-1}) for 32 size classes between 1.25 to 250 μm. Accuracy of the LISST has been documented in Bale (1996); Gartner *et al.* (2001); Pedocchi and Garcia (2006). The LISST data were compared to the SSC estimates derived from the Niskin samples, which is preferable to just using the single-point measurement of the LISST data as the Niskin samples were taken at three positions throughout the water column. The total concentration of fine particles ($<$ 63 μm) derived by the LISST was summed and compared with the Niskin concentration at 12 m (the closest depth to the LISST sensor depth). A positive correlation (Figure 6.8) was found with an $R^2 = 0.68$, showing that the concentration described by the LISST is approximately double the estimate calculated from the Niskin bottle sampling. The difference in concentration is partly due to the difference in depth between both samplers; the Niskin sample was taken at 12 m ($\sim$1 m off the bed), and the LISST was 0.45 m off the bed. There may also be errors in the calibration of the LISST, and particle loss during recovery of the grains from the water sample (settling below output pipe and loss from filtering of sand grains). This correlation showed that using the LISST was a viable alternative to using sand traps to determine suspended sand concentrations; therefore the concentration of particles larger than 63 μm was also summed from the LISST data.

The LISST-derived concentrations of both sands and fines were plotted against tidal elevation, velocity, wind speed and wind direction (strong winds can cause resuspension, and direction can affect the fetch and waves, affecting suspension), shown in Figure 6.9. Suspension of fine-grained material follows changes in velocity. Water depth is important as larger concentrations of fine-grained material occur when the water level is lower due to the thickness of the boundary layer. Velocity is also an important

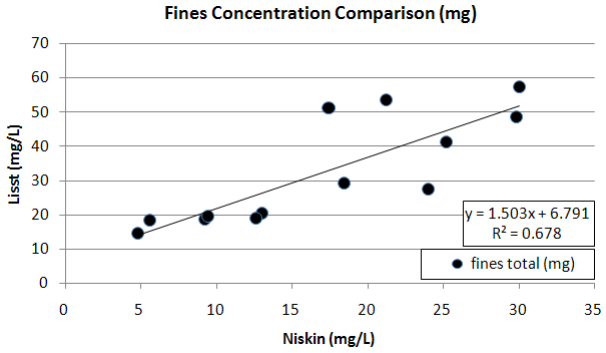

Fig. 6.8: Comparison of fines concentration as determined by Niskin bottle sampling and LISST instrumentation.

factor in controlling sand in suspension, but it appears that the sirocco (south-easterly wind) helps to maintain sand in suspension when tidal velocities fall. However, on two occasions high concentrations occurred when the wind direction was variable prior to becoming southerly; this may be the results of a predominant southerly wind causing waves, which are more effective at suspending sediment due to a thinner boundary layer (Figure 6.2A). The southerly winds coincide with maximum current velocities so the trend is not definitive. A correlation was found between the Niskin suspended fines concentrations and LISST suspended sand concentrations (Figure 6.10). It appears that up to ∼15 mg l^{-1} of fines in concentration, the proportion of sands to fines remains at around 57% (± 5%) sand. Above this concentration, the proportion of sands increases to an average of 70% (± 4%). The total correlation is shown in Figure 6.10:

$$C_s = 0.101 \ln(C_f) + 0.367 \tag{6.9}$$

where C_s and C_f refers to concentrations of sand and fines respectively. The correlation is reliable only at z =1 m, as fines concentration throughout the water column can be assumed to be almost linear (above the boundary layer, calculated to be approximately 4 m thick - Amos *et al.*, 2008), whereas sand will be concentrated nearer the bed (Soulsby, 1997). Therefore the concentration of sand relative to fines changes according to the position in the water column (z). However, the equation is useful as it provides a value for C_z (C_s at 1 m) to calculate the Rouse profile. The Rouse profile was used to calculate the concentration of sand in the water column. The value C_s/C_z is

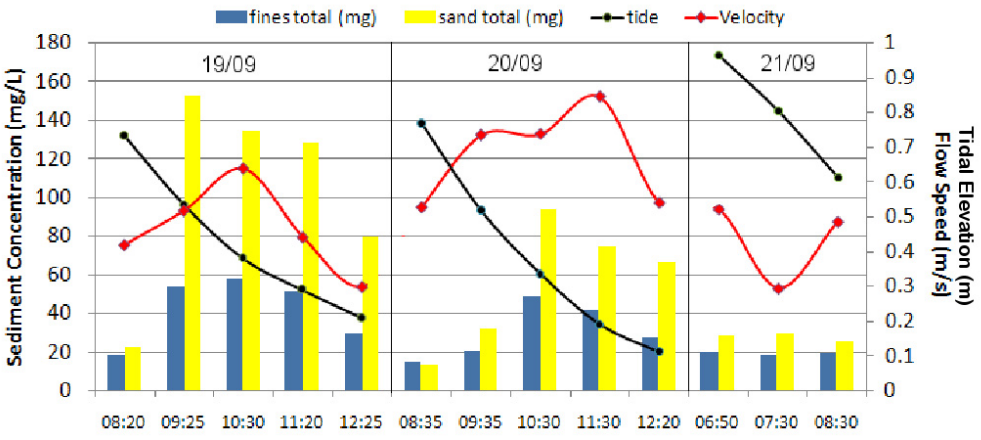

(a) tidal elevation and current velocity (Valeport current meter)

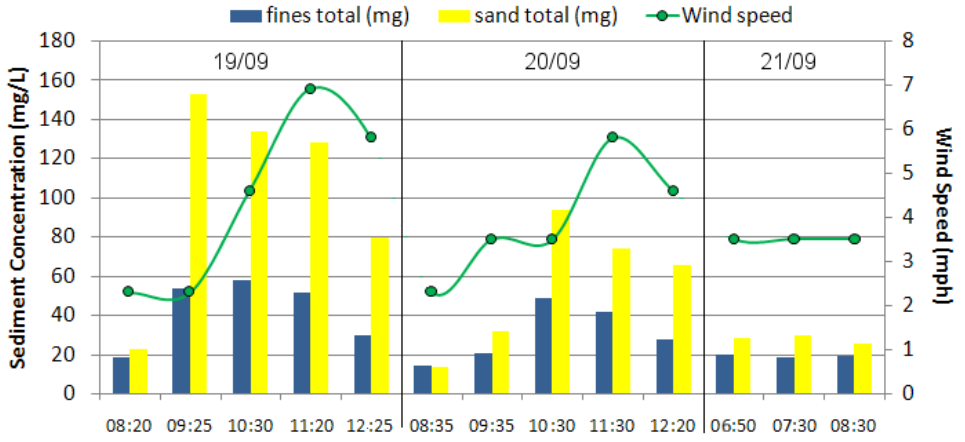

(b) wind speed

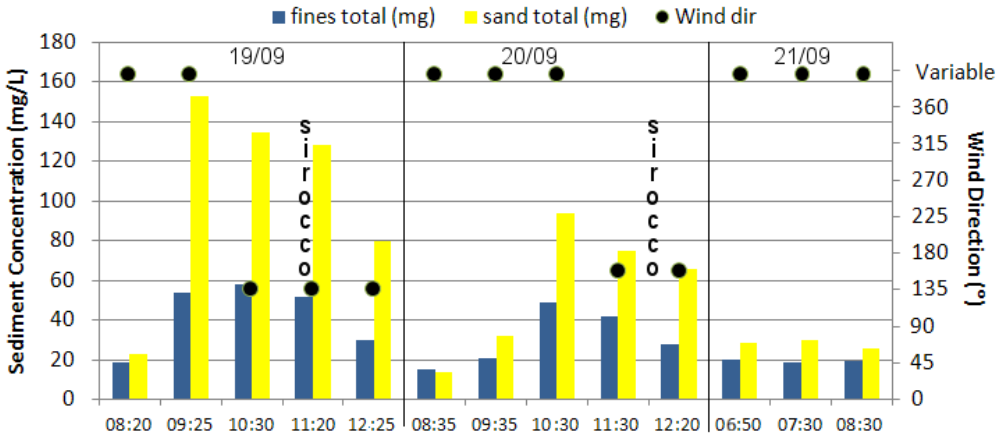

(c) wind direction

Fig. 6.9: LISST derived fines and sand concentration against possible concentration affecting variables.

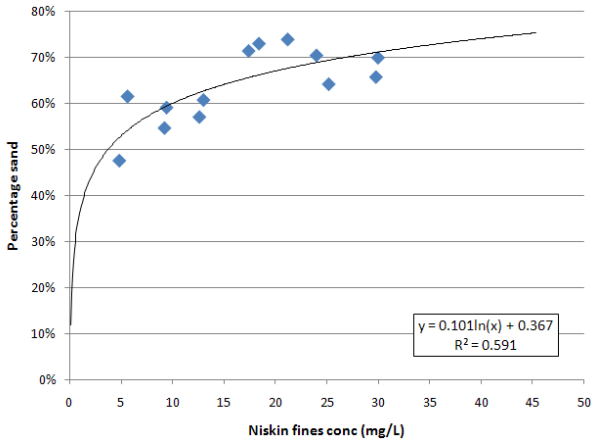

Fig. 6.10: Correlation between Niskin-derived fines concentration and LISST-derived sand concentration.

determined by solving Equation 6.9, and the changing variables of water depth and velocity taken into account at each point where C_s is known. The method is displayed in the following steps, with brackets denoting values used in this study:

1. Determine the Rouse parameter (Equation 6.1) for a range of relevant water depths (h = 14, 12, 10, 8, and 5 m) and relevant $\overline{U}$ velocities ($\overline{U}$ =0.1, 0.2, 0.3, 0.4, 0.5, 0.6, 0.8, and 1 m s^{-1}) for both fines (40 μm) and sands (98 μm).

$\overline{U}$	Fines Conc. (mg l^{-1})					Sands Conc. (mg l^{-1})				
	14	12	10	8	5	14	12	10	8	5
0.1	0.55	0.54	0.52	0.51	0.47	3.21	3.13	3.05	2.94	0.23
0.2	0.28	0.27	0.26	0.25	2.71	1.60	1.57	1.52	1.47	1.36

Tab. 6.2: Example of Step 1: Determine Rouse number (b)

2. Calculate the Rouse profile at a range of arbitrary suspended fines concentrations within bounds determined by sediment sampling (1, 5, 10, 15, and 20 mg l^{-1}) using z values every 0.1 m for the first metre above the seabed and then once every metre subsequently (1, 2, and 3).

3. Use Equation 6.9 to calculate the percentage of sand as a total and determine concentration relative to the fines (see table below).

Fines (mg l^{-1})	1	5	10	15	20
Sands (mg l^{-1})	0.58	5.63	14.97	26.73	40.53

4. Apply the Rouse profile to the calculated sand concentrations (as in Step 2) using the Rouse number for a sand d_{50} (111 μm; the mean grain size of the sand caught in the sand traps).

5. Produce a regression ($y = mx^c$) of fines and sand for each z value for every water depth (h) class chosen at Step 1.

6. Produce a regression of m (from previous step) and z for each $\overline{U}$ and h class. $m = nz^p$

7. Apply the equation $y = mx^c$ (from Step 5), where x is fines concentration, m is determined by Step 6, and c is as produced by Step 5 to produce the concentration of sand in suspension at any depth (dependent on $\overline{U}$ and h).

These steps were used to calculate fines (section 6.2.4.2) so that the concentration of sand in suspension could be calculated for any ADCP bin as long as the suspended concentration of fines was known, as well as water depth, depth-averaged velocity and height above seabed. The final steps summed the suspended concentration of fines and sand to determine the total sediment in suspension per bin and per profile so that total sediment export could be calculated.

6.2.5 Suspended Sediment Concentration: Fixed ADCP

To determine sediment transport over a longer time scale than provided by the traversing ADCP, the data calculated from the previous section must be used to calibrate SSC values derived from the fixed ADCP, which continuously collects data every ten minutes from the main channel of Lido Inlet.

The ADCP is fixed at 1 m above the seabed and can sample a vertical column of water, 13 m in height (although the top 2 bins are bad data in this study). The data from the fixed ADCP was available as velocity and echo intensity, which could not be converted into backscatter by WinADCP. The conversion corrects for sound

absorption, beam spreading, transducer temperature and power (Gordon, 1996). As the process can be complicated (Deines, 1999), the velocity was used to determine suspended sediment concentration in conjunction with the application of the Rouse profile, which was required to determine the SSC in the bottom metre of the water column where no data was available from the fixed ADCP. Sediment samples were collected by sand trap in the vicinity of the fixed ADCP at the same height as the first data bin (Venturini, 2007) but no correlation was found with the suspended sand concentration and velocity, so no C_a could be determined. A number of methods exist to calculate the sediment concentration (C_a) at a reference height (z_a) in the absence of samples (Soulsby, 1997). The formula derived by Smith and McLean (1977) is recognised to be one of the more accurate methods (Garcia and Parker, 1991; Soulsby, 1997):

$$C_a = \frac{0.00156 T_s}{1 + 0.0024 T_s} \tag{6.10a}$$

$$z_a = \frac{26.3 \tau_{cr} T_s}{\rho g \left(s - 1\right)} + \frac{d_{50}}{12} \tag{6.10b}$$

where T_s is a transport parameter ($\frac{\tau_{0s} - \tau_{cr}}{\tau_{cr}}$), τ_{cr} is threshold shear stress.
Using a d_{50} of 106 μm, which was the mean grain size of the sand traps deployed on the northern edge of the inlet (see Figure 6.3), and the depth averaged velocity ($\overline{U}$) from the fixed ADCP, C_a and z_a were calculated using the method of Smith and McLean (1977). The Rouse profile was then determined with Equation 6.2 at z values (height above seabed) every 0.1 metre to 0.9 m and every metre from 1 to 13 m.

The results provided very high concentrations when velocity exceeded around 0.4 m s^{-1}. Therefore, OBS data and Valeport velocity data were compared and a correlation of $C_a = 32.36 \ln \overline{U} + 103.4$ determined[vii]. The d_{50} was determined from grain size analysis of the sand trap data from the site near to the fixed ADCP. A logarithmic relationship between the height above the seabed and mean grain size was determined (Figure 6.11), from which, the d_{50} was determined at height z. Between the heights of the benthic frame (current meter, OBS and LISST; 0.45 m) and the fixed ADCP head ($\sim$1 m), the average d_{50} of 98 μm was assumed. The Rouse profile was recalculated to produce a transect of sediment concentration throughout the survey period (see Figure

[vii] see section 6.2.5

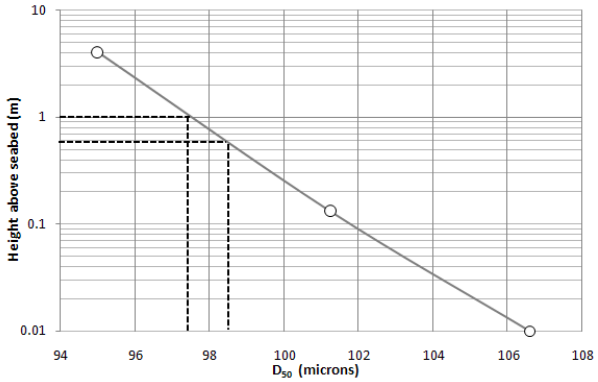

Fig. 6.11: Correlation between height above seabed and mean grain size (d_{50}). Dashed lines show heights of the fixed ADCP and LISST.

6.23 in the results section). The results were compared with the SSC results from the traversing ADCP. As the fixed ADCP collects data continuously, these calculations for the Rouse profile were run again for the entire month of September 2006 to determine net sand transport.

This method produced sensible results with suspended sediment concentrations values similar to those produced from the traversing backscatter data, although no correlation was found between the two datasets. Consequently, the suspended sediment concentrations from the traversing ADCP were compared with meteorological data as sediment can also be suspended by waves (Figure 6.2B). This was especially important as the R^2 value for velocity against OBS SSC was 0.45, suggesting than another factor had influenced the results. Three sets of data, ADCP velocity/sand trap, Valeport/OBS and $\overline{U}$/OBS were initially plotted against tidal elevation, but no significant correlations emerged. The data was then divided according to the time of collection, which revealed a significant difference between morning and afternoon samples. The afternoon samples had a much greater concentration than those collected in the morning despite being collected under similar velocities. Separate regressions (Figure 6.12) found that morning samples followed an exponential relationship, with an average R^2 of 0.88. Afternoon samples followed logarithmic relationships, with an average R^2 of 0.56 (reduced due to a bad sand trap correlation). The best fit, with an average R^2 of 0.83 was between $\overline{U}$ and OBS SSC, but cannot be applied until the reason why separa-

tion in the results occurs between morning and afternoon sampling is determined. The tide was in the last stages of ebb at 12pm before turning at 3pm near the end of the survey day. Therefore the split is not due to a simple ebb/flood difference. Wind speed increased in the afternoon but the most significant factor seems to be wind direction, which changed from NE in the morning to SE in the afternoon (with some variability between 10am and 1pm). Wind driven velocity has a thinner boundary layer, encouraging resuspension of sediments from the bed. The regressions therefore reflect the shape of the velocity profiles (see Figure 6.2A). The fixed ADCP velocity data was

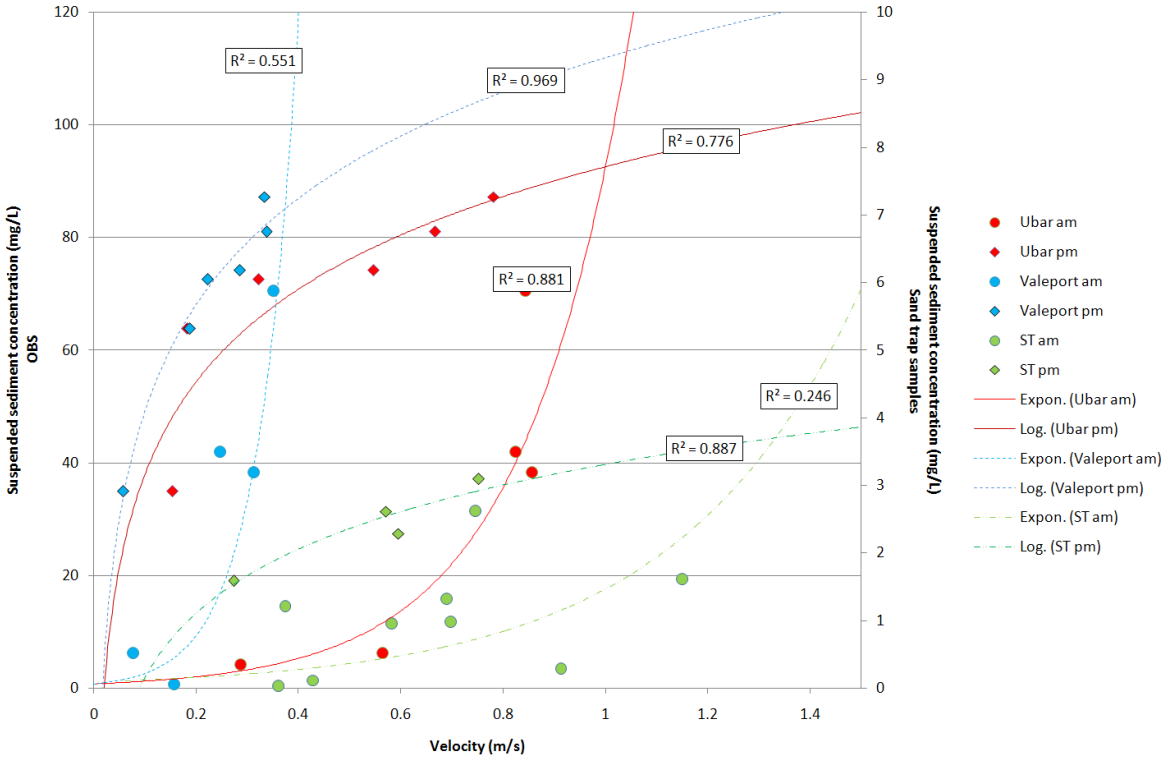

Fig. 6.12: Suspended sediment concentration vs velocity. OBS SSC has been correlated with $\overline{U}$ from the fixed ADCP (Ubar) and Valeport velocity. Sand trap (ST) data has been correlated with ADCP velocity. Note that afternoon samples (diamonds) regressed logarithmically, and morning samples (circles), exponentially.

re-processed to incorporate wind effects using $C_{(z)} = 0.789 \exp^{4.766\overline{U}}$, ($R^2$=0.88) for normal conditions, and $C_{(z)} = 23.72 \ln\left(\overline{U}\right) + 11.8$, ($R^2$=0.78) for data collected during Sirocco events. The results appeared to compare favourably with suspended fines concentration, despite the OBS being calibrated for total sediment. However, as the

calibration relied on simple laboratory based methods involving mechanical mixing in a shallow container and subsampling, the likelihood is that most sands settled before subsampling could effectively collect them. As the results were comparable to estimates of the concentration of suspended fines determined by the traversing ADCP, the same proportional-based method was used to find the concentration of suspended sand for the fixed ADCP.

6.2.6 Bedload Transport

Although the traversing ADCP cannot provide estimations of bedload transport through the conversion of backscatter data, it can provide values for $\overline{U}$ and h needed to solve the volumetric transport rate (q_b Equation 6.4); thus high resolution estimates of bedload transport can be calculated across the whole profile. As the equation (Equation 6.5) requires similar variables for the calculation of the Rouse profile, the processing script used to estimate suspended sediment concentration was altered to provide estimations for bedload transport in the inlet. The average grain size used in the calculations was 179 μm as indicated by the grain size maps described in Chapter 5. Bedforms were assumed (as it was observed that the skin friction Shield's parameter remained below 0.8 when suspended sediment concentrations were calculated - Soulsby, 1997) and estimated using the assumptions in Soulsby (1997) that ripple wavelengths are $\sim$1000 grain diameters ($\lambda_r = 1000 d_{50}$) and ripple height is 1/7 of the wavelength ($\Delta_r = \frac{\lambda_r}{7}$). These estimates were used in the calculation of the form-drag component of shear stress to find the total shear stress ($\tau_0 = \tau_{0s} + \tau_{0f}$) for the Shield's parameter (in Equation 6.4). The processing produced a single image for the three day survey (see results). To calculate the total bedload transported per hour across the whole profile the transport rate (q_b) was summed across the whole profile and plotted onto a graph. The area under the graph was calculated to find q_b m^{-1} hr^{-1} and multiplied by the average width of each ping (approximately 1.8 m) to find the total volume transported over the width of the profile. The total mass transported was calculated by multiplying the total volume transported by ρ_s (dolomite; 2860 kg m^{-3}).

6.3 Results

6.3.1 CTD

Over the survey period, water temperature varied only by 0.5 °C over most of the water column. Only in the top 4 m was there any variation with depth as surface water temperature harmonized with air temperature. The water was slightly alkali, remaining between pH 8.3 and 8.4 for the whole survey; there was also little variation with depth. Water density increased with depth from an average of 21 (σt) in the surface layers to 23.5 below 4 m. A variation of 3 σt occurred over the survey in both the surface and bottom layers, reducing during ebb flow and increasing with flood (Figure 6.13B). The trend is similar for salinity, with an average of 30 PSU at the surface increasing to an average of 34 PSU at depth. The difference between surface and deeper waters was more noticeable when current velocities were low. The CTD also recorded oxygen saturation levels (shown in Figure 6.13A) and showed them to be super-saturated, in comparison to atmospheric oxygen levels, over most of the survey. They remained relatively stable (around 118%) on the first two survey days, although the top 0.5 m of the water column became under-saturated during the 20th. The data from the 21st September showed a super-saturated oxycline (130%) between 2 and 4 m deep, although oxygen saturation was much lower in water above (minimum of 83%) and below (average of 104%).

6.3.2 ADCP Backscatter and Velocity

The first day of surveying (19th September) was conducted over a change in the tide from ebb to flood. During this time, velocity increased from around 0.4 m s^{-1} to 0.6 m s^{-1} before decreasing to 0.3 m s^{-1} during slack water (see Figure 6.14). The backscatter trend follows that of the bottom velocity, which tended to increase and decrease at a greater rate than surface velocity. The backscatter also followed the bottom velocity trend on the 20th September although in this case the surface velocity responded to a greater degree to the changing tide. Velocities were on average, 0.05 m s^{-1} faster than the previous day, with a peak velocity of 0.8 m s^{-1} (see Figure 6.14). No trends are recognised on the 21st September as data could only be collected for a few hours in the morning, resulting in few datapoints. Images of ADCP backscatter and velocity

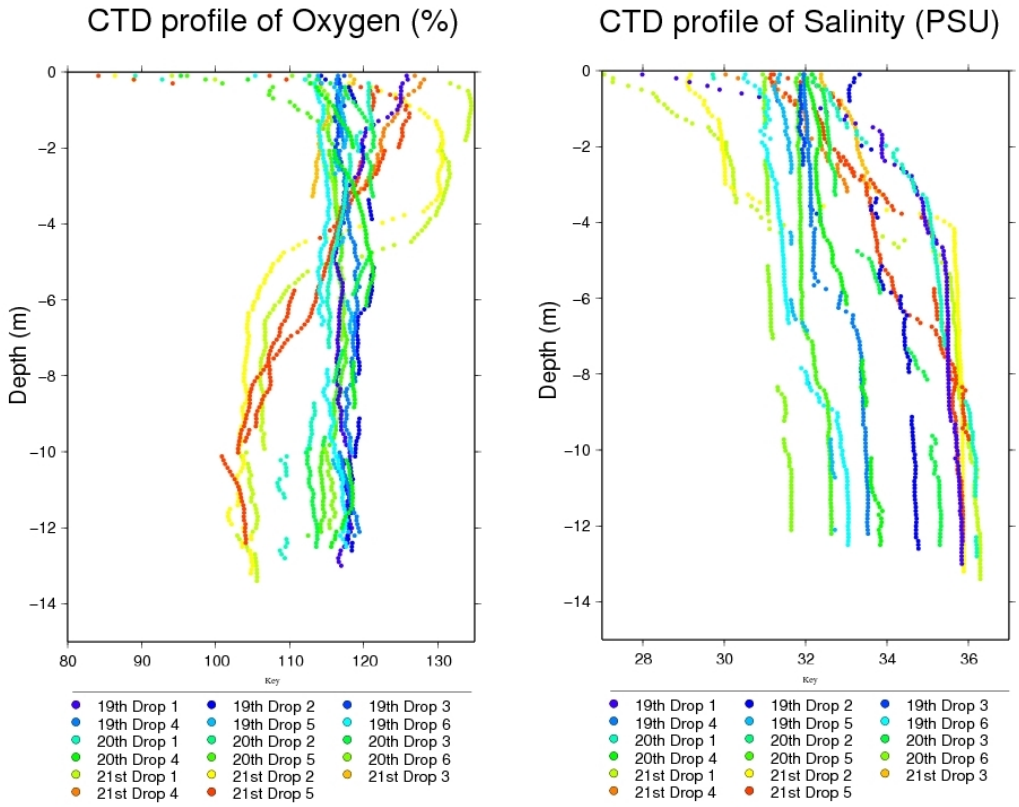

(a) Oxygen saturation (b) Salinity

Fig. 6.13: CTD profiles of oxygen saturation and salinity during the 19th to 21st September

were arranged to show a transect through time for each day (see Figure 6.15). On the morning of the 19th, the backscatter was relatively low (around 65 dB) with higher backscatter in the main channel of Lido Inlet, which gradually spread along the bottom of the whole channel with time. At 11 am (profile 5), backscatter increased to around 80 dB across the whole channel, with just the surface metres remaining below 70 dB. This area of low backscatter gradually diminished as velocities reached peak speeds, before returning gradually at 2 pm (profile 15) when velocities dropped around slack waters. The velocity was faster on the 20th, with greater speeds at depth than the previous day, although the spread across the channel was similar. The backscatter was also higher, with 'plumes' of high backscatter (90 dB) extending from the bottom of the channel, both in the deepest and shallowest area. The data collected on the 21st

shows that velocities fell initially within the main channel also, but generally showed a similar pattern to the previous survey days with an increase of backscatter from the bottom of the profile and an increase in velocity.

6.3.3 Suspended Sediment Concentration: Traversing ADCP

There is not a good correlation between ADCP velocity and backscatter (R^2=0.2); however, the general trend is an increase in backscatter with an increase in velocity until flow speeds reach approximately 0.7 m s^{-1}. The average backscatter then falls despite further increases of velocity (see Figure 6.16).

Although data on organic matter was collected from the sand trap samples, no significant correlations were uncovered between velocity or backscatter, although organic material appears to have been transported in the bottom of the water column at lower velocities, and transported in the surface waters at higher velocities. The median proportion of organics in the samples is 4.8%, and although there are samples containing up to 90% organics, the lack of any correlation and generally low presence makes any definitive organics analysis from backscatter difficult. The survey was not designed to accurately monitor floating organic matter; thus a leaf caught in the traps will make a large contribution to the proportion of organic matter. It will therefore be ignored within the processing procedure, although will be further examined in the

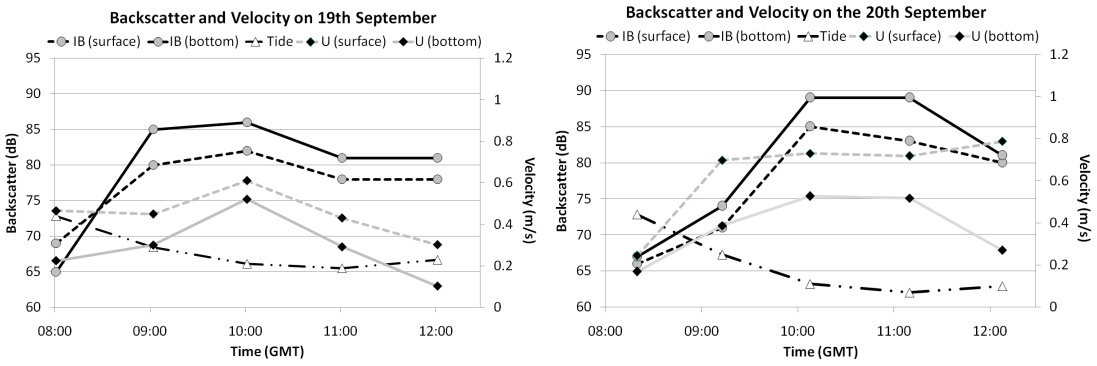

(a) 19th September (b) 20th September

Fig. 6.14: Velocity, ADCP backscatter, and tidal elevation during the 2006 survey. The 21st is not shown due to lack of datapoints.

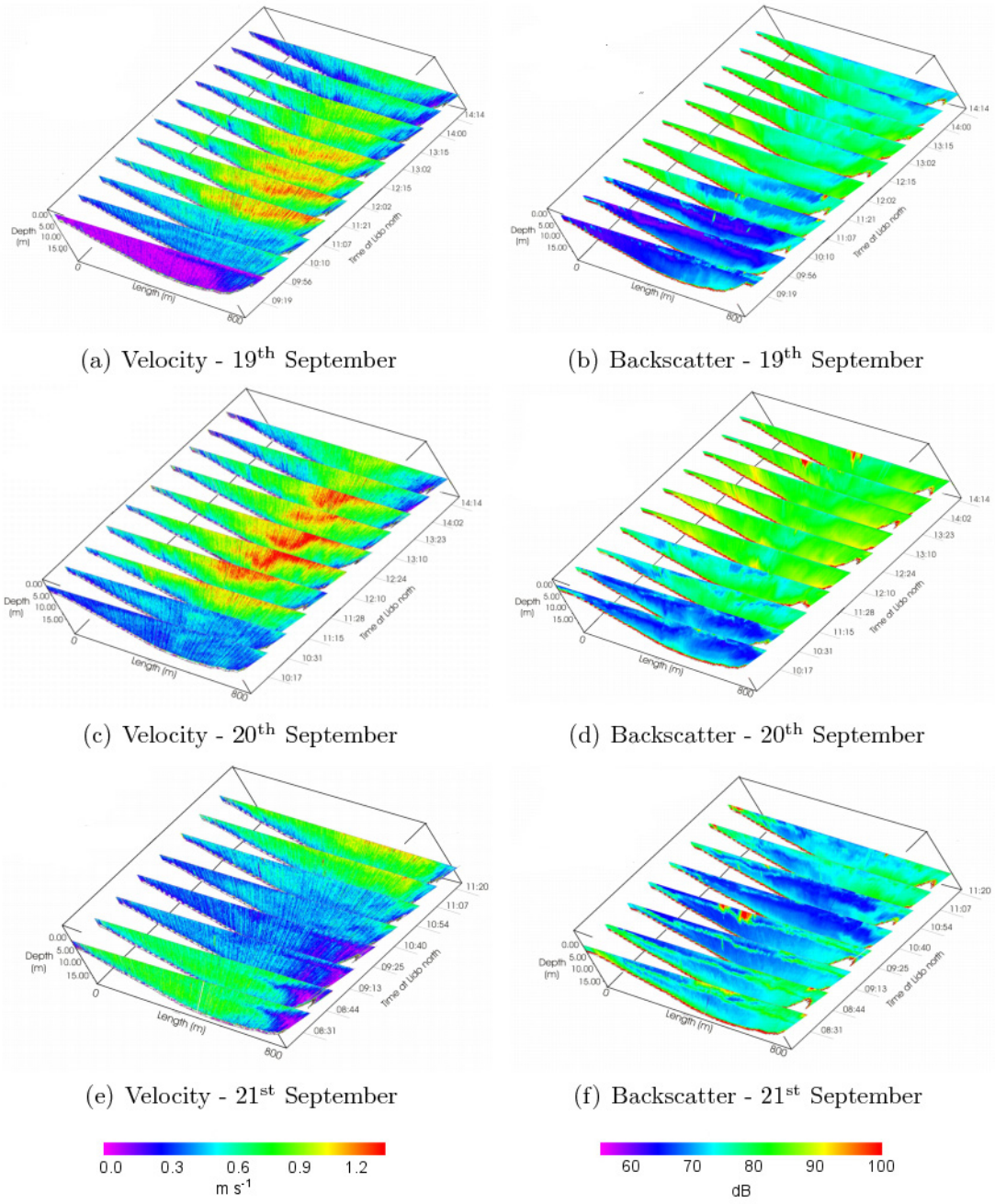

(a) Velocity - 19th September

(b) Backscatter - 19th September

(c) Velocity - 20th September

(d) Backscatter - 20th September

(e) Velocity - 21st September

(f) Backscatter - 21st September

Fig. 6.15: Backscatter and velocity on the 19th, 20th, and 21st

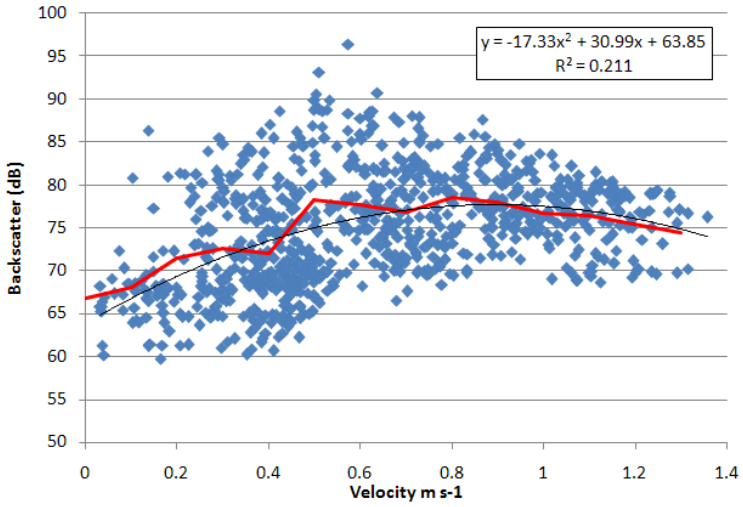

Fig. 6.16: Correlation between ADCP derived backscatter and velocity.

discussion section.

A positive correlation was found between backscatter and suspended sand concentration from the traps, although the significance was low ($R^2 = 0.36$ for surface samples and 0.22 for bottom samples) because low concentrations of sand in suspension were collected at both high and low backscatter levels, although generally, higher backscatter correlated with high sand concentration. It was impossible to determine how the signal was affected by relative proportions of fines and sands as no fine-grained sediments were collected where the sand traps were deployed by the *Litus*.

6.3.3.1 Fines Concentration

The first ADCP transect took place in the initial stages of the ebbing tide. From Figure 6.17A showing suspended fines concentration, it appears that most suspension occurred as a small plume of between 6 to 14 mg l^{-1} in the deep channel adjacent to the southern jetty. A second plume of around 12 mg l^{-1} was also present in the shallowest edge of the profile. As the tide progresses and velocity increases (Figure 6.17B), the plume reduces in height and flattens out so that only the surface 4 metres has negligible fines concentration (< 6 mg l^{-1}).

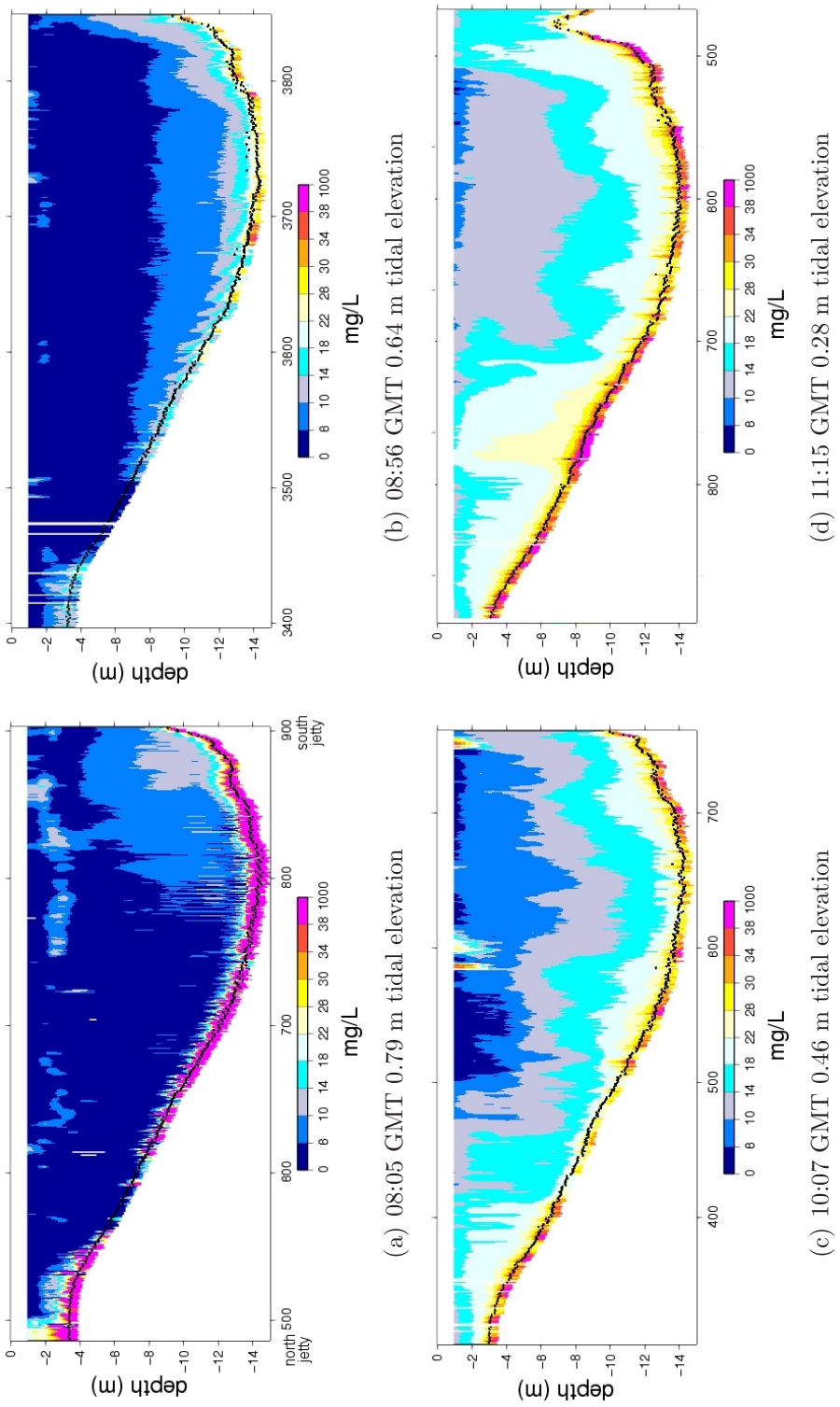

(a) 08:05 GMT 0.79 m tidal elevation

(b) 08:56 GMT 0.64 m tidal elevation

(c) 10:07 GMT 0.46 m tidal elevation

(d) 11:15 GMT 0.28 m tidal elevation

Fig. 6.17: Suspended fines concentration across Lido Inlet during an ebbing tide (19th September).

By profile 5 (Figure 6.17C), the velocity had increased and fines in suspension were present over the whole profile reducing from 22-28 mg l^{-1} at the bed to 6-10 mg l^{-1} at the surface. The shallow side of the profile (northern edge) has greater concentrations of suspended fines than over the deeper, main channel due to a large plume extending from the bed. The water column mixes further as velocity increases; concentrations reach 30 mg l^{-1} at the bed and 14-18 mg l^{-1} at the surface. A large plume with concentrations of fines of 22-26 mg l^{-1} covering most of the shallows started to build by profile 9 (mid ebb-tide; Figure 6.17D). The volume of fines in suspension and the size of the plume started to decrease as $\overline{U}$ drops to 0.3 m s^{-1} as the tide reached low water. The survey on the following day (the 21st) sampled during similar tidal conditions although velocities were higher. The pattern of suspended fines distribution was also similar to that of the previous day although the volumes involved were slightly smaller (maximum concentration of suspended fines was 28 mg l^{-1}). The final day of the survey produced very different profiles as the survey covered slack water conditions prior to flood-tidal conditions. The first two profiles showed a band of high concentrations of fines at the surface and a rapid reduction from ∼20 mg l^{-1} at the seabed to ∼10 mg l^{-1} 2 m above the seabed. During slack water conditions (covering several profiles), the concentration of fines in suspension fell to levels seen in the previous two days at slack water. As the flow started to ebb, a plume of 28 mg l^{-1} of fines emanated from the deep channel bed. The suspension threshold of fine-grained material appears to be approximately 0.2 m s^{-1}, with the densest plumes appearing at velocities exceeding 0.55 m s^{-1}. The water column appears fairly well-mixed at velocities of approximately 0.7 m s^{-1}.

6.3.3.2 Sand Concentration

There is little sand in suspension until around 9 am (profile 2: Figure 6.19B) when ebb current velocity increased past the suspension threshold (τ_{cr}) of sand (approximately 0.3 m s^{-1}). Unlike the fine-grained particles, which suspended initially as a plume, small volumes of sand (9-15 mg l^{-1}) became suspended across the bed of the main channel. Just prior to peak velocities, sand was suspended in concentrations between 51-57 mg l^{-1} near the seabed, and gradually decreased to between 0-21 mg l^{-1} at the surface. The suspended sand concentration further increased at peak velocities, to

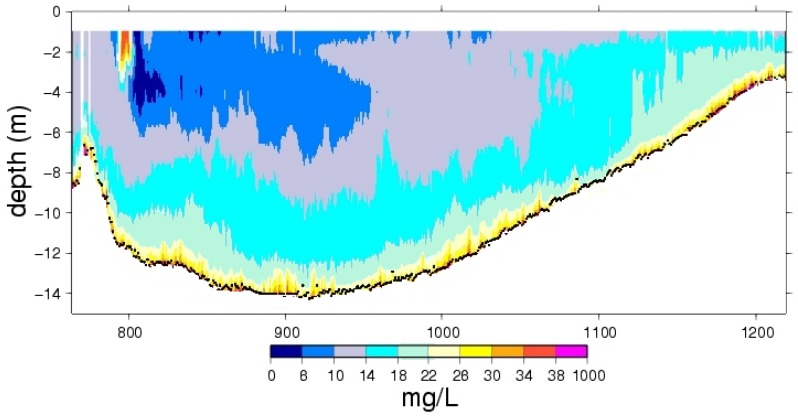

(a) Fines

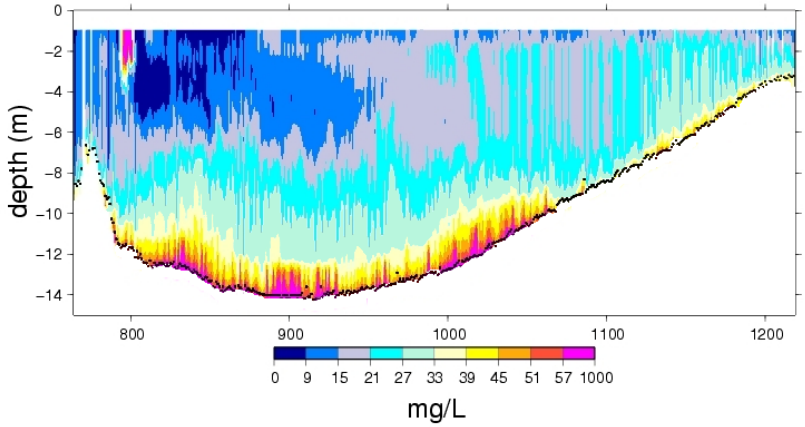

(b) Sand

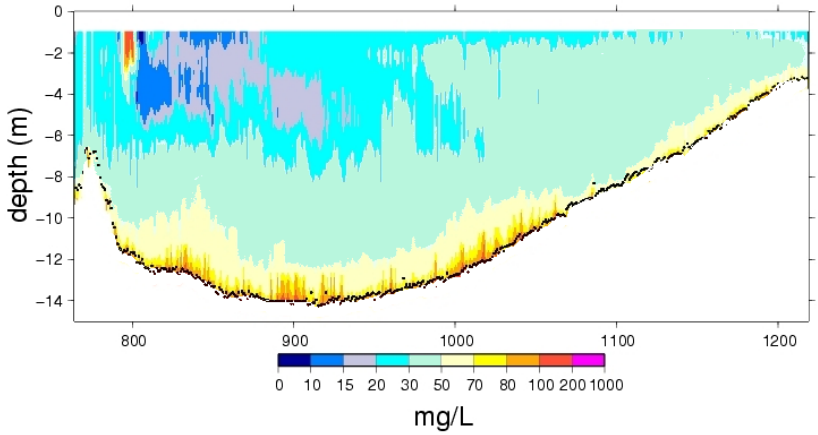

(c) Total

Fig. 6.18: Example profile (6 19/09/06 at 12:21 pm GMT) showing estimated suspended fines, sand and total concentration (mg l^{-1}). Note the fines plume in the shallows and sand plumes in the deeper channel. Note that the scales differ in each diagram so plume structure can be seen clearly for the different grains-size distributions.

over 57 mg l^{-1} at a metre above the seabed; a small plume of 27-33 mg l^{-1} suspended sand also extended from the shallow, northern side of the profile. As velocities fell, concentrations rapidly fell to an average of 9-15 mg l^{-1}, with concentrations falling more quickly at the deeper, southern edge of the profile; suspended sand concentrations here were between 0-9 mg l^{-1} compared with 15-21 mg l^{-1} along the mid-channel slope. Sand was already in suspension (9-15 mg l^{-1}) within the deeper waters at the beginning of the ebb tide on the 20th September. Concentrations rapidly increased as a plume, so that by profile 23, volumes of sand in suspension were as high as 39 mg l^{-1} 4 m above the seabed, although concentrations were less than half of this (9-15 mg l^{-1}) in the shallows. Profiles 25 to 29, taken at peak ebb velocities, showed the highest sand concentrations for the whole survey, with plumes of around 45 mg l^{-1} extending 8 m from the seabed and an average concentrations of 37 mg l^{-1}. In the final stages of the ebb tide, concentration levels gradually reduced to approximately 21-33 mg l^{-1}, and 0-21 mg l^{-1} in the shallows. The background concentration on the 21st was 9-15 mg l^{-1}, which rapidly increased to over 57 mg l^{-1} near the seabed. Concentrations were no greater than 15 mg l^{-1} when velocities reduced during slack tide but increased again when during the ebb phase.

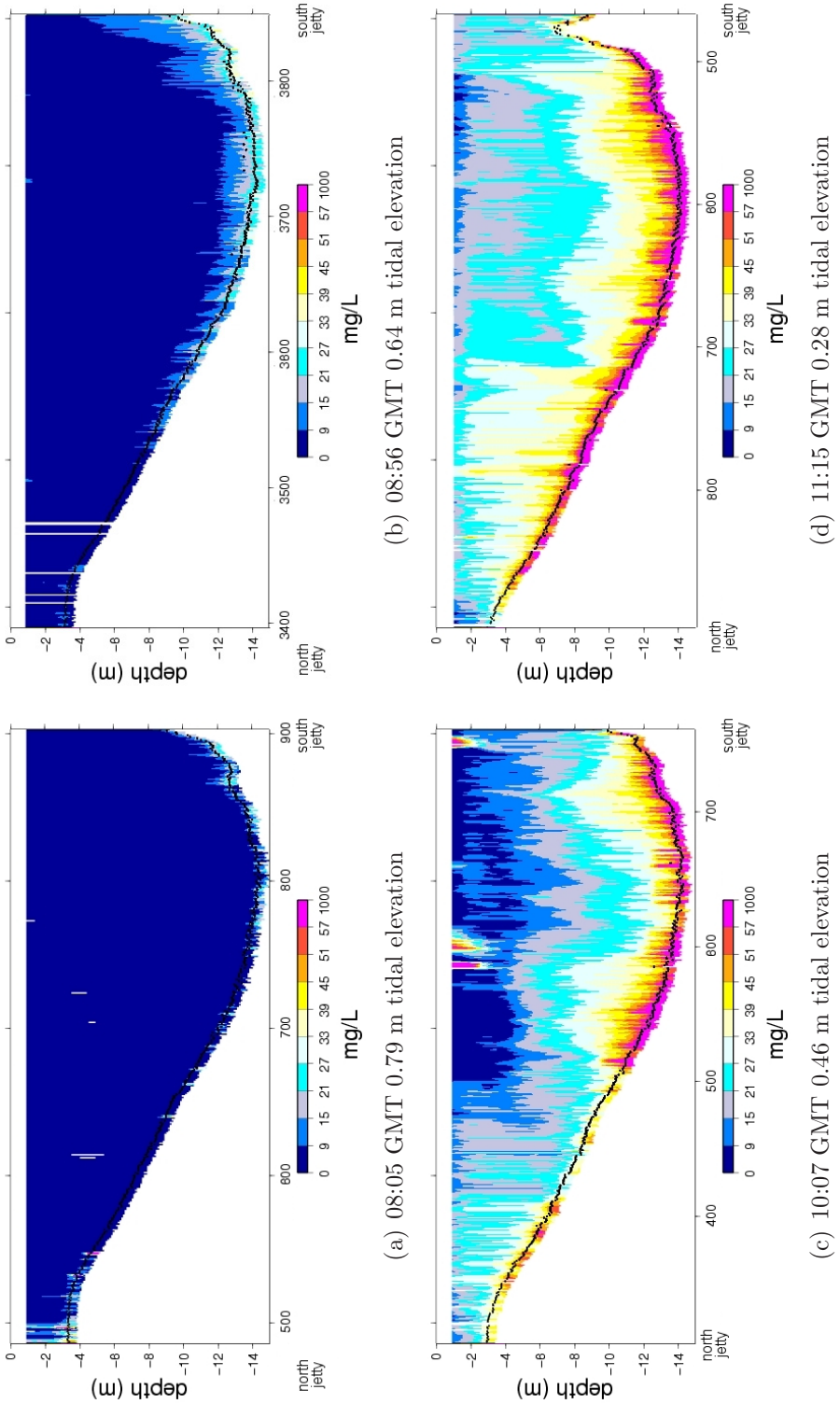

(a) 08:05 GMT 0.79 m tidal elevation

(b) 08:56 GMT 0.64 m tidal elevation

(c) 10:07 GMT 0.46 m tidal elevation

(d) 11:15 GMT 0.28 m tidal elevation

Fig. 6.19: Suspended sand concentration across Lido Inlet during an ebbing tide (19th September).

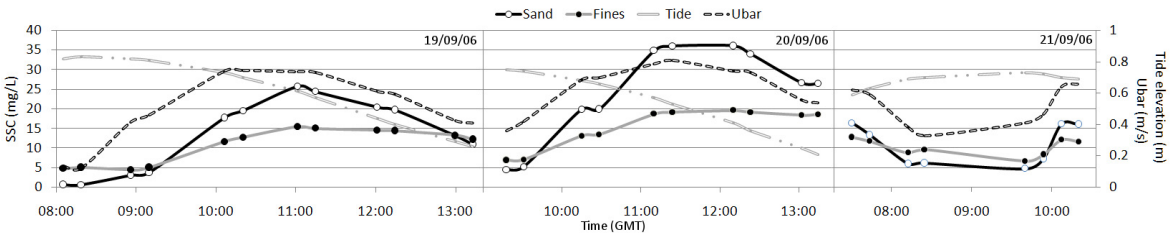

Fig. 6.20: Depth-averaged suspended sediment concentration (sand and fines) in the three survey days shown with tidal velocity and $\overline{U}$. Diagram also in Appendix D.2

Some sand is suspended when velocities are approximately 0.45 m s^{-1}, but transport begins in earnest above velocities of approximately 0.65 m s^{-1}, with plumes 4-5 m high created. The greatest densities are seen at peak velocities. Sand in suspension starts to settle below 0.5 m s^{-1}, and most sand is no longer in suspension at velocities below 0.4 m s^{-1}. Generally, the rate of change was much faster for the sands in suspension than for the suspended fines in both accelerating and decelerating flows.

6.3.3.3 Total Concentrations and Comparisons

The mean concentration of fines in the first profile is 5 mg l^{-1}, with little sand present. As ebb tidal currents accelerate, mean sand concentrations begin to exceed fines concentration increasing to 26 mg l^{-1} at peak velocities compared to just 15 mg l^{-1} of fines. Past this point, the suspended fines start to slowly settle reaching 12 mg l^{-1} at the end of the survey, with sands in suspension settling out more rapidly, falling to an average concentration of 11 mg l^{-1} in the last profile. The total dry weight of fines in suspension across the profile on the 19th, varies from 30 g during slack water to 110 g during peak velocities (see Appendix D.2); the total mass of sand in the same profile varies between 4 g to 183 g, equating to between 9,960 kg hr^{-1} transported during minimum velocities and 298,000 kg hr^{-1} during peak velocities (see Table 6.3). The second day shows higher velocities and much greater volumes of sediment in suspension; the peak load is over 35 mg l^{-1} of sand in suspension (average), and just below 20 mg l^{-1} of fines. Up to 527,000 kg of sediment is transported between the hours of 11 and 12 pm (peak velocity), 77% more than during the hour of peak transport the previous day. The final day was described by a flood to slack tide and generally showed less sand (5 mg l^{-1}) than fines (10 mg l^{-1}) in suspension, although the first

Date	GMT	Sand (kg)	Fines (kg)	Total (kg)	Sand (%)	Fines (%)	$\overline{U}_h$
19^{th}	8	9.96×10^3	2.44×10^4	3.44×10^4	29%	71%	0.22
	9	1.11×10^5	8.86×10^4	1.99×10^5	56%	44%	0.54
	10	2.91×10^5	1.85×10^5	4.76×10^5	61%	39%	0.74
	11	2.98×10^5	1.90×10^5	4.88×10^5	61%	39%	0.69
	12	1.72×10^5	1.35×10^5	3.07×10^5	56%	44%	0.54
20^{th}	9	6.73×10^4	7.33×10^4	1.41×10^5	48%	52%	0.49
	10	2.93×10^5	1.84×10^5	4.77×10^5	61%	39%	0.72
	11	5.27×10^5	2.83×10^5	8.09×10^5	65%	35%	0.78
	12	4.22×10^5	2.39×10^5	6.61×10^5	64%	36%	0.68
21^{st}	8	5.35×10^4	7.63×10^4	1.30×10^5	41%	59%	0.43
	9	5.20×10^4	6.87×10^4	1.21×10^5	43%	57%	0.50

Tab. 6.3: Total fines, sand and total sediment transported as suspension per hour. $\overline{U}_h$ is depth-averaged velocity over an hour. Note that totals represent mass from hour stated, i.e. sediment transported between 9 and 10 is listed under 9.

and last profiles, taken during higher velocities, showed up to 15 mg l^{-1} suspended sand concentration. In total, this represented a maximum of 53,500 kg of sediment transported through the whole profile per hour. Over the whole survey (11 hours in total), approximately 3,843,362 kg of sediment was transported as suspension through the Lido profile, of which 60% was sand.

The values were compared against modeled data from Coraci *et al.* (2003). Estimated values of sand export varied between 0 and 100 kg s^{-1}, whereas values in the present study (in Table D.2) ranged from 0-100 kg s^{-1} (19^{th}), 10-154 kg s^{-1} (20^{th}), and 12-61 kg s^{-1} (21^{st}). The estimates derived from both studies are variable in terms of tidal phase, wind strength and direction, but appear to be comparable to one another (considering 100 kg is approximately 14 mg l^{-1} assuming that each ADCP profile covers approximately 7.3 million litres of water[viii].

More fine-grained sediment is transported during low velocity conditions than sand-sized sediment, but as velocity increases the proportion of sand transported as

[viii])

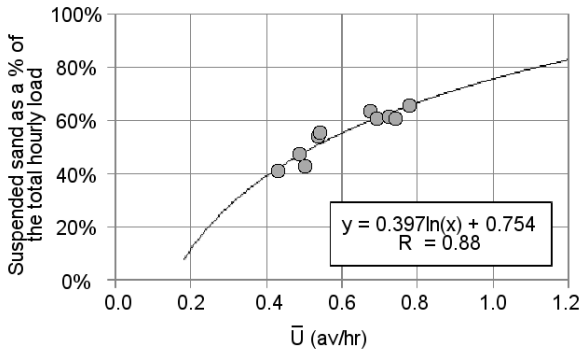

Fig. 6.21: Change in proportion of suspended sand as a total of the hourly suspended load against average $\overline{U}$ per hour.

suspension increases at a logarithmic rate of:

$$SSC_{\%} = 0.397 \ln \overline{U}_h + 0.754 \tag{6.11}$$

where $SSC_{\%}$ is the proportion of sand transported as suspension as a percentage of the hourly total load, and $\overline{U}_h$ is the average depth-averaged velocity over an hour. The critical threshold ($\overline{U}_{cr}$) of sand with a D_{50} of 100μm (h = 10 m) is approximately 0.4 m s^{-1} according to Soulsby (1997). This is also the approximate value provided by the results on page 172. The relationship detailed in Equation 6.11 provides a lower estimate of $\overline{U}_{cr}$ (0.15 m s^{-1}) defined as when the proportion of sand increases above 0%. However $\overline{U}$ is both depth and time averaged over an hour.

6.3.4 Comparison to SediView and Sediment Samples

The same sediment samples and ADCP profiles were processed with SediView software[ix] by Zaggia and Maurizio (2005). SediView uses raw binary ADCP data and sediment concentration data to provide estimates of suspended sediment concentration in profiles. The method behind both solutions to SSC estimates differs, as SediView incorporates the following algorithms[x]:

calibration of the ADCP transducer: each transducer has a unique conversion

[ix] RD instrument specific software by DRL Software
[x] Taken from the SediView website: http://drl.com/svmancont.html- 01/11/07.

(factory calibrated) from counts to dB that is dependent on temperature. This factor varies by ± 20% of the average; a potential error of 10 dB or 1000%.

beam spreading: normal procedure assumes spherical spreading, which underestimates concentrations in the top bins. SediView corrects the nearfield bins depending on frequency, transducer diameter and configuration settings.

water absorption: water conditions are not assumed to be constant in the water column, removing errors of around 100%.

sediment attenuation: a top down approach applies a value dependent on sediment density, speed of sound, kinematic viscosity and temperature.

particle variability: correlated with backscatter, dependent on time and particle concentration.

Precautions were taken within the method described herein to prevent some of the error inherent in suspended sediment estimates by ADCP. The echo intensity of each ping is corrected by WinRiver for sound absorption, beam spreading and transducer temperature, and speed of sound is a constant calculated by the ADCP.

The SediView profiles (Figure 6.22) are comparable to the concentration of fines in suspension profiles drawn up by this study. However, the SediView profiles had smaller bin sizes and no information on the bottom metre of the water column. Therefore more data on sediment transport was produced within the present study (having applied the Rouse profile). Furthermore, the data within the present study was available as the total concentration (and mass) of fines and sand in suspension, as well as the total concentration and mass of all sediment in suspension.

The low velocity profiles on the 19th are similar, although this study shows there to be higher concentrations near to the seabed and some values at the surface not present in the SediView. All of the profiles from this study show slightly higher estimates of suspended sediment, although at higher velocities, SediView begins to show much higher concentration estimates near the bed. This is the case for the data from the 19th and 20th, although the first couple of profiles from the final day (21st)

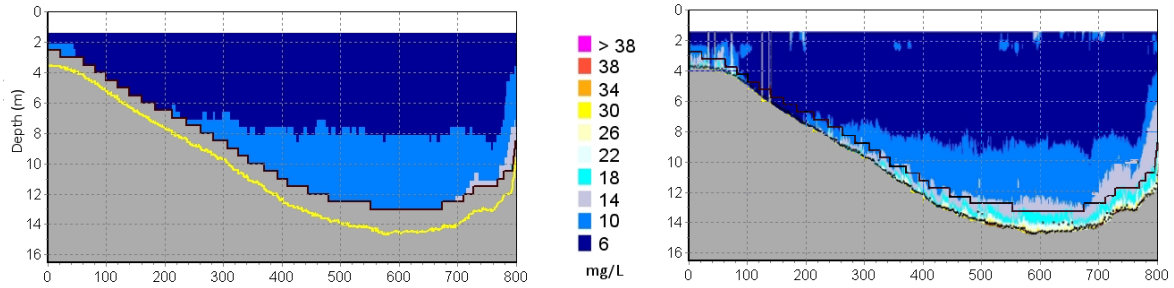

(a) 19th September, Profile 2 - early ebb

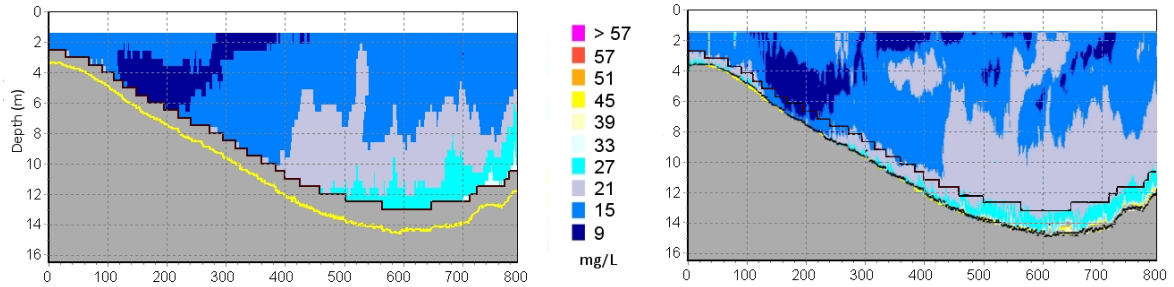

(b) 20th September, Profile 22 - early ebb

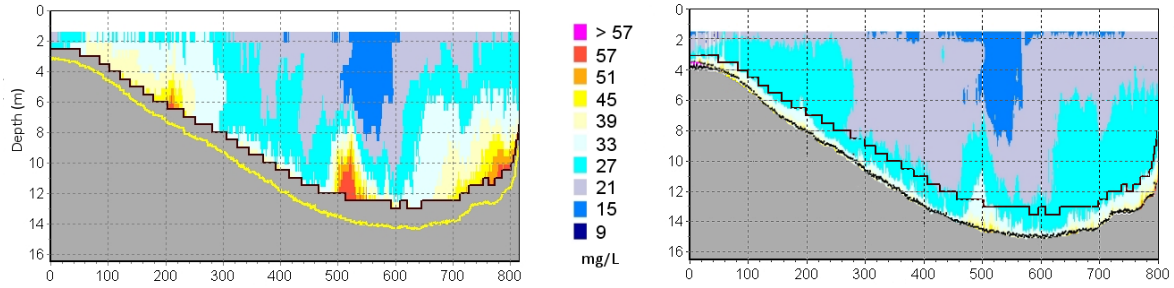

(c) 20th September, Profile 25 - mid ebb

Fig. 6.22: Comparison between SediView (left) and the technique used in this study (right). Note that both figures show suspended fines concentration; the profiles determined by this study also have concentration estimates for the bottom of the water column

show much higher concentrations than SediView predicts. Overall, the correlation between the SediView results and the fines SSC from this study is very good, with 63% of data (points picked from both sets of profiles at the same position where the Niskin samples were taken) being the same and 92% ± one class[xi]

6.3.5 Fixed ADCP: Correlation between SSC and Velocity

Velocity was used to determine estimates of suspended sediment concentrations as backscatter could not be extracted from the dataset without extensive processing. As velocity can be used to estimate sediment concentrations, it was tested for applicability. The SSC estimates using velocity data from the fixed ADCP show sensible results (comparable with those determined using the traversing ADCP data) with suspended sediment concentration increasing with faster velocities and wind speeds. Estimates vary between trace amounts to 16 mg l^{-1} for tidal driven velocity, increasing to 62 mg l^{-1} for wind driven velocity. The profiles show greater concentration of fines towards the seabed with plumes extending throughout the water column. The profiles also show a relationship with water depth as SSC plumes extend higher into the water column when water level is relatively low.

The results from the fixed ADCP were compared with estimates derived from the traversing ADCP so that a correlation could be determined for more accurate long term sediment export estimates. The estimates are generally higher than those determined by backscatter and appear to be most accurate when concentrations are between 6 and 20 mg l^{-1} with 52% of estimations calculated within 2 mg l^{-1} of the backscatter estimations. 16% of the total estimations differ by over 20 mg l^{-1} because the processing algorithm could not take into account any sediment still in suspension from previous highs in velocity (half of the SSC estimates calculated during falling velocities are within 10 mg l^{-1}, compared to 76% during increasing velocities). Also, SSC has been overestimated during sirocco wind events due to too few data points on which to base the correlation of wind and SSC. After removing the values most effected by this problem, estimates were all within 10 mg l^{-1} of backscatter-derived estimates

[xi]The SediView profiles available to this study had different colour scales for each day, which were matched for the study: the class interval for the 19th is every 4 mg l^{-1}, the 20th is every 6 mg l^{-1}, and the 21st is every 3 mg l^{-1}.

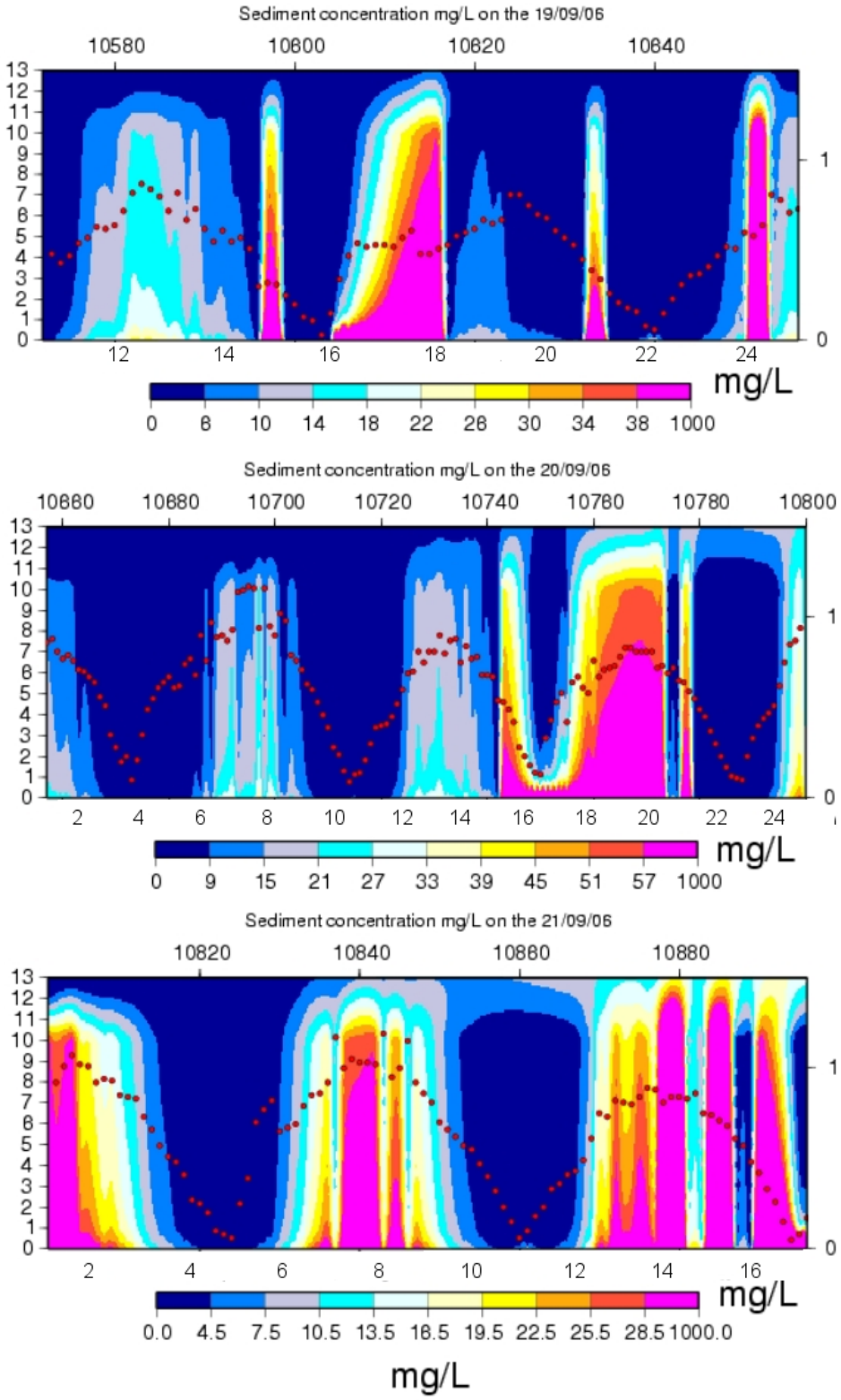

Fig. 6.23: Suspended sediment using the fixed ADCP. The red dots indicate $\overline{U}$. Note the different scales used in order for comparison with Sediview (Zaggia and Maurizio, 2005).

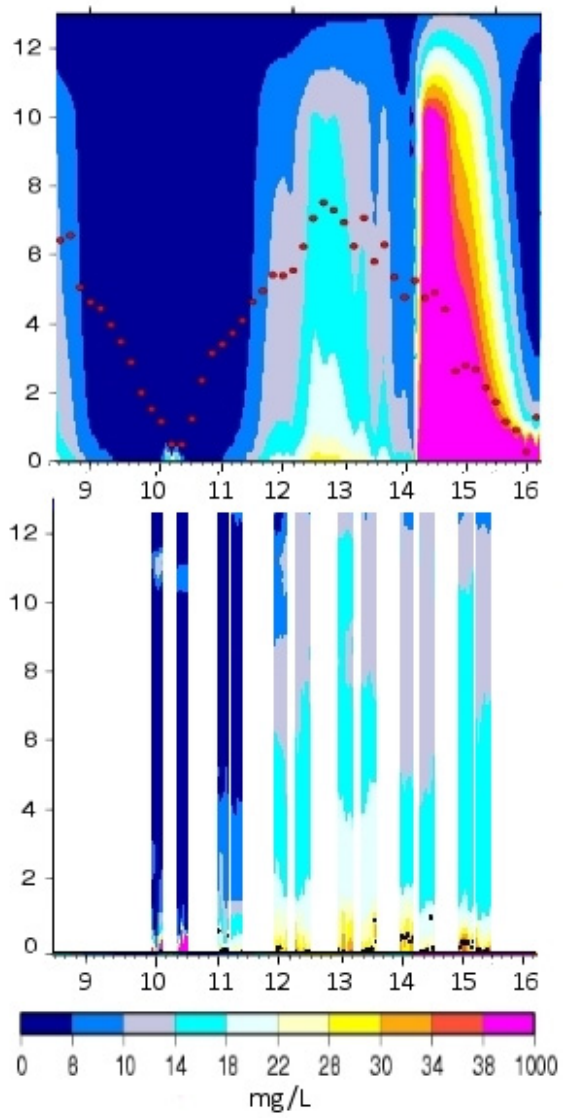

Fig. 6.24: Comparison of suspended sediment concentration estimates between the fixed ADCP (top) and traversing ADCP (bottom). The results are similar but are much too high at peak velocities and too low when velocity has recently been higher.

and 73% were within 5 mg l^{-1}.

Results from the 19th and 20th of September (Figure 6.23) show similar patterns due to similar tidal and wind patterns, but concentrations were underestimated

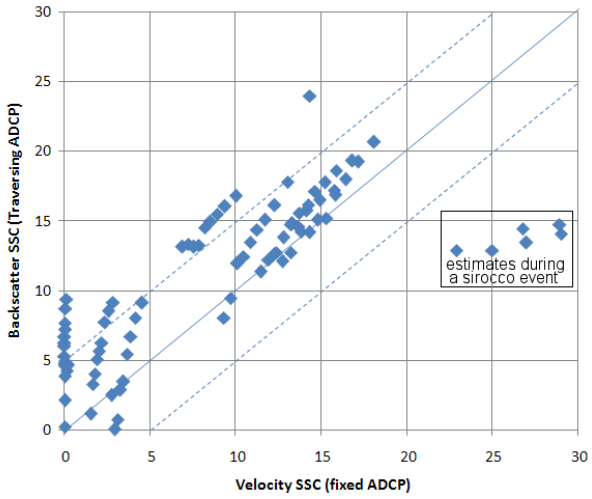

Fig. 6.25: Comparison between velocity derived and backscatter derived suspended fines concentration (mg l^{-1}). Note that SSC during Sirocco wind events have been overestimated.

when the tide changed from the last stages of flood into slack water and current speeds reduced as the fines that had remained in suspension from the earlier, stronger flood currents were not taken into account during processing.

The incorporation of algorithms that estimate the concentration of sediment remaining in the water column after the velocity had dropped requires considerable calculation as most estimates of settling velocity assume still water conditions (Soulsby, 1997). Therefore, it is more logical to apply the corrections to the echo intensity from the fixed ADCP to produce backscatter and process it in a similar way to the backscatter from the traversing ADCP. Because this conversion is beyond the scope of the thesis, the data from the fixed ADCP will be used as an indication of long term patterns rather than a complete calibration producing estimates of total import and export.

6.3.6 Bedload Estimations

The estimates of bedload showed that most transport occurred in the deep channel at high velocities, as was evident for sediment in suspension. Transport did not occur

until $\overline{U}$ exceeds 0.34 m s^{-1}, and then the rate of transport increased with velocity. The maximum volume of sediment transported as bedload was 13.39 $\times 10^{-6}$ m^2 s^{-1} (Table D.2), equivalent to 878,000 kg hr^{-1} (6.4). Bedload accounted for 8% of the total transport of sediment over the 11 hours of the survey, sand transported as suspension accounted for 55%, with suspended fines accounting for the remaining 37% (Table 6.5).

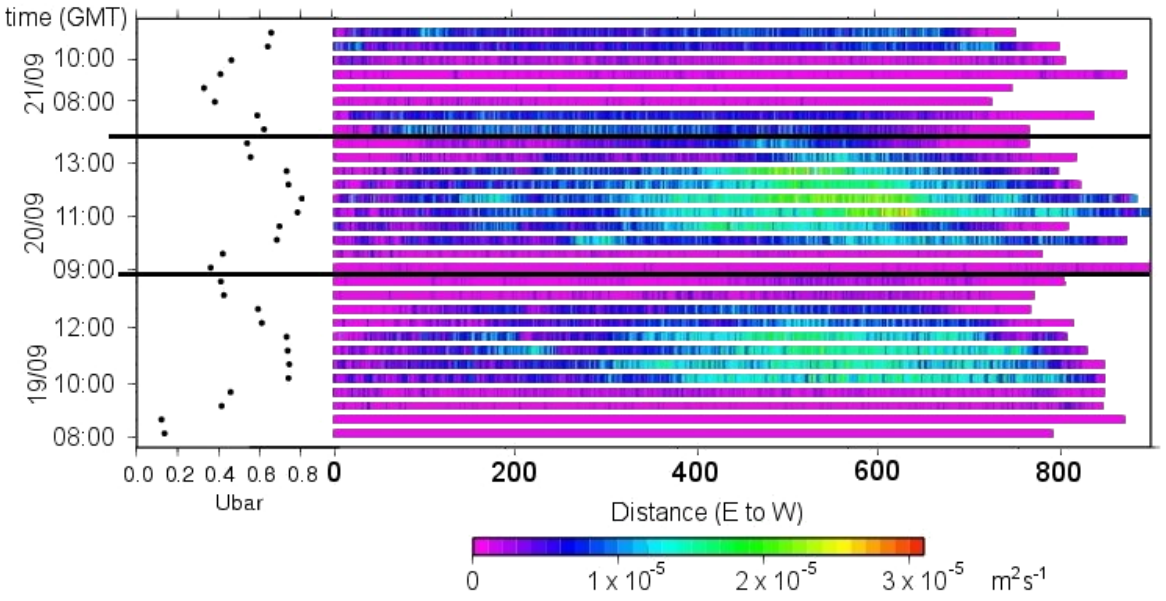

Fig. 6.26: Bedload transport in the traversing ADCP profile in Lido Inlet, with corresponding depth averaged velocity.

Date	GMT	average q_b ($m^3\ m^{-1}\ s^{-1}$)	kg hr^{-1}	total transport (kg hr^{-1})
19^{th}	8	1.53×10^{-4}	8.42×10^{2}	3.52×10^{4}
	9	2.63×10^{-3}	2.36×10^{4}	2.23×10^{5}
	10	5.77×10^{-3}	5.64×10^{4}	5.32×10^{5}
	11	4.72×10^{-3}	4.52×10^{4}	5.33×10^{5}
	12	2.04×10^{-3}	2.56×10^{4}	3.33×10^{5}
20^{th}	9	1.06×10^{-3}	7.59×10^{3}	1.48×10^{5}
	10	5.11×10^{-3}	4.70×10^{4}	5.24×10^{5}
	11	7.06×10^{-3}	6.87×10^{4}	8.78×10^{5}
	12	4.75×10^{-3}	4.69×10^{4}	7.08×10^{5}
21^{th}	8	3.97×10^{-4}	2.31×10^{3}	1.32×10^{5}
	9	5.77×10^{-4}	3.21×10^{3}	1.24×10^{5}

Tab. 6.4: Average bedload rate per hour, total sediment weight transported as bedload and total sediment transported as suspension and bedload.

Date	Suspended load		bedload %
	sand %	fines %	
19	53%	38%	9%
20	58%	35%	8%
21	41%	57%	2%
total	55%	37%	8%

Tab. 6.5: Proportion of each transport mechanism transported on each survey day and over the whole survey.

6.4 Discussion

Determining the mass of sediment transported in suspension requires many assumptions (the estimate is representative of the whole channel; the timespan over which the estimate was derived is representative of a typical tidal cycle, month, year) and accuracy of estimations is often difficult to prove as only a very small part of the total mass of sediment can be sampled. Sampling sediment accurately from the water column is subject to error due to small sampling volume (water sampling) or low sampling efficiencies (sediment trap); also, the samples collected may not be representative of the water column spatially and temporally (turbulent eddies increasing or decreasing

concentrations - Street, 2003; seasonal biological growth may alter sediment transport). This potential error can be addressed by continuous sampling; however manually collecting samples is labour intensive, and using turbidity instrumentation such as an OBS or a LISST gives only a 2D representation; a single-point measurement over time. Thus using backscatter from an ADCP can potentially determine long-term suspended sediment transport across a transect of the channel, as long as the backscatter signal from the SSC can be distinguished from other signals.

6.4.1 Velocity and Backscatter

An increase in velocity as the ebb tide progressed was reflected by an increase in the level of backscatter seen on the traversing ADCP profiles. Peak velocities occurred in the deepest part of the channel when the current direction was homogeneous across the inlet profile. Velocity profiles showed the ebb current dominating the southern edge of the channel and spreading across the channel just beneath the surface waters. The flow changed direction in the deepest part of the channel as a salt wedge of denser seawater entering the inlet along the seabed with a flood tide. This observation is representative of usual conditions (peak velocities in the deep channel) as sand and gravelly-sand are found on the bed along the deeper, southern part of the inlet, whilst muddy sands are found on the northern, shallower part of Lido Inlet (slower velocities - see Figure 4.27(b)). The fastest, and most enduring, peak velocities were seen on the 20$^{\text{th}}$ September, and this was reflected in the estimations of sediment transport; the total mass of sediment transported in the hour of peak velocity was 828 kg, compared to 535 kg on the previous day (Table 6.3). The backscatter was minimal during low velocities ($\sim$0.2 m s^{-1}), although small plumes occurred close to the seabed from small scale sediment transport. These plumes were present both in the deeper channel due to increasing velocities (thus exceeding the critical suspension threshold for sand earlier; 0.4 m s^{-1}), and in the shallow waters along the northern edge, probably due to turbulence from the boundary layer (calculated to be 4 m) and waves causing suspension of sediment. The high backscatter seen just below the surface on the 21$^{\text{st}}$ is likely to be floating organic matter, as the water column is well mixed (as shown by the CTD data in Figure 6.13) so it is unlikely that the backscatter is due to suspended sediment when lower backscatter is present below. There was also

visual evidence of increased organic matter seen from the boat. The highest backscatter emanates in the deeper part of the channel where the tide begins to change; the plume then reduces in height and spreads across the width of the inlet before increasing in reflectance from around 71 dB to 80 dB. The change in current direction is responsible for the initial plume of sediment into the water column, due to increased turbulence but as the current direction harmonizes across the profile, turbulence decreases and sediment in suspension settles slightly, reducing the height of the plume. As velocity increases with the ebb tide an increased volume of sediment is suspended closer to the inlet bed. Small 'wisps' of low reflectivity occur at the surface of the profiles in areas of peak velocity due to turbulent eddies (Street, 2003). Figure 6.16 shows that there is not a well defined correlation between backscatter and velocity; however, charting the minimum, maximum and the difference between these values of backscatter against velocity shows that the minimum backscatter does increase with velocity. The maximum backscatter value increases initially with velocity until $\sim$0.5 m s^{-1}, after which they decrease (see Figure 6.27). This may be indicative of the spatial coherence of the particles as hypothesized by Merckelbach (2006); with an increase in velocity, the particles are distributed in the water column in phase with the acoustic wave sent by the ADCP. Merckelbach (2006) states that increased velocities produce a greater echo intensity for the concentration of particles in suspension, but there is no mention of the backscatter reducing after a critical velocity. The grain size distribution did not change in the dataset of Merckelbach, but within Lido Inlet, just fines are transported at lower velocities, with sand being transported after the critical suspension threshold of $\sim$0.4 m s^{-1}, which is marginally slower than the critical velocity for the reduction in maximum backscatter. It may be the case that suspension of sand into the water column reduced the spatial coherence of the sediment in suspension, thus reflecting acoustic waves that were out of phase (producing lower echo intensities). Further investigation of this phenomenon, using the same method as Merckelbach (2006) is required to confirm the effect of changing grain size on the coherence of suspended particles.

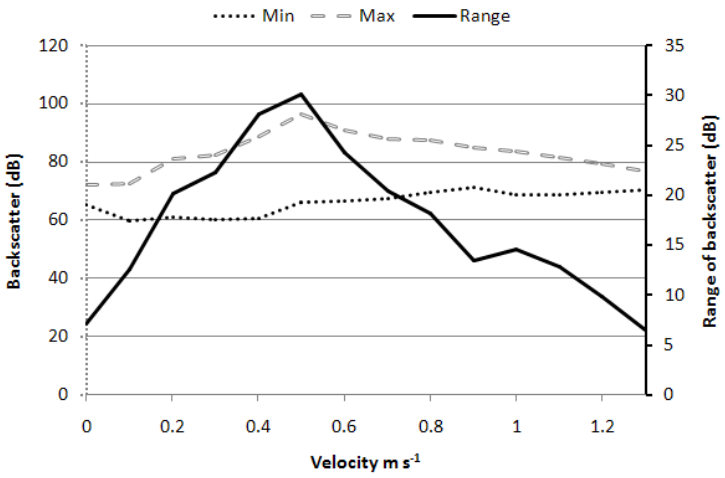

Fig. 6.27: Minimum, maximum and range of backscatter values against velocity.

6.4.2 Suspended Sediment Concentration: Traversing ADCP

The general increase of backscatter to increasing velocities suggest that an increase in velocity suspended greater volumes of particulate matter into the water column; however, the contribution between sediments and organics to the backscatter signal is unclear. The only relationship between organics and velocity appeared to be the gradual rising of organic matter from the seabed to the surface. Because segregation proved difficult, the likelihood of organics present will be discussed in this section.

The first method used to determine sand and fines in suspension gave an unrealistic representation of sand in the water column, although the calibration for fines appeared sensible. The potential error in using the values determined from the bedload traps was fairly high as no specific calibration was carried out (instead the average efficiency of the surface trap was used; 4%). The traps were also deployed within the layer of side-lobe echoes, thus the backscatter to which the concentrations were compared to, were derived from the last viable bin a metre or more above the traps. Although some correlation was found (which was used), the accuracy is highly debatable even if the method was acceptable. The premise of the method was that sand in suspension was highly unlikely in the surface waters, but as high backscatter readings from fine-grained material and organics was present, estimates of sand in suspension were

wrongly inferred. Using a probability scale to determine the accuracy of the estimate only produced stratification and no comparability to the SediView profiles.

The method was developed on the basis that backscatter is a product of the all particles in suspension; thus, as it could be assumed that the concentration of fines in suspension is fairly constant over depth, although close to the bed the concentration increases (Amos, 2006; pers comm). Therefore the differences in backscatter could mainly be attributed to the sand in suspension. Consequently, the concentration of fines in suspension as determined by the Niskin bottle were compared to backscatter and the resulting regression applied to the backscatter data. The SediView profiles appeared to show higher concentrations of fines in suspension in the bottom 3 m during higher velocities than described by the results from this study. For example, for profile 25 (Figure 6.22C), SediView estimated concentrations of between 33 to 57 mg l^{-1}, compared to estimates of 27 mg l^{-1} by the method outline in this chapter; however, the concentration of suspended fines in the original water sample was 24 mg l^{-1}, which appears to verify this method. Generally, comparisons with the results from the SediView software is very good with 63% of the points sampled being the same for both profiles. Only two profiles looked noticeably different due to organic matter appearing as high backscatter in the surface waters between 2 and 4 m deep. Samples taken at the time contained around 60% organic matter and CTD data shows an oxycline at the same depth, with 103% O_2 below 4 m, and 128% O_2 between 2 and 4 m, compared to a survey average at this depth of ∼118%. These high concentrations of oxygen are indicative of green organic matter. The method converted the high backscatter reflected off the plants into peaks of suspended fines concentration, whereas the real concentration was likely to be approximately 10 mg l^{-1} less than estimated. Occasional peaks of very high fines concentration at the surface in two of the profiles are due to reflections off boat wakes. It may be possible to remove the signal from both of these non-sediment related variables through careful averaging, but as this might remove real data also, the option was removed in preference to correlating any outlying data with the samples and CTD data. This approach will affect the estimations of total suspended sediment but has been included in error calculations.

Comparing the Niskin derived suspended fines concentration with LISST de-

rived suspended fines concentration produced a fairly good correlation ($R^2 = 0.7$), so it is probable that the LISST data for sands in suspension must also be viable. A problem with the previous method was the double-signal gained from independently deriving suspended sand, and suspended fines concentrations from the same signal, therefore it was important to determine proportions of the different grain sizes that produced the backscatter signal. Both sand and fines in suspension are controlled by the same variables (velocity, water depth etc.) so a proportional relationship between the two concentrations is probable. Niskin derived SFC and percentage LISST sand followed a logarithmic relationship, so that as fines increased, so did the percentage of sand. The R^2 was 0.6, but there were no significant outliers to sully the relationship conclusively. This method took water depth and velocity into account so no correction for 'probability' was required (as for the previous method) and although no SediView profiles were available for sand, the results looked realistic with sand increasing and decreasing in concentration at a greater rate than fines. The rate of change between surface and near bed concentrations was also greater than for the fines, as would be expected. Most importantly, the actual estimations were reasonable when compared to the sand trap and water samples.

6.4.3 Suspended Sediment Concentration: Fixed ADCP

Using velocity from the fixed ADCP provided mixed results. The estimates of SSC were comparable with backscatter derived results when velocity was increasing (and had been increasing for approximately an hour), whereas SSC was underestimated when velocity was falling or had been higher previously. This is because the processing script did not take sediment already in suspension into account. In order to incorporate settling, the processing script would have to estimate the SSC at peak velocity and then calculate how much of this sediment would settle out completely in the time between peak velocity and present velocity. The sediment remaining in suspension would then have to be added to the SSC estimate calculated for the present velocity speed. This method would have numerous obstacles not least because settling velocities would not be the same as those calculated for still water conditions due to turbulent eddies, and also the grain size is likely to change as larger particles usually have larger settling velocities; this would affect calculations of the Rouse profile. Changing grain sizes

(d_{50}) affects the accuracy of this particular study anyway as sediment samples are only available for ebb velocities. It is likely that the d_{50} would increase during flood conditions as the lagoonal fines that are transported with the ebb will not be present to the same degree.

6.5 Conclusions

The 12 m deep main channel is the most dynamical area of Lido Inlet in terms of tidal driven current flow, and consequently sediment transport. The tide starts to ebb in the waters adjacent to the southern jetty before extending across the surface waters (lower density freshwater) to the rest of the channel. Peak velocities occur in the surface waters over the deep channel, with speed rapidly falling at both edges of the inlet due to a combination of increased influences from the seabed/inlet walls and decreased free stream flow. These results are representative of general conditions as the seabed under areas of higher velocities are sandy and gravelly (as described in Chapter 5), whereas finer muddy sands are found in the lower velocity shallows opposite.

Tidal currents during flood conditions enter the inlet along the bottom of the main channel as seen in ADCP velocity direction profiles and CTD drops. The backscatter signal from the ADCP is correlated with bottom velocity, as it is bottom velocity that must exceed τ_{cr} of 0.14 m s $^{-1}$, in order to transport the sand fraction as suspension (D_{50} = 98 μm). Once this transport is initiated, the proportion of sand-sized sediment transported every hour increases logarithmically with average velocity as the water column mixes. The maximum proportion of sand transported as suspension during this survey was 65%, equating to around 539 kg hr^{-1}, an average of 37 mg l^{-1}. During lower velocities (below $\sim$0.4 m s^{-1}), more fine-grained sediment is transported as suspension, the average concentration being between 6 to 8 mg l^{-1} (around 100 kg hr^{-1}). The concentration of sand in suspension rapidly increased with faster velocities; from the point of equilibrium to peak concentrations, supended fines increased by around 150-170%, whilst suspended sand concentration increased by 330-400%. Although the first two survey days (19-20$^{\text{th}}$ September) sampled the same tidal period, and showed similar velocities, the second day saw greater masses of sediment

being transported (around a third more[xii] for the same $\overline{U}_h$). The current flow on this day had more enduring peak velocities allowing little settling, and increased scour resulting in greater volumes of sediment transported as sediment. This difference in concentration at the same velocity is partly why the use of velocity for estimates of SSC, as carried out for the fixed ADCP data, is not accurate.

The proportion method used in this study to define the concentration of sand throughout the water column appears to be successful, with comparable results to the SediView method (Land and Bray, 2000). Although the equations used in this study may not transfer, the method should be applicable to other inlets as long as organic matter does not make up the majority of suspended matter. The reasoning behind this assumption relies on the theory that sediments of any size are influenced by the same water conditions albeit in different magnitudes.

[xii] 19/09/06 11:00 am GMT: $\overline{U}_h = 0.69$, total mass of sediment transported 535.12 kg. 20/09/06 12:00 pm GMT: $\overline{U}_h = 0.68$, total mass of sediment transported 715.87 kg. Page 173.

7

Sediment Budget and Modelling

7.1 Introduction

A sediment budget provides a quantitative estimate of volumes of sediment entering and leaving a system (sources and sinks), as well as volumes within active transportation. The morphological variability and vulnerability of the system can consequently be quantified and effectively managed with understanding of the budget and how it changes. Whereas sediment-transport pathways, sinks and sources can readily be identified, the task of quantifying the sediment exchange accurately is difficult (French, 2001), especially around tidal inlets due to the complex pathways involved[i]; sediment transport magnitudes and pathways are convoluted due to bi-directional tidal currents, wave and current interactions, wave diffraction/refraction, and also engineering activities (Rosati and Kraus, 1999a). The transport pathway of sand in the northern lagoon and along the coastline of Venice has been investigated in Chapters 4 and 5, with estimates of the volumes of sediment transported through Lido Inlet as suspended load and bedload discussed in Chapter 6. The results from these chapters will be used in conjuntion with quantitative volume estimates from the lagoon-wide bathymetry datasets provided by CNR-ISMAR, to formulate a sediment budget of Venice Lagoon.

[i]http://www.csc.noaa.gov/beachnourishment/html/geo/budgets.htm

The aims of this chapter are as follows:

- What is the sediment budget of Venice Lagoon; does it compare with previous estimates of sediment exchange?
- Is the system in equilibrium; has the balance changed with the large-scale, industrial changes seen in the last century (canal building, water pumping)?
- What are the future trends in the sediment budget for Venice Lagoon?

7.1.1 Sediment Exchange

The sources, sinks and transport pathways in Venice Lagoon are complex (as shown in Table 7.1), but must be identified, and balanced in the form (French, 2001):

Volume of sediment in = Volume of sediment stored + Volume of sediment out

although if a system is not in equilibrium then change (erosion or accretion) will occur until balance is achieved. Rosati and Kraus (1999a) describe this balance in more detail:

$$\sum Q_{source} - \sum Q_{sink} - \Delta V + P - R = Residual \tag{7.1}$$

where Q is discharge, ΔV is the net change in volume within a coastal cell, R and P are the volumes artificially removed and placed into the system. The *Residual* volume represents the remaining imbalance of the sediment budget. As the actual volume of sediment in transport cannot be accurately measured, each value may be expressed as:

Reported Value = Best estimate ± Uncertainty

where uncertainty represents both error and true uncertainty in the volumetric estimate. True uncertainty includes temporal variations, unknown parameters such as sediment density and grain size, and uncertainty in estimations of the volumes of sediment removed by dredging and sediment disposal (Kraus and Rosati, 1998, 1999).

The Difference Map Method (DMM) has been cited in the literature (Stauble, 1998; Pacheco *et al.*, 2008) as a way to estimate the change in volume (thus volume added, P, or removed, R, from the sediment budget) between two bathymetry datasets

Sediment gains[i]	**Sediment losses**[i]
longshore transport	longshore transport
onshore transport	offshore transport
fluvial inputs	solution/abrasion
wind transport	wind transport
deposition of intertidal/channel sediment	erosion of intertidal/channel sediment
artificial gains (beach nourishment)	artificial losses (dredging)

Tab. 7.1: Sediment losses and gains in an open tidal inlet system

of different years. The gridded bathymetry of one year is subtracted from that of another (the method used for determining areas of erosion and deposition in Chapter 4). This method is only suitable for areas where adequate bathymetry is available. Pacheco *et al.* (2008) and Rosati and Kraus (1999b) note that estimating changes in tidal deltas are difficult to assess using this method, as most bathymetric surveys cease at the tidal inlet. In this case, or if the total volume of a delta is being investigated (requiring estimates of how the contours would look if no delta was present), an estimate of the bathymetry must be calculated, thus increasing uncertainty (Pacheco *et al.*, 2008). Error is also introduced as the boundaries of deltas are indistinct; Stauble (1998) suggests that the boundary of an ebb-tidal delta can be determined by a return to straight and parallel contour lines.

Other methods of determining the volume of exported sediment involve direct measurement of bedload and suspended sediment at all the major conduits into the system (tidal inlets, rivers etc). Estimates can be determined through the use of optical (OBS) or acoustic (ADCP) instruments, which measure the concentration of sediment in suspension; error is introduced with uncertainties in calibration (Downing, 2008). The use of ADCP to measure the backscatter (and thus the volume of sediment in transit) across a cross-section of a channel is currently being developed (Reichel and Nachtnebel, 1994; Land and Bray, 2000; Dinehart and Burau, 2005; Merckelbach, 2006; Wall *et al.*, 2006); if successful, it can improve both the efficiency and the accuracy of calculating the export and import of sediment in suspension. The use of ADCP also provides the variables required (velocity, water depth) to calculate bedload transport

(see previous chapter) and the possibility of long-term deployment, which ensures that a wide range of sediment transport conditions are sampled, decreasing estimate error. These optical or acoustical methods can only produce estimates during the period of deployment, and thus can only show the present-day sediment budget (due to the instrumentation being relatively recent developments). However, it is often possible to model the sediment exchange within the system (Kern and Westrich, 1997; Cooper *et al.*, 2001; Ferrarin, 2005), although error can be high due to the extensive list of uncertainties and assumptions.

Despite the large catalogue of scientific research that has been conducted in and around Venice Lagoon, there is very little data describing sediment exchange system-wide. Consorzio Venezia Nuova (1996) estimate that the total sediment loss from the lagoon is 1.1 million m^3 yr^{-1}, with 400,000 m^3 yr^{-1} dredge spoil dumped at sea (although the practice is now to retain this sediment for intertidal flat regeneration - D'Alpaos, 2007). Consorzio Venezia Nuova (CVN) have also published[ii] estimates stating that approximately 2.2 million m^3 yr^{-1} of sediment moves within the lagoon, of which 30,000 m^3 yr^{-1} enters via the rivers, 70,000 m^3 yr^{-1} is eroded from the salt marshes, and 2.1 million m^3 yr^{-1} is re-suspended from the bed. Of this, 700,000 m^3 yr^{-1} exits the lagoon via the inlets (Figure 7.1). No mention is made of sediment entering through the tidal inlets as CVN state that sediment supply to the coast has been reduced from anthropogenic interference to river channels, and jetties defining the inlets block any "silt, sand and any other solid materials" preventing them from reaching the lagoon and depositing. Consorzio Venezia Nuova (1996) have estimated that 300,000 m^3 yr^{-1} of sediment entered the lagoon through the inlets prior to jetty construction, with the volume decreasing to less than $\frac{1}{6}$ of this (50,000 m^3) post-construction. Tambroni and Seminara (2006b) modelled the total loss of sand from the lagoon at 58,000 m^3 yr^{-1}. They suggest that sand actually enters the lagoon during winter and summer due to sand accumulation at the jetty during bora and sirrocco wind events (Consorzio Venezia Nuova, 1996). Tambroni and Seminara (2006b) estimate that 7,800 m^3 yr^{-1} of sediment leaves the lagoon via Lido Inlet, 43,000 m^3 yr^{-1} via Malamocco, and 9,800 m^3yr^{-1} through Chioggia Inlet. Whilst 400,000 m^3 yr^{-1} of sediment is estimated to be removed by dredging, 25 million m^3 was removed between

[ii]Website - www.salve.it (February 29^{th} 2008)

1965 and 1969 during construction of the Petroli Canal (Ravera, 2000), although it is unclear whether this volume has been included in the estimates of CVN. There

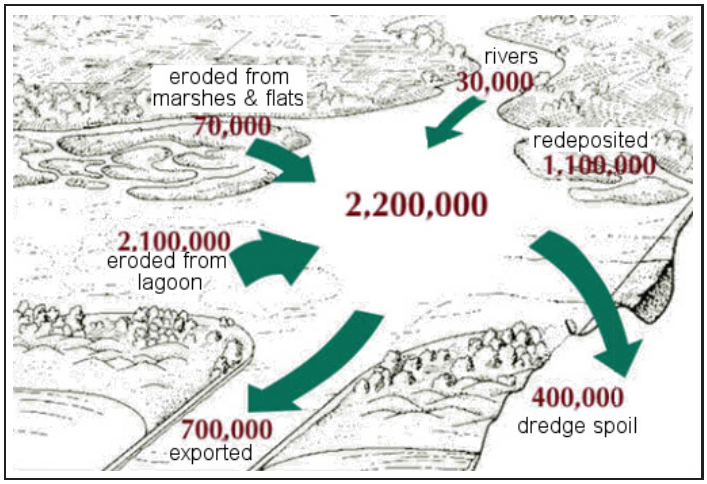

Fig. 7.1: Current sediment budget of Venice Lagoon. From Consorzio Venezia Nuova, 2008[ii]

is a need for an up-to-date sediment budget for all of Venice Lagoon as data has tended to be collected from specific sites across the lagoon rather than looking at the lagoon as a whole system (Day *et al.*, 1998; Albani *et al.*, 1998; Amos *et al.*, 2002; Helsby, 2006). This should provide a general picture of the balance between the total volume of sediment eroded and deposited within the canals and intertidal areas (salt marshes, mudflats) and whether large scale anthropogenic modifications have affected this balance (dredging, salt marsh restoration - Fletcher and Spencer, 2005). This final chapter will concatenate data used within previous chapters as well as recent data published within the literature, including results from the fixed ADCP stations (Zaggia and Maurizio, 2005).

7.2 Methods

7.2.1 Sediment Budget

The erosional and depositional trends determined from changes in the bathymetry of Venice Lagoon have been used to estimate the total loss or gain of sediment in the longterm. The canals are the main conduit for sediment transport, with secondary

inputs from fluvial sources, intertidal flats and longshore transport. Fluvial input is negligible since the diversion of the rivers (Albani and Serandrei Barbero, 2001; Mazzacurati, 1995), but has been estimated to be 33 x 10^3 kg yr^{-1}, of which 50% is deposited into the northern region.

Bathymetric datasets from 1930, 1970 and 2000 were used to evaluate the sediment budget as these are generally considered to be reliable for the whole lagoon. The 1990 dataset is believed to be inaccurate in the northern lagoon and was not used for this reason (G. Umgiesser, pers. comm.). Venice Lagoon can be partitioned into southern, central and northern basins, which are thought to be hydrodynamically separate (Solidoro *et al.*, 2004; Cucco and Umgiesser, 2005). As the boundaries of these basins are debatable, three arbitrary boundaries were defined following lines of latitude or longitude to the nearest 0.01° (positions in Figure 7.2) to provide a general overview of sediment exchange in each region, although the final sediment budget will be provided as a lagoon-wide estimate.

The 1930 bathymetry dataset was subtracted from the 2000 dataset and the resultant data gridded every 0.0005 decimal degrees (i.e. DMM/difference map method). The aim of the method was to calculate the change in volume between the two years; therefore, if the change in depth is known, and the total area that experienced this level of change is known, then it is possible to calculate the total volume that has been eroded or deposited (Table 7.2).

Change in depth (m)		Area affected (m^2)		Total Volume (m^3)
-0.375	×	2.59 ×10^7	=	-9.71 ×10^6
-0.625	×	1.51 ×10^7	=	-9.43 ×10^6
TOTAL		4.1 ×10^7		-1.91 ×10^7

Tab. 7.2: Calculating the total volume of sediment eroded by determining the total area changed by the same value between two years. Example shown is from the central region 1970-2000.

To calculate the total area subject to change at different depths, the gridded

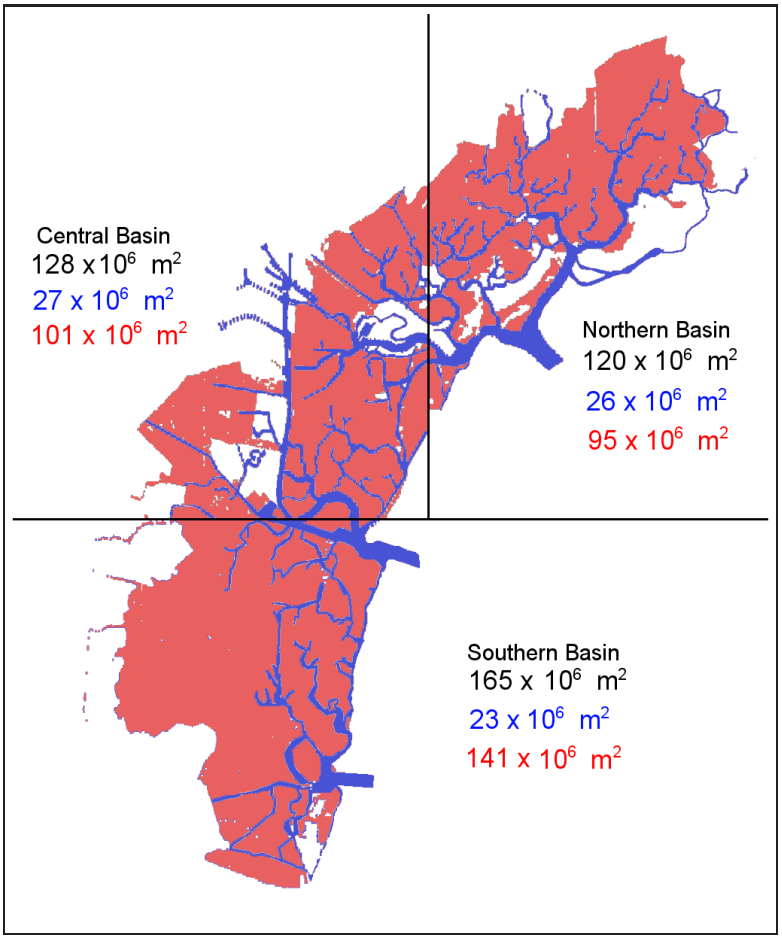

Fig. 7.2: The divisions used for sediment budget calculation, and the area of each region (black), major canals (blue) and intertidal habitat (red). Urbanized islands are not included in the calculations.

data were imaged with the scale interval representing changes in bathymetry of 25 cm between 1930 and 2000. To keep the colours perceptible between the scale interval (with changes of over 10 m in some places, there over 100 intervals in total), the data were imaged three times. The first image showed changes in bathymetry of less than 4 m (scale shown in Figure 7.3A), the second image showed changes in bathymetry greater than 4 m but less than 11 m (Figure 7.3B), and the final image showed changes greater than 11 m (Figure 7.3C). The open-source, graphics editor 'The Gimp'[iii] was used to select each colour of the scale using a masking tool. This selected pixels of the

[iii] www.gimp.org

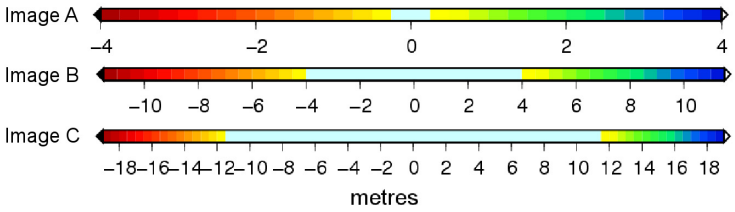

Fig. 7.3: Colour scales and increments used for the sediment budget calculations.

same colour in the whole image, with the in-built histogram revealing the number of pixels within the mask (i.e. the total area, in pixels, that has experienced change of the value represented by the colour selected). In order to determine the equivalent, real-world area that each pixel represented, the distance (in metres) over 0.1 of a decimal degree (latitude and longitude) was calculated and the number of pixels over the same distance counted as shown in Figure 7.4 (pixel area $= \frac{\text{real world distance}}{\text{number of pixels}}$).

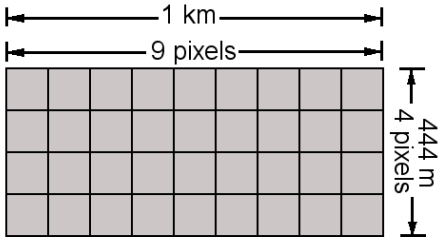

Fig. 7.4: Calculation of the pixel area. The example produces a pixel area of 111 m^2

Areas defined as canals (using Bondesan *et al.*, 2004) were painted out using lilac, a colour not used within the scale (see Figure 7.5), and the mask for each scale interval reapplied to determine the area of (i.e. number of pixels in) the intertidal area (the intertidal zone within this chapter is defined as any area not urbanised or a canal, with the definition including mudflats and salt marshes). The volume and area of sediment change within the canals was then determined by subtracting the intertidal count from the total count. The steps were repeated comparing bathymetry from 1930 to 1970 and 1970 to 2000. Using this method, a variety of data was extracted:

area - total area subject to net sediment loss, gain or experiencing relatively no

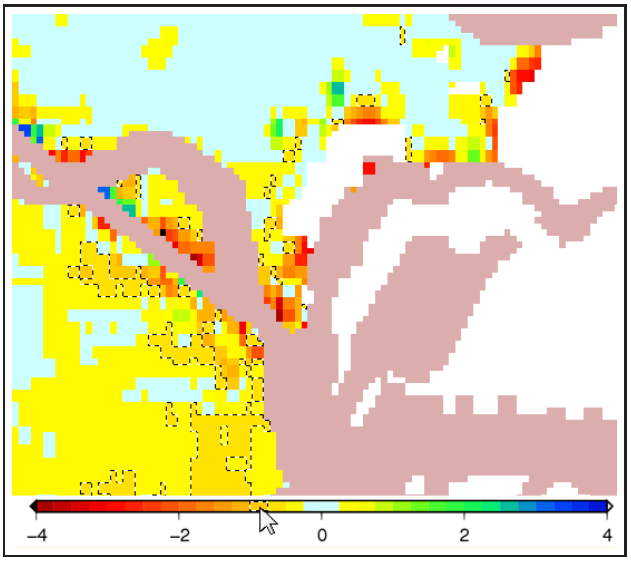

Fig. 7.5: Colour mask selection. The canals have been painted over with lilac to ensure that their pixels are not including in the mask (selecting the colour representing a loss of 1 m of sediment in the example). The histogram (not shown) reveals 58 pixels have been selected; each pixel represents 1089 m^2, thus the area subject to a loss of 1 m is 63,162 m^2; a volume of 63,162 m^3.

change (within ± 0.25 m; the smallest increment used in the scale and equivalent to between 4 (1930-2000) to 8 (1970-2000) mm maximum change per year).

volume/area - volume measurements in conjunction with area enabling comparison between regions, and/or environment.

total volume - total volumes of sediment lost or gained.

7.2.1.1 Error and Assumptions

The Petroli Canal was analysed separately in order to evaluate the error of this method as a known volume of sediment was dredged during its construction (25 million m^3 in total), which finished in 1969, one year before the 1970 dataset was collected. The sum total of sediment deficit in the Petroli Canal between 1930 and 1970, as calculated by the described method was also 25 million m^3, which suggests that the error in the technique is low.

Average subsidence levels are known for Venice Lagoon, but no correction was applied as the area of subsidence has shifted from around the centre of the lagoon (due to water extraction) between the '20s and '70s, to the northern region due to natural subsidence (Carbognin *et al.*, 2004). No corrections concerning sea-level rise were required as the bathymetry dataset had already been corrected relative to the Punta della Salute Datum. Distinguishing a difference between natural erosion and dredging activities is very difficult without complete dredging records[iv], therefore, no distinction is made, although possible regions of dredging and artificial accretions are discussed at the end of the chapter. Difference between the two bathymetry datasets of less than 25 cm is deemed to be insignificant (in relation to maximum changes of up to 19 m[v]) and therefore referred to as unchanged.

7.3 Results

The sediment budget as calculated by differences between bathymetric datasets can only provide net change rather than the gross volume of sediment gained or lost. Thus, sediment that has accreted during storms in 1947 for example, but has eroded or been dredged by 1970 will not be accounted for in a net sediment budget of 1930-1970, although the total volume of sediment lost through dredging of a canal in 1969 would mostly be included. Although the estimates will be much smaller than gross change, net change can still provide estimates to the long-term evolution of the lagoon. The results are shown as:

net change by area:

- Is the area subject to erosion increasing or decreasing?
- Is erosion around the Petroli Canal balanced by deposition in the northern region?

net volume change:

- Is the volume of sediment eroding per m^2 increasing or decreasing?
- Is Venice Lagoon balanced in terms of its sediment budget?

[iv] unable to obtain
[v] 1930-2000

7.3.1 Sediment Budget: Area

1930-1970

Over 50% of the lagoon experienced no net change between 1930 and 1970, 27% saw net erosion, and deposition characterised the remaining 22% (see Figures 7.6A and 7.10A). 85% of the canals were subject to change (erosion or deposition), whilst the intertidal area was stable in comparison (59% experienced no change). However, the total area of intertidal zone subject to erosion was greater than that subject to deposition (25% and 16% respectively). This is also evident as the gradual decline in the total area of salt marsh shown in Figure 3.5. All three regions show similar trends, although the central region was the most dynamic; 57% experienced change, compared to 43% of the southern region and 48% of the northern region. The southern region was the most stable region as 64% experienced no change. Only around 15% of the canals over the whole lagoon were stable between 1930-1970 and a slightly greater proportion of the remaining canals suffered infilling in comparison to those losing sediment. This difference in the total area of canals experiencing net loss and net gain was greatest in the central region (54% more canals were infilling than eroding) and smallest in the northern region (within 1%).

%	Total			Central			South			North		
	T	C	I	T	C	I	T	C	I	T	C	I
-	27.1	38.1	24.6	30.6	34.2	29.7	24.2	38.7	22.1	27.2	41.5	23.2
+	21.7	47.1	16.2	26.3	52.7	19.5	18.4	46.4	14.3	21.3	42.2	15.5
nc	51.2	14.8	59.2	43.1	13.1	50.7	57.3	14.9	63.7	51.5	16.3	61.3

Tab. 7.3: Proportion (%) of total lagoonal area (T), canals (C), and intertidal zone (I) subject to erosion (-), deposition (+) and no change (nc) between 1930 and 1970.

1970-2000

42% of the lagoon was stable between 1970-2000, a third suffered net erosion, whilst a quarter was depositional (see Figures7.6B 7.10B). There was an equal proportion of canals experiencing erosion and deposition (39%), although the total area of canal experiencing no change increased to 21% (from 15% in the period 1930-1970). This in-

crease was manifested by a decrease in the total area of canals experiencing deposition (reduced from 47% in the period 1930-1970, to 39% between 1970-2000). Therefore, the canals were fairly balanced as the area suffering erosion equalled the area experiencing deposition. 47% of the intertidal zone was stable between 1970 and 2000; a smaller area than that seen in the earlier period (59%) due mainly to the increase in area experiencing change in the southern region. The proportion of intertidal zone remaining stable in the southern region decreased by a third compared with the previous period to 43.2%, with the extension of areas experiencing net sediment loss increasing by two thirds on the previous period to 37%. However, 20% saw net sediment gain, an increase of 39% on the previous period. The increased dynamicism (implied by a decrease in the total area remaining stable) was also seen in the central region, where the proportion of intertidal zone eroding was greater (39%), as it was for deposition (22%). Despite this, the rate of change between the two periods was much smaller in the central region than in the southern region, as the total area of intertidal zone that was net eroded increased by 31% and the area of net gain increased by 13% (see Table 7.6). The northern region saw a decrease in the total area of eroding intertidal zone, reducing by 30% from the first period to 16%. At the same time, the proportion of intertidal zone that experienced net deposition increased to 24% (an increase of 53% on the previous period).

%	Total			Central			South			North		
	T	C	I	T	C	I	T	C	I	T	C	I
-	33.1	39.2	31.7	39.8	43.1	38.9	38.0	44.7	36.9	19.3	30.2	16.2
+	25.0	39.6	21.6	25.2	36.1	22.1	22.4	37.5	19.9	28.4	45.1	23.7
nc	41.8	21.2	46.7	34.9	20.8	39.0	39.5	17.8	43.2	52.3	24.7	60.1

Tab. 7.4: Proportion (%) of total lagoonal area (T), canals (C), and intertidal zone (I) subject to erosion (-), deposition (+) and no change (nc) between 1970 and 2000.

1930-2000

The results show that 38% of Venice lagoon was net erosional between 1930 and 2000 (Figure 7.6C). 32% remained unchanged (± 0.25 m), and only 29%[vi] experienced ac-

[vi] the remaining 1% is accounted through rounding errors

cumulation. Sediment gains are largely within the canals, of which 50% experienced deposition, compared to only 24% of the intertidal zone. 38.4% of the intertidal zone and 37.9% of canals were subject to erosion (similar proportions); however, the intertidal zone was more stable with 36.8% showing no change between 1930-2000, compared to 12.5% of the canals. Only the northern region had a stable intertidal zone; 50% remained unchanged between 1930 and 2000, and a slightly larger area sustained sediment gain (26%) than loss (24%). The northern region canals largely infilled (50%), and experienced lower than average (lagoon-wide) losses of sediment (35%). The southern and central regions were much more dynamic than the northern region: 66% and 78% of the regions experienced change (respectively), compared to 58% of the northern region. 47% of the central region experienced erosion, with a slightly larger area of intertidal zone experiencing loss than the canals did (see Table 7.5), which mainly (∼50%) infilled. The pattern is similar in the southern region, although not to the same extremes as in the central region.

%	Total			Central			South			North		
	T	C	I	T	C	I	T	C	I	T	C	I
-	38.3	37.9	38.4	44.9	38.9	46.5	41.9	40.2	42.2	26.4	34.9	24.0
+	29.3	49.5	24.8	33.6	50.7	29.1	24.5	47.6	20.7	31.5	50.1	26.5
nc	32.3	12.5	36.8	21.5	10.5	24.4	33.6	12.2	37.1	42.1	15.0	49.5

Tab. 7.5: Proportion (%) of total lagoonal area (T), canals (C), and intertidal zone (I) subject to erosion (-), deposition (+) and no change (nc) between 1930 and 2000.

%	Total			Central			South			North		
	T	C	I	T	C	I	T	C	I	T	C	I
-	22	3	29	30	26	31	57	16	67	-29	-27	-30
+	15	-16	33	-4	-31	13	22	-19	39	33	7	53
nc	-18	43	-21	-19	59	-23	-31	19	-32	2	52	-2

Tab. 7.6: Change in total area of total lagoonal area (T), canals (C), and intertidal zone (I) subject to erosion (-), deposition (+), or experiencing no change (nc), between 1930 to 1970 and 1970 to 2000.

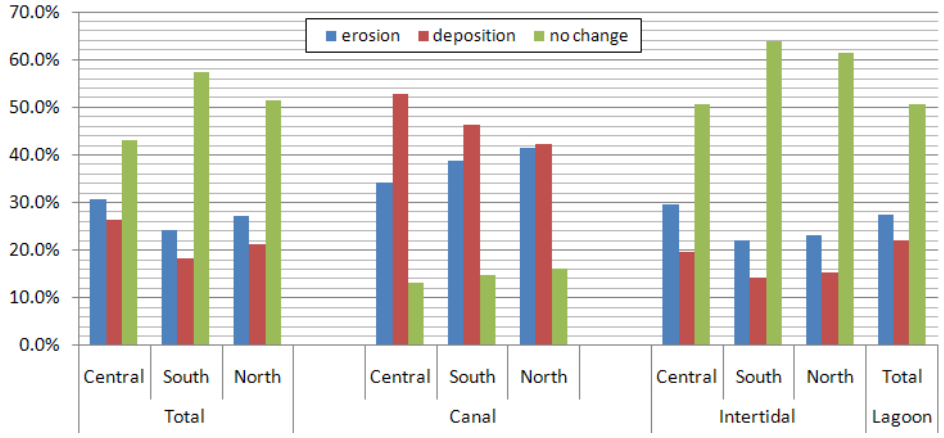

(a) 1930-1970

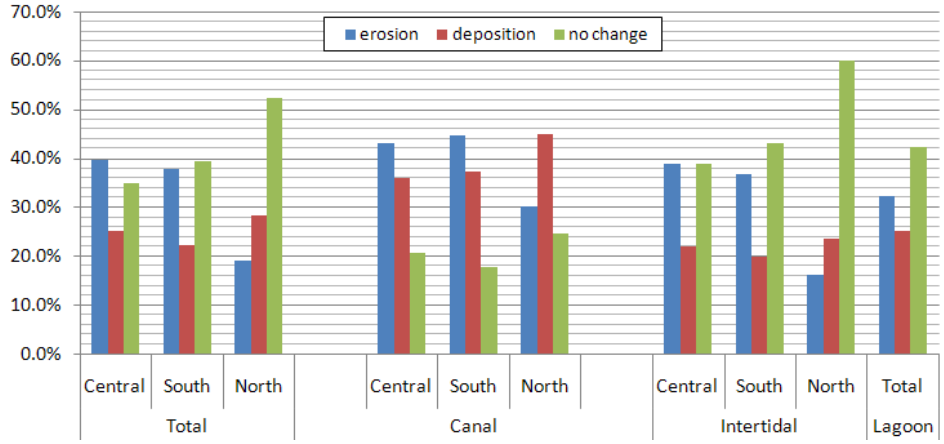

(b) 1970-2000

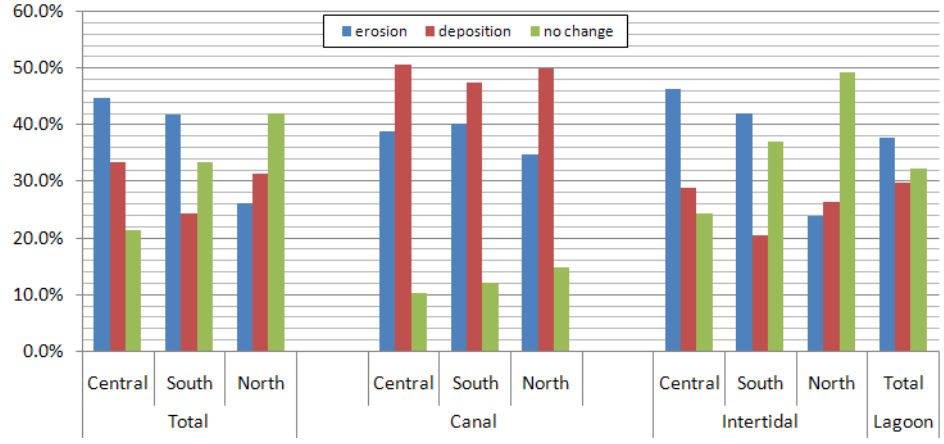

(c) 1930-2000

Fig. 7.6: Percentage of areas within Venice Lagoon experiencing erosion, deposition, or no change.

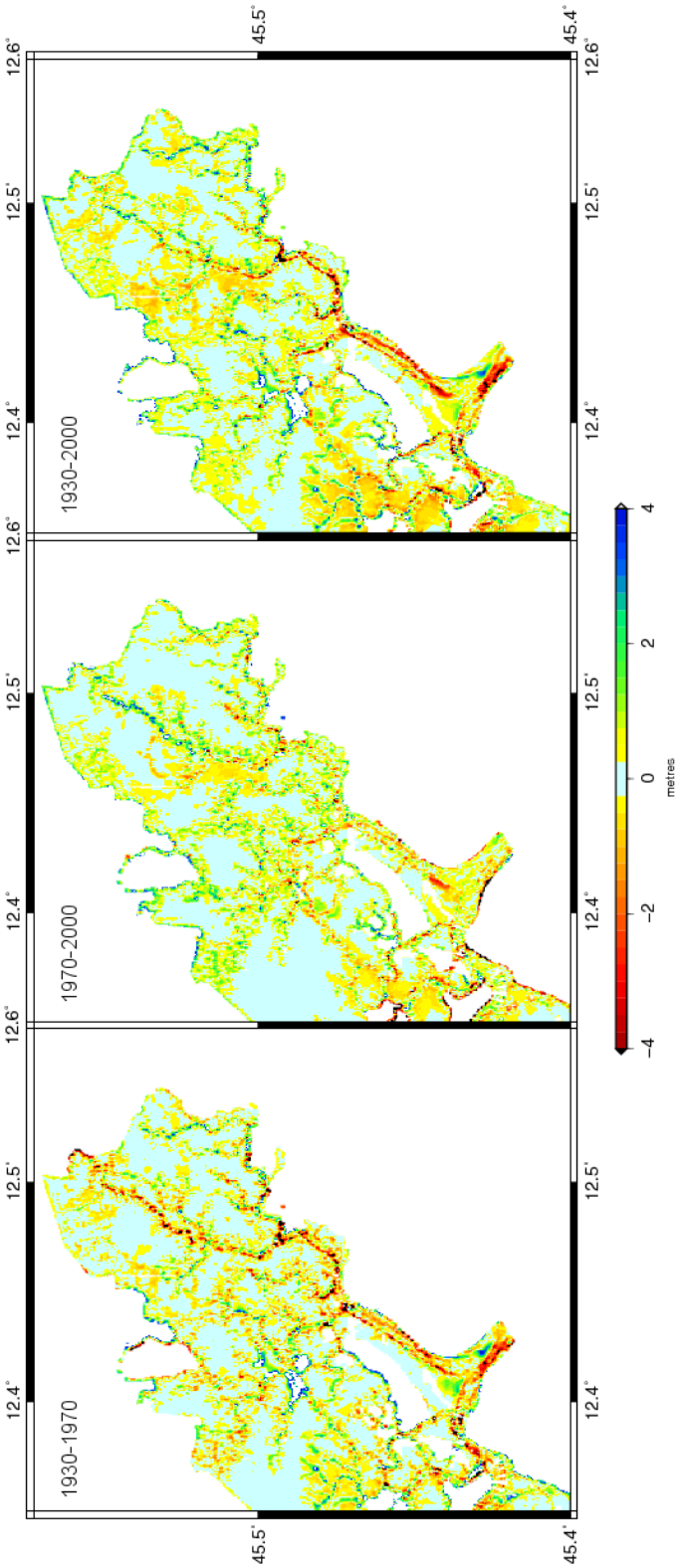

Fig. 7.7: Erosion and accretion in the northern region; 1930-1970, 1970-2000, 1930-2000.

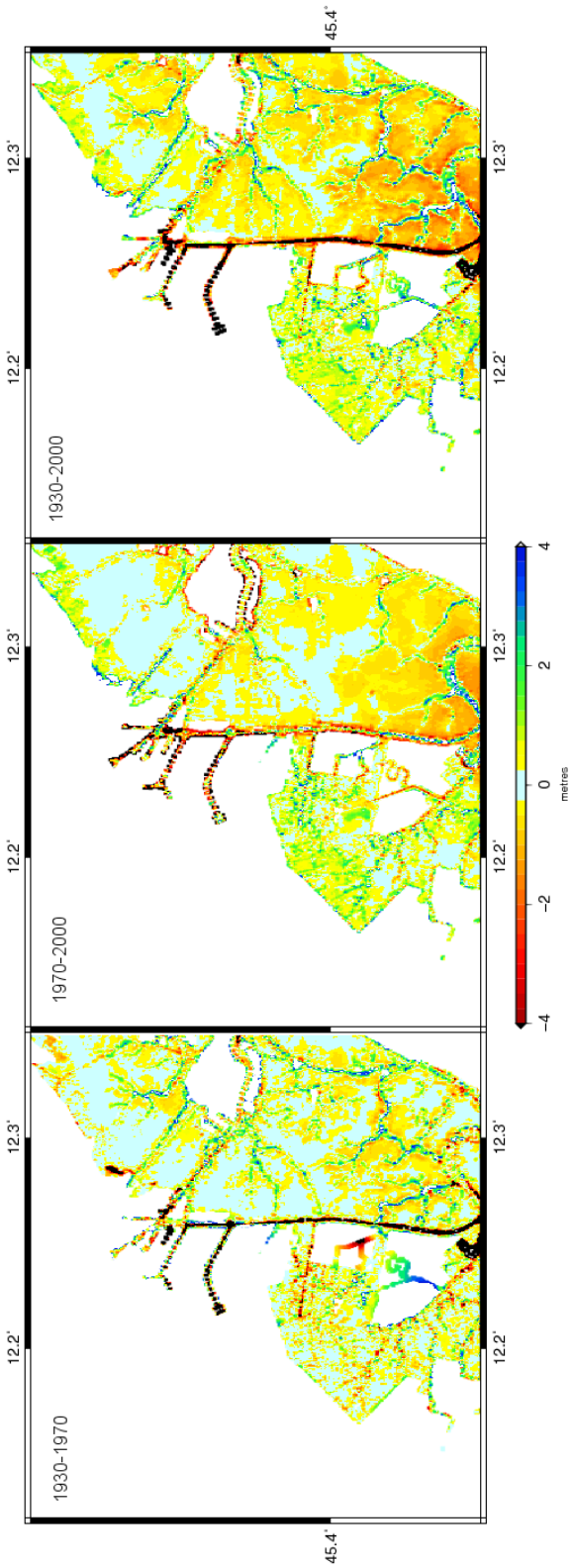

Fig. 7.8: Erosion and accretion in the central region; 1930-1970, 1970-2000, 1930-2000.

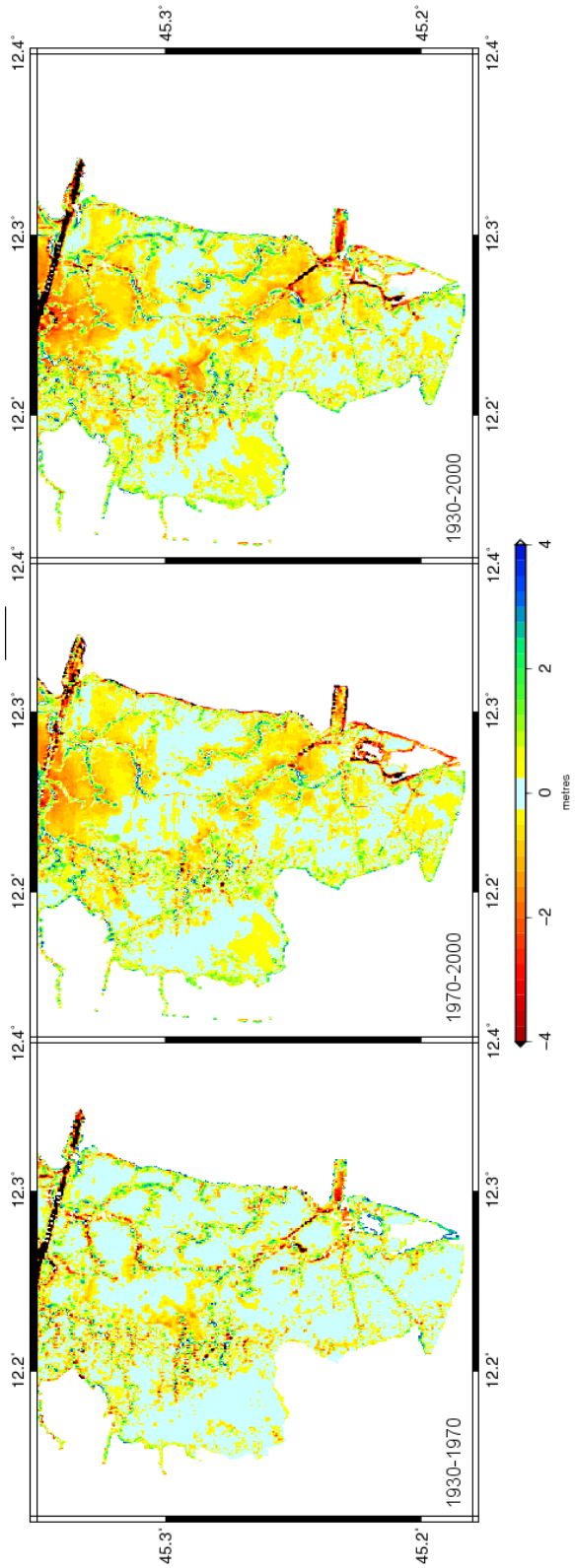

Fig. 7.9: Erosion and accretion in the southern region; 1930-1970, 1970-2000, 1930-2000.

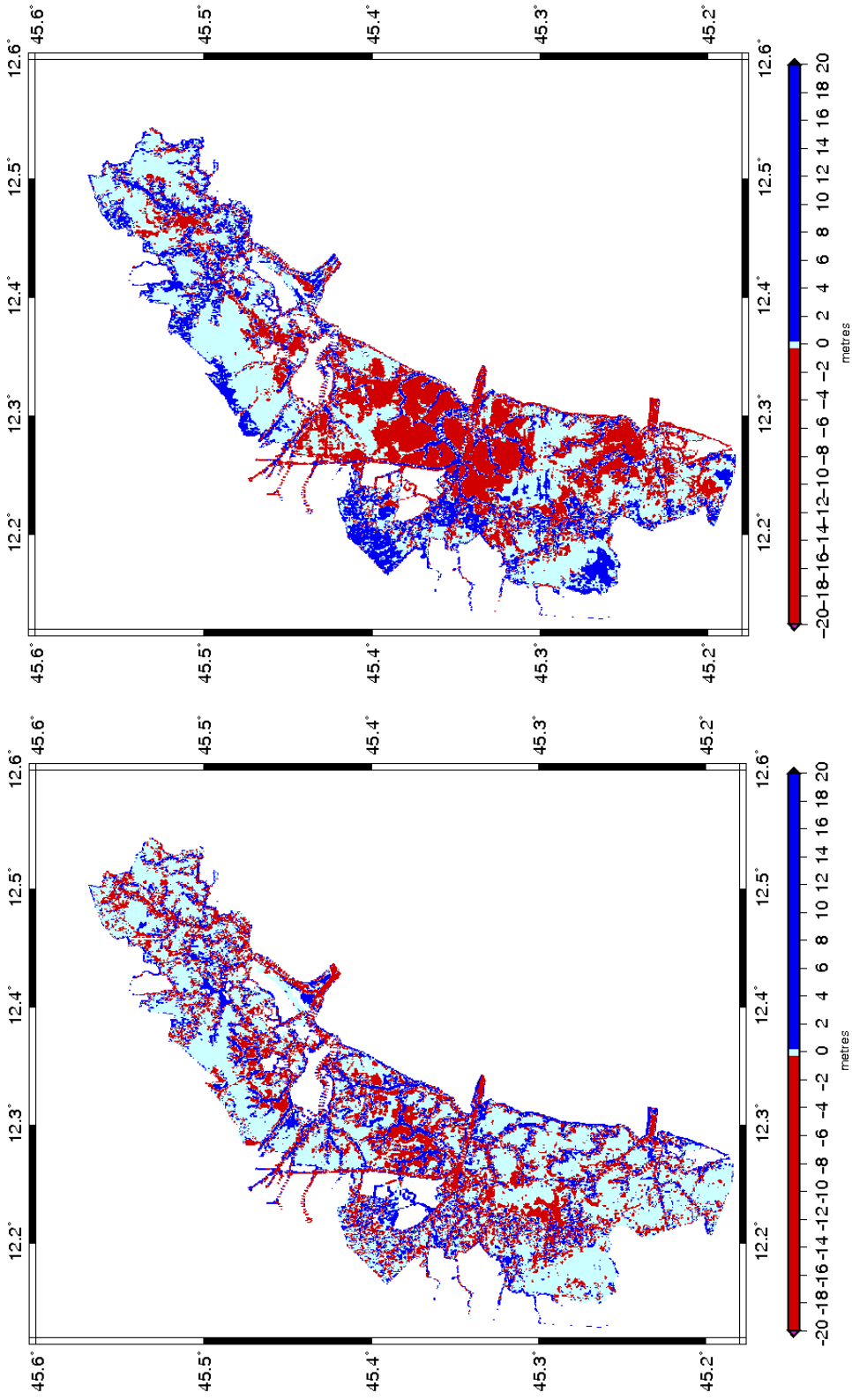

(a) 1930 to 1970

(b) 1970 to 2000

Fig. 7.10: Areas of net erosion (>0.25 m), no change (-0.25 to 0.25 m), and net deposition (>0.25 m) in 1930 to 1970 (a), and between 1970 and 2000 (b).

7.3.1.1 Summary - Intertidal Zone

The intertidal zone shows evidence of increased changes in time. Over half of the intertidal area experienced no net change (± 0.25 m) between 1930 and 1970. However, between 1970 and 2000, intertidal areas were increasingly becoming subject to erosion in the central and southern regions. Only the northern region has retained a similar area of unchanged intertidal zone (see Figure 7.7). Almost 50% of the central region was net erosional between 1930 and 2000, compared to under 25% in the northern region. However, a greater proportion of the central region experienced net deposition than the north (and south), suggesting that it was the most dynamic region of Venice Lagoon (Figure 7.8). All three regions have seen an increase in the total intertidal area subject to deposition between 1930-1970 to 1970-2000. Despite this, a concurrent and larger increase in the intertidal area subject to sediment loss results in a increasingly erosional intertidal zone in the southern and central regions. A decrease in the intertidal area experiencing erosion in the northern region effectuates the only net depositional intertidal zone in the lagoon (see Figure 7.6).

7.3.1.2 Summary - Canals

The canals are much more dynamic than the intertidal area; only 12.5% maintained stability between 1930 and 2000. Almost 50% of lagoonal canals experienced deposition, whilst 38% deepened. The northern region canals were the most stable (15% remaining stable), and had the smallest proportion of eroding canals.

Between 1930 and 1970, most canals were depositional, especially in the central region (52.7%), although the northern region had an equal proportion of canals eroding and depositing (42%). Between 1970 and 2000, the canals followed a similar pattern to the intertidal zone; the total area of eroding canals in the central and southern regions increased to over 40%, whereas the area of infilling canals in the same regions decreased to below 40%. In contrast, the northern canals became depositional in place of those which were net erosional. Between 1990 and 2000, the proportion of infilling canals had fallen to ∼25%; however, the central region canals stablized with the proportion of eroding canals returning to 1930-1970 levels.

7.3.2 Sediment Budget: Annual Volumetric Changes

In order to present the data in context, the average rates of erosion and deposition are presented as volume change per area experiencing erosion/deposition, rather than per total area, which may 'dilute' the results (see Figure 7.11). Thus, the rates shown are representative unless otherwise stated.

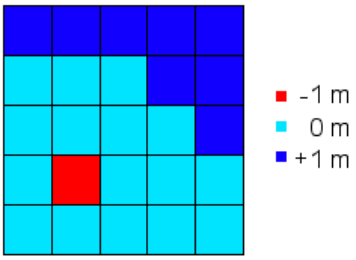

Fig. 7.11: The average loss within erosional areas would be -1 m (representative), whereas if averaged over the whole area, the result would be 0.04 m, which does not provide a good indication of the average erosion rate.

1930-1970

During 1930 to 1970, the areas of the lagoon experiencing net erosion lost an average of 2.79 cm^3 per cm^2 (hereafter noted as just cm), whilst areas of net accretion gained 3.21 cm yr^{-1} (see Table 7.7). However, as a greater area of the lagoon suffered erosion, the lagoon as a whole, experienced a net loss of 0.05 cm yr^{-1}. Erosion of the central region was greater than the other regions (-3.17 cm yr^{-1}, compared to -2.76 cm yr^{-1} in the southern region and -2.36 cm yr^{-1} in the northern region). Deposition was also greater in comparison (3.3 cm yr^{-1} compared to ~3.15 cm yr^{-1} in the other regions), although as an average over each region, the central and southern regions lost around 0.1 cm yr^{-1}, whereas the northern region gained 0.03 cm yr^{-1}. Canals deepened by an average of 5.99 cm yr^{-1} over the lagoon and infilled at an average rate of 4.67 cm yr^{-1}. The area of infilling canals exceeded those eroding; however, the higher rate of erosion resulted in the canals deepening by an average of 0.1 cm yr^{-1}.

The erosional sections of the canals in the central region deepened by an average of 8.57 cm yr^{-1}; the infilling sections gained 4.83 cm yr^{-1}, resulting in the canals

deepening by a average, net rate of 0.38 cm yr^{-1} (the greatest loss in the lagoon). The canals in the southern region deepened by a net average of 0.24 cm yr^{-1}, resulting from net loss of 6.3 cm yr^{-1} in the erosional canal sections and a net gain of 4.73 cm yr^{-1} in the sections that have accreted. The northern region canals experienced net infilling of 0.33 cm yr^{-1} due to a much lower rate of erosion (-3.69 cm yr^{-1}, 57% less than the erosion rate in the adjacent central region), and a slightly smaller depositional rate (4.41 cm yr^{-1}).

The depositional regions of the intertidal flats experienced a 2.28 cm yr^{-1} gain, compared to a average loss of 1.71 cm yr^{-1} from the erosional parts. However, as a 50% larger area experienced erosion over deposition, the intertidal zone across the whole lagoon experienced net erosion of -0.05 cm yr^{-1}. The central region intertidal zone was the most stable, with a net loss of 0.03 cm yr^{-1}, compared to a net loss of 0.06 cm yr^{-1} experienced in the rest of the lagoon. The erosional areas here experienced the smallest rate of loss (-1.58 cm yr^{-1}), compared to the southern region (-1.83 cm yr^{-1}) and the northern region (-1.7 cm yr^{-1}). The southern intertidal zone experienced the greatest rate of deposition, gaining 2.41 cm yr^{-1}, compared to the central region (2.24 cm yr^{-1}) and the northern region (2.14 cm yr^{-1}). In all cases, net erosion occurred over a larger area of intertidal zone, than net deposition, resulting in net losses despite a larger rate of deposition in all three regions.

cm yr^{-1}	Total			Central			South			North		
	T	C	I	T	C	I	T	C	I	T	C	I
-	-2.79	-5.99	-1.71	-3.17	-8.57	-1.58	-2.76	-6.30	-1.83	-2.36	-3.69	-1.70
+	3.21	4.67	2.28	3.30	4.83	2.24	3.17	4.73	2.41	3.13	4.41	2.14
nc				-0.10	-0.38	-0.03	-0.09	-0.24	-0.06	0.03	0.33	-0.06

Tab. 7.7: Annual rate of change in total lagoonal area (T), canals (C), and intertidal zone (I) subject to erosion (-), deposition (+) and net change (nc) between 1930 and 1970.

1970-2000

The period 1970-2000 saw a 5% increase in the rate of sediment loss from the eroding areas of the lagoon to 2.92 cm yr^{-1}, and a 9% increase in sediment gain in the depositional areas to 3.5 cm yr^{-1}. However, there was a 44% increase in the area subject to

erosion resulting in a net loss of 0.05 cm yr^{-1}; the same rate as in the earlier period. The rate of accretion in depositional areas in all three regions exceeded the rate of erosion. The central region continued to have the greatest rate of change in areas of erosion (-3.03 cm yr^{-1}) and deposition (3.3 cm yr^{-1}). The relative rate of deposition (in comparison to the rate of erosion) has increased from 1930-1970 due to a 5% decrease in the erosion rate, and a 17% increase in the deposition rate. Despite this, there was an average loss of 0.23 cm yr^{-1} over the whole region. The southern region lost an average of 0.37 cm yr^{-1} due to a high rate of sediment loss in its eroding areas (-2.92 cm yr^{-1}) and the lowest rate of deposition in the lagoon (3.3 cm yr^{-1}).

The average net accretion in the northern region increased by 1368% from 0.03 to 0.44 cm yr^{-1}, due to the low sediment loss rate in the eroding areas (2.7 cm yr^{-1}) and fairly high accretion rate (3.38 cm yr^{-1}). The average infill in accreting areas of the canals (lagoon-wide) remained similar to that in the first period, although average erosion in the canals fell by 6% to -5.65 cm yr^{-1}. However, the total area subject to erosion in the canals increased by 10%; the total area subject to infilling fell by 10%, resulting in a net loss of 0.37 cm yr^{-1} in the canals. The rate of erosion in the central region decreased by 27% to -6.23 cm yr^{-1}, with a corresponding 8% increase in the deposition rate to 5.22 cm yr^{-1}. Despite this, the average net change in the central canals increased from -0.38 to -0.79 cm yr^{-1}, due to a 32% increase in the extent of net erosion. The southern region has also experienced an increase in the average loss (down to -0.92 cm yr^{-1}), similar to the central region. The net gain within the canals of the northern region has increased by 84% to 0.61 cm yr^{-1}, although the rates of change in the eroding canal sections are similar to the rates of accretion in depositing sections (-4.38 and 4.28 cm yr^{-1} respectively). Unlike the other regions, a larger proportion of canals in the northern region are depositional rather than erosional, explaining the large net gain.

The lagoonal intertidal zone experienced an increase in the average area subject to erosion (up 25% to -2.13 cm yr^{-1}) and deposition (up 31% to 2.99 cm yr^{-1}). As the depositing areas enlarged at a greater rate than the eroding areas (33% compared to 27%), the net average change across the intertidal zone was +0.02 cm yr^{-1}. In contrast to the pattern of change within the canals, the rate of change has intensified in the intertidal zone. The southern intertidal zone has the greatest rate of erosion (-2.31 cm

yr^{-1}, up 26% on the first period), and the smallest rate of deposition (2.89 cm yr^{-1}, an increase of 20% on the first period), resulting in a net change of -0.28 cm yr^{-1}. The depositional intertidal areas in the central region have the greatest rate of sediment gain of all three regions (3.21 cm yr^{-1}), and an erosion rate of 2 cm yr^{-1}, resulting in a net loss of -0.07 cm yr^{-1}. The northern intertidal region achieved a net gain of 0.39 cm yr^{-1} (from being net erosional), due to a relatively low average rate of sediment loss (1.82 cm yr^{-1}) and a complementary increase of 53% in the extent of areas of net deposition and 30% decrease in the extent of net erosion.

cm yr^{-1}	Total			Central			South			North		
	T	C	I	T	C	I	T	C	I	T	C	I
-	-2.92	-5.65	-2.13	-3.03	-6.23	-2.00	-2.92	-5.94	-2.31	-2.70	-4.38	-1.82
+	3.50	4.69	2.99	3.86	5.22	3.21	3.30	4.64	2.89	3.38	4.28	2.90
nc				-0.23	-0.79	-0.07	-0.37	-0.92	-0.28	0.44	0.61	0.39

Tab. 7.8: Annual rate of change in total lagoonal area (T), canals (C), and intertidal zone (I) subject to erosion (-), deposition (+) and net change (nc) between 1970 and 2000.

1930-2000

Between 1930 and 2000, the erosional areas of the lagoon lost an average of 1.5 cm yr^{-1} of sediment per year, with area of deposition gaining an average of 1.7 cm yr^{-1}. This equates to an average annual loss of 0.06 cm over the whole lagoon; an average loss over the 70 years of 4.06 cm[vii]. The rate of change was the greatest in the central region, where erosional areas lost 1.71 cm yr^{-1} on average, and depositional areas gained 1.83 cm yr^{-1}. The depositional areas in the south and northern regions both gained ∼1.6 cm yr^{-1}, however, loss in the erosional areas of the southern region was 16% greater than in the northern region.

The greatest rates of change occurred in the canals; the erosional areas lost an average of 3.7 cm yr^{-1} with the depositional sections gaining an average of 2.52 cm yr^{-1}. This equates to an average loss in the canals of 0.16 cm yr^{-1}. The central region once again, saw the greatest rate of change; canals suffering net erosion lost 4.65 cm

[vii]note that this does not include data for urbanized islands or the barrier islands.

yr^{-1}, whilst infilling canals gained an average of 2.68 cm yr^{-1}. A similar degree of change was seen in the southern region (-4 cm yr^{-1} and 2.57 cm yr^{-1} respectively). The northern region canals experienced an inversion of this trend with higher rates of deposition (2.32 cm yr^{-1}) than erosion (-2.27 cm yr^{-1}). Consequently, the southern region canals deepened by an average of 0.21 cm yr^{-1}, while the central region canals deepened by 0.15 cm yr^{-1}; the northern region canals infilled by an average of 0.19 cm yr^{-1} over the whole network.

The intertidal areas were relatively stable over the whole lagoon with an average loss of 1.02 cm yr^{-1} in the erosional parts and an average gain of 1.34 cm yr^{-1} in the depositional areas. The larger expanse of eroded intertidal flats resulted in an average *loss* of -0.04 cm yr^{-1} despite the depositional flats experiencing a greater rate of change than those that have eroded. The southern region intertidal zone showed the greatest rate of erosion on average (-0.18 cm yr^{-1}) as the accreting flats gained less than those in the other regions (1.27 cm yr^{-1}), whilst the erosional areas lost 1.05 cm yr^{-1}. Although the central region intertidal zone lost sediment at a similar rate (-1.06 cm yr^{-1}), its intertidal depositional-rate was much higher (1.44 cm yr^{-1}), resulting in an average annual loss of 0.07 cm. The northern region intertidal zone gained sediment at a comparable rate in its accreting parts as the southern region; however, the eroded parts lost, on average, 19% less than the other two regions (-0.85 cm yr^{-1}) resulting in a net annual gain of 0.14 cm.

Overall, the lagoon as a whole has remained constant in volume, with an overall loss of 0.05 cm yr^{-1} between 1930 to 1970 and 1970 to 2000 despite many changes in the rates of erosion and deposition in the canals and intertidal zone.

7.3.2.1 Summary - Canals

The amount of sediment loss in the eroding areas has decreased between 1930-1970 and 1970-2000, although the rate of sediment gain in depositing areas has remained fairly constant. A relative increase in the total area subject to erosion has resulted in a net average loss of -0.16 cm yr^{-1} between 1930 and 2000, with the rate increasing

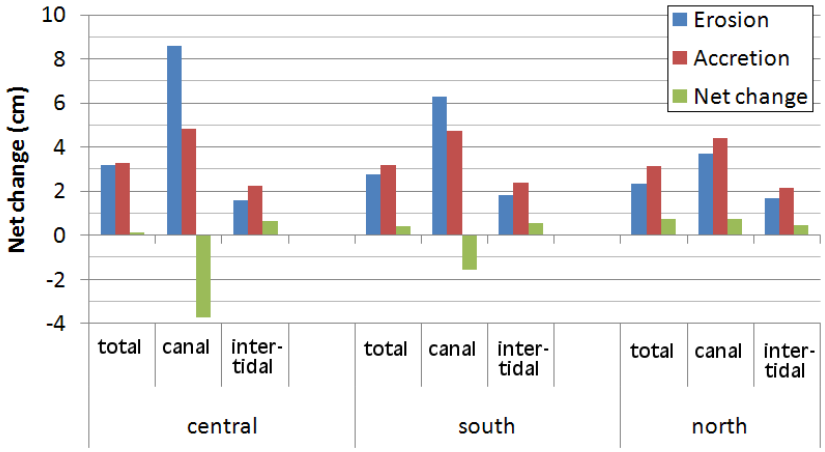

(a) 1930 to 1970

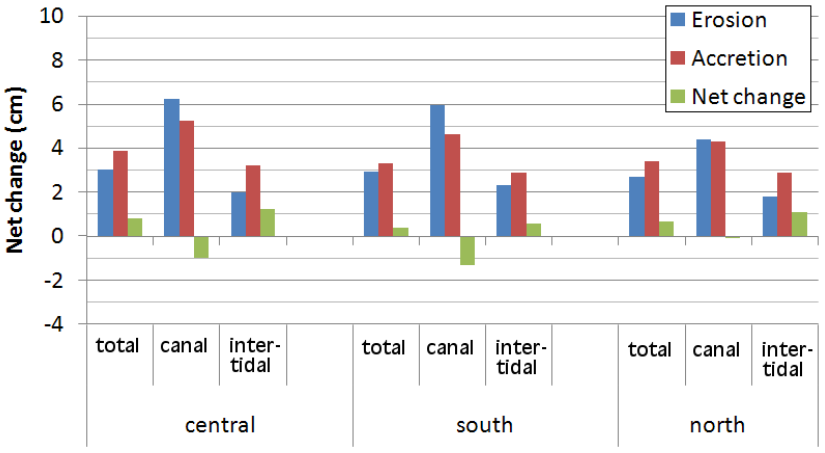

(b) 1970 to 2000

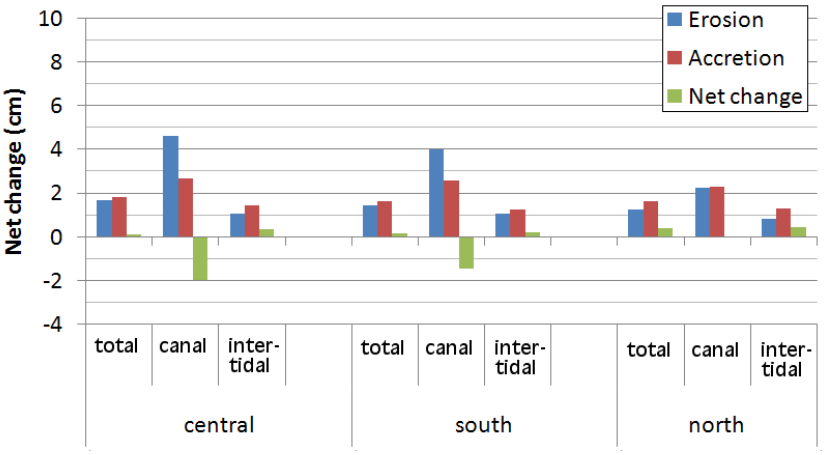

(c) 1930 to 2000

Fig. 7.12: Volume of net erosion (>0.25 m), no change (-0.25 to 0.25 m), and net deposition (>0.25 m) in (a) 1930 to 1970, (b) 1970 and 2000, and (c) 1930 and 2000. Note that values for erosion have been plotted in the positive to facilitate comparison with values of deposition; net change values remain either positive or negative.

cm yr^{-1}	Total			Central			South			North		
	T	C	I	T	C	I	T	C	I	T	C	I
-	-1.50	-3.70	-1.02	-1.71	-4.65	-1.06	-1.45	-4.00	-1.05	-1.25	-2.27	-0.85
+	1.70	2.52	1.34	1.83	2.68	1.44	1.62	2.57	1.27	1.64	2.32	1.30
nc				-0.15	-0.45	-0.07	-0.21	-0.38	-0.18	0.19	0.37	0.14

Tab. 7.9: Annual rate of change in total lagoonal area (T), canals (C), and intertidal zone (I) subject to erosion (-), deposition (+) and net change (nc) between 1930 and 2000.

substantially in the second period (see Table 7.11). Only in the northern region, have the canals shown net accretion (0.37 cm yr^{-1}) between 1930 and 2000, whereas the central region has shown the largest net loss (-0.45 cm yr^{-1}).

7.3.2.2 Summary - Intertidal Zone

The intertidal zone has changed from being a sediment exporter (-0.05 cm yr^{-1}) between 1930 and 1970, to a sediment importer (0.02 cm yr^{-1}) between 1970 and 2000. However, the rate of import in 1970-2000 has not yet exceeded the rate of export in 1930-1970 and so it remains a net exporter (-0.04 cm yr^{-1}) between 1930 and 2000 (see Table 7.11). Both the southern and central regions have seen a large increase in the rate of loss from the intertidal zone (362% and 129% respectively), with a total loss of -0.18 cm yr^{-1} -0.07 cm yr^{-1} seen respectively between 1930 and 2000. Only the northern region has experienced a change from net loss to net accretion, with an overall gain of 0.14 cm yr^{-1} between 1930 and 2000.

7.3.2.3 Total Volume Changes

Between 1930 and 1970, Venice Lagoon exported a net total of 241,000 m^3 yr^{-1} of sediment of which 74% came from the intertidal zone. The canals were balanced, importing and exporting 1.6×10^6 m^3 yr^{-1}. In comparison, net accreting areas in the intertidal zone imported 1.2×10^6 m^3 yr^{-1}, and eroding areas exported 1.4×10^6 m^3 yr^{-1}. Therefore, even though the canals transported greater volumes of sediment, the intertidal zone largely controlled the net sediment budget during this time period (see Table 7.10).

Between 1970 and 2000, the net annual loss of sediment increased as the lagoon lost 373,000 m^3 yr^{-1}. The amount of sediment eroded and deposited also increased with ~900,000 m^3 yr^{-1} extra sediment eroded from erosional areas, and 765,000 m^3 yr^{-1} extra sediment deposited on depositional areas, when compared to the previous period (1930-1970). Whilst areas of net erosion within the canals exported an extra 62,000 m^3 yr^{-1} from 1930-1970 to 1970-2000, the depositing areas imported 155,000 m^3 yr^{-1} less in 1970-2000 than in 1930-1970, resulting in greater contribution to net lagoonal export by the canals (Table 7.11 and Figure 7.13). Greater volumes of sediment were exported (2.3×10^6 m^3 yr^{-1}) from eroding intertidal flats and imported (2.2×10^6 m^3 yr^{-1}) from accreting intertidal flats in 1970-2000. This balance in the sediment exchange resulted in a net export of only 91,000 m^3 yr^{-1} from the intertidal zone (Table 7.11).

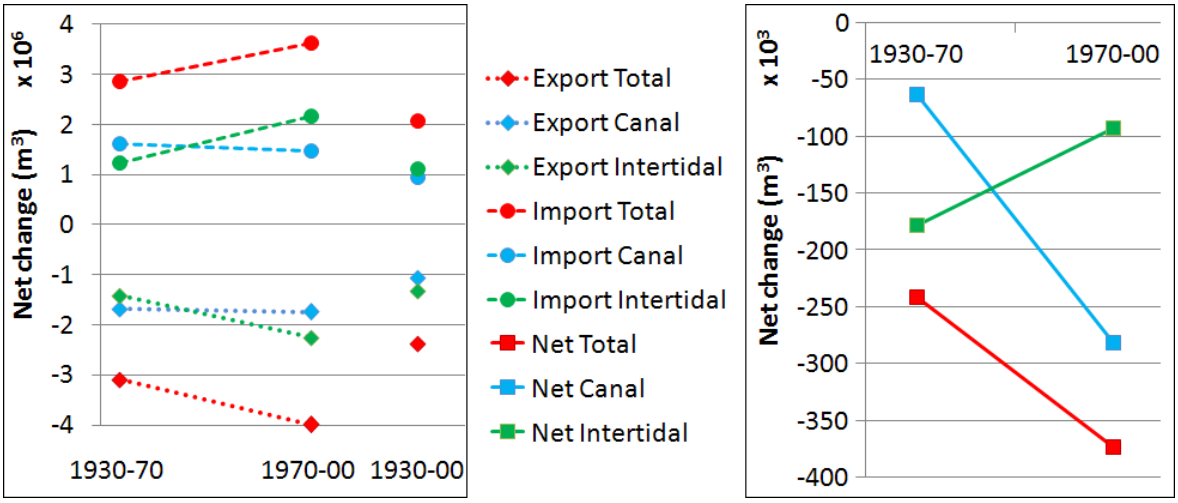

Fig. 7.13: Net export and import of sediment.

7.3.2.4 Summary

The following tables show the difference in sediment exchange between 1930 to 1970, and 1970 and 2000, as a total (Table 7.10), and within the canals and intertidal zone (Table 7.11). Changes in the total area result from differences in the coverage of data between 1930 and 2000.

Variable	Exchange	Total		
		1930-‘70	1970-‘00	1930-‘00
volume [m^3]	erosion	-124,050,439	-119,968,283	-166,612,821
	accretion	114,420,363	108,776,665	144,565,554
	sum	-9,630,076	-11,191,617	-22,047,267
volume [m^3 yr^{-1}]	erosion	-3,101,261	-3,998,942	-2,380,183
	accretion	2,860,509	3,625,889	2,065,222
	net change	-240,752	-373,054	-314,961
av. cm (m)	erosion	-30.46 (-1.12)	-28.36 (-0.88)	-39.77 (-1.05)
	accretion	28.28 (1.28)	26.77 (1.05)	35.71 (-1.19)
	change	-2.18 (0.17)	-1.59 (0.17)	-4.06 (0.14)
av. cm yr^{-1} (cm yr^{-1})	erosion	-0.76 (-2.79)	-0.95 (-2.92)	-0.57 (-1.5)
	accretion	0.71 (3.21)	0.89 (3.5)	0.51 (1.70)
	change	-0.05 (0.42)	-0.05 (0.58)	-0.06 (0.2)
area [m^2]	sum	411,141,904	413,190,748	413,270,762
	erosion	111,236,468	136,836,202	158,366,954
	accretion	89,227,500	103,486,232	121,271,544
	no change	210,677,936	172,868,314	133,632,274
area %	erosion	27.06%	33.12%	38.31%
	accretion	21.70%	25.05%	29.34%
	no change	51.24%	41.84%	32.3%

Tab. 7.10: Summary results comparing total changes between 1930-1970, 1970-2000, and 1930-2000. Data outside parentheses is an average of the total area, data within parentheses is an average of just erosional or accretional areas.

Variable	Exchange	Canal			Intertidal		
		1930-'70	1970-'00	1930-'00	1930-'70	1970-'00	1930-'00
volume [m^3]	erosion	-67,254,834	-52,324,056	74,243,721	-56,795,605	-67,644,226	-92,369,100
	accretion	64,731,540	43,890,222	66,163,483	49,688,823	64,886,444	78,402,071
	sum	-2,523,294	-8,433,835	-8,080,238	-7,106,782	-2,757,783	-13,967,029
volume [m^3 yr^{-1}]	erosion	-1,681,371	-1,744,135	-1,060,625	-1,419,890	-2,254,808	-1,319,559
	accretion	1,618,288	1,463,007	945,193	1,242,221	2,162,881	1,120,030
	net change	-63,082	-281,128	-115,432	-177,670	-91,926	-199,529
av. cm (m)	erosion	-91.98 (-2.4)	-66.58 (-1.69)	-98.2 (-2.58)	-16.9 (-0.68)	-19.25 (-0.64)	-26.59 (-0.71)
	accretion	88.06 (1.28)	55.55 (1.41)	87.31 (1.77)	88.06 (1.87)	19.73 (0.9)	23.90 (0.94)
	change	-3.93 (-0.53)	-11.04 (-0.29)	-10.89 (-0.82)	-2.06 (0.23)	0.47 (0.26)	-2.69 (0.22)
av. cm yr^{-1} (cm yr^{-1})	erosion	-2.3 (-5.99)	-2.22 (-5.65)	-1.4 (-3.7)	-0.42 (-1.71)	-0.64 (-2.13)	-0.38 (-1.02)
	accretion	2.2 (4.67)	1.85 (4.69)	1.25 (2.52)	0.37 (2.28)	0.66 (2.99)	0.34 (1.34)
	change	-0.1 (-1.32)	-0.37 (-0.95)	-0.16 (-1.17)	-0.05 (0.57)	0.02 (0.86)	-0.04 (0.32)
area [m^2]	sum	73,602,826	78,784,220	75,640,576	337,539,078	334,406,528	337,630,196
	erosion	28,068,212	30,881,852	28,701,568	83,168,256	105,954,350	129,665,386
	accretion	34,670,516	31,164,154	37,450,934	54,556,984	72,322,078	83,820,610
	no change	10,864,098	16,738,214	9,488,074	199,813,838	156,130,100	124,144,200
area %	erosion	38.13%	39.20%	37.94%	24.64%	31.68%	38.4%
	accretion	47.10%	39.56%	49.51%	16.16%	21.63%	24.83%
	no change	14.76%	21.25%	12.54%	59.20%	46.69%	36.77%

Tab. 7.11: Summary results comparing changes within the canals and intertidal zone between 1930-1970, 1970-2000, and 1930-2000. Data outside parentheses is an average of the total area, data within parentheses is an average of just erosional or accretional areas.

7.4 Discussion

Quantitative comparisons of bathymetry datasets (the difference map method - DMM) have been used to provide estimates to the terms of the sediment budget:

$$\sum Q_{source} - \sum Q_{sink} - \Delta V + P - R = Residual$$

The method has determined the net volume of sediment eroded ($\sum Q_{source} + R$), and the net volume of sediment accreted ($\sum Q_{sink} + P$). Distinguishing the natural (Q) and anthropogenic terms (R and P) is complicated but will be discussed qualitatively within this section. The final term, ΔV (net change in volume) cannot be determined through DMM, thus is also discussed in terms of direct-measurements determined within this thesis and within the literature (Zaggia and Maurizio, 2005; Ferrarin, 2005; Sfriso *et al.*, 2005a; Fontolan *et al.*, 2007; Tambroni and Seminara, 2006b).

7.4.1 Venice Lagoon in Periods of Exploitation and Remediation

The period between 1930-1970 was part of the industrial revolution of Venice; the petrochemical/chemical industrial sector at Mestre/Marghera (Figure 3.1) expanded rapidly, with groundwater extracted underneath Venice in order to provide enough water for its use (Consorzio Venezia Nuova, 1996). To allow for passage of tankers to the port, the 15 m-deep Petroli Canal was constructed between 1965 to 1969 (Ravera, 2000) from Malamocco Inlet to Marghera Port. The industrial sector and the Petroli Canal have both affected the central region (causing subsidence due to groundwater extraction and erosion from ship-generated waves), although the hydrodynamics of the whole lagoon had been altered at the beginning of the 20$^{\text{th}}$ century due to construction of jetties at all three inlets, which resulted in changed circulation and sediment dynamics (Seminara *et al.*, 2005; Di Silvio, 2005). The extreme high water in 1966 enlightened the authorities to the potential impact of continued anthropogenic exploitation and climate change (Fletcher and Spencer, 2005), and thus the period 1970-2000 encompasses a time when remedial measures were undertaken with a view to sediment retention, especially in the salt marshes and mudflats. These remedial measures include:

- Cessation of groundwater pumping in the early ‘70s (Fletcher and Spencer, 2005);

- Control of pollutants (dredging of polluted sediments, securing dumps abandoned in the '70s). Increased nutrients in the water column caused macro-algal blooms (predominantly *Ulva rigida*) in the '70s and '80s, reducing the light attenuation in the lagoon and resulting in the reduction of eel-grass beds (bioindicator of unpolluted habitat under the European Water Framework Directive - Krause-Jensen *et al.*, 2005). Eel-grass helps reduce resuspension of sediment, thus in its absence erosion of sediment increases (Bettinetti *et al.*, 1996);

- Restoration and protection of salt marshes (dredge spoil recycled into artificial marshes and mudflats, pilings installed to protect existing marshes[viii]) (Consorzio Venezia Nuova, 1996, 1997).

The effects of some of these remedial measures will have been encompassed within the results as they have changed the elevation of the seabed.

7.4.2 Alterations in the Sediment Budget: 1930-1970 to 1970-2000

The lagoon has become more dynamic, with 22% more of the lagoon accreting or eroding during 1970-2000 than during 1930-1970. This is largely due to anthropogenic intervention; the construction of the Petroli Canal has caused widespread erosion in the surrounding saltmarshes due to wave action from heavy shipping traffic (Venice Institute of Science, Letters and Arts, 2008[ix]) with the resultant suspended sediment depositing in the surrounding canals (Ravera, 2000), including the Petroli Canal. The same effect can be seen around the canal leading from Chioggia Inlet, although the erosional 'aura' has not extended as far as with the Petroli Canal (Bettinetti *et al.*, 1996). Further, artificial salt-marsh regeneration has occurred in and around the edges of the lagoon (Scarton *et al.*, 2000; Deheyn and Shaffer, 2007), appearing as accretion in the DMM maps, where it had previously been relatively stable or erosional. Some of this accretion is due to plantation of trees and shrubs, which act as a buffer between land-derived pollutants[viii] (fertilizers) and the lagoonal waters; their roots increase shear strength of the sediment bed, and pollutants are trapped within this buffer rather than entering the lagoon. Pilings have been laid elsewhere in the lagoon to prevent further loss of sediments; in total, Consorzio Venezia Nuova[viii] state that 12 km^2 of

[viii] www.salve.it - February 2008
[ix] www.istitutoveneto.it

intertidal zone has been reconstructed, along with the implantation of 30 km of pilings to reinforce existing salt marshes.

7.4.2.1 Intertidal Zone

32% of the intertidal zone eroded between 1970-2000 (a 28% increase on the period 1930-1970), whilst 22% accreted (a 34% increase on the previous period). As the rate of deposition increased more than the rate of erosion, the intertidal zone accreted 0.02 cm yr^{-1} during 1970-2000 (changing from a -0.05 cm yr^{-1} loss). This is principally due to the lagoon-edge, salt-marsh regeneration (both natural and artificial) previously described, and the combination of a high accretion rate and low erosion rate in the northern region.

Most of the intertidal area surrounding the Petroli Canal is subject to net sediment erosion ($\sim$80 km^2), as is the smaller intertidal zone surrounding the Chioggia Inlet canal system ($\sim$24 km^2) and between Venice and Burano. This erosion can be largely attributed to anthropogenic activities such as:

- waves generated by boat traffic (especially tankers in the Petroli Canal), undermining root systems in the intertidal zone, causing bank collapse;
- dredging of canals, which reduces the wave buffer zone, allowing the full impact to hit the mudflats and salt marshes (causing slumping);
- dredging for clams in the intertidal zone, which reduces cohesive strength as well as resuspending sediment. It also disrupts the surface biofilm further decreasing cohesive strength;
- increased efficiency of channels (such as Malamocco Inlet, Petroli Canal) can change circulation patterns, flooding the tidal flats with water and increasing salinities. The niche that salt marsh plants thrive in is thus altered causing the plants die, reducing soil stability and increasing resuspension (Weinstein, 1996).

A larger area of the intertidal northern region was stable during 1970 and 2000 than during 1930 to 1970. However, the canals and the intertidal zone adjacent to the canals, have infilled except for the area between Palude della Centrega and of Palude

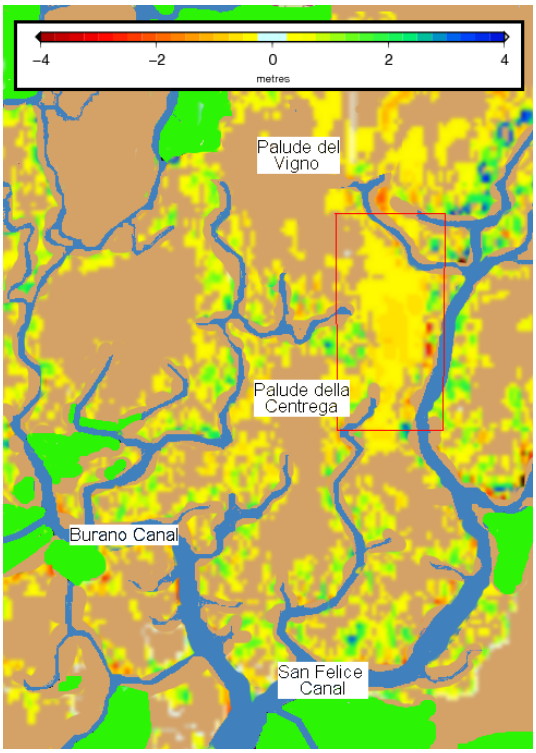

Fig. 7.14: Erosion between the salt marshes of Palude del Vigno and Palude della Centrega between 1970-2000.

del Vigno (Figure 7.14), which has experienced net erosion. Suspended sediment from these intertidal areas may be entering the nearby San Felice Canal, which has changed from being net erosional between 1930 and 1970, to becoming net depositional between 1970 and 2000. Suspended sediment concentrations have increased greatly since the '90s (Sfriso *et al.*, 2005a), due to an almost complete disappearance of the macroalgae (Ulva rigida), that previously bloomed in the lagoon (Sfriso *et al.*, 2005b). The clam *Tapes philippinarum*, introduced in 1983 (Venice Institute of Science, Letters and Arts[x]) quickly colonized areas not inhabited by macroalgae or seagrasses, and subsequent harvesting of these clams by mechanical dredges has caused a increase in the amount of suspended sediment by one order of magnitude (Sfriso *et al.*, 2005a). This suspended sediment is not exported out of the lagoon quickly, as residence times average 30 days in the lagoon (Fletcher and Spencer, 2005), which allowing it time to

[x]www.istitutoveneto.it - May 2008

settle. Furthermore, the surface biological layer in the northern region is still present, unlike in the other two regions, which are almost free of macrophyte biomass (Sfriso *et al.*, 2001). Macrophytes attenuate waves, which reduces shear stress and enhances the rate of sediment deposition; the roots also stabilize the bed reducing the rate of resuspension (Cappucci *et al.*, 2004).

Intertidal deposition in the northern lagoon occurred during 1970-2000 whilst other regions have eroded. Whilst reduction of boat-generated waves has occurred since implementation of speed limits in 2002 (Zanatta *et al.*, 2005); the effects are too recent to be seen within the available lagoon-wide bathymetry. However, wind-generated waves have been affected by the reduced frequency and velocities of Bora winds due to climate change (Pirazzoli and Tomasin, 1999). Bora winds are caused by polar air invasion in eastern Europe; cold air is steered around the Alps and wind is formed due to temperature gradients as the air reaches the warmer Mediterranean Sea. Reduced frequencies of polar air invasions into eastern Europe has had a knock-on effect on the creation of Bora winds (Pirazzoli and Tomasin, 1999). When Bora winds occur, water is 'pushed' towards the southern region, causing water levels to decrease by approximately 30 cm in the northern region (Umgiesser, 1997). The northern region is also relatively sheltered from bora-generated waves as the fetch is short. Higher waves are produced in the southern region due to the large fetch over the whole lagoon (Umgiesser, 1997). As Bora events are becoming increasingly infrequent, the level of erosion is decreasing in the northern region. If this was the only reason to why deposition is occurring in the northern region then less erosion should also be seen in the southern region, as it is this area that is affected by the largest bora-generated waves. However, the southern region has seen an increase in erosion and decrease in deposition (see Figure 7.6). It may be possible that the rivers are transporting increased sediment loads; the canals and the surrounding intertidal zone along the northern shoreline has accreted more during 1970-2000 than 1930-1970 (see Figure 7.7). Also, Cavallino Beach has migrated to the end of the northern jetty of Lido Inlet and it has been shown in previous chapters that sand is entering the inlet. Tambroni and Seminara (2006b) have also modeled that there is net import of sand into the inlet during summer and winter. Thus it may be that sand from longshore transport is now being imported into the northern region, although this has been hard to prove from the results of the

mineralogical analysis undertaken in Chapter 5. Further investigation is required to prove whether increased import is occurring and its provenance, including the longterm sediment flux of the rivers feeding the northern region and perhaps particle tracking (tracing Black *et al.*, 2004) from Cavallino Beach exploring seasonality.

Sections of Palude del Monte (the areas south of the shoreline of Campalto and Marco Polo Airport) are the only areas within the southern region that have remained stable between 1930 and 2000. The area is adjacent to accreting intertidal zone that is present along the shoreline of the mainland and has previously been described by Solidoro *et al.* (2004) as an extension of the northern region (also experiencing accretion along the shoreline of the mainland). The northern region is particularly stable with large areas of intertidal zone which have not changed (± 25 cm) between 1930-2000. However, most of the central intertidal zone away from the shoreline has been eroded between 1930 and 2000, although the canals have infilled. This flattening effect has been described by Ravera (2000); waves undercut the intertidal zone and the eroded sediment is washed into the canals.

Dredge spoil has been used to reclaim land in an effort to restore salt marsh habitat within the lagoon, and thus appears as sediment accretion in the sediment budget. The area around Lago dei Teneri and Lago Stradoni (south of the industrial area, Marghera), has been particularly affected by this type of regeneration (Fletcher and Spencer, 2005). This area represents the majority of the intertidal zone in the central region that has experienced deposition. Fish farming is prevalent in the southern region, along the mainland/lagoonal boundary, and is generally represented by intertidal zone that has remained unchanged between 1930 and 2000.

7.4.2.2 Canals

A larger proportion of canals have stopped depositing and become stable; this could be due to a reduction in the supply of sediment. The proportion of canals deepening has also increased slightly, probably due to routine maintenance dredging of canals. Treporti Canal and Lido Inlet have also stabilized in 1970-2000 compared to 1930-1970 (see Chapter 4), which may indicate dredging in the earlier period. The stabilization

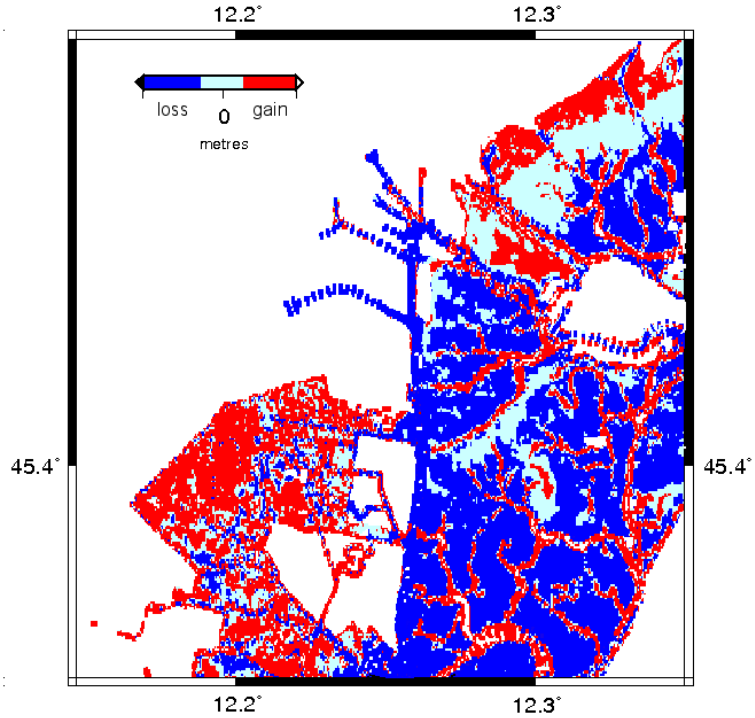

Fig. 7.15: Areas subject to no change and sediment losses or gains, between 1930 and 2000.

could be partly due to increasing hydrodynamic stability after the construction of the jetties, or deposition due to land subsidence. The only canal not to show net deposition is the Petroli Canal, due to the initial dredging project in the '60s and then subsequent maintenance dredging. However, in gross terms, it is also likely to experience a similar level of infilling as the other central canals due to the degree of local intertidal erosion and relatively low velocities (due to the large cross-sectional area to tidal prism ratio O'Brien, 1969).

7.4.2.3 Sediment Budget Volumes

The total net volume of sediment loss from the intertidal zone between 1970 and 2000 is 2.3×10^6 m^3 yr^{-1}[xi], compared with 1.4×10^6 m^3 yr^{-1} lost between 1930 and 1970 (Table 7.11); thus an extra 835,000 m^3 yr^{-1} is exported into the lagoon due to erosion of intertidal areas, and an extra 921,000 m^3 yr^{-1} is imported into areas of deposition. The

[xi] rounded figure

residual volume of sediment from the intertidal zone has thus reduced from a net export of 178,000 m^3 yr^{-1} to 92,000 m^3 yr^{-1}. These values suggest a more dynamic intertidal environment with greater volumes of sediment in transit, but also suggest that the rate of accretion is overcoming the rate of erosion. The severity of the erosion of the intertidal area around the Petroli Canal has meant that the total volume of sediment exported from the intertidal zone between 1970-2000 exceeded the volume exported from the canals (in contrast to the trend seen between 1930-1970) even though the rate of change within the canals remained greater. This reduced the total area of the lagoon inhabited by salt marsh, as marshes must accrete enough sediment to remain intertidal; too far down the tidal range results in waterlogging and dieback of the marsh (Patrick and DeLaune, 1990). Loss of salt marsh further exacerbates resuspension of sediment as waves are no longer attenuated and sediment is not stabilized by root systems.

7.4.3 Determination of Gross Export: 1970-2000

The most recent sediment budget determined within this chapter was compared to the Consorzio Venenezia Nuova budget. CVN[xii] proposed that 2.2 million m^3 of sediment was resuspended from the lagoon beds and 70,000 m^3 was eroded from the salt marshes. These figures are comparable to the results determined within this chapter, with differences most likely attributable to the definitions (intertidal zone/canals and lagoon bed/salt marsh). This study determined that 1.7 million m^3 was resuspended from the canals, which is smaller than the estimate of CVN, although 'lagoon bed' probably includes some intertidal mudflats, which are defined within the 'intertidal zone' definition within this study. An estimate of 92,000 m^3 of sediment exported from the intertidal zone is also comparable to CVNs estimate of 70,000 m^3 exported from the salt marshes (again, the difference can be explained by mudflat regions being included in different categories). CVN estimated that 95% of the sediment resuspended from the bed was redeposited in the lagoon; this study estimates a redeposition rate of 91%[xiii]; however, the estimates of total export are smaller within this study. Whereas CVN estimates that 700,000 m^3 is exported through the inlets, the present study puts the figure closer to 370,000 m^3. It may be possible that the difference is generated by dredge spoil,

[xii] www.salve.it

[xiii] 3,625,889/3,998,942; see Table 7.11

which was previously dumped outside the lagoon (producing the overall export estimate of 1.1 million m^3 that is frequently cited). This volume is now re-introduced into the lagoon for marsh regeneration and thus may be included in the results of this study (no authorship year is present for the sediment budget, although the estimate of 1.1 million m^3 annual sediment export appears in Carbognin and Cecconi, 1997, and thus predates the 2000 bathymetry dataset used by the present study).

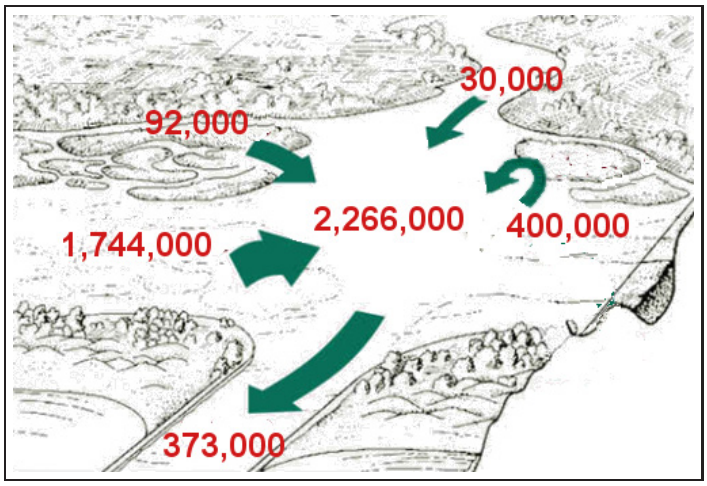

Fig. 7.16: Sediment budget of Venice Lagoon following the style of Consorzio Venezia Nuova, 2008[ii]

7.4.4 Summary and Error

Quantitative comparisons of bathymetry datasets are useful in the determination of long-term, change in sediment volumes important in the evaluation of the sediment budget. However, it is limited as the calculations only take into account net change and provide no information on through-put of sediment. For example, if sediment builds up in one area after bathymetry is collected, but is dredged before the second survey is completed, the sediment removed prior to the second survey is not included in the calculations. For this reason, the volumes calculated for the period 1930-2000 are not a simple addition of the results derived from the intermediate periods (1930-1970 and 1970-2000).

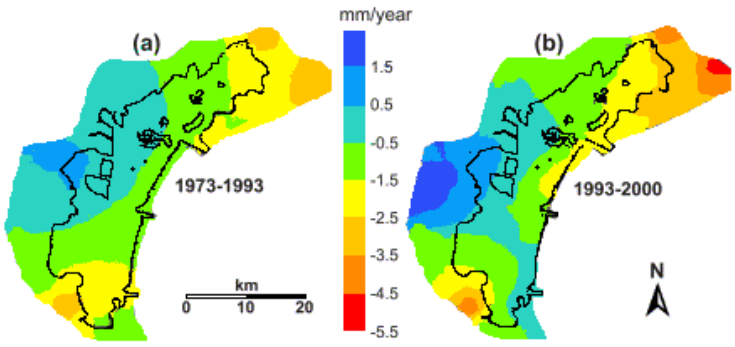

Fig. 7.17: Vertical displacement in Venice Lagoon between (a) 1973-1993, and (b) 1993-2000 (after Carbognin *et al.*, 2004)

The results show net changes in elevation of the seabed between 1930-1970, 1970-2000 and 1930-2000. During 1930-1970, approximately 25 million m^3 (approximately 6,250,000 m^3 yr^{-1} between 1965-1969) was removed from the lagoon during the building of the Petroli Canal, and a further 400,000 m^3 yr^{-1} removed through maintenance dredging of the canals. As this removal will have affected the bathymetry, the figures are included within the results discussed. Sediment from the salt marshes ($\sim$178,000 m^3 yr^{-1}) may have contributed further to the infilling of the canals, with an additional 30,000 m^3 yr^{-1} of sediment entering the lagoon from the rivers.

The bathymetry is affected by subsidence in the region; the central region has rebounded up to 1.5 mm yr^{-1} now that underground water pumping has been discontinued. However the northern region has subsided by 6 cm between 1973 and 2000 (up to 3.5 mm yr^{-1} Carbognin *et al.*, 2004 - see Figure 7.17). The average subsidence across the lagoon is approximately 1 mm yr^{-1}, thus error is introduced if data is within 3 cm (1 mm yr^{-1} $\times$ 30 years) of the previous scale boundary. Error increases in the north and south where subsidence is greater, and where change in elevation has been relatively small; therefore average error (the percentage of datapoints that fall within 3 cm of the interval boundary) and maximum error (percentage of datapoints that fall within 7.5 cm of the interval boundary) is shown in Figure 7.18. The mean average error for the whole lagoon is 0.07%; the mean maximum error is 0.19%.

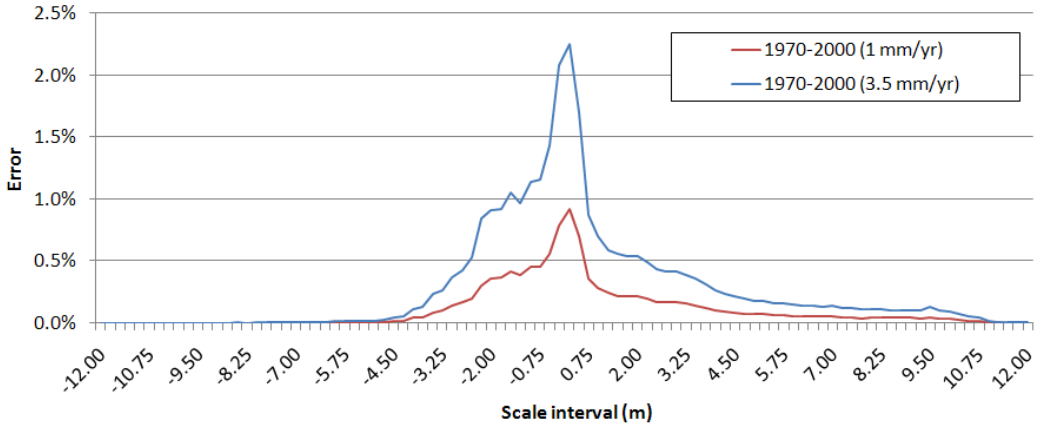

Fig. 7.18: Average and maximum error due to subsidence.

7.5 Conclusions

The net volume of sediment lost annually from the Venice Lagoon system has increased by approximately 30% between 1930-1970 and 1970-2000. This is despite 25 million m^3 of sediment being removed from the lagoon within 1930-1970 due to the excavation of the Petroli Canal (1965 to 1969), and despite increasing areas of intertidal zone becoming net depositional in the latter period (either artificially via re-integration of dredge spoil back into the lagoon for salt marsh regeneration or natural depositional trends as is occurring in the northern region). The increase in the net loss (373,000 m^3 yr^{-1} of sediment) from the system is not due to an increase in erosion, as the net volume of sediment being eroded from the lagoon has in fact decreased by 3% between the two periods. The result is due to a 4% decrease in the net volume of sediment depositing; it is likely that this sediment is remaining in suspension (it has been previously reported that the concentration of sediment in suspension has increased) and is exported out of the lagoon before conditions allow for settling. The increase in the level of suspended sediment is principally due to the excavation of the Petroli Canal; a combination of increased ship traffic, producing waves that have been eroding the shallows adjacent to the channel, and increased and altered hydrodynamics (Gatto and Carbognin, 1981) due to the increased efficiency of the channel.

8

Discussion and Conclusions

Lagoons are by nature a geologically temporary feature on a dynamic coast with tendencies towards marine or land amalgamation (Consorzio Venezia Nuova, 1997; Ravera, 2000). Throughout this investigation it has become clear that Venice Lagoon has undergone a gradual transformation towards a marine embayment since the construction of jetties at each inlet c. 1900 (Ravera, 2000).

It is suggested that lagoons will be flood dominant at conception due to the lack of intertidal zone, but as the lagoon infills and the intertidal area (A_i) increases relative to basin area (A), the ebb tide gradually becomes more dominant due to negative feedback control (see page 10). Modelled velocity for 1930, 1970, and 2000 suggests that the northern lagoon may be becoming flood dominant once more; Lido Inlet has changed from being slightly ebb dominant to flood dominant between 1930 to 2000 and Treporti Canal is becoming less ebb dominant than it was in 1930 (see Table 4.1). The erosion of the intertidal zone (A_i) is well documented (Consorzio Venezia Nuova, 1996; Day *et al.*, 1998); if current rates of loss continue, there will be no salt marsh by 2045 (Figure 3.5), and the lagoon is becoming flatter due to the deposition of eroded material into the canals (Ravera, 2000). Therefore the A_i/A ratio is reducing, the ebb currents are weakening (hypothesized by Speer and Aubrey, 1985 and shown in Table

4.1) and as a result, the flood phase is becoming dominant. If this trend continues then there should be import of sand from the Adriatic Sea, although Tambroni and Seminara (2006a) has stated that inlet geometry is a dominant factor of sediment exchange as it is more of a control on ebb-flood asymmetry. Further, the distance of jettied inlet mouths away from the breaker zone prevent wave-suspended sediment from being imported. There is a lack of knowledge about the provenance, transport processes and sinks of sand in the region despite the seabed of all three tidal inlets being composed of sand (Bondesan *et al.*, 2004). The issue of sand exchange between the lagoon and sea is becoming increasingly important as relative sea level rises and impacts from anthropogenic activities cause resuspension and erosion. However, previous engineering works to prevent siltation of the lagoon, are now aiding the gradual amalgamation into the sea. The aim of this thesis has been to investigate the transport of the sand that composes the seabed of Lido Inlet; to determine its provenance, whether this sand is being exported or imported and analyse the characteristics of transport and changes in these characteristics over time.

8.1 The Sand Transport Pathway in Northern Venice Lagoon

8.1.1 Sources

Gazzi *et al.* (1973) described the longshore, sediment-transport pathway along the Adriatic coast, interpreting a north to south, beach-parallel movement of sand from the Talgliamento river to Pellestrina where it converges with south to north transport from the River Po. The longshore transport of sand is restricted to within 2 km of the shore; beyond this is a 'mud-belt' running parallel (Albani *et al.*, 1998), which itself is restricted by a region of relic sand that has been used as a source for beach replenishment for the barrier islands of Venice (Cecconi and Ardone, 2000). The mineralogy of these replenished beaches show a higher content of quartz and feldspar than would be expected in the native, dolomite-rich sediment, and is representative of sediment found to the south of the lagoon (Gazzi *et al.*, 1973; Stefani, 2002). Although this sand is relic (re-worked from coastal structures formed during the last marine transgression - Simonini *et al.*, 2005), its high quartz content and high calcite/dolomite ratio suggests

a shared source with the southern rivers (Adige, Brenta, Po). The underlying signal of the longshore transport pathway is still evident despite this recent beach replenishment, with a gradual decrease in the grain size from north to south along Cavallino and Jesolo beaches, and from south to north along Chioggia Beach representing grain maturity. The mineralogy of the northern (Jesolo, Cavallino and Lido) and southern (Chioggia and Pellestrina) beaches is distinct as greater proportions of quartz are present in the southern beaches, and greater calcite/dolomite ratios (above 0.3) are present in the northern beaches.

Calcite/dolomite (c/d) ratios of sediment within Lido Inlet are also high, indicating relatively unworked sediment, whereas the c/d ratios of sediment in the inner lagoon are fairly low (less than 0.3 - Bellucci *et al.*, 2005); an indication of mature sediment. The higher ratios suggest that the sediment within the lagoon is not the source of the sediment within Lido Inlet. This is also indicated through grain-size statistics; lagoonal sediment is principally sandy-silt sediment (McComb, 1995), with sands present predominantly along the barrier islands and tidal inlets. It may be possible that the low ratios in the lagoon are recorded principally due to fine-grained sediments which are preferentially transported away in high-energy environments, like canals and tidal inlets, leaving the coarser-grained, and less mature sediment behind. Mineralogical comparisons indicate that little sediment from north of the Sile River is imported into the inlet as the sand of Lido Inlet is composed of much fewer carbonate grains (50-75%) than the sand north of the Sile River (75-100%), whilst proportions of quartz and feldspar are approximately double within the inlet. It may be that sand from beach replenishment has increased the proportions of quartz and feldspar, especially as Tambroni and Seminara (2006b) have hypothesized that sand enters the inlet during winter and summer months. It is unknown how much of the estimated 150,000 m^3 yr^{-1} of sand transported along Cavallino Beach (Fontolan *et al.*, 2007) bypasses Lido Inlet. However, the thickness of the beaches alongshore progressively narrows and there is a strong indication that a proportion does enter Lido Inlet alongside the northern jetty. Sediment sampling along the jetty has show that this area has a higher proportion of sand than the rest of the inlet excluding the ebb spit and flood delta. This is also shown on the sidescan as an area of high reflectivity; both of these maps (Figures 4.27B & 5.8) indicate import rather than accumulation of lagoonal sand. Comparison

of bathymetry reveal that this sand has built up post-1930, after massive accretion due to longshore transport and trapping of sand by the northern jetty, had extended Punta Sabbioni and Cavallino Beach (15.8 m yr^{-1} between 1908 and 1933 - Fontolan *et al.*, 2007) almost up to the tip of the jetty.

The results of grain-trend modelling (after Gao and Collins, 1992) show a strong likelihood of sand export from Treporti Canal, some of which is derived from continual erosion of the channel bed (as seen in the bathymetric comparison- Chapter 4). Treporti Canal drains the northern lagoon, which has received sediment from the Piave River (Collavini *et al.*, 2000) in the past (Stefani, 2002). The sediments of Treporti Canal and Lido Inlet are mineralogically similar to the Piave sediments (see Figure 5.17C), and less so with the Tagliamento River sediments, despite the fact that Cavallino/Jesolo Beach (present between Lido Inlet and the Tagliamento River) sediments are richer in Dolomite and lacking in quartz. The sediment samples used to run the grain trend model were collected during the winter months and showed a transport pathway out of the lagoon. This indicates that sand being transported as bedload is exported, despite the flood dominance of Lido Inlet and suggestions that sand is imported during winter.

The largest source of sediment is the lagoon itself; the sediment budget estimates that 1.8 million m^3 of sediment is eroded from the lagoonal floor and salt marshes every year (in agreement with older estimates by Consorzio Venezia Nuova[i]). In previous years, much of this sediment would have been redeposited; however, a combination of increasing boat traffic (and size of vessel able to navigate the lagoon), dredging for clams (reducing bed shear stresses and increasing erodibility) and a decrease in seabed macroalage and seagrass (reducing shear strength) has caused an increase in the suspended sediment concentration (Sfriso *et al.*, 2005a). As there has been a decrease in the net volume of sediment eroding, but a concurrent decrease in net sediment accretion (see Chapter 7); it appears that sediment, once eroded, remains in suspension.

A significant volume of sand has been eroded from the bed of Treporti Canal as shown by the comparisons of bathymetry in Chapter 4. This erosion has been a

[i]www.salve.it

response to an increasing tidal prism, although the sand will mostly have been exported due to the ebb dominance of this channel (albeit the ebb dominance is receding). Lido Inlet is stable in terms of the tidal prism/cross-sectional area relationship, and so is not a significant source of sand. The largest morphological change occurring in Lido Inlet since the construction of the jetties c. 1900 has been the scouring of the deep, flood-dominant channel and the concurrent growth of the ebb-tidal spit, indicating that equilibrium occurred prior to 1930, although morphological stability occurred later (between 1930-1970). The cross-sectional area has not changed by more than 2% since 1970 (see Figure 4.18).

8.1.2 Sinks

Before the construction of the jetties, the major sink in the northern-most inlet was a large tidal delta/sub-aqueous spit that extended from Punta Sabbioni and Sant'Erasmo, with the main tidal channel meandering around the northern-most extent of Lido barrier island. The jetties dissected both the channel and delta, causing major restructuring of the water circulation pattern and affecting the dynamics of sediment transport. With the channel constrained, flow speed of water exported from Treporti Canal increased (shown in Figure 3.6 as an increase in depth) and the sub-aqueous spit eroded. The delta extending from Sant'Erasmo has remained an important sediment sink for sand, with fine-grained sediment sorted and removed (although the particle-size distribution of the delta is finely skewed). The growth of the delta has not been significant; only the western edge has accreted more than 1 m over the last century (1930-2000), with the eastern edge remaining stable enough for plant growth and stabilisation. The ebb spit extending from Punta Sabbioni has regrown rapidly, depositing sand (sediment sampling proved no fines or gravels) at a net rate of 18,000 m^3 yr^{-1}[ii], suggesting that this is a sink of sand from Treporti Canal rather than longshore transport.

The constriction of the channel by the jetties has resulted in the formation of ebb-jets, able to exceed the transport threshold for sand to export it out of the lagoon. Beyond the confines of the artificial channel, flow speeds rapidly fall below the sand transport threshold and sand is built up in the form of an ebb-tidal delta. As this

[ii]Estimate is from 1930-1970, after which the ebb spit was dredged

delta extends approximately 4 km into the Adriatic Sea, it is highly likely that some of the sand is derived from the north-south longshore transport, certainly as the shape of the delta has been skewed to follow the direction of longshore transport. Grain-size statistics also support this hypothesis, as sediment both within the lagoon and nearshore north of the inlet mouth is very well-sorted. Within the inlet, the ebb-tidal delta and nearshore south of the lagoon, the sand is less well sorted, which can indicate a mixing of sediments from different sources. As the ebb-tidal delta has a gradient of grain sizes, with gravels (> 2 mm) depositing near to the inlet mouth, sands from the inlet mouth to approximately 4 km offshore, with finer-grained sediment present at the very edge (at the mudbelt), it is probable that the main component of this deltaic sand is lagoonally sourced. The delta is still experiencing growth, indicated by a gradual extension seawards.

8.1.3 Sand in Transport

The majority of sediment in Lido Inlet is transported as suspension (approximately 90%). Sand is transported when flows exceed 0.4 m s$-$1 and contributes approximately 60% to the total mass of sediment in suspension during peak flow, although only fine-grained sediment remains in suspension during low current velocities. Using ADCP backscatter, it has been determined that peak ebb flows ($\overline{U}_h = 0.78$ m s^{-1}) can transport approximately 878,000 kg hr^{-1} of sediment of which 60% is sand in suspension and a further 9% is sand travelling as bedload. Bedload transport is also minimum during low velocities although faster velocities, especially within the deeper water, are enough to transport medium to coarse sand. Both of these mechanisms have been analysed in Chapter 5.5 using backscatter and velocity data from ADCP.

8.2 Conclusions

The northern region of Venice Lagoon has been following an increasingly flood dominant trend; as such, it is more susceptible to import of sand. Evidence to support this hypothesis is plentiful. Investigations from sediment analysis and reflectivity of the seabed suggest that sand is entering the inlet from the north to south longshore transport pathway (having accreted to the tip of the northern jetty). Tambroni and Seminara (2006b) has proposed that sand export from the lagoon is much less than

previously estimated and that it is invariably imported during the winter and summer months. Sediment budget analysis has indicated that the northern region is net accretional (between 1970-2000), having previously been net erosional like the central and southern regions were and still are. This suggests an increase in the sediment supply that could only come though Lido Inlet as the rivers provide a small proportion of sediment ($\sim$30,000 m^3 yr^{-1}) and the basins (south, central and north) are thought to be hydrodynamically separate (Solidoro *et al.*, 2004).

The southern and central lagoon suffers net loss of sediment as it is more exposed to wind-generated waves (bora; Umgiesser *et al.*, 2004a), ship-generated waves (tanker route through the Petroli Canal), and aggressive fishing techniques (mechanical clam dredging). Furthermore, the supply of sand to its inlets (Malamocco and Chioggia) is much weaker than at Lido Inlet, shown by the progressive narrowing of the barrier islands from north to south. However, results from sediment budget analysis suggest that whilst the rate of erosion is falling, there has been a large increase in area subject to erosion. Deposition rates are also decreasing, most likely because resuspended sediment is unable to settle, shown by an increase in the concentration of suspended solids noted by Sfriso *et al.* (2005a).

8.3 Questions for Future Consideration

The investigations within this thesis have raised many possibilities for future study. The hypothesis that sand is imported into the northern lagoon could be further tested with field study and modelling:

- Can tracers be used to determine the pathway of sand from Cavallino Beach into Lido Inlet and the northern lagoon, and does transport vary seasonally?
- ADCPs have been used to determine sand in suspension as well as give estimates of bedload transport. However, a clearer picture of the total exchange of sand could be determined with seasonal transects taken over complete cycles of neap and spring tides, with data calibrated with coordinated LISST and water sampling of total suspended solids.

- Is the northern lagoon accreting due to an increase in the sediment flux from the rivers?
- Is the accretion seen in the northern lagoon correlated with estimates of sand import modelled by Tambroni and Seminara (2006b)?

The largest losses in the intertidal zone have been around the Petroli Canal within the central and southern basins;

- is the negative feedback cycle described by Speer and Aubrey (1985) also occurring in this area and are Chioggia and Malamocco inlets becoming flood dominant as a result?

Venice. The only place where you can get seasick by crossing the street.
-Anonymous

APPENDIX A

Introduction

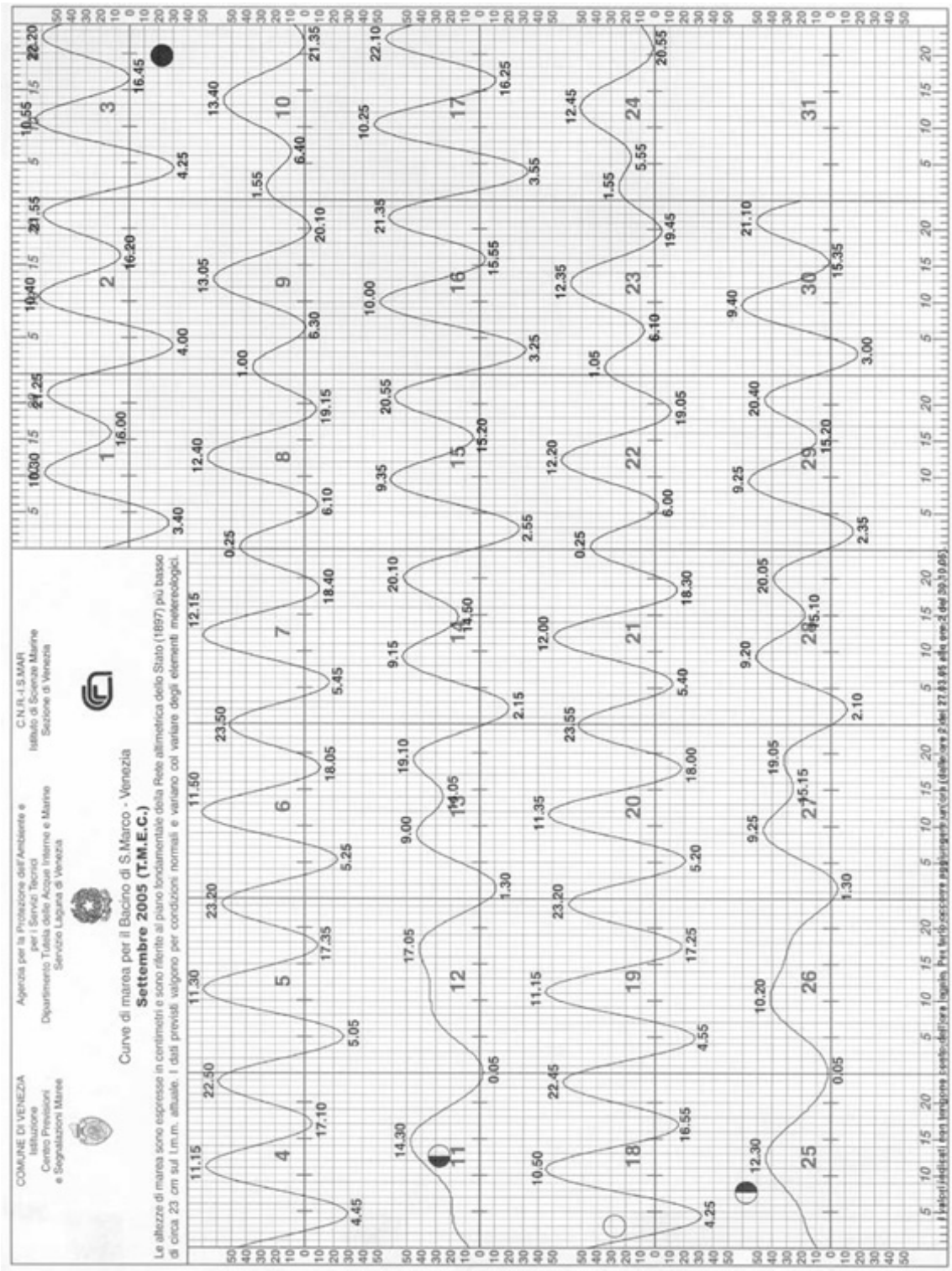

Fig. A.1: Tidal cycle for September 2005. From Comune di Venezia.

APPENDIX B

Character and Morphology

All bathymetry images including comparisons between years can be found in the electronic appendix. GMT algorithms used:

- **grdcontour** Contouring of 2-D gridded data
- **grdimage** Produce images from 2-D gridded data
- **grdvector** Plot vector fields from 2-D gridded data
- **pslegend** Plot legend on a map
- **psmask** Create overlay to mask specified regions of a map
- **psscale** Plot greyscale or colourscale
- **pstext** Plot textstrings
- **psxy** Plot symbols, polygons, and lines in 2-D
- **surface** Continuous curvature gridding algorithm
- **grdtrack** Sampling of 2-D data along 1-D track
- **project** Project data onto lines/great circles
- **gmtdefaults** List the current default settings
- **gmtset** Edit parameters in the .gmtdefaults file

- **grdinfo** Get information about grd files
- **minmax** Report extreme values in table datafiles
- **grdmath** Reverse Polish calculator for grdfiles
- **makecpt** Create GMT colour palette tables

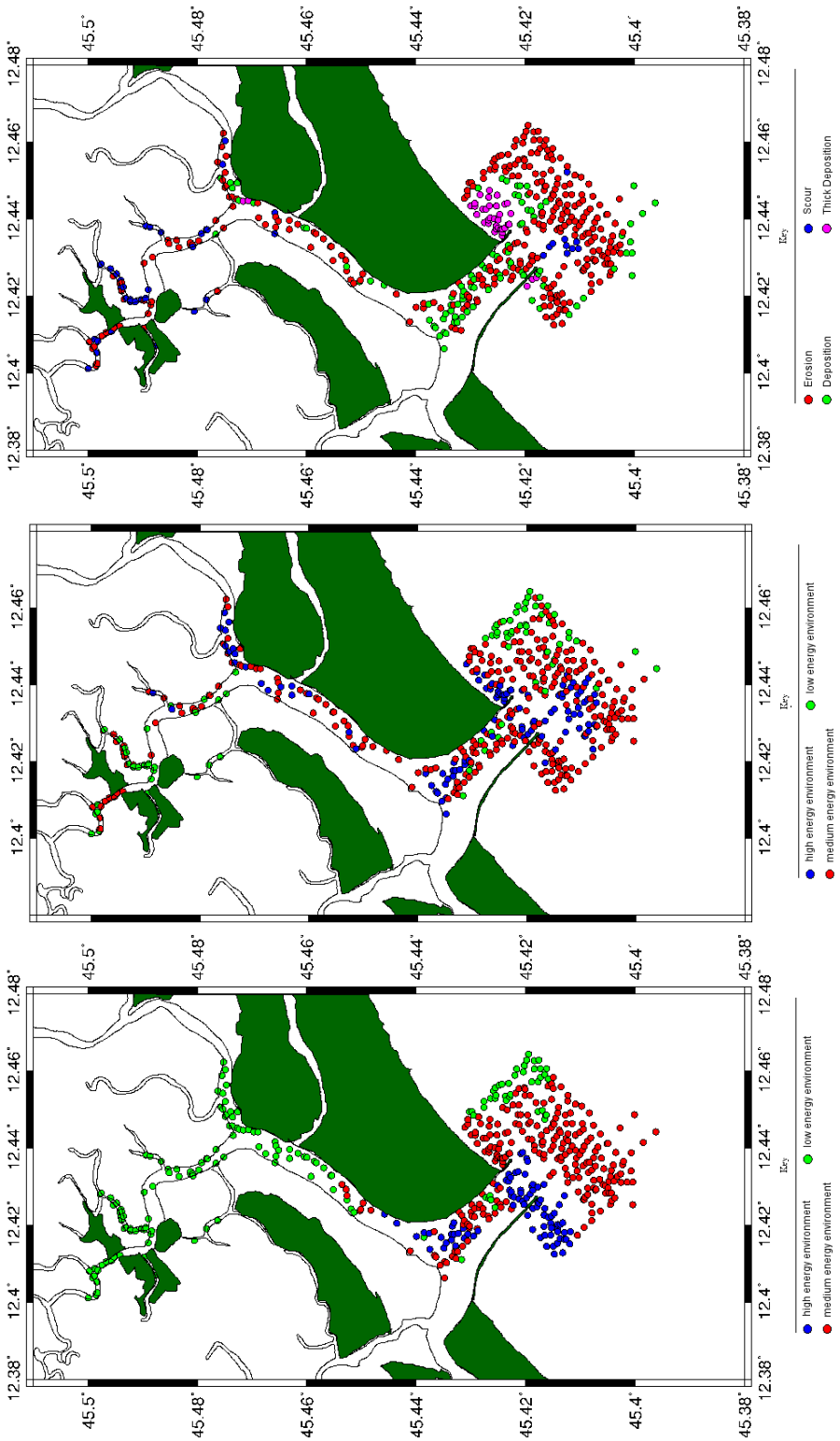

(a) Sediment type (b) Reflectivity (c) Bathymetry

Fig. B.1: Seabed classification using three datasets.

Profile	Date					
	1930-'70	1930-'90	1930-'00	1970-'90	1970-'00	1990-'00
1	7 %	2 %	0 %	-6 %	-8 %	-2 %
2	7 %	2 %	0 %	-6 %	-8 %	-2 %
3	7 %	2 %	-1 %	-6 %	-8 %	-2 %
Lido Average	7 %	2 %	0 %	-6 %	-8 %	-2 %
4	17 %	4 %	10 %	-15 %	-9 %	6 %
5	16 %	4 %	7 %	-14 %	-10 %	4 %
6	16 %	2 %	9 %	-17 %	-8 %	7 %
7	17 %	2 %	8 %	-17 %	-11 %	6 %
Treporti Average	16 %	3 %	8 %	-16 %	-9 %	6 %
8	3 %	-4 %	-16 %	-7 %	-20 %	-12 %
9	1 %	-14 %	-11 %	-15 %	-12 %	3 %
10	8 %	-1 %	3 %	-11 %	-6 %	4 %
11	5 %	-9 %	-4 %	-15 %	-9 %	5 %
Burano Average	4 %	-7 %	-7 %	-12 %	-12 %	0 %
Total average	9 %	-1 %	0 %	-12 %	-10 %	1 %

Tab. B.1: The change the tidal prism at each cross section

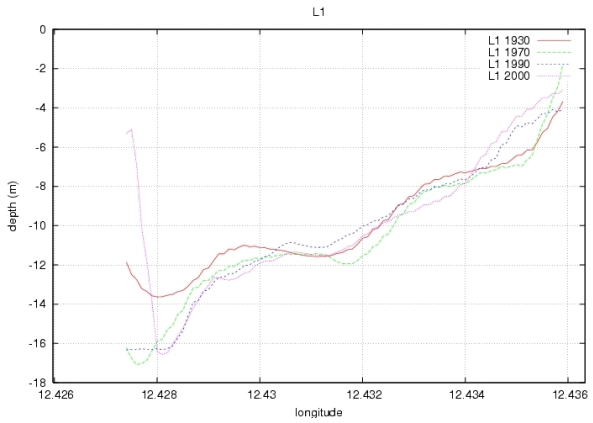

(a) Profile L1 - mouth of Lido Inlet

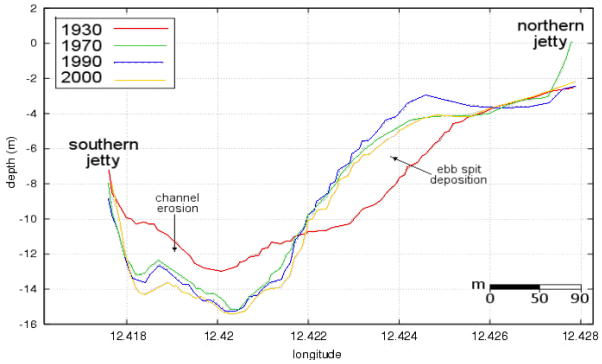

(b) Profile L2 - middle section of Lido Inlet

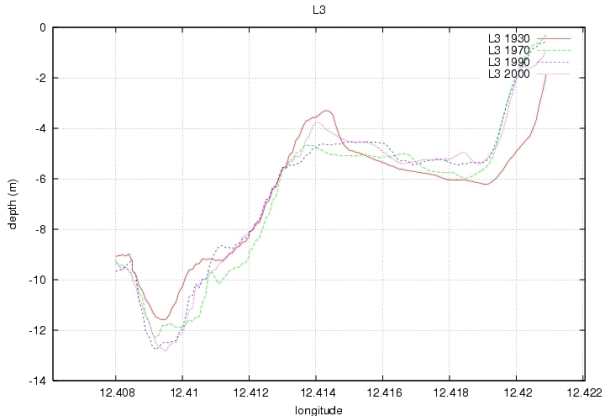

(c) Profile L3/3

Fig. B.2: Cross-sectional profiles along Lido Inlet in 1930, 1970, 1990 and 2000.

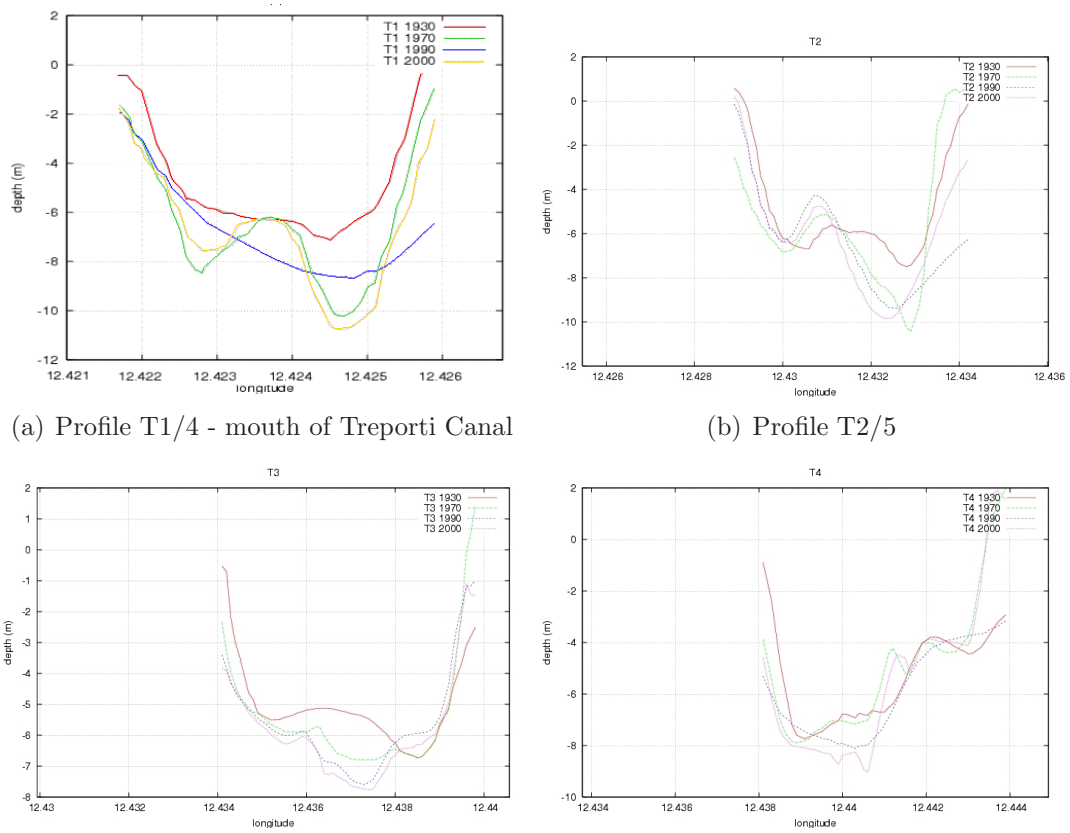

(a) Profile T1/4 - mouth of Treporti Canal

(b) Profile T2/5

(c) Profile T3/6

(d) Profile T4/7 - Just before Treporti Canal/Burano Canal scour hole

Fig. B.3: Cross-sectional profiles along Treporti Canal in 1930, 1970, 1990 and 2000.

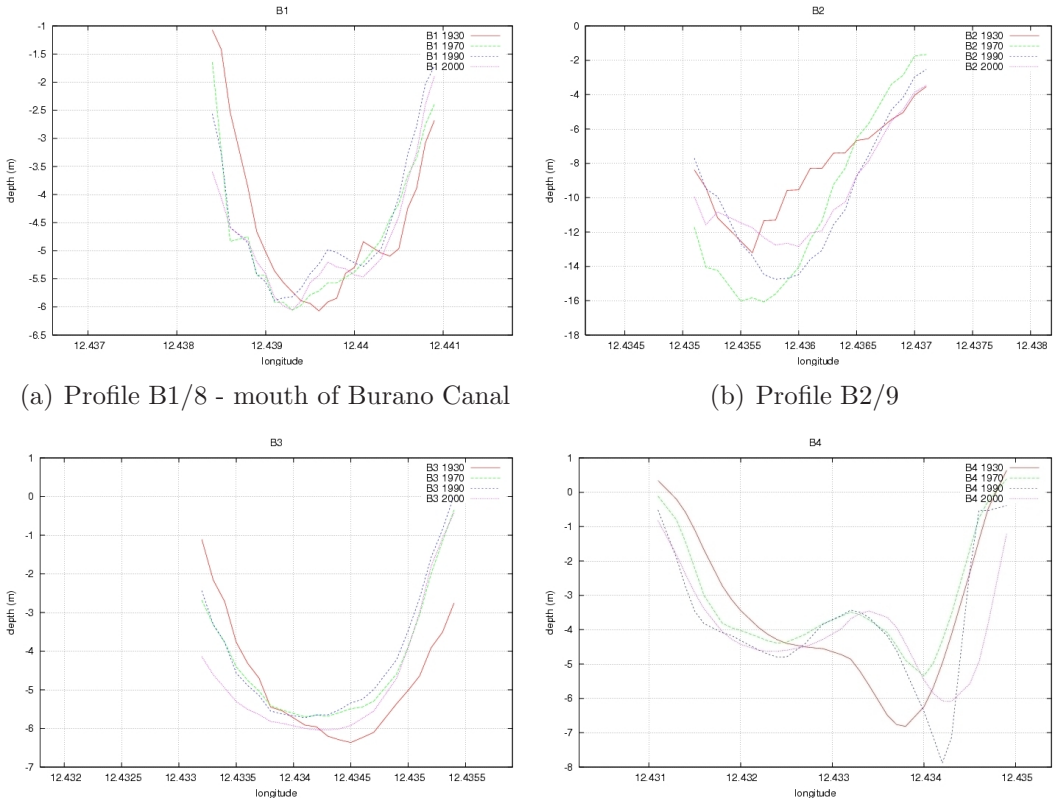

(a) Profile B1/8 - mouth of Burano Canal

(b) Profile B2/9

(c) Profile B3/10

(d) Profile B4/11

Fig. B.4: Cross-sectional profiles along Burano Canal in 1930, 1970, 1990 and 2000.

APPENDIX C

Source, Transport and Sinks

Sample	Location	Position	Sample	Location	Position
Brenta River	BR101	N45.58433 E11.75998	Cavallino Beach	B25	N45.50457 E12.64712
	BR102	N45.54320 E11.80817		B26	N45.51045 E12.66477
	B1	N45.42558 E12.43465		B27	N45.51602 E12.68283
	B2	N45.43070 E12.44043		B28	N45.52155 E12.70052
	B3	N45.43513 E12.44640		B29	N45.52587 E12.71960
	B4	N45.43935 E12.45378		B30	N45.52955 E12.72580
	B5	N45.44288 E12.46172	Chioggia Beach	S1	N45.19905 E12.30390
	B6	N45.44592 E12.46990		S2	N45.18855 E12.30972
	B7	N45.44878 E12.47768		S3	N45.20802 E12.30113
	B8	N45.45092 E12.48635		S4	N45.21718 E12.29912
	B9	N45.45303 E12.49502		S5	N45.22682 E12.30115
	B10	N45.45552 E12.50380	Lido Beach	W1	N45.41929 E12.38469
	B11	N45.45802 E12.51235		W2	N45.41248 E12.37641
	B12	N45.46053 E12.52110		W3	N45.40517 E12.36904
	B13	N45.46332 E12.53047		W4	N45.39775 E12.36179
	B14	N45.46642 E12.53913		W5	N45.38996 E12.35572
	B15	N45.47062 E12.55097		W6	N45.38181 E12.35016
	B16	N45.47332 E12.55965	Lido Inlet	A1	N45.43999 E12.40942
	B17	N45.47624 E12.56956		A2	N45.44144 E12.40869
	B18	N45.47828 E12.57870		A3	N45.44316 E12.40758
	B19	N45.48145 E12.58820		A4	N45.44444 E12.40582
	B20	N45.48505 E12.59598		A5	N45.44580 E12.40582
	B21	N45.48870 E12.60447		A6	N45.44620 E12.40709
	B22	N45.49215 E12.61268		A7	N45.44526 E12.40921
	B23	N45.49547 E12.62135		A8	N45.44419 E12.41125
	B24	N45.49878 E12.63050		A9	N45.44481 E12.41356

Tab. C.1: Sediment sample locations

Sample	Location	Position	Sample	Location	Position
Lido Inlet	A10	N45.44560 E12.41570		C17	N45.44291 E12.39479
	A100	N45.45422 E12.41486		C18	N45.44193 E12.39266
	A101	N45.45559 E12.41676		C19	N45.44430 E12.39002
	A102	N45.45278 E12.41282		C20	N45.44457 E12.39185
	A103	N45.45147 E12.41085		D1	N45.44509 E12.42132
	A104	N45.45032 E12.40892		D4	N45.44018 E12.41957
	A105	N45.44923 E12.40678		D5	N45.43798 E12.42000
	A106	N45.44798 E12.40496		D7	N45.43516 E12.42072
	A107	N45.44676 E12.40240		D8	N45.43397 E12.42155
	A108	N45.44592 E12.40015		D9	N45.43266 E12.42275
	A109	N45.44533 E12.39777		D10	N45.43136 E12.42411
	A110	N45.44443 E12.39495		D11	N45.43015 E12.42536
	C1	N45.43702 E12.41325		D12	N45.42869 E12.42685
	C2	N45.43580 E12.41079		D13	N45.42769 E12.42820
	C3	N45.43466 E12.40839		D14	N45.42680 E12.42972
	C5	N45.43103 E12.40272		D15	N45.42554 E12.43135
	C6	N45.42911 E12.40814		D16	N45.42480 E12.43270
	C7	N45.42672 E12.41412		D17	N45.42385 E12.43425
	C8	N45.42438 E12.41924		D18	N45.42229 E12.43608
	C9	N45.43144 E12.39936		D19	N45.42158 E12.43494
	C10	N45.43386 E12.39404		D20	N45.42331 E12.43257
	C11	N45.43467 E12.38725		D21	N45.42453 E12.43034
	C13	N45.43642 E12.38421		D22	N45.42643 E12.42773
	C14	N45.43788 E12.39087		D23	N45.42826 E12.42541
	C15	N45.43842 E12.39653		D24	N45.42968 E12.42370
	C16	N45.44026 E12.39562		D25	N45.43117 E12.42160

Tab. C.1: Sediment sample locations continued...

Sample	Location	Position	Sample	Location	Position
Lido Inlet	D26	N45.43282 E12.41998		O9	N45.42112 E12.42736
	D27	N45.43462 E12.41816		O10	N45.41917 E12.42980
	D28	N45.43597 E12.41565		R1	N45.42913 E12.41947
	D29	N45.43700 E12.41363		Z1	N45.42387 E12.41959
	D30	N45.43894 E12.41138		Z2	N45.42207 E12.42298
	D31	N45.44187 E12.41167		Z3	N45.41952 E12.42685
	D32	N45.44352 E12.41340		Z26	N45.43108 E12.41204
	D33	N45.44494 E12.41557		Z27	N45.43373 E12.41029
	D34	N45.44643 E12.41812		Z28	N45.43604 E12.40740
	D35	N45.44924 E12.42021		Z29	N45.43760 E12.40390
	D36	N45.45110 E12.42202		Z30	N45.43723 E12.40082
	D37	N45.45273 E12.42436	Outside lagoon	F3	N45.42670 E12.40285
	F1	N45.44460 E12.42100		F4	N45.41940 E12.39507
	F2	N45.43981 E12.41815		F5	N45.41180 E12.38807
	F12	N45.43765 E12.40657		F6	N45.40270 E12.41094
	F13	N45.44012 E12.40567		F7	N45.39463 E12.41741
	F14	N45.44146 E12.40394		F8	N45.38957 E12.42211
	L58	N45.42383 E12.42562		F9	N45.39725 E12.42899
	L59	N45.42470 E12.42744		F10	N45.40545 E12.43440
	L60	N45.42622 E12.42954		F11	N45.41943 E12.45052
	O1	N45.43780 E12.41051		O12	N45.41551 E12.43563
	O2	N45.43512 E12.40787		O13	N45.41400 E12.43859
	O3	N45.43320 E12.41076		O14	N45.41167 E12.44377
	O4	N45.43129 E12.41366		O15	N45.40851 E12.45064
	O7	N45.42535 E12.42224		O16	N45.41137 E12.45037
	O8	N45.42347 E12.42454		O17	N45.41368 E12.44910

Tab. C.1: Sediment sample locations continued...

Sample	Location	Position	Sample	Location	Position
Outside lagoon	O18	N45.41606 E12.44722		Z18	N45.42546 E12.43856
	O19	N45.41802 E12.44469		Z19	N45.41808 E12.42431
	O20	N45.42021 E12.44412		Z20	N45.41551 E12.41881
	R2	N45.40560 E12.42268		Z21	N45.41252 E12.41368
	R3	N45.40032 E12.44973		Z22	N45.41381 E12.40734
	R4	N45.38976 E12.44032		Z23	N45.41819 E12.40929
	R5	N45.42817 E12.46874		Z24	N45.42271 E12.41150
	R6	N45.42264 E12.45914		Z25	N45.41748 E12.42564
	R7	N45.40284 E12.39236	Pellestrina	P1	N45.25400 E12.30070
	Z4	N45.41507 E12.42746		P2	N45.26836 E12.30229
	Z5	N45.41916 E12.43477		P3	N45.27735 E12.30366
	Z6	N45.42251 E12.44272		P4	N45.28622 E12.30602
	Z7	N45.42411 E12.44797		P5	N45.29492 E12.30925
	Z8	N45.42664 E12.45326		P6	N45.30364 E12.31244
	Z9	N45.43177 E12.45012		P7	N45.31236 E12.31580
	Z10	N45.43527 E12.45446		P8	N45.32093 E12.31991
	Z11	N45.43804 E12.45986		P9	N45.32919 E12.32379
	Z12	N45.44107 E12.46505	Piave River	BR100	N45.71027 E12.45630
	Z13	N45.43723 E12.46879	Tagliamento River	BR4	N45.67340 E13.06708
	Z14	N45.43465 E12.46296		BR5	N45.77078 E12.99825
	Z15	N45.43221 E12.45687		BR6	N45.86033 E12.97332
	Z16	N45.42955 E12.45058		BR7	N45.96410 E12.90985
	Z17	N45.42826 E12.44399			

Tab. C.1: Sediment sample locations continued...

Fig. C.1: Satellite image showing the recirculation eddies adjacent to Lido Beach and the southern jetty, showing some south to north transport, against the predominant direction.

(a) Micrograph of calcite (stained pink) and dolomite. Note that the relief changes from high (top dolomite) to low (lower dolomite) as the stage is rotated.

(b) Micrograph of polycrystalline quartz, feldspar and dolomite under cross-polarised light. The feldspar has aligned inclusions and has parallel cleavage.

Fig. C.2: Micrographs of calcite, dolomite, polycrystalline quartz, feldspar

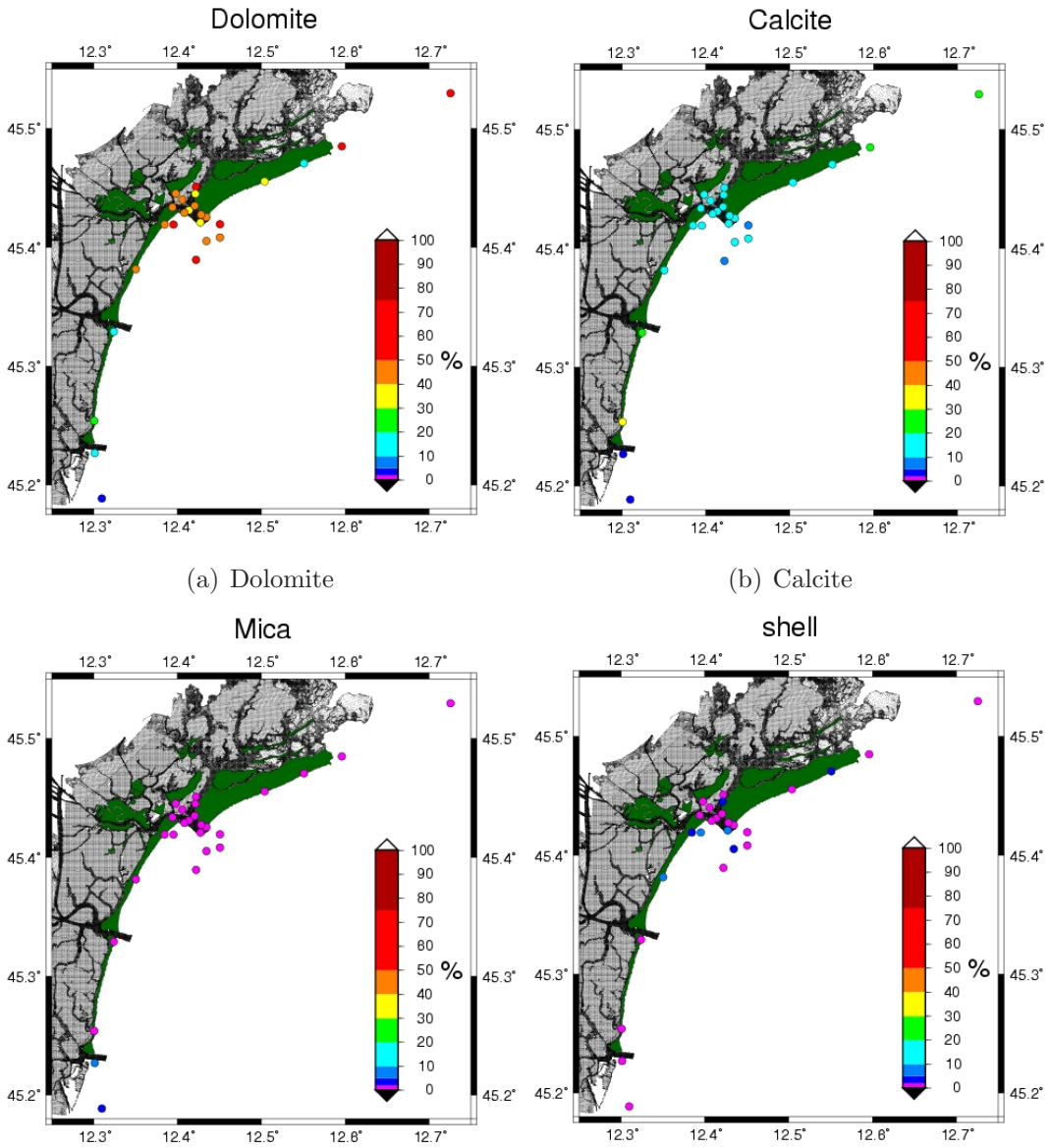

(a) Dolomite

(b) Calcite

(c) Mica

(d) Shell

Fig. C.3: Mineralogy

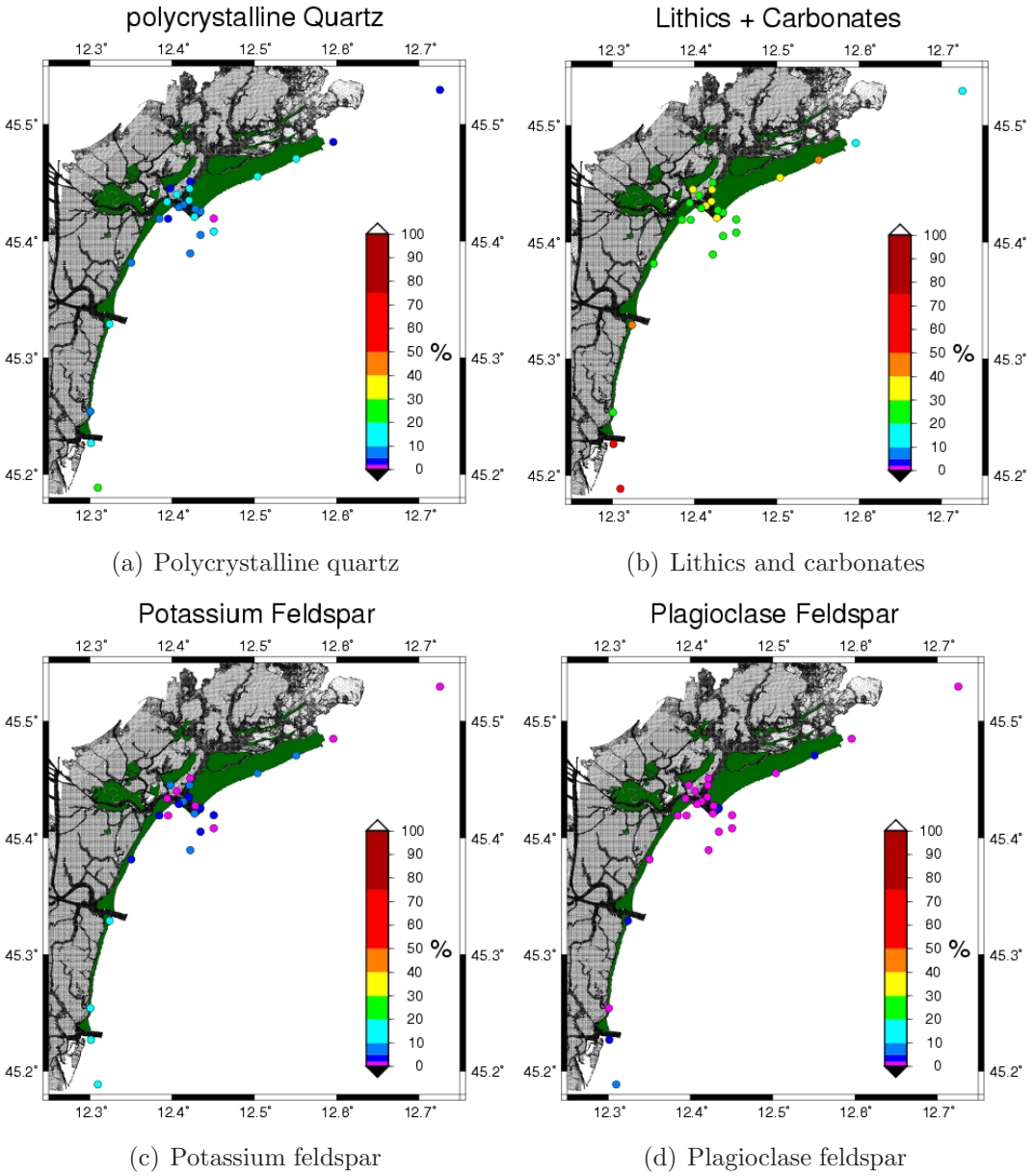

(a) Polycrystalline quartz

(b) Lithics and carbonates

(c) Potassium feldspar

(d) Plagioclase feldspar

Fig. C.4: Mineralogy

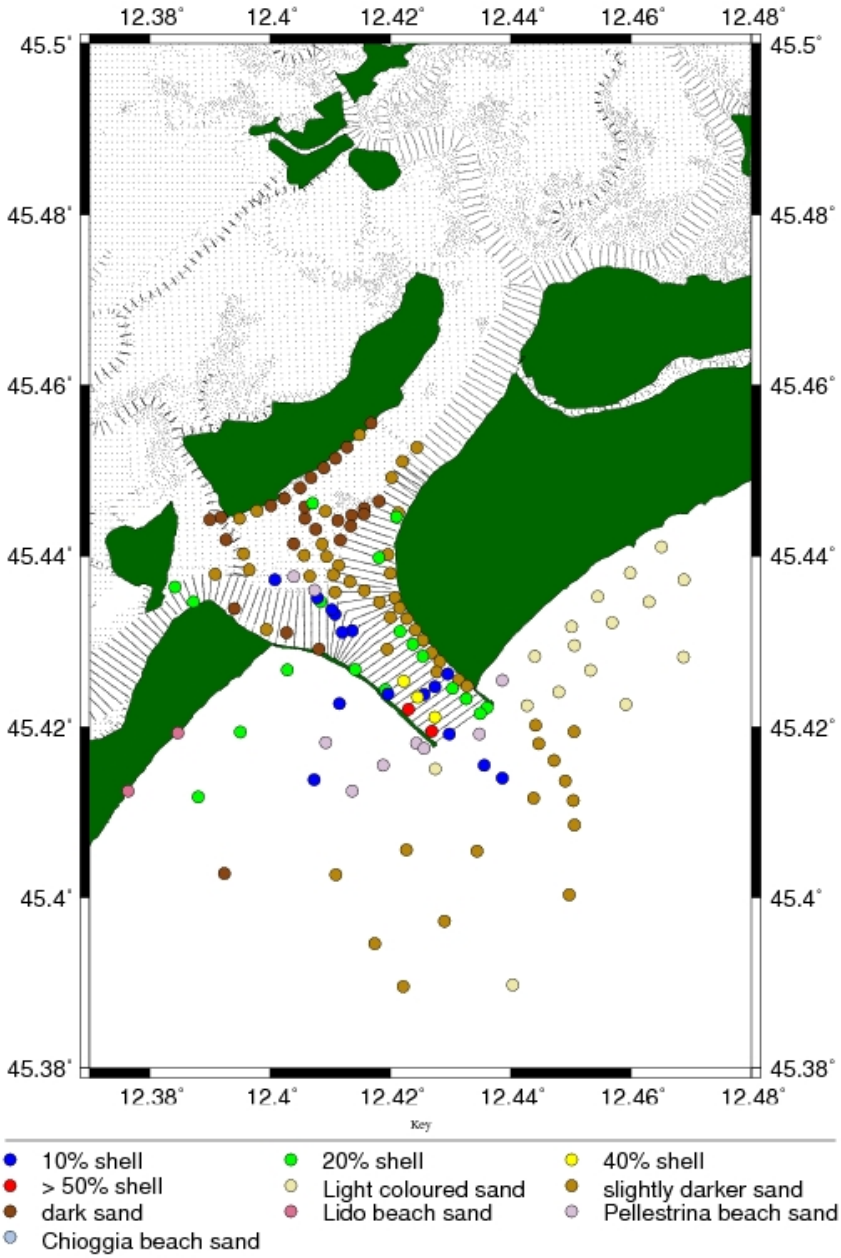

Fig. C.5: The sand was also analysis for colour (by eye); the areas are well defined by different colours of sand and proportion of shell. It appears that the sand from the ebb delta is similar to that of the ebb spit and flood delta lobe. Shells were found predominantly in the scour channel and outside the inlet. It is interesting to note that the sand immediately south of the mouth is the same colour as the beach replenished sand of Pellestina. This study was extended through the use of radiometer although the results have not been fully analysed for this study.

APPENDIX D

Channel Dynamics

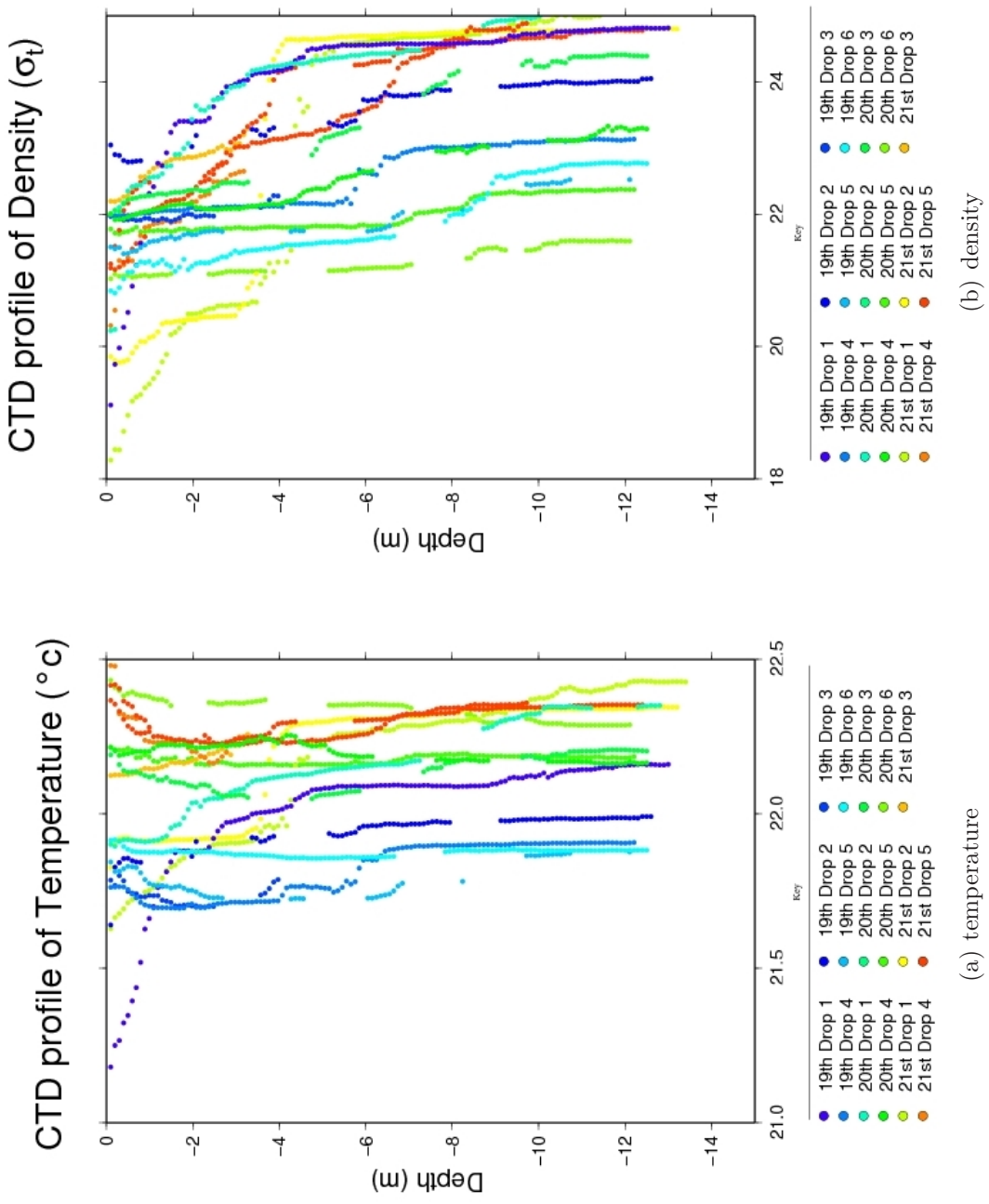

(b) density

(a) temperature

Fig. D.1: CTD

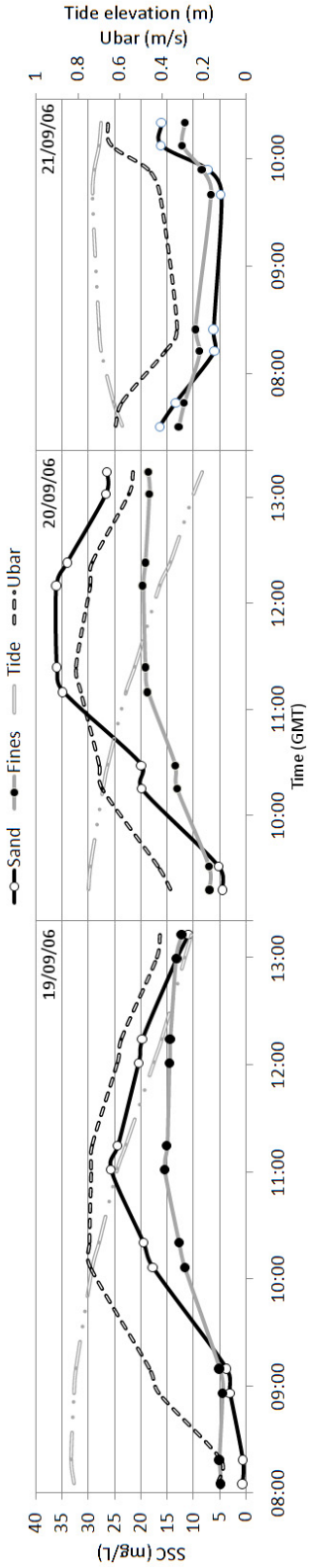

Fig. D.2: Average suspended sediment concentration (sand and fines) in the three survey days shown with tidal velocity and $\overline{U}$.

19^{th}		20^{th}		21^{st}	
Time (GMT)	$m^2\ s^{-1}$	Time (GMT)	$m^2\ s^{-1}$	Time (GMT)	$m^2\ s^{-1}$
08:05:58	2.30×10^{-6}	09:17:58	1.32×10^{-4}	07:31:06	3.53×10^{-3}
08:19:26	0	09:31:16	3.75×10^{-4}	07:44:26	3.09×10^{-3}
08:56:48	3.64×10^{-4}	10:15:12	4.85×10^{-3}	08:13:03	2.41×10^{-4}
09:10:38	7.91×10^{-4}	10:28:32	4.77×10^{-3}	08:25:10	6.61×10^{-5}
10:07:20	5.90×10^{-3}	11:10:00	7.44×10^{-3}	09:40:29	3.43×10^{-4}
10:21:24	5.91×10^{-3}	11:24:11	7.78×10^{-3}	09:54:11	8.51×10^{-4}
11:02:25	5.80×10^{-3}	12:10:31	5.77×10^{-3}	10:07:34	3.50×10^{-3}
11:15:57	5.44×10^{-3}	12:23:39	5.50×10^{-3}	10:20:30	3.62×10^{-3}
12:02:10	3.30×10^{-3}	13:02:30	2.62×10^{-3}		
12:15:28	2.75×10^{-3}	13:14:57	2.07×10^{-3}		
13:00:54	5.94×10^{-4}				
13:14:03	4.89×10^{-4}				

Tab. D.1: Total bedload transported per hour. Note that totals represent mass up until hour stated, i.e. sediment transported between 9 and 10 is listed under 10.

ADCP time	Ping length	Pings (mg $\times 10^4$)		bedload rate ($\times 10^{-4}$)	Metres		bedload rate ($\times 10^{-6}$)	bottom velocity	Total weight across profile (kg)		
GMT	(m)	Sand	Fines	$m^2\ s^{-1}$	Sand (g)	Fines (g)	$m^2\ s^{-1}$	$m\ s^{-1}$	Sand	Fines	Bedload
08:05:58	1.93	0.2	1.6	0.02	4.06	30.15	∼0	0.15	0.59	4.38	0.00
08:19:26	1.79	0.3	1.9	0	4.42	34.25	0	0.17	0.74	5.71	0.00
08:56:48	1.78	1.1	1.6	3.6	18.73	27.75	0.65	0.34	6.34	9.39	0.63
09:10:38	1.80	1.5	2.1	7.9	27.47	37.06	1.42	0.37	10.10	13.63	1.50
10:07:20	1.76	7.3	4.8	58.9	129.42	85.08	10.39	0.53	68.60	45.10	15.75
10:21:24	1.76	8.3	5.4	59.1	146.71	95.44	10.42	0.52	75.75	49.28	15.39
11:02:25	1.81	10.0	6.1	58.0	182.82	110.02	10.51	0.55	99.71	60.01	16.39
11:15:57	1.86	9.6	5.9	54.3	178.07	110.29	10.11	0.52	92.05	57.01	14.95
12:02:10	1.86	7.9	5.6	33.0	146.36	103.83	6.15	0.42	62.04	44.01	7.46
12:15:28	1.95	7.4	5.4	27.5	143.71	105.32	5.36	0.42	60.45	44.30	6.45
13:00:54	1.94	4.6	4.7	5.9	89.70	91.77	1.15	0.28	25.00	25.58	0.92
13:14:03	1.88	4.2	4.7	4.9	79.05	88.77	0.92	0.28	22.51	25.27	0.75
09:17:58	1.74	1.80	2.84	1.32	31.21	49.28	0.23	0.33	10.23	16.15	0.22
09:31:16	1.97	1.92	2.64	3.75	37.82	51.95	0.74	0.37	14.02	19.25	0.78
10:15:12	1.72	8.08	5.36	48.52	139.01	92.25	8.35	0.46	63.66	42.25	10.93
10:28:32	1.86	8.03	5.42	47.66	148.97	100.52	8.84	0.49	73.21	49.40	12.43
11:10:00	1.70	14.84	7.96	74.39	252.93	135.60	12.68	0.57	142.91	76.62	20.48
11:24:11	1.70	15.56	8.27	77.78	264.62	140.77	13.23	0.58	154.08	81.96	22.04
12:10:31	1.83	14.52	7.90	57.72	266.14	144.80	10.58	0.53	140.06	76.20	15.92
12:23:39	1.87	12.98	7.30	54.98	242.12	136.28	10.26	0.54	129.92	73.13	15.75
13:02:30	1.87	9.90	6.81	26.16	185.05	127.33	4.89	0.40	73.59	50.63	5.56
13:14:57	1.98	9.54	6.68	20.70	189.39	132.49	4.11	0.39	73.38	51.34	4.55
07:31:06	1.95	6.12	4.78	35.29	119.67	93.35	6.90	0.51	61.48	47.96	10.14
07:44:26	1.81	5.52	4.90	30.91	100.04	88.92	5.61	0.46	45.99	40.88	7.37
08:13:03	2.08	1.98	3.00	2.41	41.12	62.30	0.50	0.35	14.45	21.89	0.50
08:25:10	2.06	2.25	3.50	0.66	46.47	72.07	0.15	0.28	12.96	20.10	0.11
09:40:29	1.76	1.94	2.75	3.43	34.06	48.31	0.60	0.35	12.02	17.05	0.61
09:54:11	1.88	2.75	3.17	8.51	51.86	59.76	1.60	0.37	19.24	22.17	1.70
10:07:34	1.89	6.38	4.78	35.03	120.56	90.26	6.63	0.45	54.30	40.65	8.53
10:20:30	2.00	5.81	4.22	36.17	116.35	84.51	7.25	0.48	55.52	40.33	9.89

Tab. D.2: Total sediment transported per ADCP profile on the 19th, 20th and 21st September 2006.

Bibliography

Ackers, P. and White, W.R. (1973). Sediment transport: a new approach and analysis. *Journal of the Hydraulics Division, ASCE*, 99 (HY11):2041–60.

Albani, A.D., Favero, V.M., and Serandrei Barbero, R. (1998). Distribution of sediment and benthic foraminifera in the Gulf of Venice, Italy. *Estuarine, Coastal and Shelf Science*, 46:251–65.

Albani, A. and Serandrei Barbero, R. (2001). The distribution of surface sediments in the lagoon of Venice (Italy) in the 1980s. *Atti Dell'Istituto Veneto di Scienze, Lettere ed Arti*, 154:363–78.

Allen, J.R.L. (2000). Morphodynamics of Holocene salt marshes: a review sketch from the Atlantic and southern North Sea coasts of Europe. *Quaternary Science Review*, 19 (17-18):1155–231.

Amos, C.L. (2005). Morphodynamics Lectures-Tidal Inlets and Barrier Islands. p. 29. University of Southampton, School of Ocean and Earth Science.

Amos, C.L. and Sutherland, T. (1994). A rapid technique for the determination of dry sediment mass from saturated marine sands. *Sedimentary Research*, A64 (3):667–70.

Amos, C.L., Umgiesser, G., Reed, P., Munford, G., and Lea, J. (2002). The residual tidal circulation of water, sediment and organics in northern Venice Lagoon, Italy. *Scientific Research and Safeguarding of Venice. Research programme 2001-2003*, 2:189–202.

Amos, C.L., Villatoro, M., Helsby, R., Thompson, C.E.L., Zaggia, L., Umgiesser, G., Venturini, V., Sutherland, T.F., Mazzoldi, A., and Rizetto, F. (2008). Measurements

of sand transport in the Chioggia and Lido inlets of Venice lagoon, Italy. *Continental Shelf Research*, In review.

APAT (1960a). Carta realizzata dal servizio geologico d'Italia: Foglio N.51 Venezia (legge 2/2/1960 N.68).

APAT (1960b). Carta realizzata dal servizio geologico d'Italia: Foglio N.52 S.Dona' di Piave - foce del Tagliamento (legge 2/2/1960 N.68).

APAT (1960c). Carta realizzata dal servizio geologico d'Italia: Foglio N.65 Adria (legge 2/2/1960 N.68).

APAT (2006). Aggiornamento sulle osservazioni dei livelli di marea nella laguna di Venezia. Technical Report 69/2006, APAT.

Bagnold, R.A. (1974). Fluid forces on a body in shear-flow; experimental use of 'stationary flow'. *Proceedings of the Royal Society, London.*, A340:147–71.

Bale, A.J. (1996). In Situ laser optical particle sizing. *Journal of Sea Research*, 36 (1-2):31–6.

Balletti, C. (2006). Digital elaborations for cartographic reconstruction: The territorial transformations of Venice harbours. *e-Perimetron*, 1 (4):274–86.

Balouin, Y. and Howa, H. (2002). Sediment transport pattern at the Barra Nova Inlet, south Portugal: a conceptual model. *Geo-Marine Letters*, 21 (4):226–35.

Baso, G., Scarso, M., and Tonini, C. (2003). *La Laguna di Venezia nella cartografia storica a stampa del Museo Correr.* Publ. Musei Civici Veneziani, 137 pp.

Batalla, R.J. and Martin-Vide, J.P. (2001). Thresholds of particle entrainment in a poorly sorted sandy gravel-bed river. *Catena*, 44 (3):223–43.

Bayram, A., Larson, M., and Hanson, H. (2007). A new formula for total longshore transport rate. *Coastal Engineering*, 54 (9):700–10.

Bellucci, L., Frignani, M., Lin, S., and Muntau, H. (2005). Accumulation and metal fluxes in the central Venice Lagoon during the last century. *Chemistry and Ecology*, 21 (6):425–39.

Bertin, X., Chaumillon, E., Weber, N., and Tesson, M. (2004). Morphological evolution and time-varying bedrock control of main channel at a mixed energy tidal inlet: Maumusson Inlet, France. *Marine Geology*, 204 (1-2):187–202.

Best, J. (1988). Sediment transport and bed morphology at river channel confluences. *Sedimentology*, 35 (3):481–98.

Bettinetti, A., Pypaert, P., and Sweerts, J. (1996). Application of an integrated management approach to the restoration project of the Lagoon of Venice. *Journal of Environmental Management*, 46:207–27.

Birkeland, P.W. (1999). Topography-soil relations with time in different climatic settings. In *Soils and Geomorphology*, p. 448. Oxford University Press Inc, USA.

Black, K.S., Athey, S., and Wilson, P. (2004). Particle tracking: a new tool for coastal zone sediment management. In *Littoral 2004*, pp. 1–6. Aberdeen.

Bloesch, J. (1994). A review of methods used to measure sediment resuspension. *Hydrobiologia*, 284:13–8.

Blott, S.J. and Pye, K. (2001). GRADISTAT: a grain size distribution and statistics package for the analysis of unconsolidated sediments. *Earth Surface Processes and Landforms*, 26:1237–48.

Bonardi, M., Breda, A., Bonsembiante, N., Tosi, L., and Rizzetto, F. (2005). Spatial variations of the superficial sediment characteristics of the lagoon of Venice, Italy. In P. Campostrini, ed., *Proceedings of the Annual General Meeting of CORILA: Scientific Research and Safeguarding of Venice.*, volume 3, p. 491. Venice.

Bonardi, M., Canal, E., Cavazzoni, S. Serandrei Barbero, R., Tosi, L., Galgaro, A., and Giada, M. (1997). Sedimentological, archaeological and historical evidences of paleoclimatic changes during the Holocene in the lagoon of Venice (Italy). *World Resource Review*, 9 (4):435–46.

Bonardi, M., Tosi, L., and Rizzetto, F. (2002). Mineralogical characterization of the Venice Lagoon top sediments. *Scientific Research and Safeguarding of Venice. Research programme 2001-2003*, 2:145–55.

Bondesan, A., Meneghel, M., Rosselli, R., and Vitturi, A. (2004). Carta geomorfologica della provincia di Venezia alla scala 1:50,000.

Brambati, A., Bregant, d., Lenardon, G., and Stolfa, D. (1973). Transport and sedimentation in the Adriatic Sea. Technical report, Museo friulano di Storia Naturale.

Brambati, A., Marocco, R., Catani, G., Carobene, L., and Lenardon, G. (1978). Stato delle conoscenze dei litorali dell'Alto Adriatico e criteri di intervento per la loro difesa. *Memorie della Societa Geologica Italiana*, 19:389–98.

Bridge, J.S. (2003). *Rivers and Floodplains: Forms, Processes, and Sedimentary Record*. Blackwell Publishing, 492 pp.

Briggs, D. (1986). *Fundamentals of Physical Geography.* Rowman & Littlefield Publishers, Inc., 558 pp.

Bristow, C.S., Best, J.L., and Roy, A.G. (1993). Morphology and facies models of channel confluences. *Special Publications of the International Association of Sedimentologists*, 17:91–100.

Bruun, P. (1978). *Stability of Tidal Inlets, Theory and Engineering.* Elsevier Scientific Publishing Company, Amsterdam, 506 pp.

Bruun, P. and Gerritsen, F. (1959). Natural bypassing of sand at coastal inlets. *Journal of Waterways and Harbours Division*, 85:75–107.

Burczynski, J. (2001). Bottom Classification. Technical Report BioSonics Inc., www.biosonicsinc.com/doc_library/docs/bottom_classification.pdf.

Cappucci, S., Amos, C.L., Hosoe, T., and Umgiesser, G. (2004). SLIM: a numerical model to evaluate the factors controlling the evolution of intertidal mudflats in Venice Lagoon, Italy. *Journal of Marine Systems*, 51 (1-4):257–80.

Carbognin, L. and Cecconi, G. (1997). The Lagoon of Venice environmental problems, remedial measures. In *Meeting of Environmental Sedimentology*, p. 71.

Carbognin, L., Teatini, P., and Tosi, L. (2004). Eustacy and land subsidence in the Venice Lagoon at the beginning of the new millennium. *Journal of Marine Systems*, 51 (1-4):345–53.

Carr, E.E. and Kraus, N.C. (2001). Morphological asymmetries at entrances to tidal Inlets. Technical Report EDRC/CHL CHETN-IV-33, U.S Army Corps of Engineers.

Castelle, B., Borget, J., Molnar, N., Strauss, D., Deschamps, S., and Tomlinson, R. (2006). Dynamics of a wave-dominated tidal inlet and influence on adjacent beaches, Currumbin Creek, Gold Coast, Australia. *Coastal Engineering*, 54:77–90.

Cecconi, G. and Ardone, V. (1998). La protezione dei litorali con ripascimento delle spiagge. L'esperienza dei litorali di Cavallino e Pellestrina, in La progettazione ambientale nei sistemi costieri. In M. Pietrobelli, ed., *10th IAED Conference*, volume Notebook 12, pp. 11–31. International Association for Environmental Design, Rome.

Cecconi, G. and Ardone, V. (2000). La fonte di approvvigionamento della sabbia nel ripascimento dei litorali veneti. In *Intervento alla Presentazione della Costa ligure.* Genova.

Ciavola, P., Organo, C., Vintro, L., and Mitchell, P.I. (2002). Sedimentation processes on intertidal areas of the lagoon of Venice: Identification of exceptional flood events (Aqua Alta) using radionuclides. *Journal of Coastal Research*, (SI36):139–47.

Cohen, J.E., Small, C., Mellinger, A., Gallup, J., Sachs, J., Vitousek, P.M., and Mooney, H.A. (1997). Estimates of Coastal Populations. *Science*, 278 (5341):1209c–13. 10.1126/science.278.5341.1209c.

Collavini, F., Zonta, R., and Zaggia, L. (2000). Longitudinal distribution of heavy metals in sediments of Piave River Estuary (northeastern Italy). In *International Conference on Heavy Metals in the Environment*. Ann Harbor, Michigan.

Collier, J.S. and Brown, C.J. (2005). Correlation of sidescan backscatter with grainsize distribution of surficial seabed sediments. *Marine Geology*, 214:431–49.

Consorzio Venezia Nuova (1989). Progetto preliminare di massima delle opere alle boche: Vol 2-Descrizione dell'ecosistema parte II. Technical report, Magistrato alle Acque di Venezia.

Consorzio Venezia Nuova (1996). The morphological restoration of the Venice Lagoon. Technical report, Consorzio Venezia Nuova.

Consorzio Venezia Nuova (1997). Measures for the protection of Venice and itŹs lagoon. Technical report, Consorzio Venezia Nuova.

Consorzio Venezia Nuova (2000). La difesa del Lido di Venezia dalle mareggiate. *Quaderni Trimestrali Consorzio Venezia Nuova*, 3/4:89–109.

Cooper, N.J., Hooke, J.M., and Bray, M.J. (2001). Predicting coastal evolution using a sediment budget approach: a case from southern England. *Ocean and Coastal Management*, 44 (11):711–28.

Coraci, E., Umgiesser, G., Scalvo, M., and Amos, C.L. (2003). Modeling sand transport in the Venice Lagoon inlets. *Scientific Research and Safeguarding of Venice. Research programme 2001-2003*, 2:157–73.

Costanza, R., D'Arge, R., de Groots, R., Farber, S., Grasso, M., Hannon, B., Limburg, K., Naeem, S., O'Neill, R.V., Paruelo, J., Raskin, R.G., Sutton, P., and van den Belt, M. (1997). The value of the world's ecosystem services and natural capital. *Nature*, 387:253–60.

Cox, J.M. (2002). Appendix 9. Report on mineralogical tracers. Technical Report LOW-260938/DJ, School of Environmental Sciences, University of East Anglia.

Crossland, C.J., Kremer, H.H., Lindeboom, H.J., Marshall Crossland, J.I., and Le Tissier, M.D.A. (2005). *Coastal fluxes in the anthropocene: the land-ocean interactions in the Coastal Zone Project of the International Geosphere-Biospher Programme.* Springer-Verlag, Berlin, 231 pp.

Cucco, A. and Umgiesser, G. (2005). Modelling the Venice Lagoon residence time. *Ecological Modelling*, 193 (1-2):34–51.

Daboll, J.M. (1969). *Holocene sediments of the Parker River estuary, Massachusetts.* Msc thesis, University of Massachusetts.

D'Alpaos, A.e.a. (2007). *Modellazione matematica e fisica di alcuni processi di erosione e sedimentazione nella laguna di Venezia.* Research Program CO.RI.LA 2004-2006: 6th Meeting presentations. CORILA, Venice.

Danish Hydraulics (1996). The Venetian Coasts. *Danish Hydraulics.*

Davis, J.R.A. (1978). *Coastal Sedimentary Environments.* Springer-Verlag, 420 pp.

Davis, J.R.A. and Fitzgerald, D.M. (2004). *Beaches and Coasts.* Wiley-Blackwell, 419 pp.

Day, Jr, J.W., Rybczyk, J., Scarton, F., Rismondo, A., Are, D., and Cecconi, G. (1999). Soil accretionary dynamics, sea-level rise and the survival of wetlands in Venice Lagoon: a field and modelling approach. *Estuarine, Coastal and Shelf Science*, 49:607–28.

Day, Jr, J.W., Scarton, F., Rismondo, A., and Are, D. (1998). Rapid deterioration of a salt marsh in Venice Lagoon, Italy. *Journal of Coastal Research*, 14 (2):583–90.

De Lange, W.P., Healy, T.R., and Darlan, Y. (1997). Reproducibility of sieve and settling tube textural determinations for sand-sized beach sediment. *Journal of Coastal Research*, 13 (1):73–80.

Deheyn, D.D. and Shaffer, L.R. (2007). Saving Venice: Engineering and ecology in the Venice lagoon. *Technology in Society*, 29 (2):205–13.

Deines, K.L. (1999). Backscatter estimation using broadband acoustic Doppler current meters. In *Proceedings of the IEEE Sixth Working Conference on Current Measurement*, pp. 249–53.

di Donato, G., Negredo, A.M., Sabadini, R., and Vermeersen, L.L.A. (1999). Multiple processes causing sea-level rise in the central Mediterranean. *Geophysics Research Letters*, 26 (12):1769–72.

Di Silvio, G. (2005). Sediment balance, morphodynamics and landscape restoration. In C. Fletcher, ed., *Flooding and Environmental Challenges for Venice and it's Lagoon*, pp. 359–68. Cambridge University Press.

Dinehart, R.L. and Burau, J.R. (2005). Repeated surveys by acoustic Doppler current profiler for flow and sediment dynamics in a tidal river. *Journal of Hydrology*, 314 (1-4):1–21.

Donde, F., Brancolini, G., Tosi, L., Kovacevic, V., Baradello, L., Gačić, M., and Rizzetto, F. (2008). The ebb-tidal delta of the Venice Lagoon, Italy. *The Holocene*, 18:267–78.

Downing, J. (2008). Comparison of Suspended Solids Concentration (SSC) and turbidity. Technical Report Application Note 2Q-AA, Cambell Scientific Inc.

Dyer, K.R. (1986). *Coastal and Estuarine Sediment Dynamics.* John Wiley and Sons, Chichester, 342 pp.

Dyer, K.R. (1997). *Estuaries: a Physical Introduction.* John Wiley and Sons., Chichester, 2nd ed. edition, 195 pp.

Edwards, T.K. and Glysson, G.D. (1999). C2:Field Methods for Measurement of Fluvial Sediment. In *Techniques of Water-Resources Investigations of the U.S. Geological Survey*, volume Book 3, Applications of Hydraulics, p. 89. USGS.

Emery, K.O. (1955). Grain size of marine beach gravels. *Journal of Geology*, 63 (1):39–49.

Emmett, W.W. (1980). A field calibration of the sediment trapping characteristics of the Helley-Smith bed load sampler. Technical Report Professional Paper 1139, Geological Survey.

Escoffier, F.F. (1940). The stability of tidal inlets. *Shore and Beach*, 8 (4):114–5.

Fenster, M. and Dolan, R. (1996). Assessing the impact of tidal inlets on adjacent barrier island shorelines. *Journal of Coastal Research*, 12:294–310.

Ferrarin, C. (2005). A 3-D sediment transport model and bed reworking for the Venice Lagoon. In P. Campostrini, ed., *Proceedings of the Annual General Meeting of CORILA: Scientific Research and Safeguarding of Venice 2005*, volume 4, p. 511. Venice.

Fitzgerald, D.M. (1982). Sediment bypassing at mixed energy tidal inlets. In *Proceedings 18th coastal engineering conference, ASCE*, pp. 1094–118.

Fitzgerald, D.M. (1988). Shoreline erosional-depositional processes associated with tidal inlets. In *Hydrodynamics and Sediment Dynamics of Tidal Inlets*. Springer-Verlag.

Fitzgerald, D.M., Kraus, N.C., and Hands, E.B. (2000). Natural mechanisms of sediment bypassing at tidal inlets. Technical Report ERDC/CHL CHETN-IV-30, U.S Army Corps of Engineers.

Fletcher, C. and Da Mosto, J. (2004). *The Science of Saving Venice*. Umberto Allemandi e C, 91 pp.

Fletcher, C.A. and Spencer, T. (2005). *Flooding and Environmental Challenges for Venice and it's Lagoon: State of Knowledge*. Cambridge University Press, 718 pp.

Folk, R.L. (1974). *Petrology of Sedimentary Rocks*. Hemphill Publishing Company, Austin, TX, 182 pp.

Folk, R.L. and Ward, W.C. (1957). Brazos River bar: A study in the significance of grain size parameters. *Journal of Sedimentary Petrology*, 27 (1):3–26.

Fontolan, G., Pillon, S., delli Quadri, F., and Bezzi, A. (2007). Sediment storage at tidal inlets in northern Adriatic lagoons: Ebb-tidal delta morphodynamics, conservation and sand use strategies. *Estuarine, Coastal and Shelf Science*, 75 (1-2):261–77.

Fredlund, D.G. and Rahardjo, H. (1993). *Soil Mechanics for Unsaturated Soils*. Wiley-Interscience, 544 pp.

French, P.W. (2001). *Coastal Defences: Processes, Problems, and Solutions*. Routledge, 384 pp.

Gao, S. (1991). A critique of the "McLaren Method" for defining sediment transport paths. *Journal of Sedimentary Petrology*, 61:43–147.

Gao, S. (1993). *Sediment Dynamics and Stability of Tidal Inlets*. Ph.D. thesis, University of Southampton.

Gao, S. and Collins, M.B. (1992). Net sediment transport patterns inferred from grain-size trends based upon definition of "transport vectors". *Sedimentary Geology*, 80:47–60.

Gao, S. and Collins, M.B. (1994). Tidal Inlet Equilibrium, in Relation to Cross-sectional Area and Sediment Transport Patterns. *Estuarine, Coastal and Shelf Science*, 38 (2):157–72.

Gao, S., Collins, M.B., Lanckneus, J., De Moor, G., and Van Lancker, V. (1994). Grain size trends associated with net sediment transport patterns: An example from the Belgian continental shelf. *Marine Geology*, 121 (3-4):171–85.

Garcia, M. and Parker, G. (1991). Entrainment of bed sediment into suspension. *Journal of the Hydraulics Division, ASCE.*, 117 (4):414–35.

Gartner, J.W., Cheng, R.T., Wang, P.F., and Richter, K. (2001). Laboratory and field evaluations of the LISST-100 instrument for suspended particle determinations. *Marine Geology*, 175 (1-4):199–219.

Gartner, J.W. (2002). Estimation of suspended solids concentrations based on acoustic backscatter intensity: theoretical background. In *Turbidity and Other Sediment Surrogates Workshop*. Remo, Nevada.

Gartner, J.W. (2004). Estimating suspended solids concentrations from backscatter intensity measured by acoustic Doppler current profiler in San Francisco Bay, California. *Marine Geology*, 211 (3-4):169–87.

Gatto, P. and Carbognin, L. (1981). The lagoon of Venice: natural environmental trend and man-induced modification. *Hydrological Sciences Bulletin,*, 26 (4):379–91.

Gazzi, P., Zuffa, G.G., Gandolf, G., and Paganelli, L. (1973). Provenienza e dispersione litoranea delle sabbie delle spiagge adriatiche fra le foci dell'Isonzo e del Fogilia: inquadramento regionale. *Memorie della Societa Geologica Italiana*, 12 (January):37.

Gilbert, G.K. (1885). 5th Annual Report: The topographic features of lake shores. Technical report, U.S. Geological Survey.

Gordon, R.L. (1996). Acoustic Doppler Current Profiler: principles of operation, a practical primer. Technical report, RD Instruments, San Diego, CA.

Graham, M.H., Dayton, P.K., and Erlandson, J.M. (2003). Ice ages and ecological transitions on temperate coasts. *Trends in Ecology and Evolution*, 18 (1):33–40.

Hayes, M.O. (1975). Morphology of sand accumulations in estuaries. In L. Cronin, ed., *Estuarine Research,*, pp. 3–22. Academic Press.

Hayes, M.O. (1979). Barrier island morphology as a function of tidal and wave regime. In S. Leatherman, ed., *Barrier Islands, from the Gulf of St. Lawrence to the Gulf of Mexico*, pp. 1–27. Academic Press, London.

Heathershaw, A.D. (1988). Sediment transport in the sea, on beaches and rivers: part 2-Sediment movement. *Journal of Naval Science*, 14:221–34.

Helsby, R., Amos, C.L., and Umgiesser, G. (2005). Morphological evolution and sand pathways in northern Venice Lagoon. In P. Campostrini, ed., *Scientific Research and Safeguarding of Venice*, volume 4, pp. 388–402. CO.RI.LA, Venice.

Helsby, R. (2006). *The dynamics and origin of sand in northern Venice Lagoon with an emphasis on the tidal inlet of Lido*. Phd upgrade, University of Southampton.

Hicks, D.M. and Hume, T.M. (1996). Morphology and size of ebb-tidal deltas at natural inlets on open-sea and pocket-bay coasts, North Island, New Zealand. *Journal of Coastal Research*, 12 (1):47–63.

Hicks, D.M. and Hume, T.M. (1997). Determining sand volumes and bathymetric change on an ebb-tidal delta. *Journal of Coastal Research*, 13 (2):407–16.

Hill, S.H. and McLaren, P. (2001). A comparison between log-hyperbolic and model-independent grain size distributions in Sediment Trend Analysis (STA®). *Journal of Coastal Research*, 17 (4):931–5.

Hitchcock, D.R., Newell, R.C., and Seiderer, L.J. (1999). Investigation of Benthic and Surface Plumes associated with Marine Aggregate Mining in the United Kingdom Final Report. Technical Report Contract No. 14-35-001030763/Ref. 98-555-03, Coastline Surveys Ltd.

Hoffmans, G.J.C.M. and Verheij, H.J. (1997). *Scour Manual*. A.A. Balkema, Rotterdam, 224 pp.

Hoitink, A.J.F. and Hoekstra, P. (2005). Observations of suspended sediment from ADCP and OBS measurements in a mud-dominated environment. *Coastal Engineering*, 52 (2):103–18.

Hoyt, J.H. (1967). Barrier island formation. *Geological Society of America Bulletin*, 78:1125–36.

HR Wallingford (2002). Southern North Sea sediment transport study: Phase II (Sediment transport report). Technical Report EX 4526, HR Wallingford, CEFAS/UEA, Posford Haskoning and Dr Brian D'Olier for Great Yarmouth Bourough Council.

Hughes, S.A. (1997). Estimating scour caused by deflected ebb flows. Technical Report CETN-IV-8, U.S Army Corps. of Engineers.

Hughes, S.A. (2003). Scour prediction and protection at inlets. Powerpoint presentation - CIRP Technology Transfer Workshop (4th).

Hume, T.M. and Herdendorf, C.E. (1988). The 'Furkert-Heath' relationship for tidal inlet stability reviewed. *New Zealand Journal of Marine and Freshwater Research*, 22:129–34.

Hume, T.M. and Herdendorf, C.E. (1990). Morphologic and hydrologic characteristics of tidal inlets on a headland dominated, low littoral drift coast, Northeastern New Zealand. *Journal of Coastal Research*, Special Issue 9:527–63.

Inman, D.L. (2002). Nearshore Processes. In *Encyclopedia of Science and Technology*, volume 9. McGraw-Hill, New York.

Jarrett, J.T. (1976). Tidal prism - inlet area relationships. Technical Report GITI Report 3, Department of the Army Corps of Engineers.

Joshi, P.B. (1982). Hydromechanics of tidal jets. *Journal of the Waterway, Port, Coastal and Ocean Division*, 108 (WW2 Proc. Paper 17294):239–53.

Keahey, J. (2002). *Venice Againest the Sea: A City Besieged*. T. Dunhe Books/St Martin's Press, 304 pp.

Keijzer, M. and Bobovic, V. (1999). Error correction of a deterministic model in Venice Lagoon by locall linear models. In *Modelli complessi e metodi computazionali intensivi per la stima e la previsione*. Venezia.

Kern, U. and Westrich, B. (1997). Sediment budget analysis for river reservoirs. *Water, Air, and Soil Pollution*, 99 (1-4):105–12.

King, Jr, D.B. (2005). Influence of grain size on sediment transport rates with emphasis on the total longshore rate. Technical Report ERDC/CHL CHETN-II-48, U.S. Army Corps of Engineers.

Kirk, R.M. and Lauder, G.A. (2000). Significant coastal lagoon systems in the South Island, New Zealand: coastal processes and lagoon mouth closure. In *Science for Conservation 146*, p. 48. Department of Conversation, Wellington, New Zealand.

Kjerfve, B. (1994). *Coastal Lagoon Processes*. Elsevier Oceanography Series. Elsevier Science B.V., Amsterdam, 577 pp.

Klassen, G.J. and Vermeer, K. (1988). Confluence scour in large braided rivers with fine bed material. In *Proceedings of the International Conference on Fluvial Hydraulics, Budapest*.

Komar, P.D. (1996). Tidal inlet processes and morphology related to sediment transport. *Journal of Coastal Research*, 23:23–45.

Komar, P.D. and Cui, B. (1984). The analysis of grain-size measurements by sieving and settling-tube techniques. *Journal of Sedimentary Petrology*, 54:603–14.

Komar, P.D. and Reimers, C.E. (1978). Grain shape effects on settling rates. *Journal of Geology*, 86:193–209.

Kramer, J.R. (1959). Correction of some earlier data on calcite and dolomite in sea water. *Journal of Sedimentary Petrology*, 29 (3):465–7.

Kraus, N.C. and Rosati, J.D. (1998). Estimation of uncertainty in coastal sediment budgets at inlets. Technical Report Coastal Engineering Technical Note IV-16, US Army Corps of Engineers.

Kraus, N.C. and Rosati, J.D. (1999). Estimating uncertainty in coastal inlet sediment budgets. In *Proceedings, 12th National Conference on Beach Preservation Technology,*. Florida Shore & Beach Preservation Association, Tallahassee, FL,.

Krause-Jensen, D., Greve, T., and Nielsen, K. (2005). Eelgrass as a bioindicator under the European Water Framework Directive. *Water Resources Management*, 19 (1):63–75(13).

Krüger, J.C. and Healy, T.R. (2006). Mapping the morphology of a dredged ebb tidal delta, Tauranga Harbour, New Zealand. *Journal of Coastal Research*, 22 (3):720–7.

Krumbein, W.C. (1936). Application of logarithmic moments to size frequency distributions of sediments. *Journal of Sedimentary Petrology*, 6 (1):35–47.

Krumbein, W.C. (1938). Size frequency distributions of sediments and the normal phi curve. *Journal of Sedimentary Petrology*, 8 (3):84–90.

Land, J.M. and Bray, R.N. (2000). Acoustic measurement of suspended solids for monitoring of dredging and dredged material disposal. *Journal of Dredging Engineering*, 2 (3):1–17.

Le Conte, L.J. (1905). Discussion on river and harbor outlets, Notes on the improvement of river and harbor outlets in the United States". *D.A. Watts, Trans. ASCE 55*, paper 1009:306–8.

le Roux, J.P. (2005). Grains in motion: a review. *Sedimentary Geology*, 178:285–313.

Lees, B.J. (1981). Relationship between eddy viscosity of seawater and eddy diffusivity of suspended particles. *Geo-Marine Letters*, 1:249–54.

Li, M.Z. and Amos, C.L. (2001). SEDTRANS96: the upgraded and better calibrated sediment-transport model for continental shelves. *Computers and Geosciences*, 27:619–45.

Lied, T.T., Walday, M., Olsgard, F., Ellingsen, K.E., and Holm, S. (2004). SEABEC - a Single Beam Echo Sounder Seabed Classification System. Technical Report 0-7803-8669-8/04, IEEE.

Lucio, P.S., Dupont, H.S., and Bodevan, E.C. (2004). Sediment Transport Paths in the Westerschelde: One-Dimensional Alternative to Determine Sediment Trend. *Journal of Coastal Research*, 20 (3):771–5.

Magistrato alle Aqua (1993). Evoluzione morfologica della Laguna di Venezia. In *Confronto batimetrico tra la batimetria del 1992 e del 1970. Convenzione 7322, Sezione 20, Stralcio 2*. Servizio Informativo, Venice.

Marani, M., Belluco, E., Ferrari, S., Silvstri, S., D'Alpaos, A., Lanzoni, S., Feola, A., and Rinaldo, A. (2006). Analysis, synthesis and modelling of high-resolution observations of salt-marsh eco-geomorphological patterns in the Venice lagoon. *Estuarine, Coastal and Shelf Science*, 69:414–26.

Marino, J.N. and Mehta, A.J. (1987). Inlet ebb tide shoals related to coastal parameters. In *Coastal Sediments*, pp. 1608–22. American Society of Civil Engineers, New Orleans.

Martin, L. and Dominguez, J.M.L. (1994). Geological history of coastal lagoons. In K. B, ed., *Coastal Lagoon Processes*, pp. 41–68. Eselvier Science, Amsterdam.

MAV-CVN (1992). Valutazione degli effetti delle nuove configurazioni sulla gestione delle opere mobili. Technical Report VEN340-STUDIOB.5.58, Magistrato alle Aque di Venezia and Consorzio Venezia Nuova.

Mazzacurati, G. (1995). Water flow restoration and the active protection of the Venice Lagoon. In *Ca' Vendramin Conference on Coastal Lagoons*. Rovigo, Italy.

McComb, A.J. (1995). *Eutrophic Shallow Estuaries and Lagoons*. CRC Press Inc., 252 pp.

McGee, W.D. (1890). Encroachments of the sea. *The Forum*, 9:437–49.

McLaren, P. (1981). An interpretation of trends in grain size measures. *Journal of Sedimentary Petrology*, 51 (2):611–24.

McLaren, P. and Bowles, D. (1985). The effects of sediment transport on grain-size distributions. *Journal of Sedimentary Research*, 55 (4):457–70.

Meijer, M.C. (2005). *Wave attenuation over salt marsh vegetation*. Msc thesis, Delft University of Technology.

Melville, B.W. and Coleman, S.E. (2000). *Bridge Scour*. Water Rescources Publications, 572 pp.

Merckelbach, L.M. (2006). A model for high-frequency acoustic Doppler current profiler backscatter from suspended sediment in strong currents. *Continental Shelf Research*, 26 (11):1316–35.

Mitello, A. and Hughes, S.A. (2000). Circulation Patterns at Tidal Inlets with Jetties. Technical Report ERDC/CHL CETN-IV-29, U.S Army Engineer Research and Development Center, Vicksburg, MS.

Molinaroli, E., Guerzoni, S., Sarretta, A., Cucco, A., and Umgiesser, G. (2007). Links between hydrology and sedimentology in the Lagoon of Venice. *Journal of Marine Systems*, 68:303–17.

Mota Oliveira, I.B. (1970). Natural flushing ability in tidal inlets. In *Proceedings, 12th Coastal Engineering Conference*, pp. 1827–45. ASCE.

Nayak, I.V. (1971). Tidal Prism-Area Relationship in a Model Inlet. Technical Report HEL-24-1, University of California.

Neumeier, U. (2005). Cal_settling. A Matlab script. Technical Report Converts raw settling column data (from NOCS) into grain sizes (phi)., University of Southampton.

Nielsen, P. (1992). *Coastal Bottom Boundary Layers and Sediment Transport*, volume 4 of *Advanced Series on Ocean-Engineering*. World scientific Publishing, Singapore.

Nitsche, F.O., Ryan, W.B.F., Carbotte, S.M., Bell, R.E., Slagle, A., Bertinado, C., Flood, R., Kenna, T., and McHugh, C. (2007). Regional patterns and local variations of sediment distribution in the Hudson River Estuary. *Estuarine, Coastal and Shelf Science*, 71:259–77.

Norwich, J.J. (2003). *A History of Venice*. Penguin, London, 4 edition, 673 pp.

O'Brien, M.P. (1931). Estuary tidal prism related to entrance areas. *Civil Engineering*, 1 (8):738.

O'Brien, M.P. (1969). Dynamics of tidal inlets. In *Lagunas costeras, un simposio: Simposio Internacional sobre lagunas costeras*, pp. 397–406. Mexico City, Mexico.

Oertel, G.F. (1988). Processes of sediment exchange between tidal inlets, ebb deltas, and barrier islands. In D. Aubrey and L. Weishar, eds., *Hydrodynamics and Sediment Dynamics of Tidal Inlets*, volume 29 of *Lecture notes on coastal and estuarine studies*, pp. 297–318. Springer-Verlag, New York.

Ogston, A. (2006). Suspended sediment load and flux.

Pacheco, A., Vila-Concejo, A., Ferreira, O., and Dias, J.A. (2008). Assessment of tidal inlet evolution and stability using sediment budget computations and hydraulic parameter analysis. *Marine Geology*, 247 (1-2):104–27.

Packham, J.R. and Willis, A.J. (1996). *Ecology of Dunes, Salt Marsh and Shingle*. Kluwer Academic Publishers, 352 pp.

Patrick, Jr, W.H. and DeLaune, R.D. (1990). Subsidence, accretion, and sea level rise in south San Francisco Bay marshes. *Limnology and Oceanography*, 35 (6):1389–95.

Pedocchi, F. and Garcia, M.H. (2006). Evaluation of the LISST-ST instrument for suspended particle size distribution and settling velocity measurements. *Continental Shelf Research*, 26 (8):943–58.

Pirazzoli, P.A. and Tomasin, A. (1999). Recent abatement of easterly winds in the northern Adriatic. *International Journal of Climatology*, 19 (11):1205–19.

Pritchard, D.W. (1952). Estuarine Hydrography. *Advances in Geophysics*, 1:243–80.

Ralston, D.K. and Stacey, M.T. (2007). Tidal and meteorological forcing of sediment transport in tributary mudflat channels. *Continental Shelf Research*, 27 (10-11):1510–27.

Raudkivi, A.J. (1998). *Loose Boundary Hydraulics*. A.A.Balkema, 507 pp.

Ravaioli, M., Alvisi, F., and Menegazzo Vitturi, L. (2003). Dolomite as a tracer for sediment transport and deposition on the northwestern Adriatic continental shelf (Adriatic Sea, Italy). *Continental Shelf Research*, 23:1359–77.

Ravera, O. (2000). The Lagoon of Venice: the result of both natural factors and human influence. *Journal of Limnology*, 59 (1):19–30.

Reichel, G. and Nachtnebel, H.P. (1994). Suspended sediment monitoring in a fluvial environment: Advantages and limitations applying an Acoustic Doppler Current Profiler. *Water Research*, 28 (4):751–61.

Reynolds, O. (1883). An experimental investigation of the circumstances which determine whether the motion of water shall be direct or sinuous, and of the law of resistance in parallel channels. *Philosophical Transactions of the Royal Society*, 174:935–82.

Rosati, J.D. (1985). Sediment size and fall velocity effects on longshore sediment transport. Technical Report CETN-II-11, U.S. Army Engineer Waterways Experiment Station. (Assumed author- listed for correspondence).

Rosati, J.D. and Kraus, N.C. (1999a). Formulation of sediment budgets at inlets. Technical Report CETV IV-15, U.S. Corps of Engineers.

Rosati, J.D. and Kraus, N.C. (1999b). Sediment Budget Analysis System (SBAS). Technical Report CETN-IV-20, U.S. Corps of Engineers.

Rotaru, E., Le Coz, J., Drobot, R., Adler, M.J., and Dramais, G. (2006). ADcp measurements of suspended sediment fluxes in Banat rivers, Romania. In *BALWOIS*. Ohrid, Republic of Macedonia.

Rouse, H. (1939). Experiments on the mechanics of sediment transport. In *Proceedings of the 5th International Congress on Applied Mechanics.*, pp. 550–4. Cambridge, Massachusetts.

Scarton, F., Day, Jr, J.W., Rismondo, A., Cecconi, A., and Are, D. (2000). Effects of an intertidal sediment fence on sediment elevation and vegetation distribution in a Venice (italy) Lagoon salt marsh. *Ecological Engineering*, 16:223–33.

Schlichting, H.T. and Gersten, K. (1999). *Boundary Layer Theory*. Springer-Verlag and Heidelberg GmbH & Co, Berlin, 801 pp.

Seabergh, W.C. (2002). Inner-Bank Erosion Processes and Solutions at Coastal Inlets. Technical Report ERDC/CHL CHETN-IV-52, U.S Army Corps of Engineers.

Seabergh, W.C. (2003). Part 2.6. Hydrodynamics of Tidal Inlets. In *Coastal Engineering Manual*. U.S. Army Corps. of Engineers, Vicksburg, Mississippi.

Seminara, G., Bolla Pittaluga, M., Tambroni, N., and Garotta, V. (2005). Open problems in modelling the long-term morphodynamics evolution of Venice Lagoon. In C. Fletcher, ed., *Flooding and Environmental Challenges for Venice and it's Lagoon*, pp. 369–78. Cambridge University Press.

Serandrei Barbero, R., Carbognin, L., Taroni, G., and Cova, E. (1999). Distribution of recent benthic foraminifera in the southern basin of the Venice lagoon (Italy): statistical evaluation of taxa significance. *Micropaleontology*, 45:1–13.

Sfriso, A., Birkemeyer, T., and Ghetti, P.F. (2001). Benthic macrofauna changes in areas of Venice Lagoon populated by seagrasses or seaweeds. *Marine Environmental Research*, 52 (4):323–49.

Sfriso, A., Facca., C., and Marcomini, A. (2005a). Sedimentation Rates and Erosion Processes in the Lagoon of Venice. *Environment International*, 31:983–92.

Sfriso, A., Favaretto, M., Ceoldo, S., Facca, C., and Marcomini, A. (2005b). Organic carbon changes in the surface sediments of the Venice lagoon. *Environment International*, 31 (7):1002–10.

Sheng, J. and Hay, A.E. (1988). An examination of the spherical scatter approximation in aqueous suspension of sand. *Journal of the Acousticical Society of America*, 83:598–610.

Shigemura, T. (1981). Tidal prism-throat width relationships of the Bays of Japan. *Shore and Beach*, 49 (3):34–9.

Simon, D. and Senturk, F. (1992). *Sediment Transport Technology: Water and Sediment Dynamics*. Water Resources Publications, 919 pp.

Simonini, R., Ansaloni, I., Bonvicini Pagliai, A.M., Cavallini, F., Lotti, M., Mauri, M., Montanari, G., Preti, M., Rinaldi, A., and Prevedelli, D. (2005). The effects of sand extraction on the macrobenthos of a relict sands area (northern Adriatic Sea): results 12 months post-extraction. *Marine Pollution Bulletin*, 50 (7):768–77.

Smith, G.M. and Sayao, O.J. (1989). Definition of littoral cells for Ontario's Great Lake shorelines. In *Proceedings of the Sixth Symposium on Coastal and Ocean Management, Coastal Zone '89.*, pp. 3773–84. ASCE, Charleston, S.C.

Smith, J.D. and McLean, S.R. (1977). Spatially averaged flow over a wavy surface. *Journal of Geophysical Research*, 82 (12):1735–46.

Smith, N.P. (1994). Water, salt, and heat balance of coastal lagoons. In B. Kjerfve, ed., *Coastal Lagoon Processes*, pp. 69–101. Elsevier Science, Amsterdam.

Solidoro, C., Malaku Canu, D., Cucco, A., and Umgiesser, G. (2004). A partition of the Venice Lagoon based on physical properties and analysis of general circulation. *Journal of Marine Systems*, 51:147–60.

Soulsby, R.L. (1997). *Dynamics of marine sands: A Manual for Practical Applications.* Thomas Telford Publications, London, 249 pp.

Speer, P.E. and Aubrey, D.G. (1985). A study of non-linear tidal propagation in shallow inlet/estuarine systems, Part II: Theory. *Estuarine, Coastal and Shelf Science*, 21:207–24.

Stauble, D.K. (1998). Techniques for measuring and analyzing inlet ebb-shoal evolution. Technical Report CETN IV-13, U.S. Corps. of Engineers.

Stauble, D.K. and Morang, A. (1992). Using morphology to determine net littoral drift directions in complex systems. Technical Report CETN-II-30, U.S. Army Engineer Waterways Experiment Station. (Assumed authors- listed for correspondence).

Stefani, C. (2002). Variation in terrigenous supplies in the Upper Pliocene to Recent deposits of the Venice area. *Sedimentary Geology*, 153 (1-2):43–55.

Street, R.L. (2003). Large eddy simulation of sediment transport in the presence of surface gravity waves and complex bedforms. Technical Report N00014-00-1-0440; FY03, Stanford University, CA.

Suman, D., Guerzoni, S., and Molinaroli, E. (2005). Integrated coastal management in the Venice Lagoon and its watershed. *Hydrobiologia*, 550:251–69.

Sutherland, T., Lane, P.M., Amos, C.L., and Downing, J. (2000). The calibration of optical backscatter sensors for suspended sediment of varying darkness levels. *Marine Geology*, 162 (2-4):587–97.

Syvitski, J.M.P. (2008). *Principles, Methods and Application of Particle Size Analysis*. Cambridge University Press, 388 pp.

Tambroni, N., Bolla Pittaluga, M., and Seminara, G. (2005). Laboratory observations of the morphodynamic evolution of tidal channels and tidal inlets. *Journal of Geophysical Research*, 110 (F04009).

Tambroni, N. and Seminara, G. (2006a). Are inlets responsible for the morphological degradation of Venice Lagoon. *Journal of Geophysical Research*, 111 (F03013).

Tambroni, N. and Seminara, G. (2006b). Sullo scambio netto di sabbie a lungo termine attraverso le bocche della Laguna di Venezia. In *Presentation: Corila Linea 3.18*.

Thevenot, M.M., Prickett, T.L., and Kraus, N.C. (1992). Tylers Beach, Virginia, dredged material plume monitoring project, 27 September to 4 October 1991. Technical Report Technical Report DRP-92-7, U.S Army Corps of Engineers.

Thompson, C.E.L. (2003). *The role of the solid-transmitted bed shear stress of mobile granular material on cohesive bed erosion by unidirectional flow.* Ph.D. thesis, University of Southampton.

Tęgowski, J. (2005). Acoustical classification of the bottom sediments in the southern Baltic Sea. *Quaternary International*, 130:153–61.

Tomasin, A. (1974). Recent changes in the tidal regime in Venice. *Rivista Italiana di Geojisica*, 23:275.

Tosi, L., Carbognin, L., Teatini, P., Strozzi, T., and Wegmüller, U. (2002). Evidence of the present relative land stability of Venice, Italy, from land, sea, and space observations. *Geophysics Research Letters*, 29 (12, 1562).

Tucker, M.E. (1991). *Sedimentary Petrology: an introduction to the origin of sedimentary rocks*. Geoscience Texts. Blackwell Science Ltd., 2 edition, 260 pp.

Umgiesser, G. (1997). Modelling the Venice Lagoon. *International Journal of Salt Lake Research*, 6:175–99.

Umgiesser, G. (2000). Modeling residual currents in the Venice Lagoon. In T. Yanagi, ed., *Interactions between estuaries, coastal seas and shelf seas.*, pp. 107–24. Terra Scientific Publishing Company, Tokyo., Matsuyama, Japan 1998.

Umgiesser, G., De Pascalis, F., Ferrarin, C., and Amos, C.L. (2006). A Model of sand transport in Treporti Channel: northern Venice Lagoon. *Ocean Dynamics*, 56:339–51.

Umgiesser, G., Ferrarin, C., De Pascalis, F., and Amos, C.L. (2005). Modeling sand transport in a canal system, northern Venice Lagoon. In P. Campostrini, ed., *Scientific research and safeguarding of Venice (Co.Ri.La. Research Program 2001-2003).*, pp. 383–90. CO.RI.LA, Venice.

Umgiesser, G., Melaku Canu, D., Cucco, A., and Solidoro, C. (2004a). A finite element model for the Venice Lagoon. Development, set up, calibration and validation. *Journal of Marine Systems*, 51:123–45.

Umgiesser, G., Sclavo, M., Carniel, S., and Bergamasco, A. (2004b). Exploring the bottom stress variability in the Venice Lagoon. *Journal of Marine Systems*, 51:161–78.

U.S. Army Corps of Engineers (1998). Coastal Engineering Manual (in 6 volumes).

U.S. Army Corps of Engineers (2002). Coastal Engineering Manual. Technical Report 1110-2-1100, U.S. Army Corps of Engineers.

USACE (2007). Effects of the NY/NJ harbour deepening project on the remedial investigation/feasibility study of the Newark Bay study area: Appendix 3: Assessment of suspended sediment plumes associated with navigation dredging in the Arthur Kill waterway, New Jersey. Technical report, U.S. Army Corps of Engineers.

van Leeuwen, S.M., van der Vegt, M., and de Swart, H.E. (2003). Morphodynamics of ebb-tidal deltas: a model approach. *Estuarine, Coastal and Shelf Science*, 57:899–907.

van Rijn, L.C. (1984a). Sediment transport: part I; bed load transport. *Journal of the Hydraulics Division, ASCE.*, 110 (HY10):1431–56.

van Rijn, L.C. (1984b). Sediment Transport: part II; suspended load transport. *Journal of the Hydraulics Division, ASCE.*, 110 (HY11):1613–41.

van Rijn, L.C. (1984c). Sediment Transport: part III; bed forms and alluvial roughness. *Journal of the Hydraulics Division, ASCE.*, 110 (HY12):1733–54.

Vanoni, V.A. (1975). Sedimentation Engineering; manual and report no. 54. Technical report, American Society of Civil Engineers.

Venturini, V. (2007). *Sand Transport Dynamics in Lido Inlet, Venice Lagoon, Italy.* Msc, University of Southampton.

Vila-Concejo, A., Ferreira, O., Matias, A., and Dias, J.M.A. (2003). The first two years of an inlet: sedimentary dynamics. *Continental Shelf Research*, 23 (14-15):1425–45.

Wall, G.R., Nystrom, E.A., and Litten, S. (2006). Use of ADCP to compute suspended-sediment discharge in the tidal Hudson River, New York. Technical report, U.S. Geological Survey Scientific Investigations Report 2006-5055.

Walton, Jr, T.L. (2002). Tidal velocity asymmetry at inlets. Technical Report ERDC/CHL CHETN-IV-47, US Army Engineer Research and Development Center, Vicksburg, MS.

Walton, Jr, T.L. (2004). Escoffier curves and inlet stability. *Journal of Waterway, Port, Coastal, and Ocean Engineering*, 130 (1):54–7.

Walton, Jr, T.L. and Adams, W.D. (1976). Capacity of inlet outer bars to store sand. In *Proceedings of the 15th International Conference on Coastal Engineering.*, volume 2, pp. 1919–37. ASCE, New York.

Wang, P., Ebersole, B.A., and Smith, E.R. (2002). Longshore sand transport - initial results from large-scale sediment transport facility. Technical Report ERDC/CHL CHETN-II-46, U.S. Army Corps of Engineers.

Wang, X.H. and Pinardi, N. (2002). Modeling the dynamics of sediment transport and resuspension in the northern Adriatic Sea. *Journal of Geophysical Research*, 107 (C123225).

Weinstein, J.E. (1996). Anthropogenic Impacts on Salt Marshes- A Review. In J. Vernberg, W. Vernberg, and T. Siewicki, eds., *Sustainable Development in the Southeastern Coastal Zone: The Belle W. Baruch Library in Marine Science Number 20 (Belle W Baruch Library in Marine Science)*, pp. 135–70. University of South Carolina Press.

Weltje, G.J. (1995). Unravelling mixed provenance of coastal sands: The Po Delta and adjacent beaches of the Northern Adriatic Sea as a test case. In M. Oti and G. Postma, eds., *Geology of Deltas*, pp. 181–202. Balkema, Rotterdam.

Wessel, P. and Smith, W.H.F. (1991). Free software helps map and display data. *EOS Trans. AGU*, 72:441.

White, J.R. and Williams, E.G. (1967). The nature of a fluvial process as defined by settling velocities of heavy and light minerals. *Journal of Sedimentary Petrology*, 37 (2):530–9.

Whitehouse, R.J.S. (1995). Observations of the boundary layer characteristics and the suspension of sand at a tidal site. *Continental Shelf Research*, 15 (3):1549–67.

Winkelmolen, A.M. (1969). *Experimental rollability and natural shape sorting of sand.* Phd, University of Groningen.

Woodroffe, C.D. (2002). *Coasts: Form, Process and Evolution*. Cambridge University Press, 638 pp.

Woods Hole Group (2006). Analysis of physical changes and management alternatives for the Nauset Beach area, Cape Cod, Massachusetts. Technical report, Woods Hole Group.

Wright, C.I., Miller, W.R., and Cooper, J.A.G. (2000). The late Cenozoic evolution of coastal water bodies in Northern KwaZulu-Natal, South Africa. *Marine Geology*, 167:207–29.

Yuan, Y., Zhao, L., Wei, H., and Jang, W. (2006). Estimations of Suspended Sediment Concentration from Echo Intensity using ADCP, OBS and LISST-100. In *PICES XV*. Yokohama, Japan.

Zaggia, L. and Maurizio, F. (2005). Studies on water and suspended sediment transport at the Venice Lagoon inlets. In *Waves 2005*, p. 10. Madrid.

Zanatta, V., Rosato, P., Alberini, A., and Reppas, D. (2005). The impact of speed limits on recreational boating in the Lagoon of Venice. *FEEM Working Paper. Available at SSRN.*, 135.05.

Zuliani, A., Zaggia, L., Collavini, F., and Zonta, R. (2005). Freshwater discharge from the drainage basin to the Venice Lagoon (Italy). *Environment International*, 31:929–38.